Bayerische Julius-Maximilians-Universität zu Würzburg
Fakultät für Biologie
Lehrstuhl für Mikrobiologie

Protein dynamics in responder and non-responder solid tumor xenografts during oncolytic viral therapy

Dissertation

zur Erlangung des naturwissenschaftlichen Doktorgrades

der Bayerischen Julius-Maximilians-Universität Würzburg

vorgelegt von

Thu Ha Le

aus Vietnam

Würzburg, 2008

Eingereicht am: .....

Mitglieder der Promotionskommission:

Vorsitzender: .....

Gutachter : .....

Gutachter: .....

Tag des Promotionskolloquiums: .....

Doktorurkunde ausgehändigt am: .....

Supervisor 1: _____

(Prof. Dr. A. A. Szalay, Lehrstuhl für Mikrobiologie)

Supervisor 2: _____

(Prof. Dr. F. Grummt, Lehrstuhl für Biochemie)

Eidesstattliche Erklärung

Hiermit versichere ich, dass ich die vorliegende Dissertation selbständig und nur mit den angegebenen Hilfsmitteln und Quellen angefertigt habe.

Ich erkläre außerdem, dass diese Dissertation weder in gleicher noch in anderer Form bereits in einem anderen Prüfungsverfahren vorgelegen hat.

Neben dem akademischen Grad „Master-MD-Uni.“ habe ich keine weiteren akademischen Grade erworben oder zu erwerben versucht.

Würzburg, den …….. ……...

(Thu Ha Le)

ACKNOWLEDGEMENT

At this point I would like to take the chance to express my gratitude to all those who gave me the possibility to complete this thesis that took place at the department of microbiology, Bio center of the University of Wuerzburg, Germany, from October 1st of 2004 until December of 2008 under supervision of Prof. Dr. A. A. Szalay and Prof. Dr. F. Grummt.

I special thanks to

Prof. Dr. A. A. Szalay for providing working environment and for representing this dissertation at the faculty of biology. I am deeply indebted to you for your kindness for giving a very interesting thesis as well as stimulating suggestions, kindly recommendation, financial support of scientific projects and for your continuous encouragement.

Prof. Dr. F. Grummt for his interest on my project and for proofreading this work. I particularly thank you for encouragement helped me in all the time of research for and writing of this thesis, looked closely at the final version of the thesis for English style and grammar, correcting both and offering suggestions for improvement.

Dr. Andrea Spory from Microbiology department of Wuerzburg University for her kindly technical assistance of two-dimensional electrophoresis.

Dr. Jörg Bernhardt from Institute of Microbiology in Greifswald University for his meticulous assistance in instructing in analysis a differential protein expression by using 2D-Software and Dr. Brigit Voigt from Institute of Microbiology in Greifswald University for her responsible assistance in protein sequencing

Dr. Benedikt Brors from German cancer research centre for computative tumor protein analysis.

I was delighted to interact with Dr. Elisabeth Hofmann by her help and having her as my co-advisor, specially thank for her thorough assistance and for illuminative discussions.

My colleagues in the laboratory Christine Horchbashek, Chiristina Tietze, Stephanie Weibel, Carolin Seubert, Victoria Raab, Andrea Worschech, Ulrike Geißinger, Dr. Jochen Stritzker, Dr. Ivaylo Gentscher, Johanna Langbein, Ulrike Donat, Julia Sturm, Yvonne Dombrowski, Anja Sauer, Kerstin Richte, Claudia Stühler for their sedulous helpfulness and the comfortable working atmosphere, for advice in word and deeds and cheerful hours, the staff members of the chair of microbiology, especially Monika Goetz for kindly support working facilities, as well as the personnel of the chair of biochemistry, specifically to Anneli Kießling for her organizational talent and aid.

All members of staff of Genelux company, named Tony Yo, Qian Zhang, Nanhai Chen, Alexa Frentzen, Antonietta Jimenez Pearson, Terry Trevino, Camha Hoang, Alison

Estrada, Shahrokh Shabahang, Andrea Feathers, Tom Hagood, Valere Rollings, Albert Röder, Ron Simus and Daniela for financial support of scientific projects as well as kindly, helpful assistance during the past 4 years.

I would regret my doctoral years at Wuerzburg University if I did not join MOET and DAAD fellowships. Joining these fellowships was not only a turning point in my life, but also a wonderful experience.

Sincere thanks to my mother who always supported me and to my son and husband in Vietnam who had to live without me during the past years of my doctorade, whose patient love enabled me to complete this work. I am deeply grateful for their true understanding and trust, their help and support and much.

Contents

Zusammenfassung

Es ist bekannt, dass sich VACV GLV-1h68 sowohl als diagnostischer als auch therapeutischer Vektor eignet, der sich in Tumoren ansiedelt, darin repliziert und dass mit dessen Hilfe die Lokalisation von Tumoren bestimmen werden kann. Weiterhin konnte bereits gezeigt werden, dass der Effekt von GLV-1h68 auf die Tumor-Kolonisierung, das Tumorwachstum, die -regression und -vernichtung zustande kommt, ohne dass irgendwelche bekannten Gene mit anti-tumoraler Aktivität dazu notwedig wären. Um die differentielle Proteinexpression vergleichend sowohl zwischen uninfizierten und infizierten Tumorzellen als auch zwischen den korrespondierenden uninfizierten und infizierten Tumoren zu untersuchen, wurden proteomische Methoden angewandt. Ziel dieser Arbeit war es, mehr über die onkolytische Fähigkeit von GLV-1h68 auf Proteinebene zu erfahren.

Die dargestellten Effekte der VACV GLV-1h68 Infektion auf die zelluläre Proteinexpression legen eine selektive Vernichtung von Tumorzellen nahe. In dieser Arbeit wurde die differentielle zelluläre Proteinexpression zu verschiedenen Zeitpunkten nach Infektion mit Hilfe der zweidimensionalen Gelelektrophorese (2-DE) gefolgt von MALDI-TOF/TOF-Identifikation der Proteine analysiert. Die vergleichende Analyse mehrerer 2-DE Gele zeigte, dass sich das Proteinexpressionsmuster bei Zellen aus *in vitro* Kulturen 48 hpi dramatisch verändert. Bei Zellen aus solidem Tumorgewebe erfolgen 42 Tage nach Infektion ebenfalls derartige dramatische Veränderungen. Mittels Massenspektroskopie wurden in GI-101A-Zellen 68, in HT-29-Zellen 75 und in PC-3-Zellen 159 alteriert exprimierte zelluläre Proteine nach VACV-Infektion beobachtet. Davon werden 30, 23 bzw. 49 hochreguliert und 38, 52 bzw. 110 niederreguliert. Diese „up“- bzw. „down“-Regulation erfolgte zwischen 12 und 48 h nach Virusinfektion. In Virus-besiedelten Xenograft-Tumoren wurden mittels Massenspektroskopie in GI-101A-, HAT-29- bzw. PC-3-Tumoren 270, 101 bzw. 91 alteriert exprimierte Proteine festgestellt. Von diesen wurden zwischen 7 und 42 Tagen nach Infektion 89, 70 bzw. 40 „up“-reguliert und 181, 31 bzw. 51 „down“-reguliert.

Interessanterweise sind die in den Zelllinien differentiell regulierten Proteine meist mit metabolischen Prozessen, besonders mit dem primären Energiemetabolismus wie Glucose-Katabolismus, Zitronensäurezyklus und der Milchsäure-Produktion assoziiert. Eine VACV GLV-1h68-Infektion generall führt zur Umfunktionierung des Wirts-Translationsapparates

zur Synthese von Virusproteinen, zur Umgestaltung des Zytoskeletts und zur Derangierung des Ubiquitin-anhängigen Proteasom-Abauweges.

Insbesondere in Virus-infizierten Tumor-Xenograften ist eine weitere Palette von zellulären Prozessen alteriert. Dies umfasst die Signaltransduktion (einschließlich derjenigen, die zum Zelltod führen), Transportprozesse (hier ist vor allem der Eisentransport betroffen) und die Zellmigration. Ein gemeinsamer Signalweg, der sowohl in Zelllinien als auch in den Tumoren hochreguliert ist, ist die „unfolded protein response (UPR)". Bemerkenswerterweise beeinflusst die VACV GLV-1h68-Infektion die anti-apoptotischen Signalwege in GI-101A und PC-3-Zellen, deren korrespondierende Tumoren nach Virusinfektion eine Regression aufweisen (regressive Tumoren), nicht jedoch in HT-29-Xenograften, die nach Infektion nicht mit Regression reagieren (nicht-regressive Tumoren). So werden z.B. in Virus-infizierten GI-101A-Xenograften 12 Proteine mit Anti-Apoptose-Funktion vermindert exprimiert, darunter *tumor protein-translationally-controlled (H-TPT1), rho-GDP-dissociation inhibitor alpha (H-GDIa), ywhaq protein (M-1433T), H-PRDX4, serin/theronin-protein phosphatase-2A-catalytic subunit beta isoform PP2A (M-Ppp2cb), eukaryotic translation initiation factor 2-subunit alpha-35kDA (H-eIF2), H-actinin-α1 (ACTN1), annexn A1 (H-A1), annexin A5 (H-A5), mouse albumin 1 (M-Alb1), dimethylarginine dimethylaminohydrolase 2 (H-DDAH2)*. In PC-3-Xenograften werden lediglich drei anti-apoptotisch aktive Proteine, *ARP3 actin-related protein-3-homolog (H-ARP3), human FLNA protein und rho GDP dissociation inhibitor (GDI) alpha (H-GDIa)*, niederreguliert. Im Gegensatz dazu werden in den nicht-regressiven HT-29-Tumoren anti-apoptotische Proteine sogar verstärkt exprimiert. Diese gehören vor allem zu den Peroxiredoxin-Proteinen. Diese Erkenntnisse geben Hinweise darauf, mit welchen Mechanismen HT-29-Tumorzellen der Apoptose entgehen. Die Vaccinia-Virus-Infektion scheint vor allem die UPR und Anti-Apoptose-Proteine zu beeinflussen.

Weitere Untersuchungen sind in Zukunft nötig, um im Detail herauszufinden, wie die VACV-Infektion die UPR in Tumorzellen induziert und ob einige Elemente der UPR möglicherweise neue Ansätze zu einer verbesserten Tumortherapie darstellen könnten.

ABSTRACT

VACV GLV-1h68 was reported as a diagnostic/therapeutic vector which enters, replicates in, and reveals the locations of tumors in mice. Furthermore, the effect on tumor colonization, on tumor growth, regression and eradication by VACV GLV-1h68 without the need of any known genes with anti-tumoral activities was determined. To investigate differential protein expression between infected tumor cells and corresponding tumors, as well as between infected tumor cells, between infected tumors, proteomics is particularly used, possibly contributing to the understanding oncolytic ability on the protein level of VACV GLV-1h68.

The given effects of VACV GLV-1h68 infection on cellular protein expression support tumor cell killing. In this study, differential protein expression was analyzed at different time points with two-dimensional gel electrophoresis (2DE) followed by MALDI-TOF/TOF identification. Comparative analysis of multiple 2-DE gels revealed that the majority of protein expression changes appeared at 48 hours post infection in cell cultivation and at 42 days post infection in tumors. Mass spectrometry identified 68, 75, 159 altered cellular proteins in the GI-101A, HT-29, PC-3 infected cells, respectively, including 30, 23, 49 *up-regulated* proteins and 38, 52, 110 *down-regulated* proteins 12 to 48 hours after infection. For xenografts, mass spectrometry identified 270, 101, 91 altered cellular proteins in the infected GI-101A, HT-29, PC-3 tumors, respectively, including 89, 70, 40 *up-regulated* proteins and 181, 31, 51 *down-regulated* proteins 7 to 42 days after infection.

In general, in the cell lines, the proteins found to be differentially regulated are most often associated with metabolic processes, in particular with primary energy metabolism (glucose catabolism, TCA and lactate production). VAVC GLV 1h68 infection results in hijacking of the host translation apparatus, alteration of cytoskeleton networks, induce ubiqitin proteasome pathway (UPP) disorders.

Particularly in tumors, the responses cover a much broader panel of cellular processes, including signalling (e.g., cell death), transport (in particular of iron ions) and migration. A common pathway to be *up-regulated* in *both tumors and cell lines* is the "unfolded protein

response". Notably, VACV GLV-1h68 affected the anti-apoptosis pathways in GI-101A and PC-3 cancer cells but not in HT-29 xenografts. For example, GI-101A xenografts in mice appear 12 proteins associated with anti-apoptosis function. They were found *down-regulated*, including *tumor protein-translationally-controlled (H-TPT1), rho-GDP-dissociation inhibitor alpha (H-GDIa), ywhaq protein (M-1433T), H-PRDX4, serine/threonine-protein phosphatase-2A-catalytic subunit beta isoform PP2A (M-Ppp2cb), eukaryotic translation initiation factor 2-subunit 1 alpha-35kDa (H-eIF2), H-actinin-α1 (ACTN1), Annexin A1 (H-A1), annexin A5 (H-A5), Mouse albumin 1 (M-Alb1), dimethylarginine dimethylaminohydrolase 2 (H-DDAH2).* In PC-3 xenografts, anti-apoptosis expression is lesser than those in GI-101A cells, however 3 anti-apoptosis associated proteins were *down-regulated* such as *ARP3 actin-related protein-3-homolog (H-ARP3), Human FLNA protein, Rho GDP dissociation inhibitor (GDI) alpha (H-GDIa).* In contrast, in HT-29 xenografts, there are several anti-apoptosis-associated proteins that show even to be *up-regulated*; they mostly belong to peroxiredoxin proteins. Lesson from HT-29 had been given what various means the HT-29 cells use to escape their apoptosis fate. This suggests that VAVC GLV1h68 infection may induce unbalance of unfolded protein response (UPR) but tending to anti-apoptosis-mediated proteins and promote the destructive elements of UPR, including caspase-12 cleavage and apoptosis.

Taken together in this thesis research I have tried to compare protein profiles obtained from responder cell line and from regressing solid tumors colonized by VAVC GLV-1h68 with that of non-responding tumors. I also compared these data with PC-3 prostate cell line and tumor data on intermediate responder which alter mouse protein profiling in tumors similarly to the highly efficacious GI-101A breast tumor cell line. From these comparisons I have deduced exciting protein pattern signature characteristic for a responder or distinctly different from non-responder system. Combining these few crucial genes involved with the transcriptional test data obtained by fellow graduate student at NIH a novel national designed VACV GLV-1h68 strains with enhanced efficacy in many today non-responder cancer cell lines will be available to be tested into ongoing clinical trials.

1. INTRODUCTION

1.1 Vaccinia virus as a representative oncolytic virus

An oncolytic virus is a virus that is able to infect and lysis cancer cells, while leaving normal cells unharmed, making them potentially useful in cancer therapy. Replication of oncolytic viruses both facilitate tumor cell destruction and also produce dose amplification at the tumor site. They may also act as vectors for anticancer genes, allowing them to be specifically delivered to the tumor site.

Tremendous advances have been made in developing oncolytic viruses in the last few years. By taking advantage of current knowledge in cancer biology and virology, specific oncolytic viruses have been genetically engineered to target-specific molecules or signal transduction pathways in cancer cells in order to achieve efficient and selective replication. Oncolytic viruses utilize multiple mechanisms of action to kill cancer cells, cell lysis, cell apoptosis, anti-angiogenesis and cell necrosis. Once the virus infects the tumor cell, it compromises the cell's natural defense mechanisms, giving the virus extra time to thrive. The virus then begins to replicate. The virus continues to replicate until finally the tumor cell can no longer contain the virus and "lyses" (bursts) the host cell's membrane. The tumor cell is destroyed and the newly created viruses are spread to neighboring cancer cells to continue the cycle. It is important to remember that all oncolytic viruses are intended to replicate only in cancer cells and to pass through normal tissue without causing harm. Hence, once all the tumor cells are eradicated, the oncolytic virus no longer has the ability to replicate and the immune system clears it from the body.

In other way, the viral infection and amplification eventually induce cancer cells into cell death pathways and elicit host antitumor immune responses to further help eliminate cancer cells. Specifically targeted molecules or signaling pathways (such as RB/E2F/p16, p53, IFN, PKR, EGFR, Ras, Wnt, anti-apoptosis or hypoxia) in cancer cells or tumor microenvironment have been studied and dissected with a variety of oncolytic viruses such as adenovirus, herpes simplex virus, poxvirus, vesicular stomatitis virus, measles

virus, Newcastle disease virus, influenza virus and reovirus, setting the molecular basis for further improvements in the near future.

In one of the most successful stories in medical history, vaccinia virus (VV) was utilized as the vaccine for worldwide smallpox eradication. Recombinant VV and other related poxviruses have served as vectors for gene delivery and as vaccines for infectious disease and cancer (Guo ZS and Bartlet DL 2004). Despite the fact that it has been used as a vaccine and a gene expression vector for many years, it is only in the last decade that VV has been specifically genetically engineered and explored as an oncolytic virus (Timiryasova TM et al., 1999; Bartlett DL et al., 2001; Thorne SH et al., 2005).

1.2 Vaccinia virus biology

The biology of vaccine viruses makes them suitable for adaptation to oncolytic vectors, the extensive use of vaccinia virus for both clinical and research purposes has led to the emergence of multiple strains with unique properties. Their large genome size makes them ideal promising vectors as it allows insertion of large numbers gene for viral therapeutic approaches.

1.2.1 Vaccinia virion structure and life cycle

Vaccinia virus (VV) is a member of the Poxviridae family (Esposito JJ and Frenner F 2001; Moss B 2001). The true origin of VV remains obscure. When Edward Jenner, an English country physician, used the material that he isolated from a milkmaid as a vaccine for smallpox, he was in fact using cowpox virus (Jenner E 1798). In the 1930s, it became clear that the strain being used at that time for smallpox vaccination was distinct from the cowpox. Later, this strain was identified as vaccinia (Fentiman IS et al., 1986). The genome consists of 191,636 bp and encodes for 2063 proteins of 65 or more amino acids. These proteins are used to construct the mature virion, which includes a double membrane. The infectious mature virion or extracellular enveloped virus (EEV) is released from the cell by membrane fusion and is responsible for cell-to-cell spread of the virus. The intracellular mature virus (IMV) is released from the cell upon lysis, and is the

form of the virus that is produced under laboratory conditions. The EEV is too fragile to withstand the purification process. The mechanism of vaccinia attachment and uptake into cells is still under intense investigation. This process is likely to involve the A27L and D8L proteins, which are found in the IMV membrane and appear to bind heparin sulfate and chondroitin sulfate on the cell surface (Hsiao JC et al., 1999; Chung CS et al., 1998) Fusion is quickly followed by release of viral-transported transcriptional enzymes that transcribe early viral mRNA. These early mRNA typically encode for proteins that are involved with uncoating of the viral DNA and transcriptional factors for intermediate mRNA production. Intermediate mRNA encodes for the late transactivators that lead to late mRNA synthesis. The late proteins include viral structural proteins and early transcriptional factors to be incorporated into the mature virion (Moss B and Earl PL 1998). Viral DNA replication occurs, forming concatemers, which are then resolved into individual genomes and assembled into mature virions. The mature virus contains three membranes after assembly; the outer fuses with the cell membrane, resulting in release of a double-membrane viral particle (EEV). The EEV remains attached to the cell surface through the A34R gene product, allowing for cell-to-cell spread of the virus (McIntosh AAG and Smith GL 1996). The EEV form is resistant to antibody neutralization. It is interesting to note that the vaccinia virus, like the other poxviruses, spends its entire lifecycle in the cytoplasm and has never been shown to integrate into the genome (Moss B and Earl PL 1998). IMVs represent the most abundant form of the virus and are retained in the cell until lysis. CEVs and EEVs are important for virus dissemination (Payne LG 1980; Smit G-L 2002).

1.2.2 Interactions with host cells

In order to make the cell an ideal environment for virus survival and replication, the invading VV must alter the cell in several ways.

To inhibit of host cell macromolecular synthesis, VV were found to inhibit DNA, RNA, and protein synthesis in the cells they have infected. Vaccinia has very few interactions with host cellular proteins, allowing for rapid, efficient replication without negative effects from host cell defenses (Stephen McCraith et al., 2000). The virus induces a

profound cytopathic effect very soon after viral entry, as early viral enzymes completely shut down host cell function. By 4–6 hours after infection, there is almost complete inhibition of host protein synthesis. This allows for very efficient expression of viral genes and viral replication (Avirup Bose et al., 1997). In fact, approximately 10,000 copies of the viral genome are made within 12 hours of infection; half of these are incorporated into mature virions and released. The success of vaccinia as an oncolytic vector relies on its efficiency in vivo. This is dependent on the rapidity of replication and spread, and evasion of host defenses (Geoffrey L Smith 1999).

To defend against host antiviral mechanisms, there are several ways. Firstly, VV encode virokines which are secreted from infected cells and mimic host cytokines and therefore attach to and block host cytokine receptors (Johnston JB and Grant McFadden 2003), encode viroceptors which are essentially cellular receptors that do not contain a transmembrane domain, they are secreted from infected cells and bind their ligands, preventing their normal activity (Johnston JB and Grant McFadden 2003), intracellular proteins which can block the cytokine or complement-induced pathways within the cell itself, and encode complement regulatory protein. These products of the VV infection cause combat the host's antiviral complement and cytokines. Secondly, following the interferon patways, VV produce a dsRNA-binding protein (E3L, K3L) that blocks the PKR-mediated cellular reponse to IFN (Garc MA et al., 2007). Thirdly, VV can induce interleukins (secreted protein that mimics the mammalian proteins cause sequesters and blocks its pathways) or tumor necrosis (Johnston JB and Grant McFadden 2003; Bruce T Seet et al., 2003). Fourthly, VV produces chemokine that binds chemokine receptors and prevents their normal ligand from binding or bind to the chemokines themselves and prevent leukocyte stimulation (Jens Y Humrich et al., 2007). The last, E3L protein of VV can block apoptosis pathway (John M Taylor and Michele Barry 2006).

1.3 Genetic engineering for tumor-selective replication

Vaccinia virus strains may possess a natural tumor tropism after systemic delivery in mouse models (Acres B et al., 1994; Peplinski GR et al., 1996; McCart JA et al., 2001). Part of the reason for this may be in the fact that VV activates cell-signaling pathways

and alters the progression of the cell cycle upon infection by inactivation of the tumor suppressors' p53 and pRb. This may contribute to more efficient replication of the virus in rapidly growing cells such as many cancer cells (Yoo NK et al., 2008). As a large virus, 250×350 nm in size, it may also require leaky vasculature for extravasations from circulation and into tissues. Tumor tissues are well documented for their vascular endothelial growth factor (VEGF) production and leaky vasculature. A number of strategies have been designed to further enhance viral replication in cancer cells and reduce replication in normal cells and thus maximize its safety.

To determine the location of viral particles in the rodents with tumors, vaccinia virus carrying the firely luciferase expression cassette has been injected intravenously (Grant MFX et al., 1999). Subsequent luciferase assays of homogenates of excised individual organs and tumors reveal 3 to 500 fold enhancement of light emission in the tumor samples, showing the accumulation of viral particles. The Renilla reniformis luciferase-Aequorea victoria green fluorescent (GFP) fusion protein (RUC-GFP) (Wang Y et al., 1996; Wang Y et al., 2001) allows real-time monitoring of gene activation in the live animals base on luciferase activity and GFP fluorescence (Wang Y et al., 2002), the activity of the RUC-GFP expression cassette inserted into vaccinia virus DNA (rVV-RUC-GFP) has been imaged in both virus-infected mammalian cell cultures and in virus-infected live animals (Tymiryasova T et al., 2000). Interestingly, authors show that vaccinia virus survived and replicated in the tumors for weeks without causing viremia, this was observed in both immunocompromised and immunocompetent animals with allergenic and syngeneric tumors (Yu YA et al., 2004). Base on their "Tumor-finding" nature. Viruses may be designed to carry multiple genes for detection and treatment of cancer.

Aberrant epidermal growth factor receptor (EGFR) signaling is a major characteristic of a number of human malignancies including breast cancer, lung cancer, colon cancer, and head and neck cancer. Alterations in the functions of the EGFR signaling pathway are associated with oncogenic transformation and are associated with essentially all of the key features of cancer, such as autonomous cell growth, invasion, angiogenic potential, and development of distant metastases (Yarden Y 2001). Vaccinia growth factor (VGF), a 19-kD secreted glycoprotein encoded by the virus, shares sequence homology and

functional properties with cellular growth factors, EGF and TGF-α. Like EGF and TGF-α, VGF binds and induces tyrosine phosphorylation of the EGF receptor. Early work by Moss and associates demonstrated that viral genes encoding both thymidine kinase (tk) and vaccinia growth factor (vgf) are virulence genes and are needed for efficient viral replication in normal cells in vivo (Buller RM et al., 1985; Buller RM et al., 1988). When the tk gene was deleted from the viral genome of the WR strain of VV, the resulting virus displayed reduced replication in normal cells and yet retained full capacity to replicate in cancer cells (McCart JA et al., 2001; Puhlmann M et al., 2000). When both viral genes for VGF and TK were deleted, the resulting virus (vvDD) retained its ability to target and replicate in cancer cells both in vitro and in vivo, and displayed significant oncolytic potency in multiple tumor models (McCart JA et al., 2001; Chalikonda S et al., 2008). This virus was found to be dependent on cellular TK for viral replication, which is expressed to high levels in cancer cells as a result of aberrant EGFR signaling leading to E2F-mediated TK expression. The additional deletion of the vgf gene prevented activation of EGFR signaling in noncancer cells, further restricting viral replication to cancer cells (Thorne SH et al., 2007). The addition of GM-CSF gene to this virus was further found to be very useful for combination oncolytic immunotherapy. Systemic administration of this virus (JX-963) led to systemic efficacy against both primary carcinomas and widespread metastases in immunocompetent hosts (Thorne SH et al., 2007). In addition, by taking advantage of cancer cells' ability to evade apoptosis, the deletion of two viral genes (B22R and B13R) encoding anti-apoptotic proteins and serpins SPI-1 and SPI-2 was examined. The resulting virus, named vSP, displayed enhanced tumor targeting, yet significant oncolytic potency in a tumor model (Guo ZS et al., 2005). The tumor selectivity could be explained at least partly by the fact that normal cells infected with vSP die with faster kinetics and thus viral replication is limited, while viral replication in cancer cells is sustained. However, there is a limitation to the strategy of deleting nonessential viral genes as illustrated in a new VV (vSPT) with a triple deletion of viral genes, spi-1, spi-2 and tk. This virus showed remarkable tumor selectivity, yet lost significant oncolytic potency in tumor models in vivo (Yang ST et al., 2007). Other strains of VV have also been explored as oncolytic virus which Szalay et al. have described an oncolytic VV based on insertion of reporter genes into three viral sites

[J2R (TK), A56R (HA) and F14.5L] in the LIVP strain (Zhang Q et al., 2007). This virus, GLV-1h68, replicated poorly in normal mouse cells yet replicates well in cancer cells. It was also found to cause tumor regression in a human breast cancer xenograft in nude mice. Gene expression profiling of regressing tumors revealed gene expression signatures consistent with immune defense activation. A replication-competent vaccinia virus has significant infectious and oncolytic activity against a panel of human anaplastic thyroid carcinoma (ATC), these results encourage future in vivo and clinical studies for this novel agent to treat this fatal cancer (Lin SF et al., 2007). So far, genetic engineering may further enhance the oncolytic potency and safety of viruses.

1.4 Mechanisms of tumor escape

Understanding the escape immune mechanism of tumors help to manipulate and estimate effectively using oncolytic viruses for cancer therapy appropriately. Despite an active and apparently normal immune response by a healthy immune system, tumor cells can grow, invade and metastasize in the host (Pardoll D 2003). Tumor cells can escape or fail to elicit anti-tumor immune responses by various mechanisms. They are phenotypically and genetically less stable than normal cells and can rapidly change to escape immune destruction. One of these escape mechanism is production of inhibitory cytokines by the tumor.

Targeting tumor-associated macrophages (TAMs) is a novel trategy against cancer (Yunping Luo et al., 2006). TAMs are known as factors associated with tumor progression and metastasis. Decreasing the number of TAMs in the tumor stroma effectively altered the tumor microenvironment involved in tumor angiogenesis and progression to markedly suppress tumor growth and metastasis. Gaining better insights into the mechanisms required for an effective intervention in tumor growth and metastasis may ultimately lead to new therapeutic targets and better anticancer strategies (Luo Y et al., 2006). In recent studies, anti-TAM effects induced by small molecule inhibitors contributed to tumor suppression (Lewis C and Murdoch C 2005; Mantovani A et al., 2004). For example, the anti-neoplastic agent Yondelis has a selective cytotoxic effect on TAMs, thereby significantly reducing their production CCL2/MCP-1

(Monocyte chemotactic protein-1), which, in turn, contribute to growth suppression of inflammation-associated human tumors (Allavena P et al., 2005). MCP-1, a specific chemotactic and activating signal for monocytes, is expressed mainly by tumor cells as well as by endothelial cells, fibroblasts, and macrophages in human tumors (Mantovani A 1994). Some studies have suggested that MCP-1 may be the main determinant of the macrophage content in tumors (Graves DT et al., 1989). and it is highly expressed in a wide range of tumor types including glioma (Leung SY et al., 1997), meningioma (Sato K et al., 1995), ovarian carcinoma (Negus RP et al., 1995), and squamous cell carcinoma of uterine cervix (Riethdorf L et al., 1996). Indeed, in a study of the poorly differentiated lymphoepithelioma-like carcinoma of the lung, Wong et al. (Wong MP et al., 1998) identified a close association between the up-regulation of MCP-1 by tumor cells and TAM accumulation. Moreover, MCP-1 expression by both tumor cells and TAMs themselves was positively associated with TAM accumulation in breast carcinoma (Ueno T et al., 2000). It also correlated significantly with levels of the angiogenic factors vascular endothelial growth factor (VEGF), thymidine phosphorylase (TP), tumor necrosis factor alpha (TNFa), and interleukin-8 (IL-8). The authors also noted that increased expression of MCP-1 as well as VEGF was a significant indicator of early relapse and suggested that MCP-1 may play an important role in the regulation of angiogenesis. MCP-1 may therefore be considered a pro-tumorigenic protein. Moreover, in a study by Sica et al. (Sica A. et al., 2000), the chemokine receptor CCR2, to which MCP-1 binds, was found to have a potential pro-tumorogenic role. TAMs from solid ovarian carcinoma or ascites displayed defective CCR2 mRNA and surface expression and did not migrate in response to MCP-1. This suggested that receptor inhibition may serve as a mechanism to arrest and retain recruited TAMs at sites of tumor growth. As neutralizing antibodies for TNFa restored the CCR2 levels expressed by monocytes (cultured in the presence of ascitic fluid), the authors suggested that down-regulation of CCR2 expression by such pro-inflammatory molecules as TNFα may account for the defective migration of macrophages and their inability to mount an effective inflammatory response to the tumor.

In a different experimental model, the chemokine CCL5/RANTEST (regulated upon activation, normal T-cell expressed and secreted) was shown to be key in the recruitment

of TAMs, and an antagonist of this chemokine reduced the tumor infiltrate and slowed tumor growth (Robinson SC et al., 2003). CCL5 (or RANTES) is an 8 kDa protein classified as a cytokinechemotactic or chemokine CCL5 is chemotactic for T cell, eosinophils and basophils, and plays an active role in recruiting leukocytes into inflammatory sites. To investigate the role of tumor-derived CCL5 (regulated upon activation, normal T cell expressed and secreted, RANTES) in tumor immunity, Adler et. al., 2003 indicate that tumor-derived CCL5 can inhibit the T cell response and enhance the in vivo growth of murine mammary carcinoma (Evan P Adler et al., 2003).

Tumor immune escape is a critical trait of cancer but the mechanisms involved have to be fully described yet. VCAM-1, also known as CD106, is a molecule with a well-characterized role in the human immune system. It contains six or seven immunoglobulin domains and is expressed by many different cell types, including activated endothelial cells, bone marrow stromal cells, spleen stromal cells, thymic epithelial cells, peripheral lymph node (LN) and mesenteric LN high endothelial venules, and some dendritic cells in the spleen. Up-regulation of VCAM-1 in endothelial cells is induced by the cytokines IL-1h, IL-4, tumor necrosis factor-a, and IFN-g. VCAM-1 is an endothelial ligand for very late antigen-1 (VLA-4; or a4h1 integrin) and a4h7 integrin. The interaction between VCAM-1 and VLA-4 or a4h7 integrin, expressed on leukocytes, is thought to be involved in the extravasation of leukocytes through the endothelium to sites of inflammation (Petruzzelli L et al., 1999; Kobayashi H et al., 2007). One recent study has shown that tumor cells can escape T cell immunity by overexpressing the endothelial cell adhesion molecule vascular cell adhesion molecule-1 (VCAM-1), which normally mediates leukocyte extravasion to sites of tissue inflammation. Renal cell carcinoma was identified as one tumor type where VCAM - 1 is commonly highly overexpressed (Wu T-C 2007).

VCAM-1 expression by tumor cells led to decreased apoptosis of the tumor cells and a significant decrease in the number of tumor-infiltrating CD8+ T cells in the tumors expressing VCAM-1 (Wu T-C 2007).

1.5 Proteomic strategies and their application cancer research

1.5.1 Cancers

Cancer is a complex disease and represents the end product of a multistep biological process including growth and survival of neoplastic cells at the primary tumor site, invasion of the host tissue, angiogenesis, intravasation and survival in the circulatory system, arrest and extravasation into a new tissue and finally growth at the secondary site (Alessandro R and Kohn EC 2002; Fidler IJ 2003). Despite the knowledge of genetic mechanisms driving some of these events at the tissue level, biochemical endpoints are not fully characterized nor are treatments optimized. The ability to accurately profile cancer on a molecular level would have a profound effect on the quality of treatment. Research activities in cancer have focused on the genomic characteristics of cancer cells. Until now, the output from this strategy has not been enough in itself and needs to be paired with a conceptual return to proteins as the real key players in all physiological and pathological processes (Wiesner A 2004).

1.5.2 Cancer proteomic

The proteome is defined as complete set of proteins encoded by the genome, including splice variant and post translational modifications, for particular organism, tissue, cell or subcellular component (Wilkins MR et al., 1996). Proteomics represents technologies for analysis of the proteome under a given set of physiological or developmental conditions. The term “cancer proteome” refers to the collection of proteins expressed by a given cancer cell and should be considered as a highly dynamic entity within the cell, which affects a variety of cellular activities. The emerging proteomic analysis platforms including 2D-PAGE, mass spectrometry technologies, and protein microarrays represent powerful tools to study and understand cancer. These systems aim to not only identify, catalogue, and characterize cancer proteins, but also to unveil how they interact to affect overall tumor progression. In neoplastic cells, proteins encoded by oncogenes or tumor suppressor genes are the effecter molecules in malignancy since they are critical

components or regulate the multiple interconnected signaling pathways that drive the metastatic phenotype (McCormick F 1999; Blume-Jensen P and Hunter T 2001). High-throughput genomic techniques have facilitated a better understanding of gene expression in cancer but are not adequate for thorough dissection of such a complex disease as cancer at the molecular level. Genomic techniques suffer a limitation in their ability to monitor changes in protein levels, co- and post-translational modification events, protein-protein interactions, topographical distribution and distribution of factors across the varied cellular compartments. Moreover, genomic techniques cannot predict the activation state of signaling molecules in important protein networks. Our understanding of the molecular basis of tumor progression and metastasis needs to be developed through a detailed study of the proteins themselves. Although cancer is a genetic disease, it is a disease of proteins from a functional point of view in where the phenotype is often the result of deranged signaling pathways. (Herrmann PC et al., 2001; Petricoin EF et al., 2002). Therefore, cancer proteomics aims not only to identify, catalogue, and characterize relevant proteins, but also to understand how they interact to affect the overall initiation and metastatic progression.

1.5.3 Principles and technological platforms

At the beginning of proteomics, the field was mainly decribed by the use of two-dimensional polyacrylamide gel electrophoresis (2D-PAGE), traditionally performed to separate complex mixtures of proteins. Although this technique has some limitations for generally research applications, it still represents a powerful tool to study the protein profile of cell lysates or biological fluids. A major advantage to the use of 2D gels was the ability to identify gel-separated proteins by mass-spectrometry techniques as matrix-assisted laser desorption ionization time of flight (MALDI-TOF) and electrospray ionization tandem MS (ESI-MS/MS) (Pandey A and Mann M 2000). Another emerging technique in proteomic research is the on-line reversed phase liquid chromatography tandem mass spectrometry (LC/MS/MS) that permits the sequencing of thousands of peptides produced by trypsinization of proteins from a single sample (cell lysate or serum

sample) (Peng J and Gygi SP 2001). A refinement of MALDI, involving the spotting of the biological sample onto a treated surface, is the surface-enhanced laser desorption and ionization time-offlight (SELDI-TOF).

1.5.3.1 Two-dimensional polyacrylamide gel electrophoresis (2-DE)

This procedure is based on the use of immobilized pH gel gradients to separate proteins by their isoelectric points, followed by SDS PAGE to further separate the proteins on the basis of their molecular mass. A map of several hundred spots can be resolved in a single gel where each spot represents a different protein, different isoforms of the same protein, or its post-translational modifications (Sivakumar A 2002). Protein profiles can be scanned and quantified to search for changes in the levels of pre-existing proteins, for mutated proteins, or for other types of variants. The qualitative and quantitative analysis of 2D maps is supported by specific powerful software packages, such as 2D-DECODON. However, a major limitation of 2-DE is the inability to resolve and quantify proteins of low abundance. Other disadvantages of this method are due to the complexity and time-consuming nature of the procedure, the difficulty in separating hydrophobic as well as very large or very small proteins, and the inability to distinguish changes due to modification of truly novel proteins (Riccardo Alessandro et al., 2005).

1.5.3.2 Mass spectrometry

Matrix-assisted laser desorption ionization time of flight (MALDI-TOF) is currently the most accessible technique for most researchers and is used to identify proteins by peptide mass fingerprinting (PMF). In this technique the masses of tryptic peptides, generated after enzymatic degradation of gel-separated proteins, are measured at high accuracy (100 ppm or better). Molecular ions from the peptide samples are produced using a laser source and then introduced in an analyzer that resolves ionized fragments on the basis of their mass-to-charge (m/z) ratio. MALDI-TOF is extensively used to determine peptide mass fingerprinting, allowing the identification of proteins by matching the experimental calculated peptide masses with spectra predicted by a “theoretical” trypsin digest of a

protein database. MALDI-TOF data are relatively easy to interpret since most peptides carry only one charge and are present as single peaks in a spectrum (Henzel WJ et al., 1993; Srinivas PR et al., 2000; Rowley A et al., 2000). The limitations of MALDI-TOF are that only about 60% of proteins can be identified. Furthermore, factors that alter peptide masses from those stored in the database (e.g. post-translational modifications) can invalidate the search method. Also small proteins do not often generate sufficient numbers of digestion products for identification. When MALDI-TOF fails to unequivocally identify a protein, it is necessary to employ electrospray ionization tandem MS (ESI-MS/MS) to generate partial sequence information for database searching. MS/MS is a powerful separation tool of great value because in the presence of many other co-detected peptides, a single peptide ion can be selected, isolated, fragmented and sequenced (Peng J and Gygi SP 2001; Srinivas PR et al., 2000; Rowley A et al., 2000). Today, mass spectrometry techniques (both MALDI-TOF and MS/MS) are employed as a technology base for the relatively fast identification of proteins separated by 2D gels. These technologies have allowed a notable accumulation of knowledge concerning the proteomic profiles of several tumors. Recently, Friedman et al. (Friedman DB et al., 2004) used 2D-DIGE coupled with mass spectrometry to investigate tumor-specific changes in the proteome of human colorectal cancer and adjacent normal mucosa. This approach detected over 40 statistically significant changes in protein abundance levels across the paired samples including alterations in vinculin, vimentin, microtubule-associated protein, F-actin capping protein, cathepsin, and calgranulin B expression. Comprehensive proteomic expression profiles of normal mucosa, polyps, primary tumors and metastases from the same patients were generated by the group of Roblick and colleagues (Roblick UJ et al., 2008) using 2D PAGE and MS/MS sequence analysis in order to trace modifications of the proteome pattern corresponding to colon cancer development and progression at both the intra- and inter-patient level. Tissue biopsies from 15 patients were used and a total of 72 protein spots were identified and shown to be differentially regulated. These proteins belonged to cell cycle (elongation factor 1, translation initiation factor), cytoskeleton (mainly cytokeratins) or metabolic pathways (succinate dehydrogenase, 5-lipooxygenase, heat shock family proteins) (Gygi SP et al., 1999). However, this approach has several limitations, especially when whole cell lysates

are analyzed. In 2D gels, very acidic or basic proteins, extremely large or small proteins, and membrane proteins are often excluded or underrepresented. Moreover, proteins of low abundance cannot be detected by two-dimensional electrophoresis without some method of previous enrichment. However, fractionation of whole cell lysates by itself can alter the results of quantitative analysis because some proteins are disproportionately distributed into different fractions. For all these reasons 2D/MS may not represent the most appropriate approach for large-scale, global proteome analysis (Peng J and Gygi SP 2001). An alternative separation technique used as a new proteome analysis platform is reversed-phase liquid chromatography (LC) coupled with tandem MS (LCMS/MS). This method offers the possibility to isolate and sequence hundreds of selected peptides from one sample without previous 2D separation.

Recently, the differentially expressed transcripts of vaccinia virus-infected tumor cells were analyzed by cDNA microarrays which provide an overview of the mRNA expression profiles of infected cells (Susana Guerra et al., 2004; Krystyna W et al., 2003). The mRNA abundance is not always consistent with the protein level (Gygi, S. P. et al., 1999) and viral infection involves in post-translational modifications of diverse proteins, such as ubiquitination (Shackelford J and Pagano JS 2005), phosphorylation and glycosylation (Meredith DM et al., 1991), without affecting their transcription rate. Therefore, the proteomic analysis of host cellular responses to virus infection is more promising to probe potential cellular factors involved directly or indirectly in viral infection and to identify potential drug targets of antiviral treatment. To date, a small but increasing number of studies have used proteomic approaches to reveal the effects of viral infection on the cellular proteome (Maxwell KL and Frappier L 2007). The comparative proteomic approaches coupling 2-DE and mass spectrometry (2-DE/MS) effectively help the study of the molecular profiles of virus-infected cells (Tang H et al., 2000). In plant viruses, 2-DE/MS has been used to study the cellular changes in rice yellow mottle virus-infected cells in susceptible and partially resistant rice cultivars (Ventelon-Debout M et al., 2004) and in tobacco mosaic virus-infected tomato (Casado-Vela J et al., 2006) In animal viruses, 2-DE/MS has been utilized to investigate the cellular changes in Vero cells infected with African swine fever virus (Alfonso P et al., 2004), rhabdomyosarcoma cells infected with enterovirus 71 (Leong WF and Chow VT

2006), nuclear proteome changes in A549 alveolar type II-like epithelial cells infected with respiratory syncytial virus (Brasier AR et al., 2004), and expression changes in B cells infected with Epstein-Barr virus (EBV) or with EBV nuclear antigen EBNA-2 (Schlee M et al., 2004). In addition, several studies have used distinct protein separation methods, including difference gel electrophoresis (DIGE), isotope-coded affinity tags (ICATs), or multidimensional liquid chromatographic separations followed by liquid chromatography/tandem mass spectrometry (LC-MS/MS) identification to investigate the cellular response to infection by severe acute respiratory syndrome-associated coronavirus (SARS-CoV), flock house virus (FHV) and hepatitis C virus (Xiaojuan Zheng et al., 2008; Alexander Rassmann et al., 2006; Alessandro R and Kohn EC 2002). Therefore, the proteomic strategies provide an overall understanding of the cellular factors involved in various stages of infection and give an insight into the alteration of signaling pathways to further understand viral pathogenesis.

1.5.4 Proteome analysis of human cancer

1.5.4.1 Proteome analysis of human breast cancer

Interesting results have been obtained from comparisons between human breast ductal carcinoma and histologically normal tissue. Proteins which express highly in all carcinoma specimens and less expressed and occasionally undetectable in normal tissue are GRP94, GRP78, GRP75, mitochondrial HSP60, calreticulin, protein disulfide isomerase, peptidyl-prolyl cis-trans isomerase, collagen-binding protein 2, fructose bisphosphate aldolase, glyceraldehyde-3-phosphate dehydrogenase, thioredoxin, cytochrome c oxidase Va subunit, tubulin beta isoform and macrophage migration inhibitory factor (MIF) were identified (Bini L et al., 1997). Also specific contributions to the overall knowledge of breast cancer biology have been provided by the study of proteomic profiles of cancer cells in culture. For example, analysis of the proteomic map of the 8701-BC cell line, which is derived from a primary ductal infiltrating carcinoma, has shown the coexpression of several forms of cytokeratin 8, cytokeratin 18 and vimentin. These are cytoskeletal markers of lumenal mammary epithelium and of

mesenchymal cells, respectively. This study has demonstrated that many features related to cancer cells (e.g. loss of polarity, defective cell-cell contacts, increased motility) reflect an epithelial-mesenchymal transition, as postulated for many carcinomas of different origins (Pucci-Minafra I et al., 2002). In particular, among the proteins with higher relative expression levels in cancer cells, several glycolytic enzymes and their isoforms were identified (Pucci-Minafra I et al., 2002). A proteomic approach by means of 2D-PAGE was also applied to investigate the effects on protein expression in breast cancer cells by specific collagen molecules. With the use of a multivariate statistical procedure it was demonstrated that chaperons and heat shock proteins contributed most to changes in the observed protein expression, suggesting that this class of proteins may be involved in cellular responses following substrate interactions (Fontana S et al., 2004). Protein expression data obtained by 2D-PAGE analyses are stored in databases available world-wide that document protein expression in several cell lines and normal and tumoral tissues. These databases provide an important and unique resource for scientists to identify changes in known protein levels or in new proteins in specific cancer histotypes, and can be exemplified by the EXPASY server in Geneva (SWISS-2DPAGE).

1.5.4.2 Proteome analysis of human colon cancer

Colorectal cancer represents an ideal model system to study the development and progression of human tumors, because epithelial cells of the colon mucosa often follow a systematic process of cellular proliferation, differentiation, adenoma formation, and, eventually, cancer transformation (Roberto Mazzanti et al., 2006). The first data describing the alteration of protein expression in transformed colon mucosa were published in the beginning of the 1980s (Jellum E et al., 1984; Tracy RP et al., 1982). In 1983, Anderson et al. (Anderson KM et al., 1983) described differential distribution of acidic proteins in normal colon mucosa, primary colon adenocarcinoma, and colon metastases to the liver. With the use of the two dimensional gel electrophoresis (2DE) approach, several differences in protein expression in the cytosol of colon cancer samples, at various differentiation levels, were observed (Nalty TJ et al., 1988). Unfortunately, none of these proteins were identified. Keesee et al. (Keesee SK et al.,

1994) detected the tumor-specific expression of six nuclear matrix proteins that were also present in a panel of colon tumor cell lines. This study reinforced the concept of differential protein expression by cancerous tissue, and it raised the problem of accuracy at extrapolating results from cancer cell lines to in vivo scenarios (Zhang L et al., 1997; Ramaswamy S et al., 2003). Specific expression of several nuclear proteins was observed by Szymczyk et al. (Szymczyk P et al., 1996) in human colorectal cancer tissue compared with normal matched mucosa. One of these proteins was a 36-kDa polypeptide that was absent in the normal colonic epithelium but present in 83% of the studied carcinomas. This protein might have served as a potential marker for colon malignancy, but, unfortunately, it was not identified, thus limiting its use and understanding of its function. The data on specific cancer-related proteins or cancer-related protein expression down-regulation are still controversial. Recently, a 2-D electrophoresis database for human colon crypts, colorectal cancer cell lines (i.e., LIM 1215 and HT29), and colonic polyps of multiple intestinal neoplasia and p53-null mice has been set up by the Ludwig Institute for Cancer Research (Ji H et al., 1997; Simpson RJ et al., 2000; Stulik J et al., 1999). Stulik et al. (Stulik J et al., 1999) identified proteins that exhibit differential expression by comparing normal and malignant colon tissues.

The most important cytosolic glycolytic and mitochondrial tricarboxylic acid cycle enzymes are basic proteins as demonstrated by the proteomic analysis of human colon crypt (Li, X. M. et al., 2004). Glycolysis has been shown to be elevated in almost all cancers, the so-called “Warburg effect” (Warburg O 1956). And many cancers show dysfunction of mitochondria (Verma M et al., 2003; Warburg O 1956; Altenberg B and Greulich KO 2004). The increased aerobic glycolysis for ATP generation in cancer cells is frequently associated with mitochondrial respiration defects and hypoxia (Isidoro A. et al., 2004). A recent report showed that inhibition of glycolysis in colon cancer cells could overcome drug resistance (against common anticancer agents) associated with mitochondrial respiratory defect and hypoxia (Xu RH et al., 2005). The mitochondrial enzyme succinate dehydrogenase, which links tricarboxylic acid cycle dysfunction to oncogenesis via hypoxia-inducible factor (HIF)-1_ was also demonstrated recently (Selak MA et al., 2005). 2-DE data for colon protein analysis showed up-regulation of glycolytic enzymes such as aldolase A, enolase 1, GAPDH, etc., The 2-DE data also revealed an

impaired tricarboxylic acid cycle in CRC as evidenced by down-regulation of enzymes at the early entrance steps such as aconitase and aconitate hydratase and up-regulation of malate dehydrogenase at the exit step. These findings suggested extensive alterations in metabolic pathways that have not been well defined before (Xuezhi Bi et al., 2006). A recent report using 2-D DIGE and MS with the pH range of 4–7 found that in colon cancer some proteins such as succinate dehydrogenase subunit A, succinyl-CoA 3-ketoacid coenzyme A transferase, aldehyde dehydrogenase, and carbonic anhydrase I were down-regulated, whereas several other proteins such as triosephosphate isomerase and keratins 8 and 18 were up-regulated (Friedman DB et al., 2004). Some new proteins (aconitase, phosphoenolpyruvate carboxykinase, UGDH, and UDP-glucose pyrophosphorylase 2) that exhibited altered expression level that have not been reported in CRC previously (Xuezhi Bi et al., 2006). It will be interesting to see whether the mechanism proposed above is applicable to other cancers.

1.5.4.3 Proteome analysis of human prostate cancer

A recent 2-DE-based analysis of surgical prostate cancer specimens found that they contained significantly increased levels of proliferating cell nuclear antigen (PCNA), calreticulin, heat shock protein 90 (HSP), HSP 60, oncoprotein 18(v), elongation factor-2, glutathione-S-transferase pi (GST-pi), superoxide dismutase, and triose phosphate isomerase (Alaiya A et al., 2000) This study also reported lower amounts of tropomyosin-1 and -2 and cytokeratin 18 in prostate cancer than in BPH. The same group reported in a subsequent study that 23 proteins out of 800 were somewhat different in amount between BPH and prostate cancer specimens (Alaiya AA et al., 2001).

In other study, forty tumor-specific changes were identifed, and they included proteins involved in cellular morphology (tropomyosin-b), metabolism (aldolase A, L-lactate dehydrogenase M chain), and signal transduction (laminin receptor-67 kDa, phosphoserine-threonine-tyrosine interaction protein). Among the identifed proteins were two novel gene products that were downregulated in prostate cancer. One spot contains a putative kinase domain homologous to ATP-binding proteins, and the other is homologous to the thioredoxin peroxidase family. Several of the tumor-deregulated

proteins have been reported previously [tropomyosin-b (Alaiya AA et al., 2001, Wang FL. et al., 1996) laminin receptor-67K (Waltregny D et al., 1997), and lactate dehydrogenase (Vrubel F et al., 1979)].

Transcription factor (nucleoside diphosphate kinase 1) and enzyms involved in gene silencing (chromobox protein), protein synthesis (39-ribosomal protein L12, BiP protein, protein disulfide isomerase), degradation (cytosol aminopeptidase, endopeptidase, isocitrate dehydrogenase, NADH-ubiquinone oxidoreductase, pyruvate dehydrogenase) are among overexpressed proteins in the study of differential proteins expression in anatomical zones of prostate cancer (Lexander H et al., 2005). Other overexpressed proteins were heat-shock proteins (60 and 70 kDa), structural proteins (cytokeratins) and membrane proteins (stomatin-like protein 2). Nucleotide diphosphate kinase 1 is the product of NM-23H1, a metastasis suppressor gene known to be upregulated in early stage of prostate cancer. (Jensen SL et al., 1996). Lysophospholipase is related to proliferation and migration in cells and has been found at increased levels in ovarian cancer (Xie Y and Meier KE 2004).

1.5.5 Proteomics analysis the differentially expressed of cancer cells infected with viruses

Proteomics is the large-scale, systematic study of proteins, particularly their interactions, modifications, localization, and functions. Usually, the tools of proteomics are used to analyze modifications induced during the course of cell activation, differentiation, or transformation. However, several shortcomings have been noted in the proteomic study of host–microorganism interactions. These restrictions are mainly due to technical challenges arising from the high complexity of these systems (Anna Walduck et al., 2004). Nevertheless, infection by intracellular parasites is a privileged model for this type of study, as it permits one to have a precise experimental control (for example, a non-infected cell or infected cell variants) to compare protein profiles during infection. Depending on the different levels of interaction between microoganism and host, proteomics is of particular use in the following aspects such as: firstly, comparison of microbial proteomes from the same family but presenting a high or low expression in

different cell lines. Secondly, study of the modifications of cell proteins induced by viral infections, the impact on the host proteome by selective expression of parasite proteins can be also analyzed to understand their function. Thirdly, analysis of post translation modifications caused by the infection, especially phosphorylation, which may result in the activation of transcription factors or induction of metabolic routes involved in apoptosis. Fourthly, study of interactions between parasite and host proteins at different levels: taking over the transcriptional and translational machinery, association with intracellular transport structures, generation of parasite protein production factories, or sequestering of cell factors involved in morphogenesis and cell exit processes. Fifthly, both viruses and more complex parasites incorporate proteins from the infected cell once they emerge from it, proteomic analysis can define which proteins are incorporated into the parasite and their function in the life cycle; Finally, by using proteomics, it might also be possible to study complex interactions such as those related to the host–vector–microorganism interplay, not only from the viewpoint of the vector, but also from that of the host and of the microorganism.

Modification of host cell by infection with intracellular microorganism: this can modify the host cell metabolic pathways for their own benefit. In fact, microorganism often requires the replacement of existing host cell signaling pathways or membrane traffic machinery. Therefore, microorganism exposure may elicit changes in host proteins that can be gathered in many categories, including cell signaling pathways, protein degradation, cytokine and growth factor production, phagocytosis, apoptosis, as well as cytoskeletal rearrangement. These effects may be exerted immediately after the binding of the microorganism to the receptor on the cell surface, either by a new protein encoded by modifying the activity of a cellular protein, or by a microbial protein mimicking a cellular protein. Some of the most important cellular pathways modified by intracellular pathogens are explained and are summarized (Margo H Furman and Hidde L Ploegh 2002).

1.5.5.1 Modification of apoptotic pathways in the host cell

In any case, the tumor cell is killed by the oncolytic virus as it takes over the cellular translational and transcriptional machinery, ultimately leading to an induction of cell necrosis or apoptosis (Figure 1).

Figure 1. **Infecting and killing tumor cells by an oncolytic virus**. **a**. Viruses interact with specific cell-surface receptors. As these proteins are overexpressed by tumor cells (blue) compared with normal cells (yellow), the virus will probably infect the tumor cell. **b**. Following binding to the cell surface receptor, the virus is internalized by endocytosis or membrane fusion, and its genome is released into the cell. Depending on the type of virus, replication and viral gene expression can take place entirely in the cell cytoplasm (such as for vesicular stomatitis virus), or in the nucleus and cytoplasm (such as for adenovirus). In either case, the virus is largely dependent on cellular machinery for viral gene expression and synthesis of viral proteins. Viral gene expression and replication leads to the activation of cellular antiviral defenses, such as apoptosis, that are operational in normal cells but are often inactivated in tumor cells. Expression of viral proteins will eventually lead to immune-mediated lysis of infected cells by CD8+ T cells, which recognize viral peptide epitopes that are presented by major histocompatability complex (MHC) class I molecules on the surface of the infected cell. Alternatively, cells might be lysed owing to an overwhelming amount of budding and release of progeny virions from the cell surface, or by the activation of apoptosis during the course of viral replication and gene expression (Kelley A Parato et al., 2005).

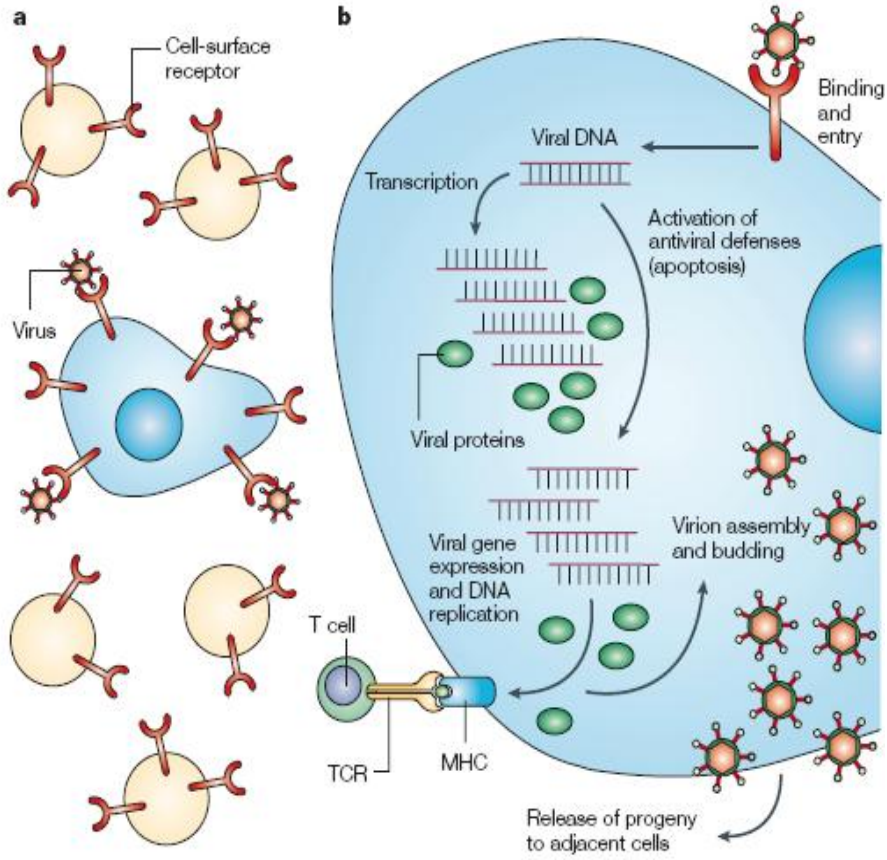

Induction of apoptosis is one of the mechanisms that infected normal cells use to prevent further spread of viruses. In turn, viruses often encode gene products that block this process (Lee CJ et al., 2005; Reboredo M et al 2004; Wright CW 2005). Tumor cells accumulate defects in apoptotic programmers, so another design strategy for oncolytic viruses would be to delete viral anti-apoptotic genes, creating mutants that only replicate in apoptosis deficient tumor cells.

Understanding how cancer cells evade apoptosis is one approach to engineer oncolytic viruses. The concept of programmed cell death, termed apoptosis, was introduced above in terms of the role of p53 in eliminating cells that have either acquired activating oncogenes or excessive genomic damage. Because apoptosis is such an effective mechanism of eliminating cells progressing to malignancy, it is not surprising that in

addition to inhibiting p53 function by mutation, other p53 independent mechanisms are also utilized by many cancers as survival factors. Apoptosis is triggered by external plasma membrane associated receptors and internal sensors, principally involving the p53 gene. Both these external and internal mechanisms are perturbed in diferent cancers. Regardless of initial stimulus, pathways of apoptosis all appear to converge on the mitochondria causing loss of membrane integrity and release of cytochrome C. Cytochrome C is a potent mediator of apoptosis and appears to directly stimulate activity of a family of intracellular proteases, called caspases, whose function is to rapidly degrade cellular organelles and chromatin so as to induce cell destruction without inflammatory responses that are typically seen after cell necrosis (Earnshaw WC et al., 1999). In addition to protecting the host against developing cancer cells, apoptosis is widely utilized during embryogenesis to eliminate populations of cells such as those between the digits or in the tail of human embryos and to eliminate self-recognizing immune cells. Apoptosis is also utilized to destroy viral genetic material and the infected cell after viral infection. As a consequence, many viruses have evolved mechanisms to evade apoptosis and several viral gene products interfere with mammalian proteins involved in apoptotic pathways (Thompson CB 1995.)

1.5.5.2 Modification in the cytoskeleton structure of the host cell

Targeting the cytoskeleton of the host cell is a common strategy among organism and reflects the alteration of many cellular activities, recent evidence demonstrates that various viruses manipulate and utilize the host cytoskeleton to promote that viral infection. Viruses induce rearrangements of cytoskeletal filaments so that they can utilize them as tracks or shove them aside when they represent barriers. Viral particles recruit molecular motors in order to a hitchhike rides to different subcellular sites which provide the proper molecular environment for uncoating, replicating and packaging viral genomes. Interactions between subviral components and cytoskeletal tracks also help to orchestrate virus assembly, release and efficient cell-to-cell spread. There is probably not a single virus that does not use cytoskeletal and motor functions in its life cycle (Radtke K et al., 2006). The actin cytoskeleton mediates a variety of essential biological functions

in all eukaryotic cells. In addition to providing a structural framework around which cell shape and polarity are defined, its dynamic properties provide the driving force for cells to move and to divide. There are several proteins act as molecular switches such as Rho GTPases which induce coordinated changes in the organization of the actin cytoskeleton and in gene transcription to drive a large variety of biological responses including morphogenesis, chemotaxis, axonal guidance, and cell cycle progression. These proteins could be changed by virus infection. It can be predicted with some confidence that the biochemical and genetic analysis of the signaling pathways controlled by these proteins will lead to a better understanding of these fundamental processes (Alan Hall et al., 1998). The actin cytoskeleton system is also crucial for active recruitment in cells such as lymphocytes and macrophages that rapidly have to move to the infection and inflammation sites (Gruenheid, S and Finlay BB 2003).

1.5.5.3 Modification of cell host intracellular signaling pathways

Many viruses have evolved sophisticated mechanisms to imitate host proteins and to occupy intracellular signal transduction systems for their own benefit (Kahn RA et al., 2002). In fact, the binding of viruses to target cells is known to be mediated by several intracellular signaling events.

When eukaryotic cells encounter adverse physiological conditions that impact on protein folding in the endoplasmic reticulum, a signal-transduction cascade is activated; this is termed the unfolded protein response (UPR). A number of cellular stress conditions, such as perturbation in calcium homeostasis or redox status, elevated secretory protein synthesis, expression of misfolded proteins, sugar/glucose deprivation, altered glycosylation, and overloading of cholesterol can interfere with oxidative protein folding and subsequently lead to accumulation of unfolded or misfolded proteins in the endoplasmic reticulum (ER) lumen, which constitutes a fundamental threat to the cells. The ER has evolved highly specific signaling pathways to alter transcriptional and translational programs to cope with the accumulation of unfolded or misfolded proteins in the ER lumen (Lee AS 1992; Brodsky JL et al. 1999). The UPR is also induced in response to viral infection (Lee AS 2001), apparently because of the high volume of viral

proteins that are being synthesized in the ER, although it has not been established whether this contributes to or limits the disease.

Inside the solid tumor themselves, there is evidence of ER stress which can activate of the UPR. Neoplastic progression requires several genetic alterations that allow the cell to ignore growth controls and disable apoptotic signalling. As the tumor becomes larger, it experiences increasing hypoxia, nutrient starvation and acidosis until the microenvironment becomes limiting. Cells respond by producing pro-angiogenic factors to initiate the formation and attraction of new blood vessels to the tumor.Although many studies have focused on the hypoxic state of tumors, the stabilization of hypoxia inducible factor-1α (HIF1α), and the activation of protective downstream responses, there is increasing evidence to show that the UPR can also be activated in tumors. Although no direct link between these two pathways has been established, they share several downstream targets, and it is conceivable that the two pathways could synergize in some cases and be antagonistic in others. The UPR normally acts as a short-term cytoprotective mechanism. Cells subjected to especially severe or prolonged microenvironmental stress normally undergo UPR mediated apoptosis by both mitochondria-dependent and mitochondria-independent pathways. It is unclear how UPR activation in solid tumors balances cell-survival and celldeath signals. Figure 2 illustrates how ER stress and subsequent activation of the UPR can lead to one of four outcomes: (Guo ZS and Bartlet DL, 2004) apoptosis and tumor resolution, (Timiryasova TM et al., 1999) tumor dormancy, (Bartlett DL et al., 2001) tumor growth and disease progression and (Thorne SH et al., 2005) altered chemotherapeutic sensitivity.

Figure 2. **ER stress and activation of the UPR** might result in Ire1/TRAF2-mediated apoptosis and disease resolution, PERKmediated G1 arrest and dormancy or an anti-apoptotic, pro-angiogenic drive, thereby resulting in disease progression via PERK/NF-κB and molecular chaperones (Peter Scriven et al., 2007).

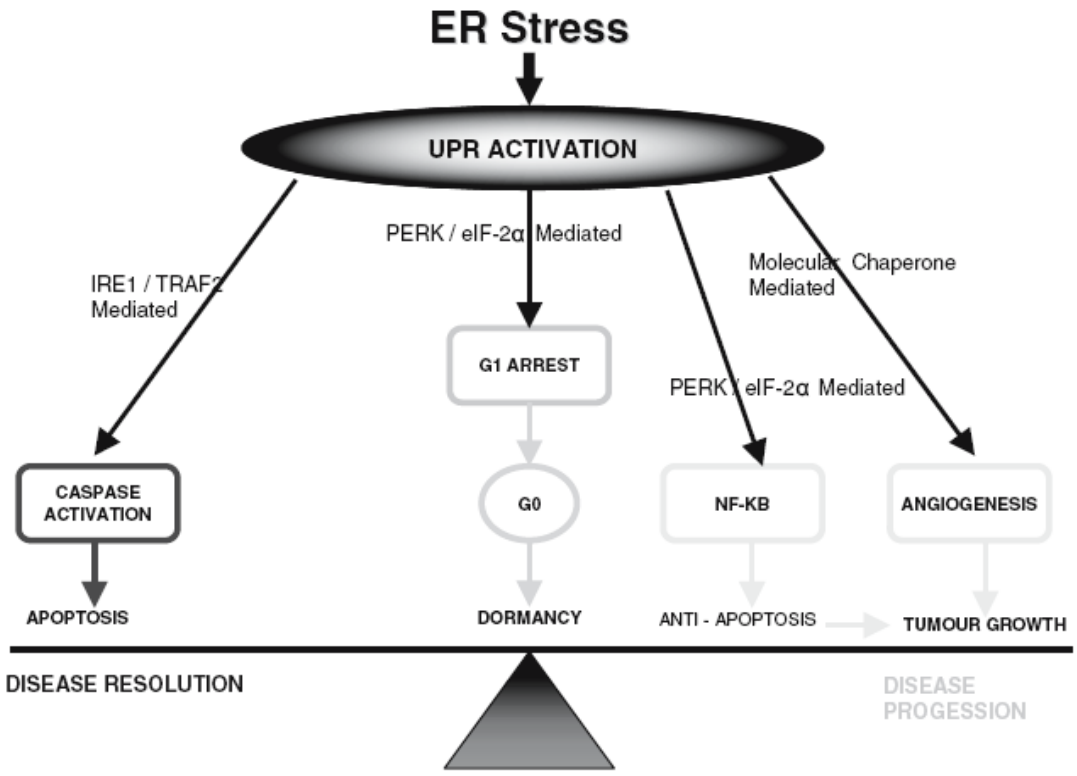

1.5.5.4 Modification of cell host metabolic pathways

Some microorganisms modify their metabolism to adapt to their specific host. The interaction between host and microorganisms not only entails alteration of protein expression levels, but also post-translational processing of the specific proteins involved. This is the case of post-translation modifications in some proteins from bacteria and viruses, which are mediated by the cellular protein machinery. Such modifications are generally reversible and play key roles in protein functional regulation. Among many reported types of post translation modifications, phosphorylation in serine, threonine, and tyrosine residues has received significant attention, since this reversible modification is a key event in signaling processes (Pawson T and Scott J D 1997). Phosphorylation is also common in virus proteins implicated in the control of virus replication, transcription, and assembly. This is the case for Rubella virus capsid protein (Ficarro SB et al., 2002),

influenza virus nucleoprotein (Neumann G et al., 1997), and Rabies virus nucleoprotein (Wu X et al., 2002). Therefore, great effort has been directed towards developing methods for detecting and characterizing these modifications. However, identification of phosphorylated residues was a difficult task, involving direct labeling of proteins with 32^{P} (Chalmers, M. et al., 2004). ESI is one of the softest ionization techniques for MS (Fenn JB et al., 1989) which allows the detection and characterization of numerous post-translation modifications, as direct sequence information is obtained. Highly complex protein mixtures can be identified directly, and the possible PTM characterized by MS (Washburn M et al., 2001). For example, MudPIT coupled to MS has been used to study the nucleocapsid protein phosphorylation of transmissible gastroenteritis virus (TGEV) in infected cells (Calvo, E. et al., 2005) which led to the identification of at least four phosphorylations in the TGEV nucleocapsid protein. Interestingly, previous work had suggested that phosphorylation/dephosphorylation processes could play an important role in coronavirus assembly (Laude H et al., 1995). The phosphorylation state of the human respiratory syncytial virus (HRSV) phosphoprotein (P protein) has been also assessed by LC-MS (Asenjo A et al., 2006).

Generally, results of studies analysis interactions of tumor cells infected with virus by proteomics are still unobtrusive. The differentially expressed transcripts of virus-infected tumor cells were analyzed by cDNA microarrays, which provide an overview of the mRNA expression profiles of infected cells (Susana Guerra et al., 2004; Krystyna W et al., 2003). However, the mRNA abundance is not always consistent with the protein level (Gygi SP et al., 1999) and viral infection involves in post-translational modifications of diverse proteins, such as ubiquitination (Shackelford J and Pagano JS 2005), phosphorylation and glycosylation (Meredith DM et al., 1991), without affecting their transcription rate. Therefore, the proteomic analysis of host cellular responses to virus infection is more promising to probe potential cellular factors involved directly or indirectly in viral infection and to identify potential drug targets of antiviral treatment. To date, increasing number of studies has used proteomic approaches to reveal the effects of viral infection on the cellular proteome (Maxwell KL and Frappier L 2007). For example, in animal viruses, 2-DE/MS has been utilized to investigate the cellular changes in Vero cells infected with African swine fever virus (Alfonso P et al., 2004), rhabdomyosarcoma

cells infected with enterovirus 71 (Leong WF and Chow VT 2006), nuclear proteome changes in A549 alveolar type II-like epithelial cells infected with respiratory syncytial virus (Brasier AR et al., 2004), expression changes in B cells infected with Epstein-Barr virus (EBV), proteome alterations in HeLa and HepG2 cells infected with coxsackievirus B3 (Alexander Rassmann et al., 2006), and EBV nuclear antigen EBNA-2 (Schlee M et al., 2004) or characterized response of the chicken embryo fibroblasts to Bursal disease virus infection (Xiaojuan Zheng et al., 2008). In addition, several studies have used distinct protein separation methods, including difference gel electrophoresis (DIGE), isotope-coded affinity tags (ICATs), or multidimensional liquid chromatographic separations followed by liquid chromatography/tandem mass spectrometry (LC-MS/MS) identification to investigate the cellular response to infection by severe acute respiratory syndrome-associated coronavirus (SARS-CoV), flock house virus (FHV) and hepatitis C virus (Xiaojuan Zheng et al., 2008; Alexander Rassmann et al., 2006; Alessandro R and Kohn EC 2002). Therefore, the proteomic strategies provide an overall understanding of the cellular factors involved in various stages of infection and give an insight into the alteration of signaling pathways to further understand viral infection.

AIMS OF THE STUDY

The purposes of this thesis are to determine protein dynamic upon oncolytic vaccinia virus infectious activity of cells and tumors. Specifically, the aims of the study are to characterize the infection of attenuated vaccinia virus VACV GLV-1h68 which were generated and studied as a live vector engineering for tumor selective replication with oncolytic efficacies.

- To characterize vaccinia virus VACV GLV-1h68
- To estimate imaging of tumors based on light emission
- To describe the proteome profile of the tumor cell and tumor xenograft in mice with and without VACV GLV-1h68 infection. To identify proteins which increase or decrease expression in the different tumor cell line and tumors, possibly contributing to the understanding ability oncolytic in the protein level of VACV GLV-1h68.
- To compare the differential protein expression between the non-regressing and regressing tumors xenograft in nude mice treated with VACV GLV-1h68.

2. MATERIALS AND METHODS

2.1 MATERIALS

2.1.1 Equipments

Biophotometer	Eppendorf, Hamburg
Cell counting chamber	Marienfeld, Lauda-Königshofen
Cell culture bottles	Greiner, Frichenhausen
Cell culture incubator	RS Biotech,UK-Irvine
Cell culture scraper	TPP, Schwerin
Centrifuge	Eppendorf, Hamburg
CO_2 incubator	Nunc^{Tna}-GaluxyS-RS Biotech
Cold centrifuge	Heraeus, Hanau
Cuvettes	Sarstedt, Nümbrecht
Electrophorstic vertical system	Hoefer DALT
Ettan IPGphor	Amersham
Film	Kodak
Film cassette	Hartenstein
Flow-Hood Lamin Air	Kendro, Langenselbold
IPG strips	Amersham
Microscopes	
• Axiovert 40CFC	Zeiss, Göttingen
• DMR	Leica, Wetzlar
• DMIRB	Leica, Wetzlar
• M2 16 FA	Leica, Wetzlar

Microscopes

• Axiovert 40CFC	Zeiss, Göttingen
• DMR	Leica, Wetzlar
• DMIRB	Leica, Wetzlar
• M2 16 FA	Leica, Wetzlar

Model 1000/500 Power supply	Bio-Rad
Multi Temp III	Pharmacia-Biotech
Nitrocellulose transfer membrane	Schneider & Schuell, Dassel
PH Electrode SenTix 61	Hartenstein
Power supply Power Pac	Bio-Rad & PEQLAB Biotechnology
Refrigerator	Liebherr
X-ray film	Konica
Scale $KERN_{ABS}$	A-Hartenstein
Semi-Dry Blot apparatus	Peqlab, Erlangen
Sonicator Branson 450	Heinemann
Spectrophotometer	Pharmacia Biotech-Novapec II
Themomixer comfort	Eppendorf, Hamburg
Vertical Gel-electrophoresis	Own construction, Biocentre University of Wuerzburg
Vortex	Hartenstein
Whatman 3MM Filter paper	Hartenstein

2.1.2 Reagents, solutions and media

2.1.2.1 Reagents

1 x BSS	PAA, A- Pasching
1 x BBS	PAA, A- Pasching
Acetic acid	Merck
Aceton	Roth, Karlsruhe
Acrylamide, Bisacrylamide	BioRad, Munchen
Agarose	Roth, Karlsruhe
Ammoniumperoxidisulphate	Merck, Darmstadt
Bovin Serum Albumin	Applichem, Darmstadt
Bromophenol blue	Sigma, Steinheim
Carboxymethylcellulose	Sigma, Steinheim
Cells chamber	Hartenstein
Coomassie brilliant blue G-250	Serva, Heidelberg
Coomassie brilliant blue R-250	Serva, Heidelberg
Crystal violet	Sigma, Steinheim
Dithiothreitol	Roth, Karlsruhe
DMEM	PAA, A- Pasching
EDTA	Serva, Heidelberg
Ethanol 96%	Chemical of Uni-Würzburg
Formaldehyde 37%	Sigma, Steinheim
Glycerin	Merck, Darmstadt
Glycin	Roth, Karlsruhe
H_2O_2	Merck, Darmstadt
Hepes	PAA, A-Pasching
Isopropanol	Roth, Karlsruhe
L-Glutamin	PAA, A- Pasching

Magenesiumchloirid	Merck,Damstadt
Magermilchpulver	Roth, Karlsruhe
Methanol	Roth, Karlsruhe
N,N,N',N'-Tetramethlethylendiamin	Fluka
Na_2CO_3	Merck, Damstadt
NaOH	Merck, Damstadt
Na-thiosulphate 43%	Merck, Damstadt
Natrium dedocylsulphate	Roth, Karlsruhe
Natriumcarbonat	Roth, Karlsruhe
Nonidet P-40 (Igepal)	Sigma, Steinheim
Ostradiol/Progesteron	PAA, A- Pasching
Penicillin/ Streptomycin	PAA, A- Pasching
Ponceau S	Sigma, Steinheim
Prestained protein marker	Fermentas, St. Leon-Rot
Protease inhibitor	Roch, US-Indianapolis
RPMI- Medium 1640	PAA, A-Pasching
Silver nitrat	Riedel deHaen, Seelze
Trichloressigsäure	Roth, Karlsruhe
Tris-Base	Roth, Karlsruhe
Tris-HCl	Roth, Karlsruhe
Trypan blue	Fluka, CH-Buchs
Trypsin-EDTA	PAA, A-Pasching
Tween 20	Roth, Karlsruhe
Urea	Roth, Karlsruhe
β-mecaptoethanol	Roth, Karlsruhe

2.1.2.2 Solutions and media

10x TBT buffer
890 mM Tris-base
890 mM H_3PO_4
25 mM Na_2EDTA

1x Towbin buffer pH 8,3
0,025 M Tris-base
0,192 M Glycin
20% MeOH

1x SDS Probe buffer
200 mM Tris-HCl pH 6,8
5% SDS
1 mM Na_2EDTA
8 M Urea
0,1 % (w/v) β-mecaptoethanol
0,2 % Bromophenol

Rehydration stock solution
8 M Urea
2 % CHAPS
0.5 % or 2 % IPG buffer
0.002 % Bromophenol blue

Displacing Solution
0.375 M Tris-HCl pH 8.8
50% Glycerol
0.002 % Bromophenol blue

SDS equilibration buffer
50 mM Tris-HCl pH 8.8
6 mM Urea
30% Glycerol
2 % SDS
0.002 % Bromophenol

SDS electrophoresis Buffer
25 mM Tris-HCL pH 8.8
192 mM Glycine
0.1 % SDS

Lysis buffer
150 mM NaCl
1 mM EDTA
10 mM Hepes

Bradford solution
50 mg Coomassie Blue G250
25 ml Ethanol 96%
50 ml Phosphor acid
25 ml Deionized H_20

10% SDS-PAGE gel
12.5 ml Deionized H_20
7.5 ml 1.5M Tris-HCl pH 8.8
150 µl 20%SDS
150 µl 10%APS
15 µl TEMED

5% staking-gel
9.23 ml Deionized H_20
1.95 ml 30 % Acrylamide/Bis
3.75 ml 0.5 M Tris-HCl pH 6.8
75 µl 20 % SDS
75 µl 10 %APS
15 µl TEMED

Coomassie solution
100 ml Deionized H_20
100 ml Phosphoric acid
1.2 g Coomassie G250
800 ml Deionized H_20
200 ml Methanol

Solution for Silve staining

Fixative
38 % Ethanol
12 % acetic acid
50 % Deionized H_20

Wash-solution
30 % Ethanol
70 % Deionized H_20

Thiosulfate reagent: (per gel)
62.5 µl Na-thiosulphate 43 %
84 µl Formaldehyde 37 %,
125 ml Deionized H_20

Silver nitrate reagent: (per gel)
0.25 g AgN03
84 µl Formaldehyde 37%
125 ml Deionized water

Developer: (per gel)
2.25µl Na-thiosulfate 43%
62.5 µl Formaldehyde 37%,
7.5g Na_2CO_3
125 ml Deionized water

Stop-reagent: (per gel)
3,5 g EDTA
250 ml Deionized water

Cell culture medium

GI-101A cultivation
500 ml RPMI 1640
6 ml Glucose
6 ml HEPES
6 ml Natrium pyruvat
5 ml Antibiotics (Pen/Strep)
100 ml FKS
300 µl BE2 (Oestradiol/Progesteron)

CV-1 cultivation
500 ml DMEM
50 ml FKS
5 ml Antibiotics (Pen/Strep)

HT-29 cultivation
500 ml RPMI 1640
100 ml FCS
5 ml Antibiotics (Pen/Strep)
2,2 g/L Na-bicarbonate

PC-3 cultivation
500 ml RPMI 1640
100 ml FCS
5 ml Antibiotics (Pen/Strep)
2,2 g/L Na-bicarbonate

2.1.3 Cell lines

1. CV-1, a kidney fibroblast of African green monkey
2. GI-101, a human breast tumor cell line
3. HT-29, a human colon tumor cell line
4. PC-3, a human prostate tumor cell line

2.1.4 Recombinant Vaccinia virus VACV GLV-1h68

VACV GLV-1h68 is provided by Genelux-Corporation. A new recombinant Vaccinia virus strain VACV GLV-1h68 is constructed by carring triple insertion mutations of *Renilla luciferase-green fluorescent protein (ruc-gfp)* in the *F14.5* gene, *β-galactosidase* into *thymidine kinase (TK)* gene, and *β-glucuronidase* into *hemagglutinin (HA)* gene of the *LIVP* genome.

Recombinant virus VACV GLV-1h68 was constructed by insertional inactivation the LIVP at the location of three genes: F14.5 gene, TK gene, and HA gene. In the locus of thymidinkinase (TK), there is the reverse transferrin receptor (rtfr) gene and marker β-galactosidase (lacZ) gene which are under the control of promoter p7.5. In the gene of F14.5L, a fusion of protein Renilla-luciferase (RUC) and Green Fluorescent Protein (GFP) gene expressed under the control of promoter E/L (early/late). A marker gene β-

glucuronidase (gus) is inserted in the locus og hemaglutinin (HA) gene which is under the control of the promoter p11.

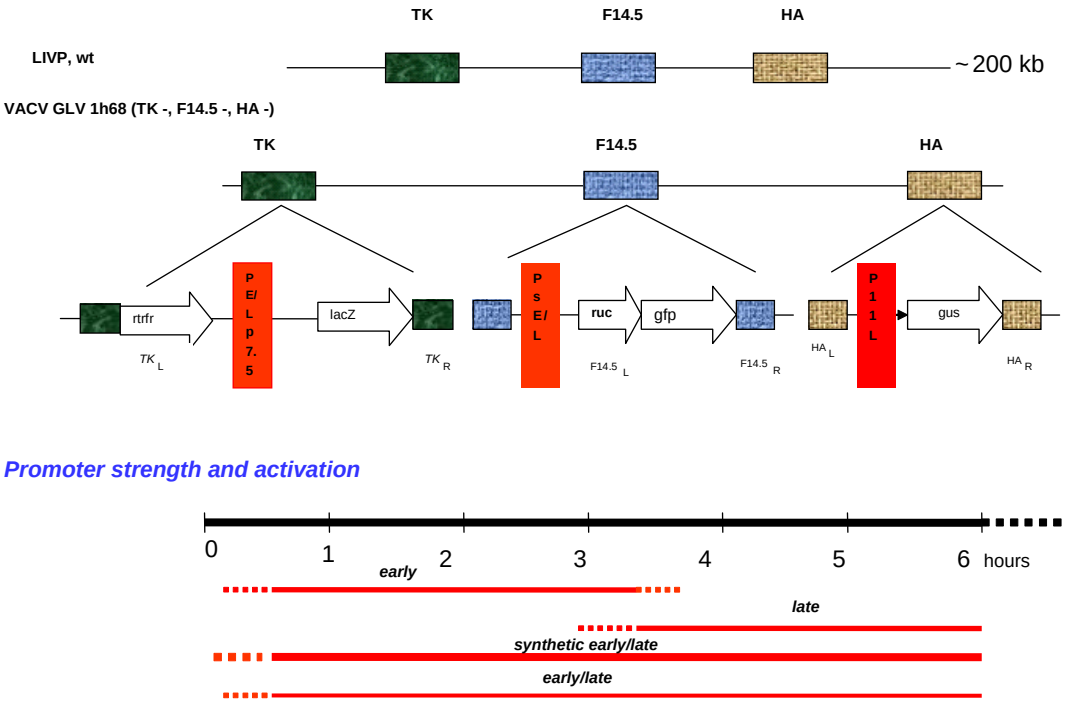

Figure 3. Construction of VACV GLV 1h68

2.1.5 Antibodies

Primary antibodies

Anti Beta-Actin	α-mouse	Abcam, Cambridge
RUC	α-sheep	AG Szalay, Uni-Würzburg
GFP	α-rabbit	Santa Cruz
Anti β-galactosidase	α-rabbit	Molecular Probes
Anti β-glucuronidase	α-rabbit	Santa Cruz

Secondary antibodies

α-rabbit, HRP	Sigma, Steinheim
α-sheep, HRP	Sigma, Steinheim
α-mouse, HRP	Sigma, Steinheim
α-goat/sheep, HRP	Sigma, Steinheim

2.2 METHODS

2.2.1 Cell biological method

2.2.1.1 Cell culture

To ensure that all cell culture procedures are performed to a standard that will prevent contamination from bacteria, fungi and mycoplasm and cross contamination with other cell lines, Chloros/Presept solution and 70% ethanol in water are used. Personal protective equipment (sterile gloves, laboratory coat, and safe visor) and microbiological safety cabinet at appropriate containment level are used.

Adherent cell lines were growing in appropriate nutrients medium. At this point the cell lines were sub-cultured in order to prevent the culture dying. View cultures using an inverted microscope to assess the degree of confluence and confirm the absence of bacterial and fungal contaminants. Media was replaced by pre-warmed medium. The cell monolayer was washed with BSS without Ca^{2+}/Mg^{2+}. Flasks were rotated to cover the monolayer with 1xTrypsin. Decant the excess trypsin. Return flask to the incubator and leave for 5-10 minutes. Examine the cells using an inverted microscope to ensure that all the cells are detached and floating. The side of the flasks may be gently tapped to release any remaining attached cells. Resuspend the cells in a small volume of fresh serum-containing medium to inactivate the trypsin. Centrifuge cell medium at 13.000 rpm/min, then remove medium, add fresh medium and perform a cell counting. Transfer the required number of cells to a new labeled flask containing pre-warmed medium.

2.2.1.2 Cell quantification

It is necessary to quantify the number of cells prior to use. Haemocytometer and inverted phase contrast microscope are used. Suspension using trypsin/EDTA as above and

resuspend in a volume of fresh medium at least equivalent to the volume of trypsin. For cells that grow in clumps centrifuge and resuspend in a small volume and gently pipette to break up clumps. Cell suspension is viewed under a light microscope using 20 x magnification. Then count the number of viable (seen as bright) cells. The central area of the counting chamber is subdivided into 4 smaller squares ($1/25mm^2$). Each of these is subdivided into 16 smaller squares. Counting cell number in 4 smaller squares in each and multiply with 10^4. This data is cell number/ml.

Cell/ml = (The mean cell count per quare) x (the dilution factor) $\div 10^{-4}$ ml

2.2.1.3 Virus infection

CV-1, GI-101A, HT-29, PC-3 (3×10^5) cells were seeded on 6 well plates. 3 ml of appropriate media was added into each well then placed into 5% CO_2/ 37 ^oC condition. Cells were checked 2-3 days after seeding for confluence. Cell number in each well of the plate is counted and cells are infected with individual virus strain VACV GLV-1h68 at MOI 0.5

Total cell number = (cell/ml) x (the original volume from which the cell sample was removed)

$$\frac{\text{Total cell number x MOI}}{\text{volume of cell culture}} = \text{number of plaque (pfu)}$$

Incubate plates for 1 hour in a humidified, 5% CO_2 incubator at 37^oC. Plates were rotated briefly every 20 to 30 minutes during incubation period to allow infection to occur. After 1 hour, cells were incubated in the fresh growth medium for monitoring in real time at 0, 2, 4, 6, 8, 10, 12, 24, 36, 48, 60, 72 hours post infection.

2.2.2 Gene expression

2.2.2.1 Fluorescent microscopy

Fluorescence illumination and observation is the most rapidly expanding microscopy technique employed today.

We are using fluorescence microscopy to detect proteins within the cells infected with VACV GLV-1h68 which is constructed by inserting *Renilla luciferase Green Fluorescent protein* including into the Vaccinia genome *(ruc-gfp)*. Fluorescent molecules absorb light at one wavelength and emit light at another, longer wavelength.

The expression of GFP in GI-101A, HT-29 and PC-3 cells, respectively, infected with VV-RVGL21 was monitored at 0, 2, 4, 6, 8, 10 12, 24, 36, 48, 60 hours post infection. GFP-images were visualized by a Zeiss Axicvert 40 CFL fluorescence microscope with UV light. Visible image and GFP image were overlaid by using Adobe PhotoShop version 7.0.

2.2.2.2 Western blot

Western blots were performed essentially by the method of Towbin et al., (1970). 15µg protein of the extract was separated using minigels (10% acrylamide). Proteins were transferred into nitrocellulose membrane. Gels, membranes and Whatmann papers were soaked in 1X Towbin buffer then placed following description underneath. Power supply is calculated at 0.8 mA/cm^2 and electrical transfer in 2 hours at room temperature condition. Band signals on the nitrocellulose membrane were detected by staining membrane with Ponceau solution and then blocked by milk solution for 2 hours at room temperature. Membranes were incubated with primary monoclonal antibodies raised against ß-actin, RUC, GFP, ß-galactosidase, ß-glucuronidase, and then was washed with 1x TBT in 5 minutes , repeated 4-5 times on the rocker. The membranes were then incubated with horseradish peroxidase (HRP)-conjugated anti-mouse, anti-rabbit, anti-goat, anti-sheep respectively, and visualized by using ECL substrate. Bound antibodies were detected on the X-ray film chemiluminescence subtrate.

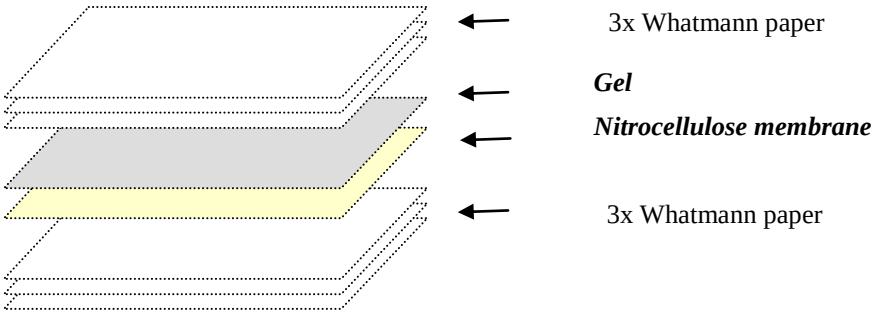

2.2.3 Trypan blue staining

Trypan blue staining was vital recommended for use in estimating the proportion of visible cells. In case the chromophor is negatively charged it does not react with the cell unless cell membranes are damaged. Staining facilitates the visualization of cell morphology. Trypan blue is derived from toluidine, that is, any of several isometric bases, $C_{14}H_{16}N_2$ derived from toluene. Trypan blue is a vital stain that colors dead tissue and cells. It is a diazo dye. Live cells or tissues with intact cell membranes will not be colored. Since cells are very selective in the compound that pass through the membrane, in a viable cell trypan blue is not absorbed; however, it traverses the membrane in the dead cell. Hence, dead cells are shown as a distinctive blue colour under a microscope.

Non-infected and infected GI-101A, HT-29 and PC-3 cell suspensions in BSS were prepared. 0.5 ml of 0.4% trypan blue solution is added in mixture of 0.3 ml of BSS and 0.2 ml of the cell suspension. Allow the cell suspension –Trypan blue mixture to stand for 5-15 minutes. Finally, live cell and dead cells are quantified by using counting procedure as described above.

2.2.4 Titration of vaccinia virus by plaque assay

The Plaque assay is a method for determine virus titer in cell lysate and suspension. Serial dilution of the virus samples at time point 0, 4, 8, 12, 24, 48, 60 hours post infection were used to infected the appropriate cell line, here CV1 cell line was used for this aim. After several days of growing, the medium was removed and the cells were stained with crystal violet. Plaques appear as 1-2 mm in diameter of diminished staining due to the retraction, rounding and detachment of infected cells.

Seed 24 well plates with $2.5x10^5$ cells per well of CV1 cells in 2 ml complete DMEM-10. Place the plates in the humidified, 5% CO_2 incubator at 37 ^oC for 2 days. After 2 days, prepare 7 tubes for dilutions by adding 1 ml of media to tube #1 and 900 ml media to tube #7. Infected cells were harvested in 1ml of PBS and 50 µl of suspension were collected for virus titer samples. Prepare the virus samples from cell lysates and suspension for titration by sonication 3 times for 30 seconds in the cold water. Make 7 fold serial dilutions from 10^{-2} to 10^{-8} of the virus samples in DMEM. Add 10 µl of virus samples to the tube #1, mixing well by pipetting up and down. Then 100 µl of virus dilution was transferred to the tube #2 and so on. Aspirate of old media from cells, add 250 µl of virus dilutions as assigned per well. The CMC (Carboxymethylcellulose) overlay media was warmed up and after virus samples were incubated in the humidified 5% CO_2 incubator at 37 ^oC for 1 hour, virus samples were overlaid by CMC in the humidified 5% CO_2 incubator at 37 ^oC for 2 days. After 2 days of incubation, CMC was removed and 250 µl of crystal violet and incubated for 1-2 days at room temperature. Wash off crystal violet and determine the titer by counting plaque within the wells and multiplying by the dilution factor.

$$\frac{\text{Number of plaques}}{\text{Dilution factor x infection volume}} = \text{Virus titre (pfu/ml)}$$

2.2.5 Protein analysis

2.2.5.1 Sample preparation and protein solubilization

To take advantage of the high resolution of 2-DE, proteins of the sample have to be denatured, disaggregated, reduced and solubilized to achieve complete disruption of molecular interactions and to ensure that each spot represents an individual polypeptide.

For cell samples: at 12 , 24 and 48 h post-infection (hpi) the viral infected and non-infected cells were washed in 1 ml washing *buffer* (1x PBS) and manually scraped in 400 µl of 1x lysis buffer and transferred into a small screw-cap tube. Cells were lysed by 40 times repeated suction pump using a tuberculin syringe system in the cold condition (all steps were carried out on ice). The lysates were then clarified by centrifugation at 13.000 rpm/20 minutes at 4 °C. The supernatants were collected and stored in single-use aliquots at - 80 °C.

For tumor tissue samples tumor tissue samples were collected as rapid as possible and freeze immediately in liquid nitrogen at –196 °C. Disrupt the samples while still deep-frozen. Small tissue specimens were homogenized and solubilized in 1x lysis buffer. Keep the centrifuge tube at 4 °C, centrifuge at 13,000*g* for 20 minutes at 4°C, supernatant was collected and centrifuged again. The proteins were collected and frozen in liquid nitrogen for using in one and two dimension electrophoresis.

2.2.5.2 Protein precipitation

Proteins were mixed with 15% TCA and incubated for 2 hours on ice then centrifuged at 13000 rpm for 20 min at 4 ^{o}C. The protein pellet was washed 3 times with cold aceton, centrifuged at 14000 rpm/ min for 10min again. Protein pellet is incubated in 2-5 min to dry for one dimensional gel and two dimensional gel electrophoresis.

2.2.5.3 Determination of protein concentration by Bradford assay

The standard care was made by using 1, 2, 3, 5, 7, 10, 15 µl of BSA 1µg/µl stock solution in 20 µl buffer each. 1 ml Coomassie brilliant blue solution was added into each tuble and incubated for 10 minutes at room temperature. A standard curve was generated by plotting. The absorbance at 594 nm measured in 1 cm path length (1 ml) microcuvette. Standard curves is generated to representative concentrations, the samples were diluted, measured according to a generated standard curve and then calculated following dilution ratio diluted.

2.2.5.4 Separation of proteins in one dimensional gel electrophoresis and two dimensional gel electrophoresis

2.2.5.4.1 One dimensional gel electrophoresis

Sodium dodecyl sulfate polyacrylamide gel electrophoresis (SDS-PAGE) is a very common method for separating proteins by electrophoresis uses a discontinuous polyacrylamide gel as a support medium and sodium dodecyl sulfate (SDS) to denature the proteins. Protein pellets precipitated from above steps were soaked in *1x SDS sample buffer* in 3 µg/µl, vortexed at 750 rpm/ 24 ^{0}C for 10 min, incubated for 5 min at 95 ^{o}C. Then 15 µg proteins were placed in 10% separating SDS-PAGE gel and 5% stacking gel. Power supply is arranged at 100 Volt for 4-6 hours.

Proteins were detected by staining with Coomassie Blue for 24 hours or more. Gels were washed with SDS removing solution (30 % v/v methanol, 10 % v/v acetic acid) and finally soaked in fixing solution (10% v/v acetic acid) for storing up to scanning.

2.2.5.4.2 Two dimensional gel electrophoresis

High-resolution two-dimensional gelelectrophoresis (2-DE) for the separation of complex protein mixtures was introduced by O'Farrell in 1975 by combining isoelectric focusing (IEF) in the first dimension in presence of urea, detergents and DTT, with sodium

dodecyl sulfate polyacrylamide gel electrophoresis (SDS-PAGE) in the second dimension. Proteins are separated according to isoelectric point (pI) and molecular mass (Mr), and quantified according to relative abundance. Depending on the gel size and pH gradient used, 2-D PAGE can resolve more than 5,000 proteins simultaneously (~2,000 proteins routinely), and can detect under 10 ng of protein per spot. Furthermore, it delivers a map of intact proteins, which reflects changes in protein expression level, isoforms or post-translational modifications.

To prevent protein degradation that otherwise may result in artifactual spots and loss high molecular weight protein, protease inhibitors were added. TCA/acetone precipitation was used for minimizing protein degradation, for removing interfering compounds, such as salt, or polyphenols, and for the enrichment of very alkaline proteins such as ribosomal proteins from total cell lysates (Görg et al., 1999).

In this work firstly, protein preparation and the linear immobilizing pH 3-10 IPG strip was applied for testing the distributions of proteins extracted from GI-101A cells infected with VACV GLV-1h68. Next, according to detections of protein separation on 2DE which tended to appear at the narrow pH range of the gel based on the test distribution of protein obtained with an immobilizing pH of 3-10, a linear gel with an immobilizing pH gradient of 4-7 and SDS 10% gel were chosen to be optimal for protein resolution-particularly for major proteins.

To minimize the analytical variation between gels, the 2-DE conditions suitable for the analysis of 36 gels were optimized by dividing 36 independent samples into 3 independent sections for isoelectric focusing (IEF) under the same conditions, and then simultaneously applying the 36 isoelectric-focused samples to sodium dodecyl sulfate polyacrylamide gel electrophoresis (SDS-PAGE).

Isoelectric focusing step

Rehydration step: protein probes of 150 µg and 250 µg proteins, respectively, were mixed with 400 µl of rehydration solution. Add rehydration solution with protein onto pH 3-10 IPG strips and pH 4-7 IPG strips, long 18 cm. These strips were rehydrated in 20 ^{o}C plate for overnight (18–20 h).

Then strips were place in the tray with the anodic (+) end of the strip resting on the appropriate mark etched on the bottom of the Manifold track with the gel side up. Pads were wetted with 150 µl deionized water and placed on the end of the IPG strip, overlay the IPG strip with 2 ml of dry strip cover fluid.

Program for first dimensional gel electrophoresis

Length	*pH*	*Step and Voltage mode*	*Voltage*	*Step duration*
18cm	*3-10*	*Step and hold*	*300 V*	*3 h*
		Gradient	*1000 V*	*6 h*
		Gradient	*8000 V*	*6 h*
		Step and hold	*8000 V*	*Until to 50-60000 Volt-hours.*

Equilibration step: Prior to the second-dimension separation (SDS-PAGE), it is essential that the IPG strips are equilibrated to allow the separated proteins to fully interact with SDS. The IPG strips are equilibrated in presence of SDS, DTT, urea, glycerol and iodoacetamide (IAA), and then placed on top of a vertical SDS gel. Dissolve 14 mg of DTT in 4 ml of equilibration buffer (= equilibration buffer I) for each strip. Take out the focused IPG gel strips from the freezer and place them into equilibration buffer I. Rock them for 15 min on a shaker and then pour equilibration buffer I off.

Dissolve 180 mg of iodoacetamide in 4 ml of equilibration buffer (= equilibration buffer II) for each strip. Equilibrate for another 15 min on a rocker. After the 2nd equilibration, place it on a piece of filter paper at one edge to drain off excess equilibration buffer. Cover the SDS-polyacrylamide gel with 1xSDS running buffer. Place the IPG trip on top of the 12% and 10% SDS-PAGE gels with the plastic back touching the behind glass plate. Discard the excess of 1x SDS running buffer and seal the IPG strip by 0.5% Agarose resolved in 1xSDS running buffer.

Separation of IPG strips in vertical gels The equilibrated IPG strips were further resolved with 10% SDS-PAGE gels at 100 V until the dye front reached the bottom of the gels.

Gel detection

Coomassie Brilliant Blue (CBB) staining methods have found widespread use for the detection of proteins on 2-D gels, ease of use and compatibility with most subsequent protein analysis and characterization methods such as MS. However, in terms of the requirements for proteome analysis, the principal limitation of CBB stains lies in their insufficient sensitivity, which does not permit the detection of low abundance proteins (the detection limit of CBB stains is in the range of 200-500 ng protein per spot). Hence, typically no more than a few hundred protein spots can be visualized on a 2-D gel, even if milligram amounts of protein had been loaded onto the gel.

Gels were fixed in 250 ml of fixation solution (50% Ethanol, 12% acetic acid , 0,5 ml per litre of 37% formaldehyde for 1-3 hours at room temperature. Then gels were washed 2 times with deionised water. Then the detection is carried out by staining gels with Coomassie blue solution. Staining gels for 1-2 days then wash with deionised water until background is clear.

Silver staining methods (Merril *et al*., 1981; Oakley *et al*., 1980) are far more sensitive than CBB or imidazole-zinc stains (detection limit is as low as 0.1 ng protein/spot). They provide a linear response with over a 10-40 fold range in protein concentration, which is slightly worse than with CBB staining. However, silver staining methods are far from stoichiometric, and are much less reproducible than CBB stains due to the subjective end-point of the staining procedure which makes them less suitable for quantitative analysis.

Silver staining steps

Fixing	*50 % MetOH/12 % acetic acid/ 38% d_2H_20*	*> 1 h or over night*
Washing	*30% EtOH*	*2 x 30 min*
Sensitizer	*Thiosulfate reagent*	*1 min*
Washing	*Deionized water*	*3 x 1 min*
Silver	*Silver nitrate*	*>1h or over night*
Washing	*Deionized water*	*2 x 30 sec*
Development	*Developer*	*3-5 min*
Stopping	*Stop reagent*	*> 20 mis or overnight*

The detected gels were scanned at a resolution of 200 dpi using the EPSON PERFECTION 4990 Scanner.

However, the 2D technique has some limitations. Proteins expressed at low levels, so called low abundance proteins (transcription factors, and some cell-signalling proteins), hydrophobic membrane and nuclear proteins with extreme pI as well as very large or very small proteins are very difficult to separate and/or detected in 2D gels.

2.2.5.5 Computerized 2-D image anylysis

One of the key objectives of proteomics is to identify the differential expression between control and experimental samples run on a series of 2-DEs. Protein spots that have been inhibited (disappeared), induced (appeared) or have changed abundance (increased or decreased in size and intensity). Once these gel features have been found, the proteins of interest can be identified using MS. This goal is usually accomplished with the help of computerized image analysis systems (Dowsey et al., 2003; Dunn 1992 & 1993; Garrels 1989).

Spot detection, spot matching, and quantitative intensity analysis were performed using Delta2D of DECODON Company.

Working with Delta 2D

Gels were organized into analysis projects. A project consists of 6 gel groups. Quantitation of results was analyzed on a gel-by-gel basis and aggregated by groups.

Wrapping and visual comparison of 2-DE images

Wrapping compensates for the differences in spot positions between gels. These differences are due to variations in running conditions and the gel casting process.

Delta2D's warping algorithms generate dual channel images on which corresponding spots are perfectly overlaid. The same algorithm that is used in producing dual channel images was used in the subsequent quantitation step to obtain accurate and reliable spot matching information.

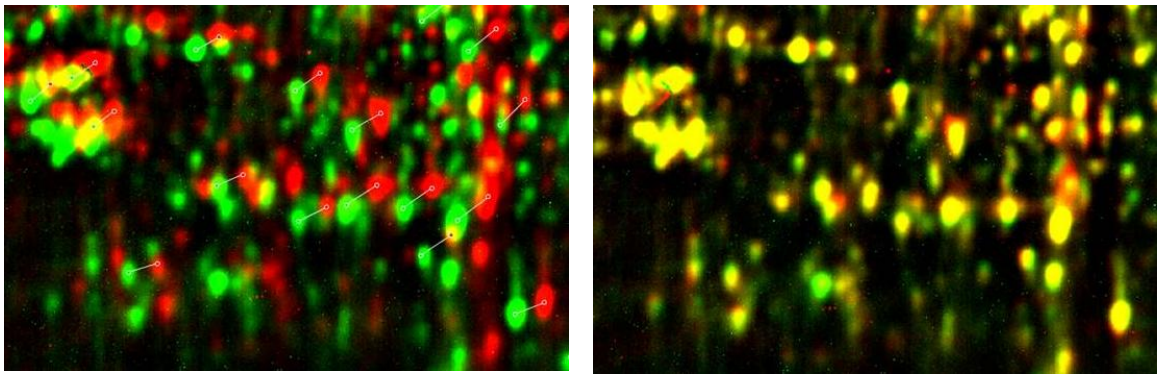

Figure 4. **A region 2D image, before and after exact wrapping**. Corresponding spots are overlaid exactly, allowing for easy identification of spots with changed expression level.

Working with quantitation table

Expression intensity ratios infected/uninfected larger than 2.0 ($p \leq 0.05$) or smaller than 0.5 ($p \leq 0.05$) were set as a threshold indicating significant changes. The numerical expression ratio was used for analysis. The column shows the ratio as mathematical ratio or as fold change. Additionally it can contain colour coded representation of the ratio.

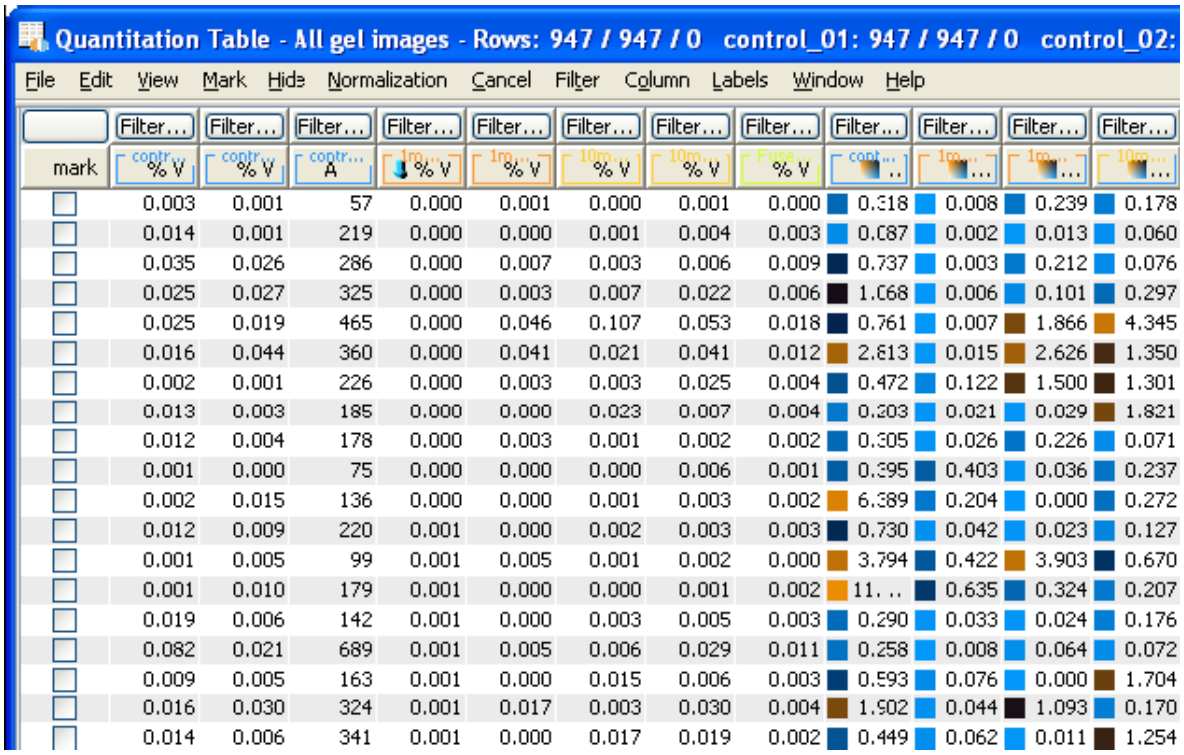

	0.003	0.001	57	0.000	0.001	0.000	0.001	0.000	0.318	0.008	0.239	0.178
	0.014	0.001	219	0.000	0.000	0.001	0.004	0.003	0.087	0.002	0.013	0.060
	0.035	0.026	286	0.000	0.007	0.003	0.006	0.009	0.737	0.003	0.212	0.076
	0.025	0.027	325	0.000	0.003	0.007	0.022	0.006	1.068	0.006	0.101	0.297
	0.025	0.019	465	0.000	0.046	0.107	0.053	0.018	0.761	0.007	1.866	4.345
	0.016	0.044	360	0.000	0.041	0.021	0.041	0.012	2.613	0.015	2.626	1.350
	0.002	0.001	226	0.000	0.003	0.003	0.025	0.004	0.472	0.122	1.500	1.301
	0.013	0.003	185	0.000	0.000	0.023	0.007	0.004	0.203	0.021	0.029	1.821
	0.012	0.004	178	0.000	0.003	0.001	0.002	0.002	0.305	0.026	0.226	0.071
	0.001	0.000	75	0.000	0.000	0.000	0.006	0.001	0.395	0.403	0.036	0.237
	0.002	0.015	136	0.000	0.000	0.001	0.003	0.002	6.389	0.204	0.000	0.272
	0.012	0.009	220	0.001	0.000	0.002	0.003	0.003	0.730	0.042	0.023	0.127
	0.001	0.005	99	0.001	0.005	0.001	0.002	0.000	3.794	0.422	3.903	0.670
	0.001	0.010	179	0.001	0.000	0.000	0.001	0.002	11. ..	0.635	0.324	0.207
	0.019	0.006	142	0.001	0.000	0.003	0.005	0.003	0.290	0.033	0.024	0.176
	0.082	0.021	689	0.001	0.005	0.006	0.029	0.011	0.258	0.008	0.064	0.072
	0.009	0.005	163	0.001	0.000	0.015	0.006	0.003	0.593	0.076	0.000	1.704
	0.016	0.030	324	0.001	0.017	0.003	0.030	0.004	1.502	0.044	1.093	0.170
	0.014	0.006	341	0.001	0.000	0.017	0.019	0.002	0.449	0.062	0.011	1.254

Figure 5. **Part of quantitation tables**. The quantitation tables gives access to data in three basic types of representation: *Single gel tables* show all available quantitive data to one single gel image. *Multi gel tables* show the same data as the above type plus data comparing the spots of the gel images to each other, whereas the *Statistics table* shows one selectable subset of the above data in a statistical evaluation for each group plus data comparing the spots groupwise. The single gel tables are labeled each with the name of the respective gel image. The multi gel tables are labeled with either the names of the gel images involved, or, if containing all gel images, simply with all gel images.

2.2.5.6 Mass spectrometry for protein identification

Preparation of peptide mixtures for MALDI-MS

Mass spectrometry has its origins in the studies performed by J. J. Thomson and his student F. W. Aston around the turn of the last century (Griffiths WJ et al 2001). An advantage of mass spectrometers over other analytical instruments is that it affords a high

degree of accuracy (~0.01–0.001%) and sensitivity (detection of 10^{-9} – 10^{-18} mol of sample required) when determining the molecular weight of biological compounds (Poland GA et al 2001). A mass spectrometer is an instrument that produces ions from a sample, separates them according to their mass-to-charge ratio (m/z) and records the relative abundance of each of the ions to obtain a mass spectrum (Bonner PLR, Lill JR et al 2002).

Proteins were excised from colloidal CBB-stained 2-D gels using a spot cutter (Proteome Works™, Bio-Rad) with a picker head of 2 mm diameter and transferred into 96-well microplates loaded with 100 ml Lichrosolv water per well. Digestion with trypsin and subsequent spotting of peptide solutions onto the MALDI targets were performed automatically in the Ettan Spot Handling Workstation (Amersham Biosciences) using a modified standard protocol. Briefly, gel pieces were washed twice with 100 mL 50mM ammoniumbicarbonate/ 50% v/v methanol for 30 min and once with 100 ml 75% v/v ACN for 10 min. After 17 min drying 10 ml trypsin solution containing 20 ng/ml trypsin (Promega, Madison, WI, USA) in 20 mM ammoniumbicarbonate was added and incubated at 37°C for 120 min. For peptide extraction gel pieces were covered with 60 ml 50% v/v ACN/0.1% w/v TFA and incubated for 30 min at 37°C. The peptide-containing supernatant was transferred into a new microplate and the extraction was repeated with 40 mL of the same solution. The supernatants were dried at 40°C for 220 min completely. Peptides were dissolved in 2.2 ml of 0.5% w/v TFA/50% v/v ACN and 0.7 ml of this solution were directly spotted on the MALDI target. Then, 0.4 ml of matrix solution (50% v/v ACN/0.5% w/v TFA) saturated with a-cyano-4-hydroxycinnamic acid (CHCA) was added and mixed with the sample solution by aspirating the mixture five times. Prior to the measurement in the MALDI-TOF instrument the samples were allowed to dry on the target for 10–15 min.

Peptide analysis and identification of proteins by using MALDI-TOF-MS

The MALDI-TOF measurement of spotted peptide solutions was carried out on a Proteome-Analyzer 4700 (Applied Biosystems, Foster City, CA, USA). The spectra were recorded in reflector mode in a mass range from 900 to 3700 Da with a focus mass of

2000 Da. For one main spectrum 25 subspectra with 100 shots per subspectrum were accumulated using a random search pattern. If the autolytical fragment of trypsin with the mono-isotopic $(M+H)^+$ *m/z* at 2211.104 reached a signal-to-noise ratio (S/N) of at least 10, an internal calibration was automatically performed using this peak for one-point-calibration. The peptide search tolerance was 50 ppm but the actual standard deviation was between 10 and 20 ppm. Calibration was performed manually for the less than 1% samples for which the automatic calibration failed. After calibration the peak lists were created using the "peak to mascot" script of the 4700 Explorer™ Software with the following settings: mass range from 900 to 3700 Da; peak density of 50 peaks per range of 200 Da; minimal area of 100 and maximal 200 peaks per protein spot and minimal S/N ratio of 6. Peak lists were compared with a specific *Homo sapiens, Vaccinia virus and Mus musculus* sequence database using the mascot search engine (Matrix Science, London, UK). Peptide mixtures that yielded at least twice a mowse score of at least 49 and a sequence coverage of at least 30% were regarded as positive identifications. Proteins/peptide mixtures that failed to exceed the 30% sequence coverage cutoff level were subject to MALDI-MS/MS. MALDI-TOF analysis was performed for the three strongest peaks of the TOF spectrum. For one main spectrum 20 subspectra with 125 shots per subspectrum were accumulated using a random search pattern. The internal calibration was automatically performed as one-point calibration if the mono-isotopic arginine $(M+H)^+$ *m/z* at 175.119 or lysine $(M+H)^+$ *m/z* at 147.107 reached an S/N of at least 5. The peak lists were created using the "peak to mascot" script of the 4700 Explorer™ Software with the following settings: mass range from 60 Da to a mass that was 20 Da lower than the precursor mass; peak density of 5 peaks per 200 Da; minimal area of 100 and maximal 20 peaks per precursor and a minimal S/N ratio of 5. Database searches employed the *Homo sapiens, Vaccinia virus and Mus musculus* specific database and the MASCOT search engine (Matrix Science) mentioned above. Proteins with a mowse score of at least 49 in the reflector mode that were confirmed by subsequent measurement of the strongest peaks (MS/ MS) were regarded as positive identification. MS/MS analysis was particularly useful for the identification of spots containing more than one component.

3. RESULTS

3.1 Verification of marker expression of VACV GLV-1h68

3.1.1 GFP-fluorescence microscopy study

Here we are using a novel vaccinia virus strain VACV GLV-1h68 which is constructed by carring triple insertions of *Renilla luciferase-green fluorescent protein (ruc-gfp)* in the *F14.5* gene, *β-galactosidase* into *thymidine kinase (TK)* gene, and *β-glucuronidase* into *hemagglutinin (HA)* gene of the *LIVP* genome.

During the infection, viral infection in the cells was monitored in real time with different methods. The expression of *ruc-gfp* which is encoded by inserted gene in VACV GLV-1h68 genome was confirmed by fluorescence microscopy.

GI-101A, HT-29, PC-3 cell lines were seeded in 6 well plates. As cell growths achieve 100% confluence, they were infected with VACV GLV-1h68 with MOI 0.5. The replication of VACV GLV-1h68 was monitored by GFP images at different time: 2, 4, 6, 8, 12, 24, 36, 48 hpi. The first images of GFP expression were cycled to estimate the initial expression of GFP for each cell line infected with VACV GLV-1h68. The morphology of non-infected and infected cells was performed under both visible light and UV light. Addition, merge images were made by Photoshop 7.0 to determine position of GFP brighten in the field of cell cultivation.

GI-101A cells infected with VACV GLV-1h68 exhibited initial distribution at 4 hours after infection with a dramatic increase of light emission in the cells in next time point of infection. We can see simultaneously the image of viral replication by emission of GFP in the culture and cell morphology image was changed by infection. The cells in which they were infected eventually detach from the plastic cell culture plate. The more cell are

infected the more changes become visible. These changes include the rounding up and detachment of the cell from the plastic culture dish, cell lysis can be seen under the visible light of microscope (Figure 6)

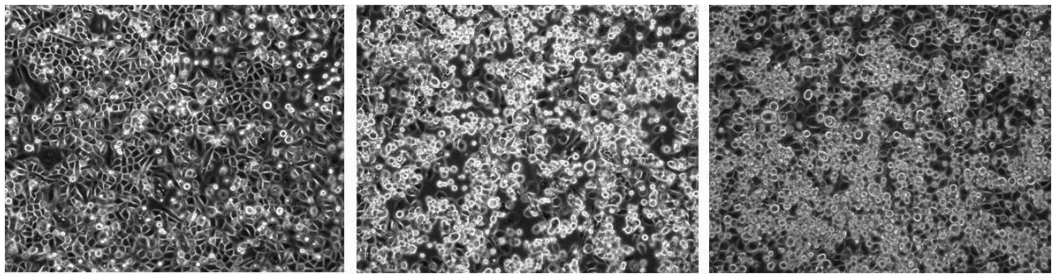

A B C

Figure 6. **Morphology of infected cells**. Uninfected PC-3 cells (A), at 12 hours after infection many cells round up (B), at 24 hours after infection more cells have rounded up and detached from the culture dish (C).

To discover whether there is any difference in details of expression of RUC-GFP fusion protein encoded by inserted gene in the F14.5 of VACV GLV-1h68 genome which are monitored by promoter early/late in other tumor cell line we did experiments in the same model with a human colon cell line (HT-29) and a human prostate tumor cell line. Three times monitoring of GFP for each cell line were performed to investigate the rule of VACV GLV-1h68 replication. Surprisingly, there is no difference of the first GFP expression in infected cells between GI-101A, HT-29 and PC-3 cells. All red cycles for beginning of GFP expression were marked at 4 hour post infection and being increased in the next time points of infection (Figure 7, 8, 9). The result show that VACV GLV-1h68 can express GFP-independent in cell line indicating efficient replication of the virus at least in three cell lines in this study.

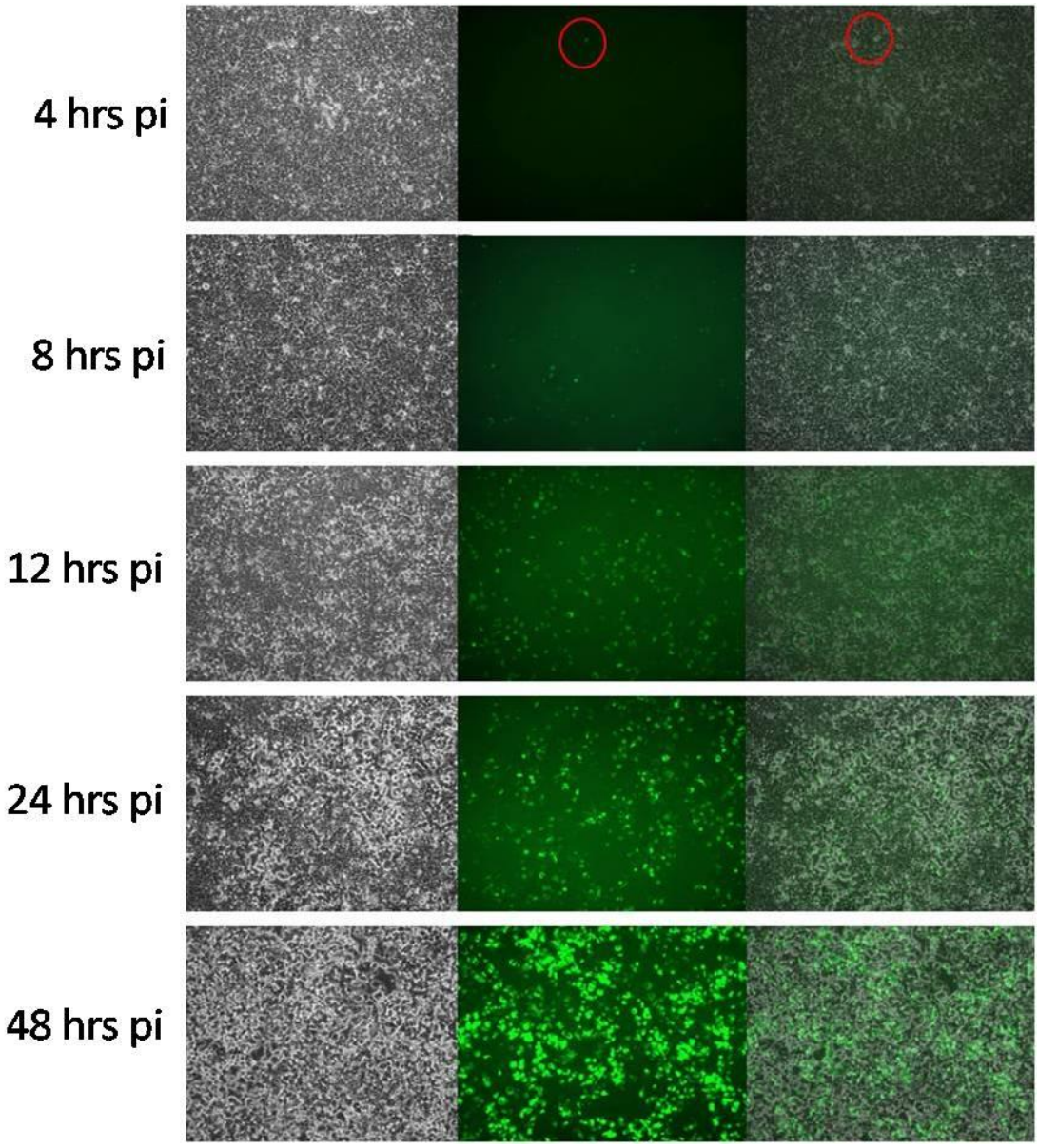

Figure 7. **GFP expression in GI-101A cells infected with VACV GLV-1h68**. Cells expressing GFP protein show green fluorescence under a fluorescence microscope. The image was acquired using a microscope (Zeiss Axiovert)

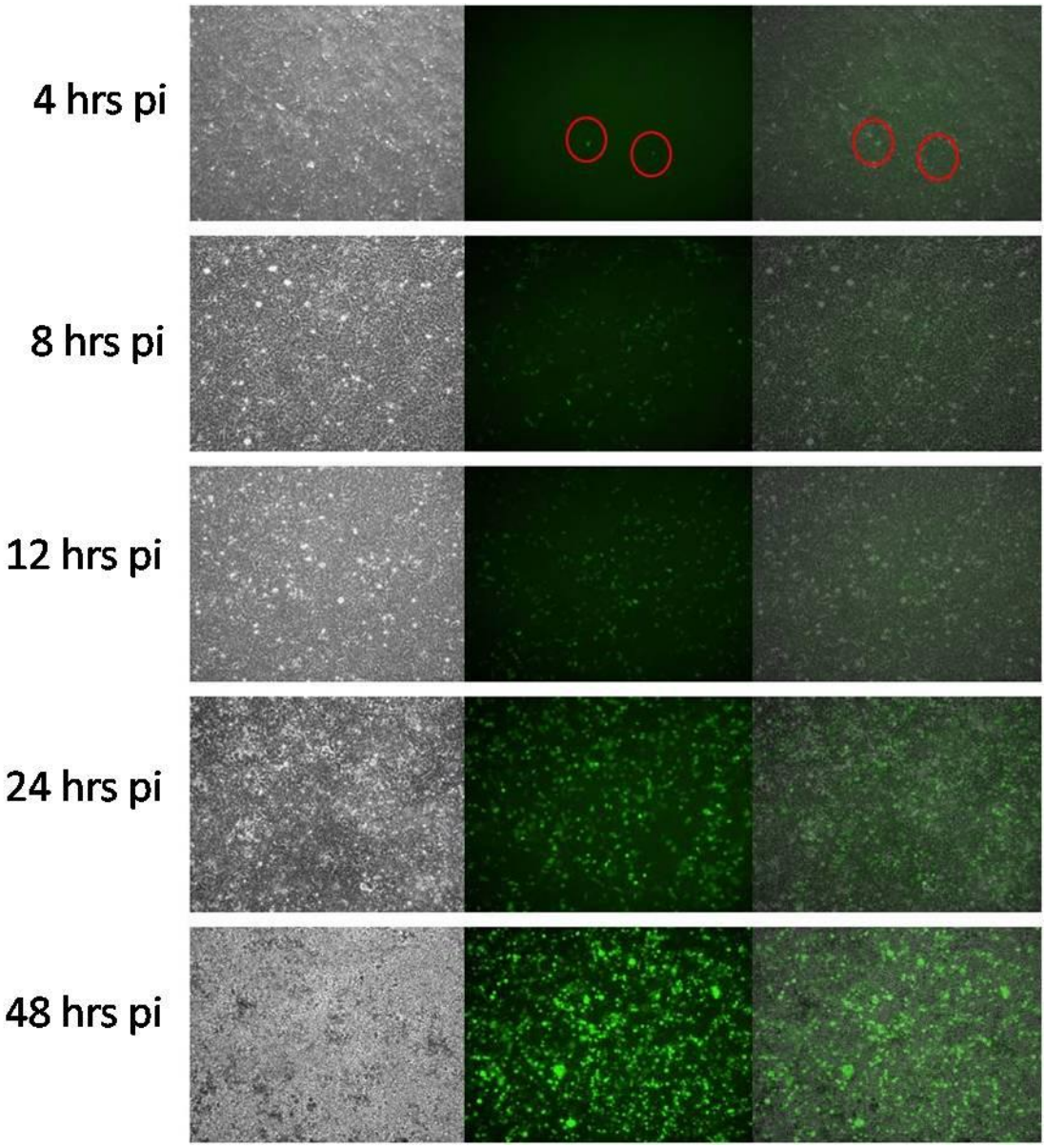

Figure 8. **GFP expression in HT-29 cells infected with VACV GLV-1h68**. Cells expressing GFP protein show green fluorescence under a fluorescence microscope. The image was acquired using a microscope (Zeiss Axiovert)

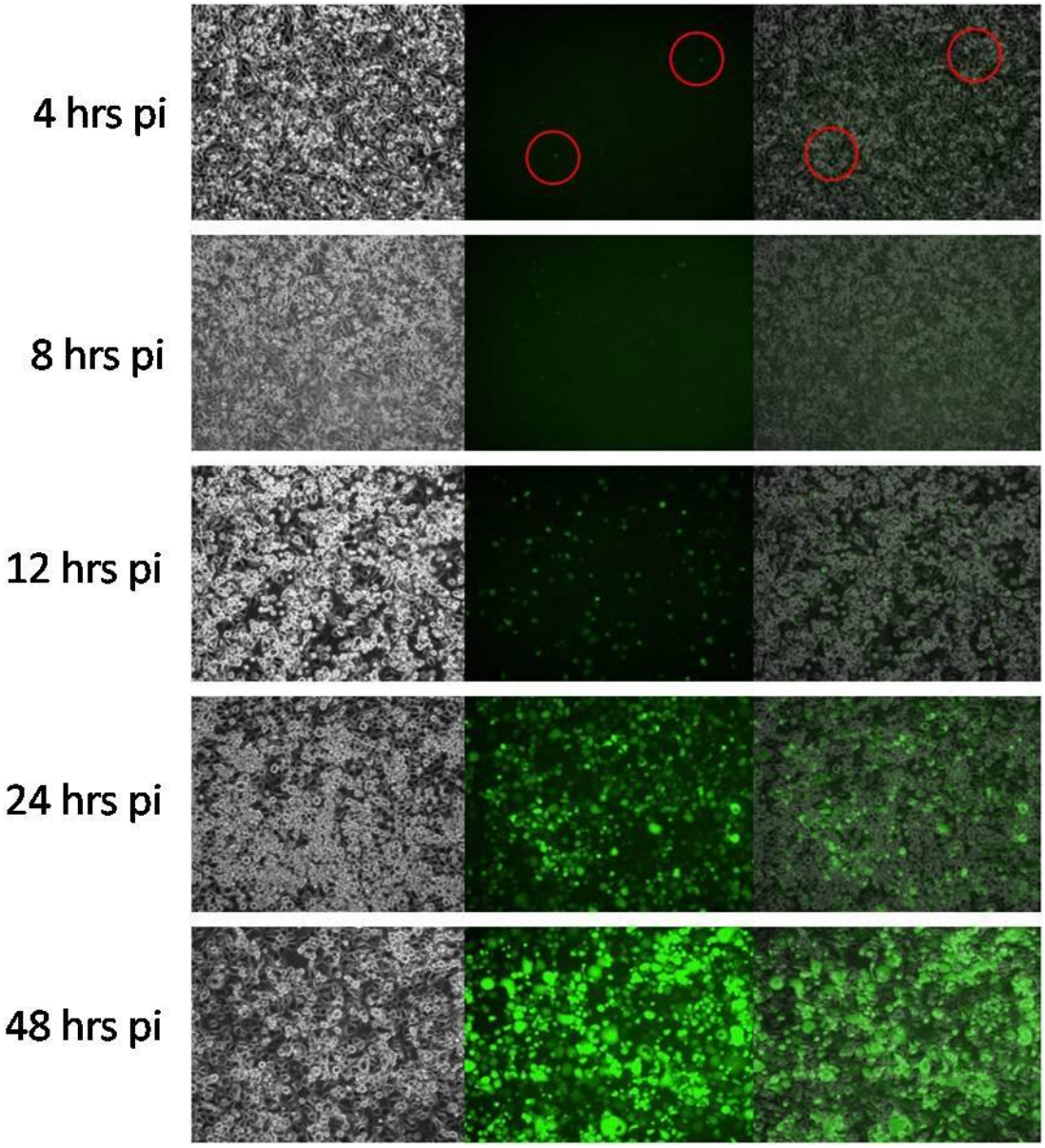

Figure 9. **GFP expression in PC-3 cells infected with VACV GLV-1h68**. Cells expressing GFP protein show green fluorescence under a fluorescence microscope. The image was acquired using a microscope (Zeiss Axiovert)

3.1.2 Biochemical analysis of cell lysate

Successful tumor-directed gene therapy is dependent upon a high percentage of tumor cells expressing a large quantity of gene product after systemic injection of a vector. To further confirm the dynamic alterations of protein expression during VACV GLV-1h68 infection, 15 μg of protein extracted from GI-101A, HT-29, PC-3 cells infected with VACV GLV-1h68 at MOI of 0.5 were separated in one dimensional SDS-PAGE gels, lysates at 4, 6, 8, 10, 12, 24 and 48 hpi were examined, separated in the SDS-PAGE gels and the transferred onto nitrocellulose membrane (0.45 μm pore). These membranes were incubated with special antibodies against Green Fluorescent proteins, β-galactosidase, and β-glucuronidase for Western-blot analysis.

Image of Ponceau S staining give first evidence that proteins were transferred to the cellulose membrane by using appropriated power supply (Figure 10), marker proteins were detected by incubating membranes with special antibodies.

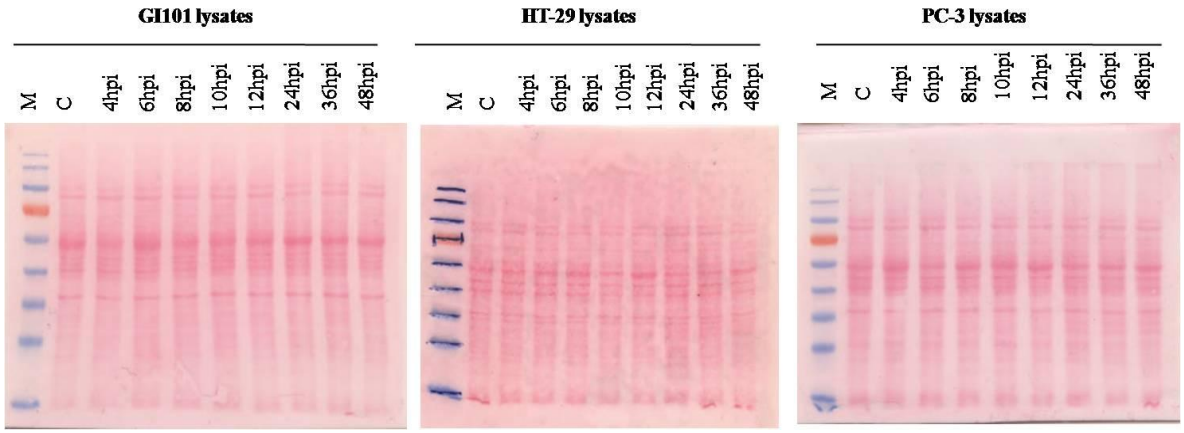

Figure 10. Blotting of proteins lysates of un-infected and infected GI-101A, HT-29, PC-3 cells.

3.1.2.1 Expression of GFP-RUC fusion proteins encoded in the VACV GLV-1h68 infected cells

Figure 11 show a sign of the expression of GFP-RUC fusion protein in both three cell line GI-101A, HT-29 and PC-3 cells.

The first fusion protein expression was produced in VACV GLV-1h68 infected GI-101A cells at 10 hpi, elevated at the next time point of infection and reached a peak in time series at 48 hpi. Early but not much distinguished from GI-101A cells, the expression of RUC-GFP fusion protein was produced in VACV GLV-1h68 infected HT-29 cells at 8 hpi and reached a peak in time series at 36 hpi. For infected PC-3 cells, evidence of the RUC-GFP fusion protein can be seen latest compared with other cell line where it was coming up since 24 hours after infection and keeping a very weak signal. This result indicates that GFP expression by Western-blot was lesser sensitive than the expression changes shown by the GFP image analysis by microscope.

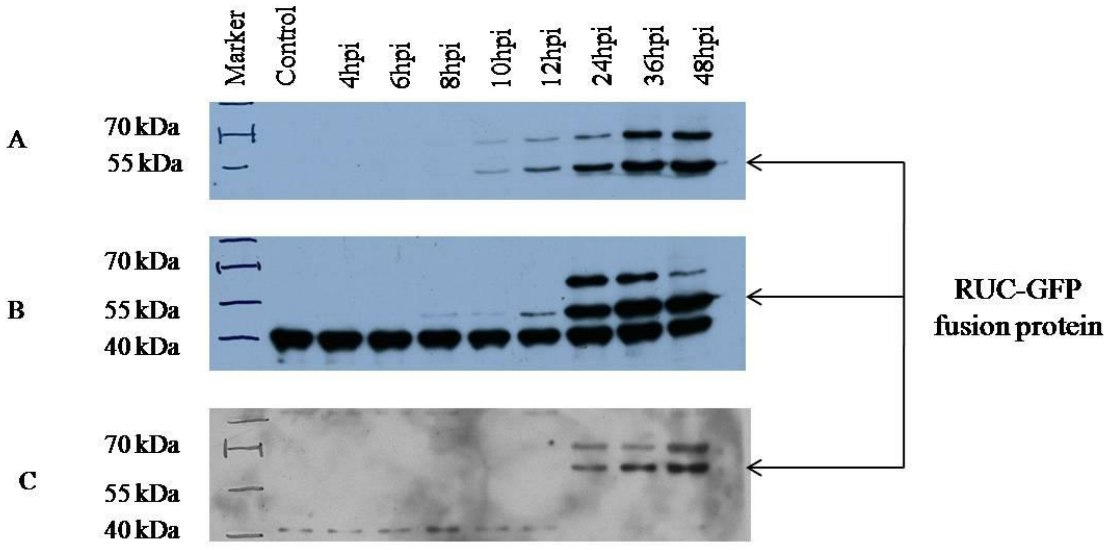

Figure 11. **Western-blot with GFP** of GI101 cell lysate (A), HT29 cell lysate (B), PC-3 cell lysate (C), 3 seconds exposure, 15 µg of proteins from lysate of cells infected with VACV GLV-1h68 were separated in SDS-PAGE 10%.

3.1.2.2 Expression of β-galactosidase proteins in the VACV GLV-1h68 infected cells

To examine the level of the β-galactosidase protein produced in the VACV GLV-1h68 infected cells, SDS-PAGE gels containing protein lysates extracted from VACV GLV-1h68 infected GI-101A, HT-29, PC-3 cells were transferred to nitrocellulose membrane. β-galactosidase was detected by using anti-β-galactosidase antibody. As shown in Figure 12, signal of β-galactosidase was manifested in VACV GLV-1h68 infected cells at a level that was beginning detected readily from the 24 hpi of infection in both three cell lines and the protein level reached a peak on the 48 hpi of infection, results is similar to HT-29 cells and PC-3 cells. This study were supposed that β-galactosidase gene which was inserted in the *thymidine kinase (TK)* gene controlled by promoter early/late p7.5 could be strongly activated at the late phase of replication but not in the early infection phase or/and reason is might be of the Western-blot is not sufficient sensitive to detect β-galactosidase earlier or protein was degraded by proteasome in the early time. However, this data can compare with RUC-GFP fusion protein expression by the same Western-blot method and analysis, noteworthy.

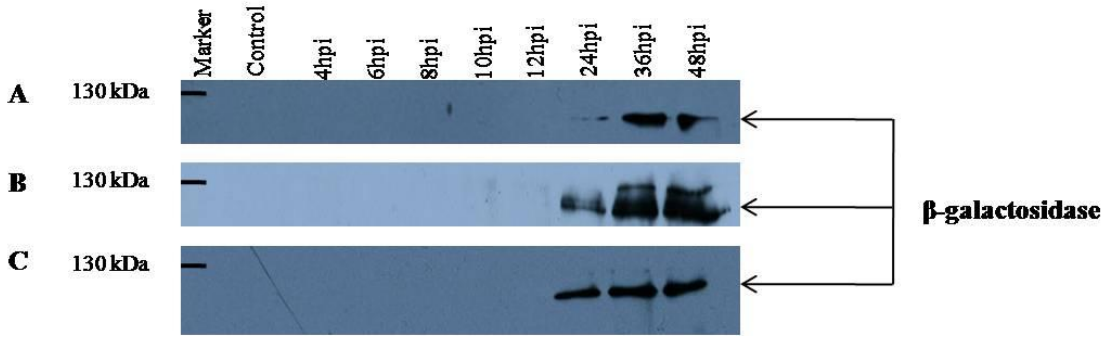

Figure 12. **Western-blot with β-galactosidase** GI101 cell lysate (A), HT29 cell lysate (B), PC-3 cell lysate (C), 3s exposure, 15 µg of proteins from lysate of cells infected with VACV GLV-1h68 were separated in SDS-PAGE 10%.

3.1.2.3 Expression of β-glucuronidase proteins encoded by marker genes in the tumor cells

As shown above, the first expression of RUC-GFP fusion protein was shown in different time point. For example, that is at 10 hpi in GI-101A cells, that is 8 hpi in HT-29 cells and 24 hpi in PC-3 cells. Besides, the first expression of β-galactosidase protein was shown in VACV GLV-1h68 infected GI-101A cells at 24 hpi, results shown is similar in HT-29, PC-3 cells. To examine expression of of β-galactosidase which were one of three genes which were inserted into *LIVP* genome then converted to VACV GLV-1h68 (β-glucuronidase were encoded by GUS gene in the *hemagglutinin (HA)* gene which were controlled by promoter p11), antibody against β-glucuronidase was using for Western-blot analysis. Three time of doing experiment in the same condition to confirm the data, that β-glucuronidase expression is also point out the first bands in the GI-101A cells, HT-29 cells and PC-3 cells at 24 hpi (Figure 13).

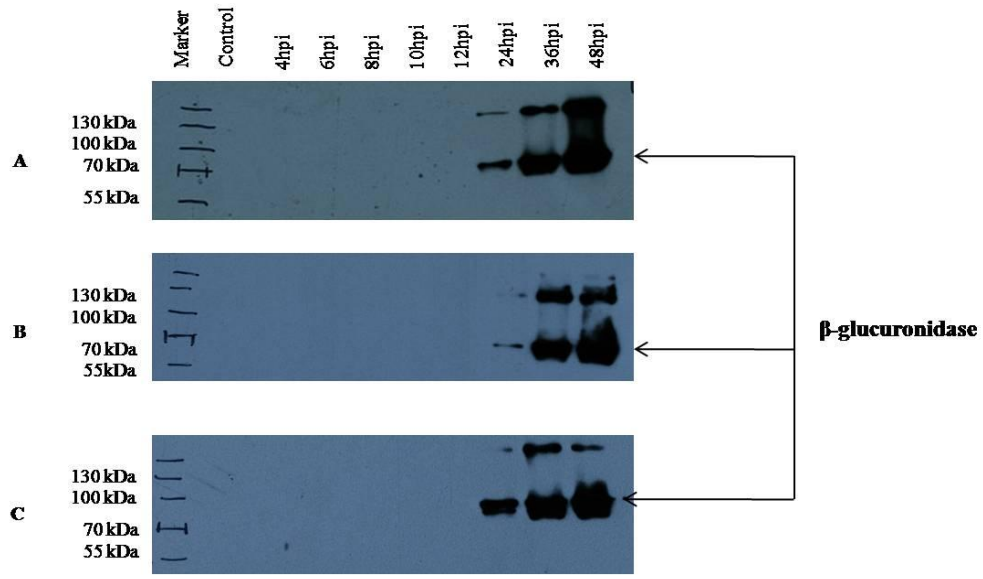

Figure 13. **Western-blot with β-glucuronidase** of GI101 cell lysate (A), HT29 cell lysate (B), PC-3 cell lysate (C), 3s exposure, 15 µg of proteins from lysate of cells infected with VACV GLV-1h68 were separated in SDS-PAGE 10%.

3.1.2.4 Expression of marker proteins of the tumor xenograft in mice

To determine expression of marker proteins which are encoded by VACV GLV-1h68 gene in the mice bearing tumor, the tumor xenografts in the mice with GI-101A, HT-29 and PC3 cell lines were surgeries and homogenized in the lysis buffer, then supernatant were collected for Western-blot analysis. Result is shown in the figure 14 below point out the expression of almost proteins which were extracted from tumor tissue then were separated in the 10% SDS-PAGE gels, protein bands were detected by Coomassie blue staining. We would to compare how different between uninfected sample (control) with infected samples after mice were subcutaneously injected with VACV GLV-1h68 virus. In general, some bands were disappeared compared with control one. In contrast, there are some bands shown appearance which have no in the control sample or shown a sign of more intensive (Figure 14). These bands may be derived from viral proteins extracted in tumor cells where viruses using host factors to produce their own products or/and host proteins which were degraded or induced by host-virus interaction.

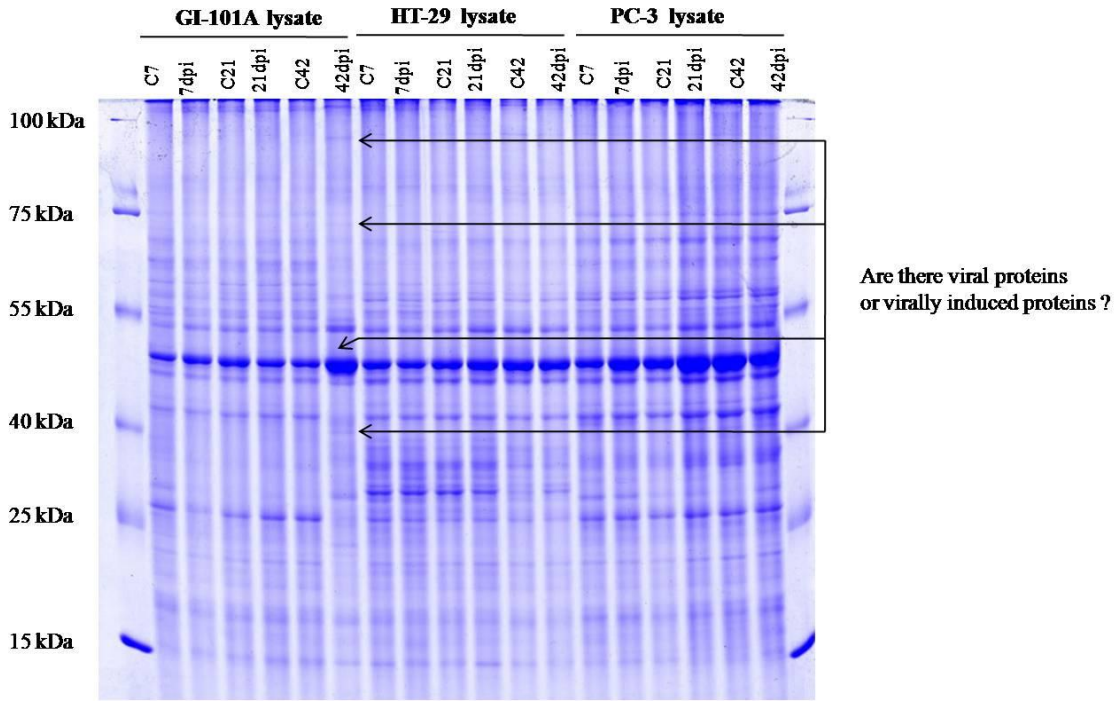

Figure 14. Protein analysis from tumor lysate by using SDS-PAGE electrophoresis and detection by Coomassie blue

To determine in detail of the marker proteins expressed in the tumor from mice, Western-blot analysis were necessary to detect protein expression level. We were also using antibodies against proteins green fluorescent, β-galactosidase, and β-glucuronidase. Figure 15 indicate that expression of the marker genes in the GI-101A tumor were obvious, relatively. Protein bands of both three markers have shown right first tumor growing phase where tumors were not yet regressed by infection. They also were keeping persistent during tumor progression. These results indicate that a recombinant VACV GLV-1h68 can replicate in the tumor, they use the home tumor to evade hunt of the host immune system.

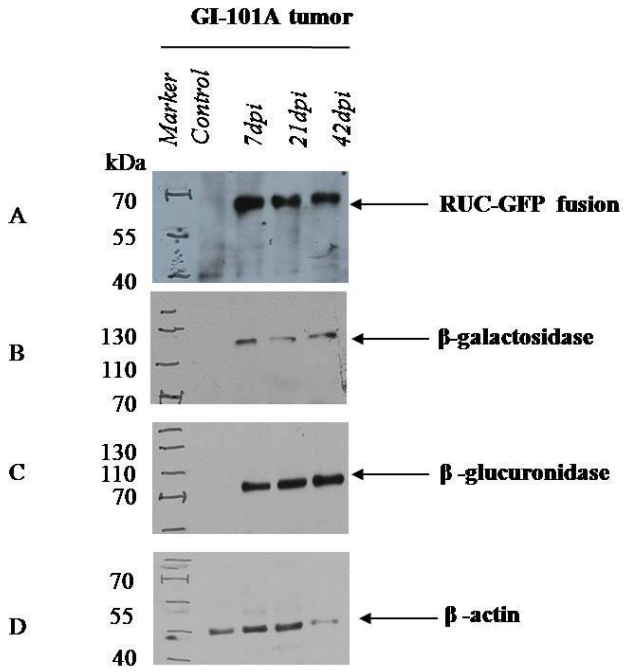

Figure 15. Western-Blot detection of marker proteins of GI-101A tumor lysate. RUC-GFP fusion protein(A), β-galactosidase (B), β-glucuronidase (C), β-actin (D), 3s exposure, 15 µg of proteins from lysate of cells infected with VACV GLV-1h68 were separated in 10% SDS-PAGE gels.

In comparison, RUC-GFP fusion protein, β-galactoside and β-glucuronidase could be found in HT-29 and PC-3 tumor but not equal levels (Figure 16). In HT-29 tumors, marker proteins could initially found at intermediate tumor phase and were present during to the late tumor phase. In PC-3 tumors only found at 21 day post infection were present. Evidence of marker gene expression in mice bearing tumors showed modifications in each of the tumors.

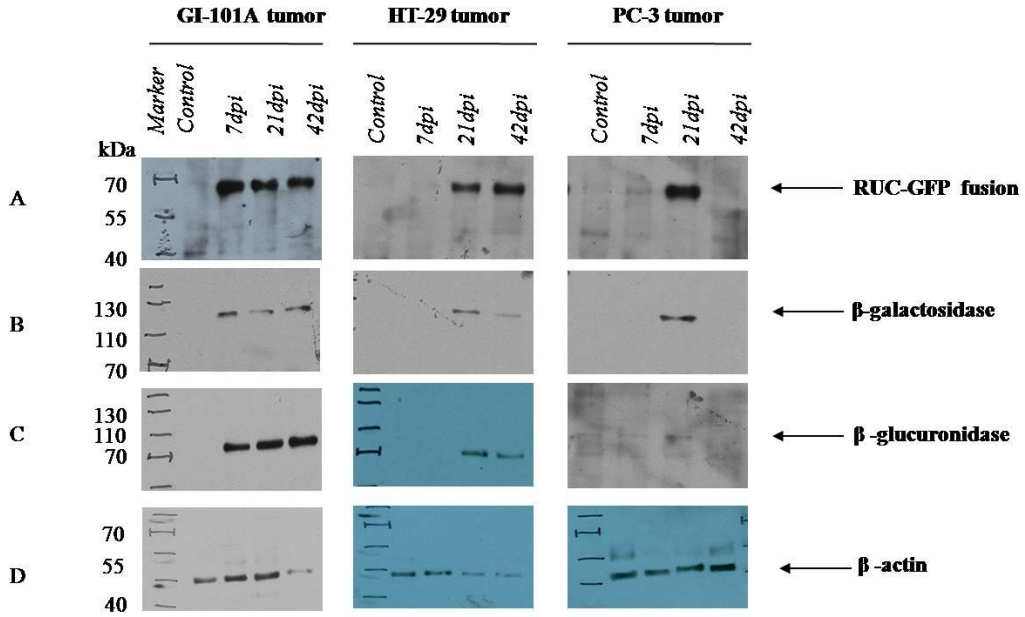

Figure 16. Western-blot detection of marker proteins of GI101, HT-29, PC-3 tumor lysate. RUC-GFP fusion protein(A), β-galactosidase (B), β-glucuronidase (C), β-actin (D), 3s exposure, 15 µg of proteins from lysate of cells infected with VACV GLV-1h68 were separated in SDS-PAGE 10%.

3.2. Growing characteristic of tumor cells non-infected and infected with VACV GLV-1h68

GI-10 1A, PC-3, HT-29 non-infected and infected cells with VACV- 1h68 at MOI 0.5 in the 6-well plate were determine number staining cells with Trypan-blue. Experiment were examined at 0, 4, 8, 12, 24, 36, 48, 60 hpi. With the help of counting chamber, a diagram of live cells and dead cells number was estimated. Figure 17 (G-co) showed result of Trypan-blue staining of non-infected GI-101A cells and elucidate a minor part of dead cells. Whereas live cells number was induced following monitoring time. Thereby, the total cell line and the live cell line were closed identically. At 72 hours maximum of cells achieve $5x10^6$. The figure 17 (G-inf) shows results of Trypan Blue staining of GI-101A cells infected with VACV- 1h68. After infection at 12 hpi, a live cell number was start reduced and dead cell increased notably. Live cell number from $2.3x10^6$ at 24 hpi fall of $1.2\ x10^5$ at 72 hpi.

The figure 18 (H-co) shows result of Trypan Blue staining of non-infected HT-29 cells and determine a minor part of dead cells too. However, live cell line was increased following time point of monitoring until 36 hours only and maximal cell number is 6,08 $x10^6$. After that live cell curve start reducing from 6,08 $x10^6$ and down to 1.74 $x10^6$ at the 72 hours, total cell number and the live cell number were resulted reducing identically, achieved 1,85 $x10^6$. Figure 18 (H-inf) is also results of Trypan Blue staining of HT-29 cells infected with VACV GLV-1h68. After 24 hours of infection, a live cell number was start reduced and there are no cells anymore at 72 hours. The dead cell number was increasing unstable until 40 hpi then decreasing companied the live cell number.

Finally, to determine survival state PC-3 cells with and without infection with VACV-1h68, experimental result gave a diagram of the total, live and dead PC-3 cell non-infected in which they can also remain the maximal number at 36 hours, achieved 2.34 $x10^6$ cells [Figure 19 (P-co)]. Later, PC-3 cells continued to grow insecurely. Figure 19 (P-inf) is results of Trypan Blue staining of PC-3 cells infected with VACV- 1h68. At 12^{th} hours of infection, a live cell number was start reduced and there is nothing at 72 hours. There is few dead cells in each real time of infection, their number was also decreased companied the live cell number.

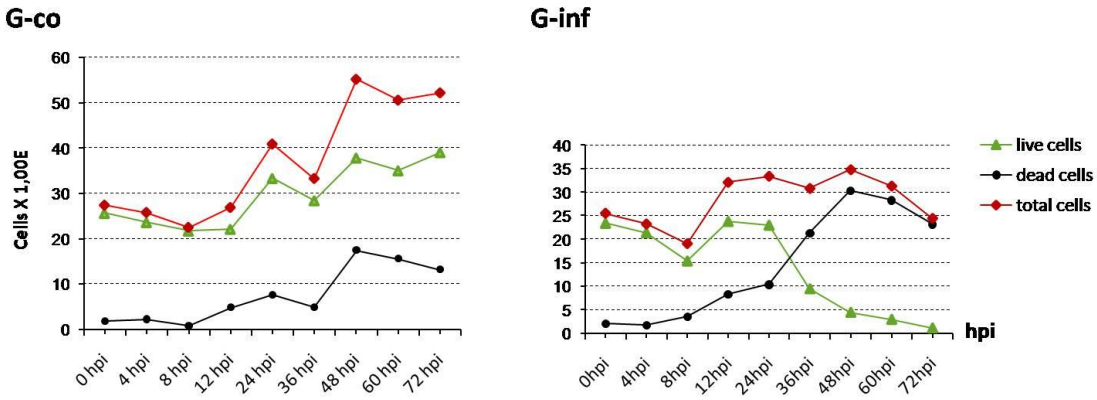

Figure 17. Distribution of live and dead non-infected GI-101A cells (G-co) and infected GI-101A cells (G-inf)

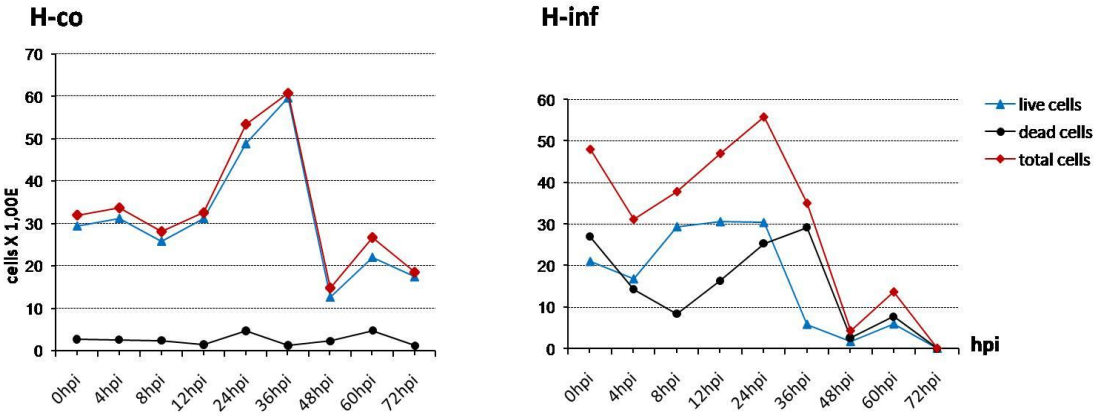

Figure 18. Distribution of live and dead non-infected HT-29 cells (H-co) and infected HT-29 cells (H-inf)

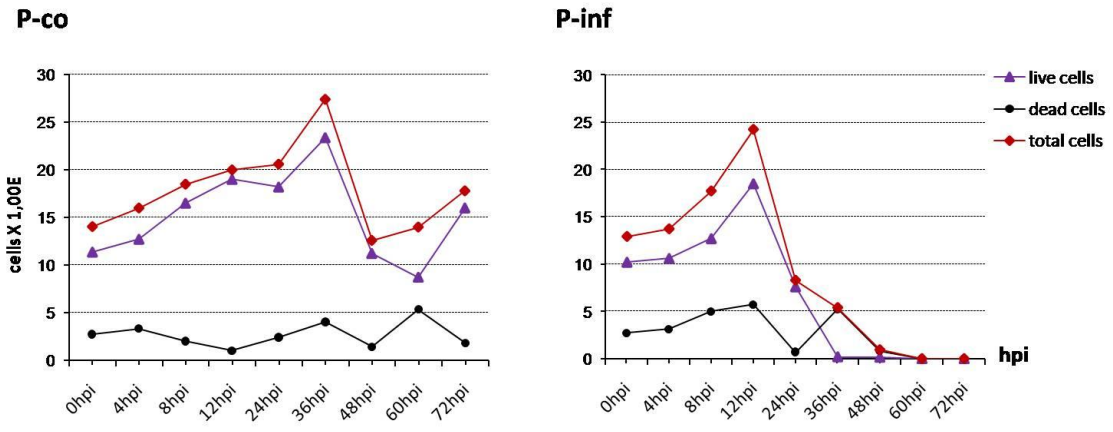

Figure 19. Distribution of live and dead non-infected PC-3 cells (P-co) and infected PC-3 cells (P-inf)

In figure 20, shows the relation of live cell percentage of GI-101A cells, HT-29 cells and PC-3 cells infected with VACV GLV-1h68. This study indicated that a curve of GI-101A cells infected with VACV- 1h68 was most decreased. This result was very different in comparison with HT-29 cells and PC-3 cells infected with VACV GLV-1h68. Therefore, it is evident that VACV- 1h68 virus had more effects on the GI-101A cells in culture than on HT-29 cells or on PC-3 cells.

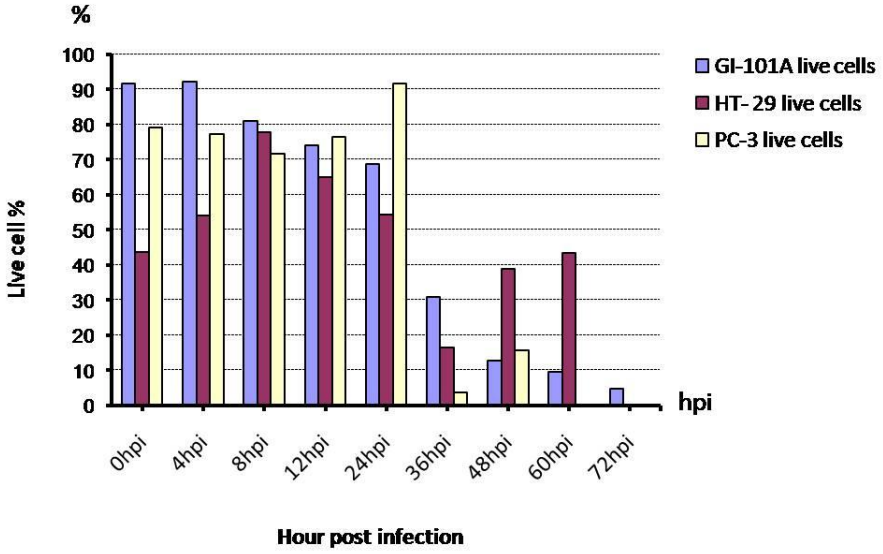

Figure 20. The relation of live cell percentage of cell lines infected with VACV GLV-1h68

3.3 Replication of VACV GLV-1h68 in cell cultures

GI-101A cells, HT-29 cells, PC-3 cells were grown in 24-well plates flat surface until forming a monolayer of cells covering a plastic dish. They were then infected with VACV GLV-1h68 at MOI 0.5. The infection medium was removed, and cells were incubated in fresh growth medium until cell harvest at 0, 4, 8, 12, 24, 36, 48, and 60 h after infection. Viral particles from the infected cells were released by a quick freeze-thaw cycle, and the titers determined as medium (pfu/ml) in duplicate by plaque assay in CV-1 cell monolayers. The liquid growth medium is replaced with a semi-solid one so that any virus particles produced as the result of an infection cannot move far from the site of their production. A plaque is produced when a virus particle infects a cell, replicates, and then kills that cell. Surrounding cells are infected by the newly replicated virus and they too are killed. This process may repeat several times. The cells are then stained with a dye which stains only living cells. The dead cells in the plaque do not stain and appear as unstained areas on a colored background. Each plaque is the result of infection of one cell by one virus followed by replication and spreading of viruses. However, viruses that do not kill cells may not produce plaques.

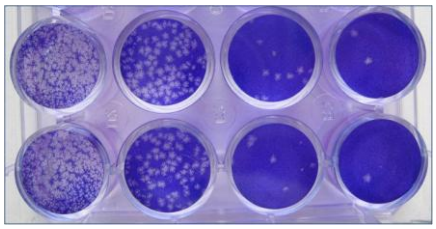

Figure 24. A viral plaques. Serial dilutions of virus have been plated on confluent monolayer cultures of cells. The cells are stained after a period of time in which a single virus infects a cell, produces new virus particles and infects surrounding cells. The white areas show areas of the culture in which the cells have been killed. Each "plaque" is the result of the presence of one original infectious virus particle.

VACV GLV-1h68 indicated its replication capacity in all three cell lines. Compared between GI-101A cell lysate, HT-29 and PC-3 cells infected by VACV GLV-1h68 derivatives showed differential replication in confluent CV-1 cells. That were

approximately one-sixth as efficient at initial hour after virus inoculation for HT-29 cells (3000 plaques/17400 plaques, respectively) and one-second for PC-3 cells (3000 plaques/ 6200 plaques, respectively) (Figure 25). Compared with GI-101A cell supernatant, the infection and replication of VACV GLV-1h68 were very different one-third from those of HT-29 (200 plaques/600 plaques, respectively) but similar to PC-3 cell supernatants (the same 200 plaques), suggesting that the VACV GLV-1h68 affect the entry, replication and egression in PC-3 cells than GI-101A cells and HT-29 cells (Figure 25 A-B-C).

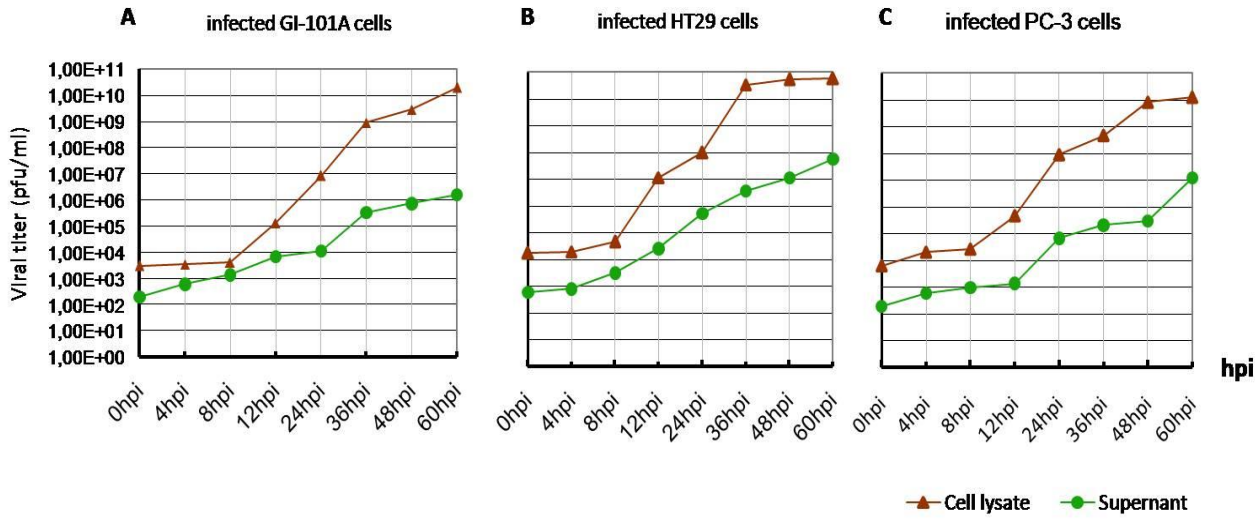

Figure 25. Viral titer of VACV GLV-1h68 in GI-101A infected cells (A), in HT-29 infected cells (B), in PC-3 infected cells (C).

Tissue samples were collected, weighed, dissected and added to 9 times of volume of lysis buffer. The samples were homogenized (or the samples be frozen in liquid N_2 and stored at - 80^{o}C if not used immediately). Tumor homogenisates were centrifuged at 13000rpm for 20 min, aspirate a supernatant for plaque assay. Experiments were performed under the same condition with viral titration of infected cells. Then plaques were calculated within weight of tumor. VACV GLV-1h68 indicated its replication

capacity quite well in all three tumors. After comparison of plaques data between infected GI-101A, HT-29 and PC-3 tumors we found differences in replication. VACV GLV-1h68 replicated most strong in GI-101A tumors. This is shown in the second tumor state and remains stable in the last tumor state. HT-29 tumor does not seem to be a perfect environment for VACV GLV-1h68 compared with GI-101A tumor but virus replication still keeps increasing (Figure 26).

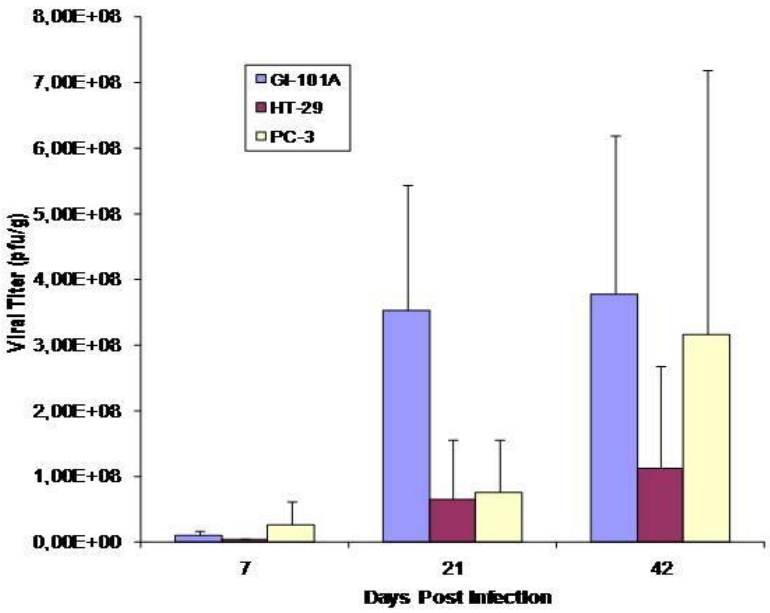

Figure 26. Viral titer in VACV GLV-1h68 infected GI-101A, HT-29, PC-3 tumors at 7, 21, 42 days post infection.

3.4 Enzyme linked immunoabsorbent assays (ELISAs) using a 'two-site' sandwich detection assay for CCL2/MCP-1, CCL5/RANTES and VCAM-1

The growth and progression of tumor cells depend not only on their malignant potential, but also on the multidirectional interactions of secreted substances. Secreted substances are produced by all the cell types including tumor, stroma, endothelial cells, and immune system cells within the local microenvironment (Bonin-Debs et al., 2004). Secreted substances in tumor microenvironment including extracellular matrix are constituted by proteins, receptors, proteoglycans, and adhesive molecules as well as a milieu of secreted proteins including growth factors, angiogenesis factors, proteases cytokines, and chemokines (Wiseman BS and Werb Z 2002; Pupa et al., 2002). It implied that chemokines play a key role in the recruitment of TAMs, (Robinson SC et al., 2003; Leek RD and Harris AL 2002). It has been also established that TAMs have pleiotropic functions, which can influence tumor growth. This differential effect of TAMs is believed to be regulated by modulation of the host immune system (Mills CD et al., 1992; Elgert KD et al., 1998). The influence tumor growth is both in terms of progression and regression. In term of progression, contribute to cancer initiation, proliferation, metastasis due to the immune tolerance, or suppression associated with malignant disease, in this hand, there is convincing data for TAMs demonstrating tumor cell growth-promoting effects through release of various cytokines and prostanoids (Grabbe S et al., 1994; Blachere NE et al., 1997). In term of regression, such as cytotoxic to the tumor cells (Condeelis J 2006; Luo Y 2006)-tumor growth reduction by TAMs can be mediated by non-specific anti-tumor cytotoxic mechanisms or induction of specific cell lytic effects. (Sunderkotter C 1994; Parajuli P and Singh SM 1996). An understanding of the complex regulatory mechanisms, therefore, that control macrophage functions during tumor growth is critical to planning therapeutic approaches to achieving improvement of patient well being and control of the malignant process.

To investigate differences of chemokines CCL2/MCP-1, CCL5/RANTES and VCAM-1 between tumors in the mice untreated and treated with VACV GLV-1h68, we assayed ELISA. The tumor was surgically removed from mice and a tumor extract was prepared in lysis buffer supplemented with protease inhibitor cocktail. Supernatant was kept frozen

at -80 °C until analyzed. Chemokines were determined by using enzyme-linked immunoabsorbent assays (ELISAs). ELISAs is method using a 'two-site' sandwich detection assay, that is, one antibody is used to capture cytokine antigen(s) and another detection antibody, is the most broadly used methods to quantify cytokines in biological matrices because of their acceptable specificity, sensitivity, rapid turnaround time, convenience, the ease of performance. However, a typical ELISA can only measure one cytokine at a time and requires at least 100 µl sample volumes. Quantification of cytokines and chemokines in tumor extract were determined. All experiments were done in, at least, triplicate was determined. We would to determine that how VACV GLV-1h68 injection into mice bearing tumor could change the patterns of cytokines and chemokines within the tumor microenvironment. Results show that in GI- 101A tumor, CCL5 decrease at 7 day post infection nearly 6 folds, while CCL2 decrease at the 21 dpi. For VCAM-1, we did not see differential changes significantly. In the HT-29 tumor, infection effect changes CCL5 level at the last tumor state (2 folds). Variously, CCL2 is decreased at 7 dpi but coming up at 21 dpi 7 folds then notably decrease 9 folds at 42 dpi. For PC-3, CCL5 show decrease at 42dpi, CCL2 increase at 21 dpi. In general, CCL5 and CCL2 seems specific decrease for GI-101A (Table 7, 8, 9).

Table 7. **Chemokine RANTES/CCL5 change** (ng/ml) in the tumor microenvironment of tumor-bearing mice following treatment in control mice or VACV GLV-1h68 mice.

GI101A	Monitoring day	1h68(-)	1h68(+)	Fold Increase
	7 days	91-135	16-22	-5,7
	21 days	16-17	17-20	+1,1
	42 days	106-112	114-138	+1,1
HT29				
	7 days	1,72-1,78	1,8-2,0	+1
	21 days	9,9-10,2	9,9-10,7	+1
	42 days	12,3-13,4	7-9	-1,8
PC3				
	7 days	nd	nd	nd
	21 days	10	10	+1
	42 days	12,5	1,7-2,0	-7,4

Table 8. **Chemokine MCP-1/CCL2 change** (ng/ml) in the tumor microenvironment of tumor-bearing mice following treatment in control mice or VACV GLV-1h68 mice.

GI101A	Monitoring day	1h68(-)	1h68(+)	Fold Increase
	7 days	0,94	0,94-0,97	+1,0
	21 days	1,15-1,28	0,5	-2,3
	42 days	1,47-1,75	1,7	+1,2
HT29				
	7 days	0,41-0,48	0,16	-2,6
	21 days	0,1-0,3	0,7-0,8	+7
	42 days	1,57-1,64	0,2	-8,5
PC3				
	7 days	nd	nd	nd
	21 days	0,1	0,9	+9
	42 days	nd	nd	nd

Table 9. **Chemokine VCAM-1 change** (ng/ml) in the tumor microenvironment of tumor-bearing mice following treatment in control mice or VACV GLV-1h68 mice.

GI101A	Monitoring day	1h68(-)	1h68(+)	Fold Increase
	7 days	63,7	55,6	-1,2
	21 days	53	48	-1,1
	42 days	99	80	-1,2
HT29				
	7 days	60	56	-1,1
	21 days	44	44	+1
	42 days	65	39	-1,7
PC3				
	7 days	nd	nd	nd
	21 days	53	41	-1,3
	42 days	68	65	-1,1

3.5 Two-dimensional gel electrophoresis profiles of infected tumors/cells with VACV GLV-1h68

Total cytosolic soluble protein including nuclear and organellar proteins from cells and tumor tissues were resolved by using 2-DE. During cell lysis, interfering compounds (e.g., proteolytic enzymes, salts, lipids, polysacarides, nucleic acids…) were removed. To prevent protein degradation that otherwise may result in artifactual spots and loss of high molecular weight protein, protease inhibitors was added. TCA/acetone precipitation was used for minimizing protein degradation, for removing interfering compounds, such as salt, or polyphenols, and for the enrichment of very alkaline proteins such as ribosomal proteins from total cell lysates (Görg A and Weiss W 2000).

Initially, the simple method for protein preparation and the linear immobilizing gel pH 3-10 was applied for testing the distributions of GI-101A cell protein, 150 µg of protein from GI-101A cells infected with VACV GLV-1h68 were separated in the first dimension on IPG strips pH 3-10 and in the second dimension on 12.5% SDS-PAGE gels. As show in figure 27 (A), proteins were incompletely separated in 2-DE gels following horizontal direction. This may happen by many low molecular weight proteins extracted from infected cells accumulated in low pH charge field but other places. In this case, it will be difficult for analyse precisely when many proteins would be overlaid with others. Therefore, this would be not helpful within this study framework for first overview to investigate tumor cell protein profiling using the novel oncolytic virus VAVC GLV 1h68.

To overcome overlapping obstacles of using IPG strip pH 3-7, 250 µg of protein were separated in the first dimension on IPG strip pH 4-7 and in the second dimension on *12.5% SDS-PAGE gels*, result in figure 27 (B) shows that protein extracted from GI-101A infected with VACV GLV-1h68, detected by Coomassie blue G-250 staining, exhibited also incompletely separation following vertical direction. This might be caused by SDS-PAGE gradient. *12% SDS-PAGE* gel might not be favourable for separating of high molecular proteins. Separation of GI-101A samples were further continued with 250 µg of protein separated in the first dimension on an IPG strip at pH 4-7 and in the second dimension on softer *SDS-PAGE* gel of 10%, 2-DE gels were detected by Coomassie blue G-250 staining. Noteworthy, result indicated that protein separation reached higher

resolutions [figure 27 (C)]. Finally, a linear gel with an immobilizing *pH gradient of 4-7* and *SDS 10% gel* were chosen to be optimal for protein resolution particularly for the rest of project.

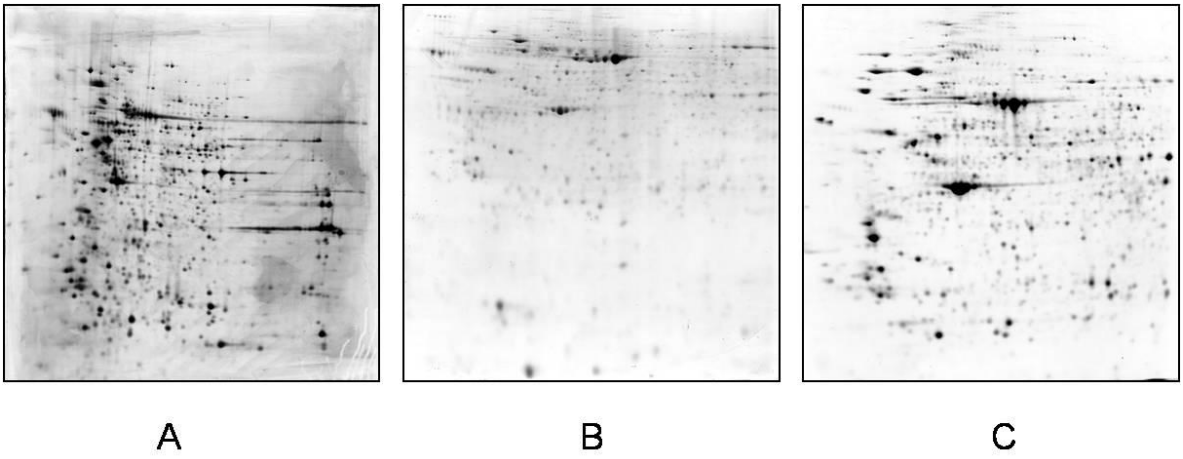

Figure 27. **Selection of optimal 2-DE condition**. 2-DE of protein extracted from GI-101A tumor infected with VACV GLV-1h68. 150 µg of protein were separated in the first dimension on an IPG strip at *pH 3-10* and in the second dimension on a *12.5% SDS-PAGE gels* (A). 2-DE of protein extracted from GI-101A tumor infected with VACV GLV-1h68. 150 µg of protein were separated in the first dimension on an IPG strip at *pH 4-7* and in the second dimension on a *12.5% SDS-PAGE* gel (B). 2-DE of protein extracted from GI-101A tumor infected with VACV GLV 1h68. 250µg of protein were separated in the first dimension on an IPG strip at *pH 4-7* and in the second dimension on a *10% SDS-PAGE gel*. All gels were stained with Coomassie blue G-250 (C).

Although silver staining methods are far more sensitive than Coomassie blue or imidazole-zinc stains (detection limit is as low as 0.1 ng protein/spot). They provide a linear response with over a 0-40 fold range in protein concentration, which is slightly worse than with CBB staining. However, silver staining methods are far from stoichiometric, and are much less reproducible than CBB stains due to the subjective end-point of the staining procedure which makes them less suitable for quantitative analysis. Silver staining methods using aldehyde-based fixatives/sensitizer are the most sensitive ones, but prevent subsequent protein analysis (e.g., by MS) due to protein cross-linkage. Coomassie staining methods have found widespread use for the detection of protein on 2-

DEs, ease of use and compatibility with most subsequent protein analysis and characterization methods such as mass spectrophometry (MS). However, in terms of the requirements for proteome analysis, the principal limitation of CBB stains lies in their insufficient sensitivity, which does not permit the detection of low abundance proteins [the detection limit of Coomassie stains is in the range of 1-10 ng protein per spot (Giovanni Candiano 2004; Brian D Wolf 2007)]. Hence, typically no more than a few hundred protein spots can be visualized on a 2-DE, even if milligram amounts of protein had been loaded onto the gel. For all the reasons, Coomassie staining is still the most appropriate chois of protein identification by MS.

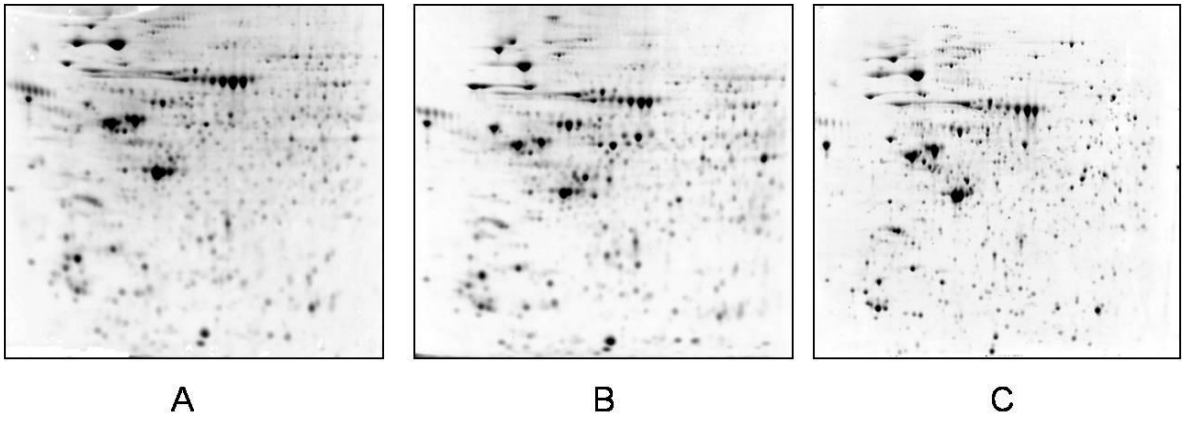

Figure 28. 2-DE of protein extracted from GI-101A cells (A), HT-29 cells (B), PC-3 cells (C)-uninfected. 250 µg of total protein were separated in the first dimension on an IPG strip at pH 4-7 and in the second dimension on a 10% SDS-PAGE gel. Gel was stained with Coomassie blue G-250.

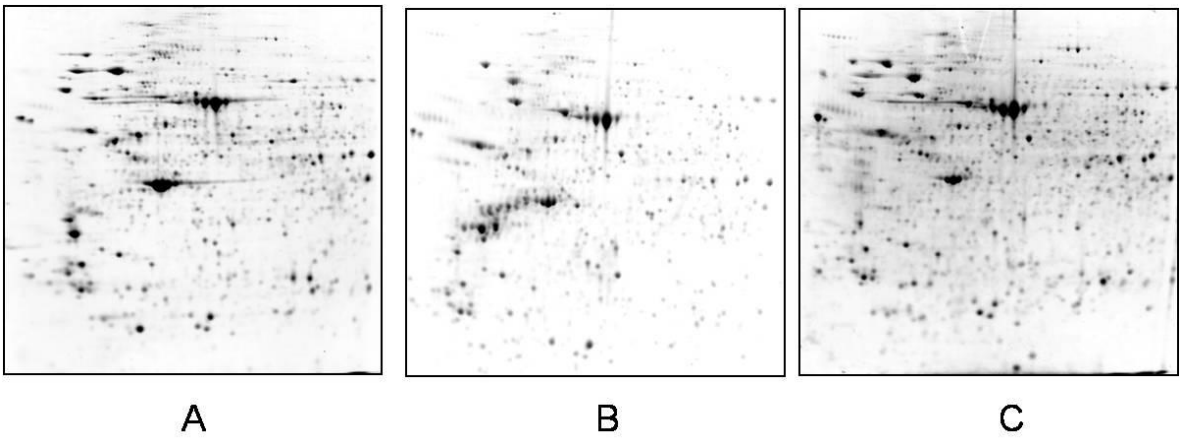

Figure 29. 2-DE of protein extracted from un-infected GI-101A tumor (A), HT-29 tumor (B), PC-3 tumor (C). 250 µg of protein were separated in the first dimension on an IPG strip at pH 4-7 and in the second dimension on a 10% SDS-PAGE gel. Gel was stained with Coomassie blue G-250.

Around 700, 500, 800, 850, 900, 950 individual protein spots from GI-101A cells, HT-29 cells, PC-3 cells, GI-101A tumor, HT-29 tumor, PC-3 tumor, respectively, were detected in 2-DE gels. All visible protein spots were excised by both automatically and manually and subjected to MS/MS analysis. Results of identification by MS/MS data were scored by the Mascot programs, and the top-scoring gene products were considered to be the corresponding proteins.

By using Delta2D software which can match correlative spots between infected gels with infected gels of the same cell or tumor species, we showed analysis of proteomic differences between early and advanced stages of infection. Protein spots of uninfected cell/tumor were marked in green. Infected one with VACV GLV-1h68 was marked in red. The protein expression difference was illustrated by the dual channel images of 2-DEs. Although recent modern 2-DE research often utilizes software-base image analysis tools. Incompletely separated (overlapping spots), less-defined and/or separated (weak spots/noise e.g., “ghost spots”), running differences between gels (e.g., protein migrates to different positions on different gels), differences in software algorithms and therefore affect the analysis tendencies.

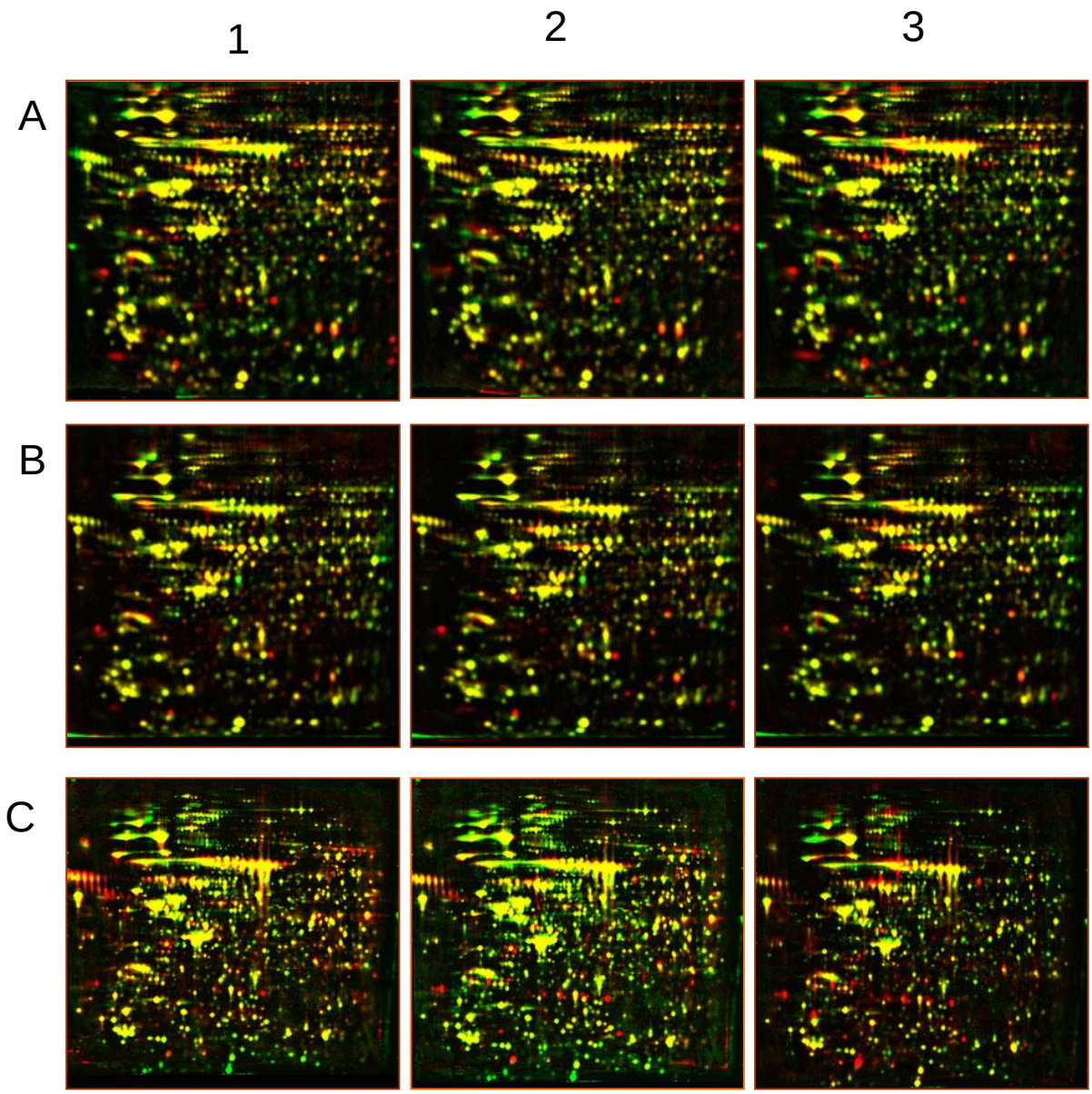

Figure 30. Differential protein expression in infected cells. Row A1, A2, A3: The differences of protein pattern of the GI-101A uninfected cells (green) and infected cells with VACV GLV-1h68 (red) at 12, 24, 48 hpi, respectively. Row B1, B2, B3 are those of HT-29 cell and C1, C2, C3 are those of PC-3 cell, respectively.

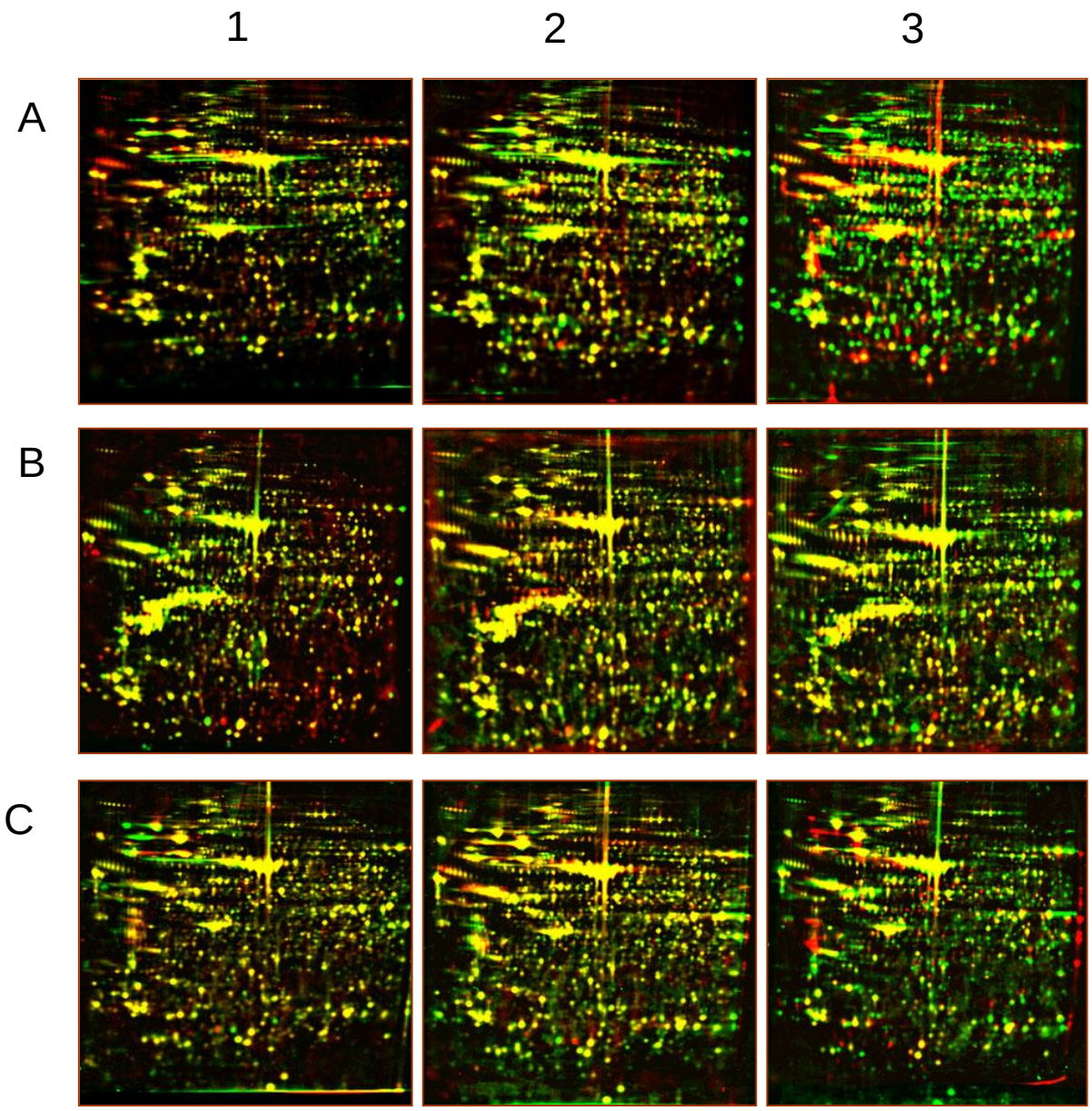

Figure 31. **Differential protein expression in infected tumors.** Row A1, A2, A3: The differences of protein pattern of the GI-101A uninfected tumor (green) and infected tumors with VACV GLV-1h68 (red) at 12, 24, 48 hpi, respectively. Row B1, B2, B3 are those of HT-29 and C1, C2, C3 are those of PC-3, respectively.

There are 436 protein spots excised from GI-101A cell culture, 423 protein spots were excised from HT-29 culture, 591 protein spots were excised from PC-3 cell cultivation

project, 597 protein spots were excised from GI-101A tumor xenograft project, 615 protein spots were excised from HT-29 tumor xenograft project, 542 protein spots were excised from PC-3 tumor xenograft project. The spots obtained were subjected to trypsin digestion for subsequent MALDI-TOF analysis.

Infection of virus produces a general shut off of protein synthesis, for example affects to the Vero cells infected with African swine fever virus increased up to 65% of cellular proteins (314). To investigate cellular proteins whose synthesis and changes were enhanced by VACV GLV-1h68 infection, we focused on proteins that are probably significant to the cellular response to infection particularly in tumor cells. Several changes in the analyzed cellular protein patterns during the infection were observed by 2-DE analysis.

3.5.1 Comparison of differential protein expression

3.5.1.1 Comparison of differential protein expression in VACV GLV-1h68 uninfected and infected GI-101A cells

To obtain a detailed comparison of the differences in protein expression profiles, the protein lysates extracted from GI101-A cells infected with VACV GLV-1h68 at 12 h, 24 h and 48 hpi and GI101-A control were separated on the 2-DE for analysis. Spot number was observed about 580 to 670. In this experiment, very little obvious changes were observed in the number of spots of the detectable proteins in controls compared with infected protein spots (from 539 to 611 spots at 12 hpi, 671 at 24 hpi and 583 at 48 hpi) (Figure 38). Total of 436 major protein spots among them were excised automatically and manually from gels and subjected to trypsin digestion for subsequence MALDI-TOF analysis, including 225 spots among them were labelled (Figure 32). Some proteins were separated in two or three spots on the 2-DE (called “multiple spots”), that why there are 178 individual protein spots were counted (30 up-regulated, 38 down-regulated and 110 equal protein spots).

On the basis of average intensity ratios of protein spots, a total of 76 protein spots were found to be dynamically changed by infection, including 30 significantly up-regulated

protein spots (ratio infection/control ≥ 2). Among this 30 up-regulated protein spots including spots shown increasing in one state of infection but decreasing in other states (Table 3). There are 38 significantly down-regulated protein spots (ratio infection/control ≤ 0.5) (Table 3). As shown in table 1, 13 protein spots showed signs of up-regulation at 12 hpi, there are more 17 protein spots were up-regulated at 24 hpi and remains 11 protein spots were up-regulated at 24 hpi. There are 4 protein spots which remains were up- regulated at 48 hpi from 12 hpi and 24 hpi. 15 protein spots were remained up-regulated at 48 hpi from 24 hpi and 3 protein spots are observed up- regulated at 48 hpi only.

Among 38 down regulated, 20 protein spots showed signs of decreasing at 12 hpi. There is no evidence showed about down-regulated protein spots at 24 hpi. That pointed out proteins identified at 24 hpi are equal and up-regulated proteins. Among that down-regulated proteins at 12 hpi, 13 protein spots displayed continuously decrease at 48 hpi. 4 spots almost completely inhibition at 48 hpi. In general, the majority of protein expression changes appeared at 48 hours post infection.

3.5.1.2 Comparison of differential protein expression in VACV GLV-1h68 infected GI-101A tumors

To determine a difference in GI-101A tumor protein expression profile, subcutaneous GI-101A tumors in nude mice with and without VACV GLV-1h68 treatment were taken 7, 21 and 42 days after virus intravenous injection. The protein lysate extracted from VACV GLV-1h68 infected GI101-A tumors was separated on the 2-DE for analysis. Spot number was observed about 449 to 861. In this study, obvious changes were observed at 42 dpi. Remarkably, the spot number in infected samples about half of the control ones, (Figure 39). Total of 597 major protein spots were excised automatically and manually from GI-101A tumor gels and subjected to trypsin digestion for subsequence MALDI-TOF analysis, 368 spots among them were labelled. Many of the same proteins were separated in two, three or four spots on the 2-DE, they may be results of post-translational modification during infection. Therefore, 178 individual protein spots were identified from 368 labelled (Figure 33).

In the same basis comparison of the average intensity ratios of protein spots analysis through the study, a total of 295 protein spots were found to be dynamically changed in GI101-A tissue tumors, including 103 significantly up-regulated protein spots, and 192 significantly suppression protein spots showed in table 1.

As shown in table 1, 49 protein spots showed signs of up-regulation at 7 dpi, including 20 human protein and 29 mouse protein spots. There are more 17 protein spots were up-regulated at 21 dpi and remains 10 protein spots were up-regulated at 42 dpi from 7 dpi and 21 dpi. They are all mouse protein spots, 6 spots are unknown proteins. All of them are shown most intensive at the last infection time point. 22 protein spots were coming at 21 dpi. The rest 27 protein spots just up-regulated at 42 dpi only. In general, the majority of protein expression changes about enhancement appeared at 42 day post infection.

Total 36 human up-regulated spots including 31 individual protein, and 53 individual mouse protein among 66 mouse protein spots were found.

Among 192 the down-regulated spots, 30 protein spots observed at 7 dpi (4 protein spots displayed decreasing at 21 and 42 dpi, 4 protein spots continue decreasing then stop down- regulation a 21 dpi. 16 other spots start their decreasing at 21 dpi and remains down- regulated at 42 dpi, including 12 human protein spots and 9 human protein spots. At 42 dpi, there are 184 of down-regulated proteins spots (observed 50% in total spots in GI-101A tumor profile), 130 human spots and 54 mouse spots.

3.5.1.3 Comparison of differential protein expression in VACV GLV-1h68 uninfected and infected HT-29 cells

To investigate the effects of oncolytic VACV GLV-1h68 on different tumor cell lines we performed experiments in human tumor colon HT-29 cell line. In the 2-DE analysis, spot number observed were about 440 to 500. There were some changes were observed in number of spots in the controls compared with infected protein spots at 12 hpi (Figure 38). Total of 423 major protein spots among them were excised automatically and manually from HT-29 cell gels and subjected to trypsin digestion for subsequence MALDI-TOF analysis, 238 spots were labelled (Figure 34). Some proteins were separated in two or three spots o the 2-DE and 176 individual protein spots were counted.

Table 5 shows total of 82 protein spots were found to be dynamically changed in HT-29 cells infected with VACV GLV-1h68, including 25 significantly up-regulated protein spots (ratio infection/control ≥ 2) and 57 significantly down-regulated protein spots (ratio infection/control ≤ 0.5). As shown in table 5 of the up-regulated proteins in infected HT-29, 18 protein spots showed signs of up-regulation at 12 hpi , there are 5 more protein spots up-regulated at 24 hpi but 5 spots do not change at 24 hpi. There are 12 protein spots which remained up- regulated at 48 hpi from 12 hpi and 24 hpi. 2 protein spots were observed up-regulated at 48 hpi only.

16 protein spots were found showing signs of down-regulation at 12 hpi, 12 spots continued to decrease at 48 hpi. 3 spots showed almost reduction at 48 hpi. Other 29 showed signs of a decrease at 48 hpi only.

3.5.1.4 Comparison of differential protein expression in VACV GLV-1h68 infected HT-29 tumors

To determine differences in HT-29 tumor protein expression profile, subcutaneous HT-29 tumors were generated in nude mice with and without VACV GLV-1h68 treatment. Tumors were harvested at 7, 21 and 42 days after VACV GLV-1h68 intravenous injection. Spot number observed were about 662 to 881. In this study, obvious decrease changes were observed in the number of spots of the detectable protein in controls compared with infected tumor protein spots also at late tumor state (42 dpi) (Figure 39). About 615 major protein spots were excised from HT-29 tumor gels. 264 spots among them were identified and labelled (Figure 35).

Table 2 shows that total of 129 protein spots were found to be dynamically changed in HT-29 tissue tumors. They include 57 human protein spots and 72 mouse spots. Many of the same proteins were separated in two, three or four spots on the 2-DE, that explains why there are 92 individual protein spots counted. 62 protein spots showed signs of up-regulation at 7 dpi, which included 33 human protein and 29 mouse protein spots. 16 protein spots were up-regulated at 21 dpi and 15 protein spots remained up-regulated at 24 dpi. 7 of them are human protein spots. There are only 9 protein spots which were coming up at 42 dpi. 4 spots just from 21 dpi and 5 other spots continued show a signs of

down-regulation from 7, 21 dpi. In general, the majority of protein expression changes occurred at 7 day post infection.

Among the down- regulated proteins, 24 protein spots were observed at 7 dpi, 25 at 21 dpi and 42 at 42 dpi. Among 42 down-regulated spots at 42 dpi, there were 8 spots that showed a signs of decrease very early at 7 dpi, 3 spots started a decrease at 21 dpi and remained their low concentration levels at 42 dpi.

3.5.1.5 Comparison of differential protein expression in VACV GLV-1h68 infected PC-3 cells

The growth, development and function of the prostate gland are dependent of the presence of hormone, i.e. androgens. This hormone can be converted in the prostate by enzymes (i.e. 5α-reductase). Prostate cancers as well as prostate cells require the presence of androgens to survive. To determine how VACV GLV-1h68 interacts with prostate cancer cells, proteomic analysis was performed. Protein lysates extracted from infected and uninfected PC-3 cells at 12 h, 24 h and 48 hpi were separated in the 2-DE for analysis. Spot number observed to be about 530 to 780. A few obvious changes were determined at 48 hpi (Figure 38). Total of 591 major protein spots were excised automatically and manually from PC-3-3 cell gels and subjected to trypsin digestion for subsequence MALDI-TOF analysis, including 322 spots among them were ladled (Figure 36). Some proteins were separated in two or three spots on the 2-DE and 268 individual protein spots counted.

On the basis of the average intensity ratios of protein spots, a total of 181 protein spots were found to be dynamically changed in PC-3 cells infected with VACV GLV-1h68 (ratio infection/control ≥ 2) (Table 6). 29 spots showed signs of up-regulation at 12 hpi, there are 15 more protein spots up-regulated at 24 hpi but 6 spots slowed up-regulation at 24 hpi. There are 16 protein spots which remained up-regulated at 48 hpi through 12 hpi and 24 hpi. 10 protein spots were observed to be up-regulated at 48 hpi only.

There are 57 spots which showed a sign of down-regulation at 12 hpi, 57 at 24 hpi and 107 at 48 hpi.

Among 107 protein spots were signs of down-regulation at 48 hpi, 50 spots continued to decrease up to 48 hpi from 12 hpi and 24 hpi. 13 spots started to be inhibited at 24 hpi and continued to decrease at 48 hpi. 19 spots showed almost complete inhibition at 48 hpi. Other 54 showed signs of a decrease at 48 hpi only. In general, the majority of protein expression changes appeared at 48 hours post infection.

3.5.1.6 Comparison of differential protein expression in VACV GLV-1h68 infected PC-3 tumors

In PC-3 tumor protein expression profile, spot number was observed about 553 to 945. In this study, decreasing changes were observed in each time point of infection (Figure 39). Total of 542 major protein spots were excised for trypsin digestion and for subsequence MALDI-TOF analysis, 162 spots among them were labelled (Figure 37). Total of 101 protein spots were found to be dynamically changed in PC-3 tissue tumors (Table 3). Many the same proteins were separated in two, three even four spots on the 2-DE, that explains why there are 69 individual protein spots counted.

In infected PC-3 tumors, at 7 dpi no evidence was shown in protein increase. We found 15 proteins started to increase their amount at 21 dpi but stopped to be enhanced at 41 dpi. While 30 protein spots were enhanced at the late of infection time (42 dpi), 19 spots of them gave evidence for equal or to be down-regulated at early infection time.

19 protein spots showed down-regulation at 7 dpi, also 19 at 21 dpi and 52 at 42 dpi. There are 21 spots showed complete disappearance at 42 dpi. In general, the majority of protein expression was found to be down-regulated at 42 days post infection.

3.5.2 Comparison of regulated and modified reproducibly identified upon VACV GLV-1h68 infection

Proteins that reproducibly regulated differentially or modified upon VACV GLV-1h68 infection of the indicate cells/tumor were sorted according to their cellular function, the identified cellular proteins were involved in the viral proteins, in cytoskeleton, in stress

response, in translation , in RNA processing, in ubiquitin-proteasome pathway (UPP), in signal transduction, and in metabolic enzymes (Table 1-6).

In VACV GLV-1h68 infected GI-101A cells

In GI-101A cell protein profiling, the percentage of up-regulated and down-regulated protein spots was 44% and 56%, respectively. Thirty-four up-regulated spots corresponded to the following 30 proteins: 10 viral proteins (33,3%), 3 cytoskeletal proteins (10,0%), 3 macromolecular biosynthesis proteins which including translation associated and RNA processing (10,0%), 10 metabolism associated and transport proteins (33,3%) and 2 signal transduction proteins (6,7%) (Figure 41, 42). Some obviously up-regulated proteins are cytosolic malate dehydrogenase (H-MDH1), Rho GTPase activating protein 1 (H-Arhgap1) (Table 4)

11 viral proteins were identified produced by VACV GLV-1h68 very clear during infection in infected GI-101A cells. As well as infected GI-101A cells, viral proteins were also identified produced in infected HT-29 and PC-3 cells. Surprisingly, in infected HT-29 cells, infected PC-3 cells, VACV GLV-1h68 replicate strongly with evidence of the protein differential expression almost over than 5 folds. Particularly, enzymes like a serine protease inhibitor-like SPI-1 (V-C12L) as known as enzymes belong to serpin family, this viral protein may be involved in the regulation of the complement cascade (315). This protein is strongly increasing in all three infected cell lines. Other protein, dsRNA-dependent PK inhibitor (V-E3L), found increase in GI-101A and HT-29 infected cells, this protein may inhibit protein synthesis by phosphorylating of eukaryotic cell for its own protein synthesis, using ribonucleotide reductase [(Ribonucleoside-diphosphate reductase (V-I4L)] encoded by vaccinia virus as a model for the mammalian enzyme (316). In this study, V-I4L was found greatly increase in HT-29 and PC-3 infected cells. Vaccinia virus A6L (V-A6L) encodes a virion core protein required for formation of mature virion (317) shows up-regulated in three infected cells. We could not find viral proteins in infected tumors. Perhaps that viral protein amount was not enough for MS detection or they might be modificated and digested by host enzymes in tumor environmental. (Table 4, 5, 6 and figure 40A-B-C).

Fourty two down-regulated spots corresponded to the following 38 proteins: 4 cytoskeletal proteins (10,5%), 8 stress response (21,1%), 5 macromolecular biosynthesis proteins which including translation associated and RNA processing (13,2%), 4 ubiquitin proteasome pathway (10,5%), 9 metabolism associated and transport proteins (23,7%) and 5 signal transduction proteins (13,2%). Strongly down-regulated proteins are heat shock 70kDa protein 1A variant (H-hsp701a), proteasome activator subunit 2 (H-PSME2) (Figure 42).

In VACV GLV-1h68 infected GI-101A tumors

The percentage of up-regulated and down-regulated protein spots was 33% and 67%, respectively. 103 human and mouse up-regulated spots corresponded to the following 89 individual proteins: 10 cytoskeletal proteins (11,2%), 8 macromolecular biosynthesis proteins which including translation associated and RNA processing (9%), 18 metabolism associated and transport proteins (20,2%), 13 signal transduction proteins (14,6%) and 29,2% other proteins (Figure 41).

Recently it was reported that adenylate kinase-1 (M-ADK1) knockout mice (AK-/-) exhibit elevated rates of glucose uptake following repeated contractions and hypoxia (318), it is interesting to find that M-ADK1 in infected GI-101A cells strongly up-regulated in the intermediate tumor phase. Or up-regulated mouse ferritin heavy chain M-Fth1, this protein stores iron in a soluble, non-toxic, readily available form, important for iron homeostasis, has ferroxidase act, iron is taken up in the ferrous form and deposited as ferric hydroxides after oxidation. Some more other protein show strongly up-regulated in GI-101A infected cells like as mouse vimentin (M-Vim), prolyl endopeptidase (H-PREP) ceruloplasmin isoform b (M-Ceru), ferritin heavy chain 1 (M-Fth1), Ferritin light chain 1 (M-Ftl1), cathepsin Z (M-Ctsz), fibrinogen, B beta polypeptide (M-Fibrb), HMW kininogen-I variant (M-KngnI), serine (or cysteine) peptidase inhibitor, clade A, member 3K (M-SPIC3K), thrombospondin (M-Thbs). Otherwise, many unknown proteins strongly increasing in infected GI-101A tumor were identified. Most of them are proteins with molecular mass from 20 to 70 kD (Table 1).

191 human and mouse down-regulated spots corresponded to the following 181 proteins: 19 cytoskeletal proteins (10,5%), 17 stress response (9,4%), 19 macromolecular biosynthesis proteins which including translation associated and RNA processing (10,5%), 8 ubiquitin proteasome pathway (4,4%), 48 metabolism associated and transport proteins (26,5%) and 14 signal transduction proteins (7,7%), 36 unknown proteins (19,9%) (Figure 42). In particular, many proteins were inhibited in the late stages of VACV GLV-1H68 infection such as 3-phosphoglycerate dehydrogenase (H-PHGDH), acetyl-Coenzyme A acetyltransferase 2 (H-Acat2), Acidic ribosomal phosphoprotein P0 (M-ARPP0), Adenosine kinase (H-AK), aldehyde dehydrogenase 1A3 (H-ALD1A3), aspartyl-tRNA synthetase (H-AspS), brain glycogen phosphorylase (H-Pygb), chaperonin containing TCP1 (H-CCT2, H-CCT6a, H-CCT8) (Table 1)

In VACV GLV-1h68 infected HT-29 cells

The percentage of up-regulated and down-regulated protein spots was 29% and 71%, respectively. 25 human up-regulated spots corresponded to the following 23 individual proteins: 10 viral proteins (43,5%), 3 cytoskeletal proteins (13,0%), 3 stress reponse (13,0%), 4 metabolism associated and transport proteins (17,4%) (Figure 41).
Proteins show strongly up-regulated in HT-29 infected cells like as heat shock 70kDa protein 8 isoform 2 (H-hsp708), keratin 1 (H-Krt1), KRT8 protein (H-Krt8) (Table 5).
57 down-regulated spots corresponded to the following 52 proteins: 2 cytoskeletal proteins (3,8%), 4 stress response (7,7%), 5 macromolecular biosynthesis proteins which including translation associated and RNA processing (9,6%), 23 metabolism associated and transport proteins (44,2%) and 7 signal transduction proteins (13,5%) (Figure 42).
Some cytoskeleton proteins show obviously down-regulated such as actin, gamma 1 propeptide (H-ACTG), ARP1 actin-related protein 1 homolog A, centractin alpha (H-ARP1). Strongly decreased proteins are annexin A13 isoform b (H-A13B), hypothetical protein (H-Hyp) (Table 5).

In VACV GLV-1h68 infected HT-29 tumors

The percentage of up-regulated and down-regulated protein spots was 69,3% and 30,7%, respectively. 82 human and mouse up-regulated spots corresponded to the following 70 individual proteins: 1 viral proteins (1,4%), 9 cytoskeletal proteins (12,9%), 3 stress reponse (4,3%), 22 metabolism associated and transport proteins (31,4%), 8 signal transduction (11,4%) (Figure 41).

Proteins show strongly up-regulated in HT-29 infected tumors like as keratin 20 (H-Krt20), peroxiredoxin (H-PRDX2, H-PRDX3, H-PRDX4), RAB14, member RAS oncogene family (M-RAB), proteasome (M-PSMA1, M-PSMD7). In this profiling, elongation factor 2 (M-EF2), TALDO1 protein (H-Tal1), IDI1 protein (H-IDI1), Triosephosphate Isomerase (H-TPI1) shown significant increased in the first tumor state but strong down in the late tumor state (Table 2).

42 down-regulated spots corresponded to the following 31 proteins: 4 cytoskeletal proteins (13,3%), 1 stress response (3,3%) 2 macromolecular biosynthesis proteins which including translation associated and RNA processing (6,6%), 8 metabolism associated and transport proteins (26,7%) and other proteins (20%) (Figure 42).

Protein show obviously down-regulated is albumin 1 (M-Alb1). While Elongation factor 2 (M-EF2), M-ENO3, Ig gamma-1 chain C region (15C5) - mouse (fragment) (M-IgGc) express up-regulated in the early state and inhibited in the last state (Table 2).

In VACV GLV-1h68 infected PC-3 cells

The percentage of up-regulated and down-regulated protein spots was 30,8% and 69,2%, respectively. 54 human up-regulated spots corresponded to the following 49 individual proteins: 11 viral proteins (22,4%), 6 cytoskeletal proteins (12,2%), 2 stress reponse (4,1%), 8 macromolecular biosynthesis proteins which including translation associated and RNA processing (16,3%), 12 metabolism associated and transport proteins (24,5%), 3 signal transduction (6,1%) (Figure 41).

Proteins show strongly up-regulated in PC-3 infected cells like as tropomyosin 3 isoform 2 (H-Tpm3), DNA replication licensing factor MCM4, CCT2 (H-TCP1), PPA1 protein (H-PPA1), many proteins in the RNA process, COMT protein (H-COMT). Keratin group shows up-regulated in the last infection time. (Table 6).

127 down-regulated spots corresponded to the following 110 proteins: 13 cytoskeletal proteins (11,8%), 11 stress response (10%), 13 macromolecular biosynthesis proteins which including translation associated and RNA processing (11,8%), 37 metabolism associated and transport proteins (33,6%) and 16 other proteins (14,5%) (Figure 42).
Proteins show obviously down-regulated are L-plastin variant (H-LCP1), group of actins (H-ActB, H-ActG, H-ACTN4), heat shock 70kDa proteins (H-Hsp704, H-hsp708, H-HSP90), oxygen regulated protein precursor (H-Orp), eukaryotic translation initiation factor 4B (H-EIF4B), ubiquitin activating enzyme E1(H-UBE1), dipeptidylpeptidase 9 (H-DPP9Ê) (Table 6).

In VACV GLV-1h68 infected PC-3 tumors

The percentage of up-regulated and down-regulated protein spots was 44% and 56%, respectively. 45 human and mouse up-regulated spots corresponded to the following 40 individual proteins: 2 cytoskeletal proteins (5%), 3 stress reponse (7,5%), 10 macromolecular biosynthesis proteins which including translation associated and RNA processing (10%), 8 metabolism associated and transport proteins (20%), 8 signal transduction (20%) and 14 unknown proteins (35%) (Figure 41).
Proteins show strongly up-regulated in PC-3 infected tumors like calreticulin (H-Calr), Chain A, Crystal Structure Of 14-3-3 Gamma In Complex With A Phosphoserine Peptide (H-1433G), apolipoprotein A-I (M-ApoA1) show up-regulated at 7dpi but down-regulated at 42dpi (Table 3).
56 down-regulated spots corresponded to the following 51 proteins: 6 cytoskeletal proteins (11,8%), 4 stress response (7,8%), 4 macromolecular biosynthesis proteins which including translation associated and RNA processing (7,8%), 12 metabolism associated and transport proteins (23,5%) and 16 unknown proteins (31,4%) (Figure 42).
Proteins show obviously down-regulated are BiP protein (H-BiP), HSP90AA1 protein (H-HSP90AA1), EBNA-2 co-activator variant (H-p100), enolase 1 variant (H-Eno1), epsilon subunit of coatomer protein complex isoform c (H-COPE), Ferritin light chain 1 (M-Ftl1), Rho GDP dissociation inhibitor (GDI) alpha (H-GDIa), vinculin isoform meta-VCL (H-mVCL), 3 unknown proteins with molecular mass of 50-70 kD (Table 3).

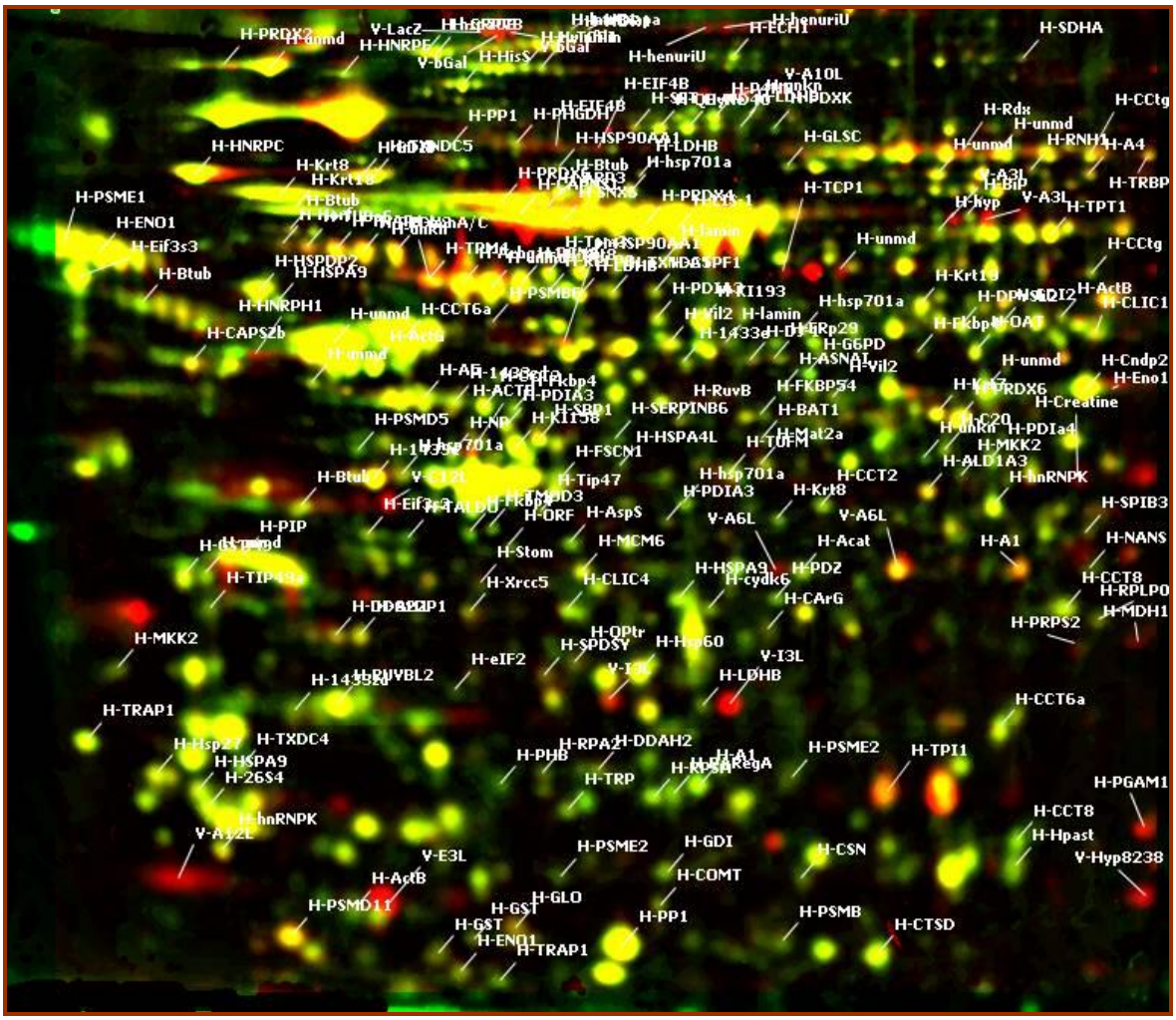

Figure 32. **The differences in protein patterns of GI-101A cell** uninfected (green) and VACV GLV-1h68 infected GI-101A cells (red) were illustrated by the Dual channel images of 2D-gels produced with Delta 2D Software.

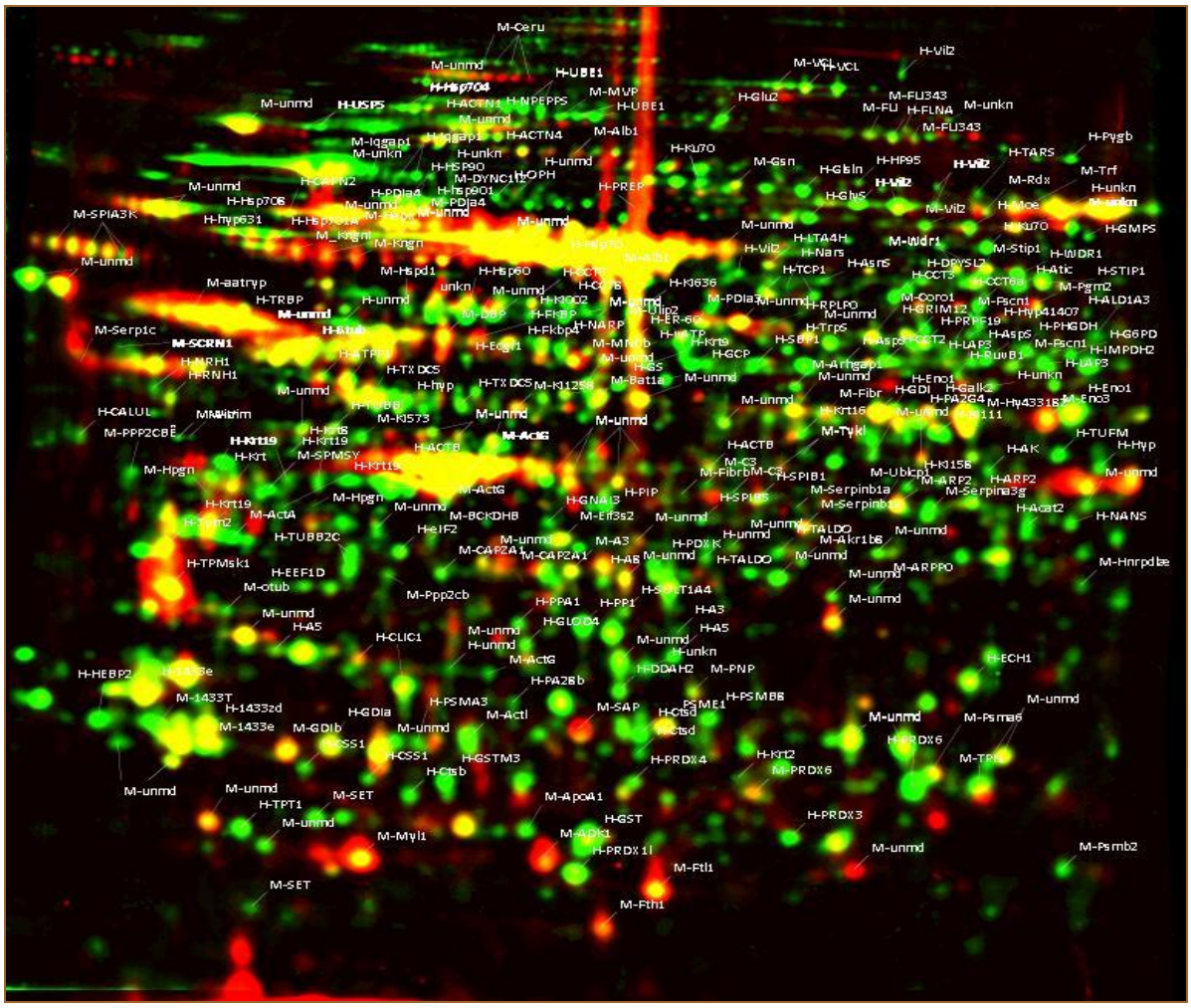

Figure 33. **The differences in protein patterns of GI-101A tumor** uninfected (green) and the GI-101A tumor infected with VACV GLV-1h68 (red) were illustrated by the Dual channel images of 2D-gels produced with Delta 2D Software.

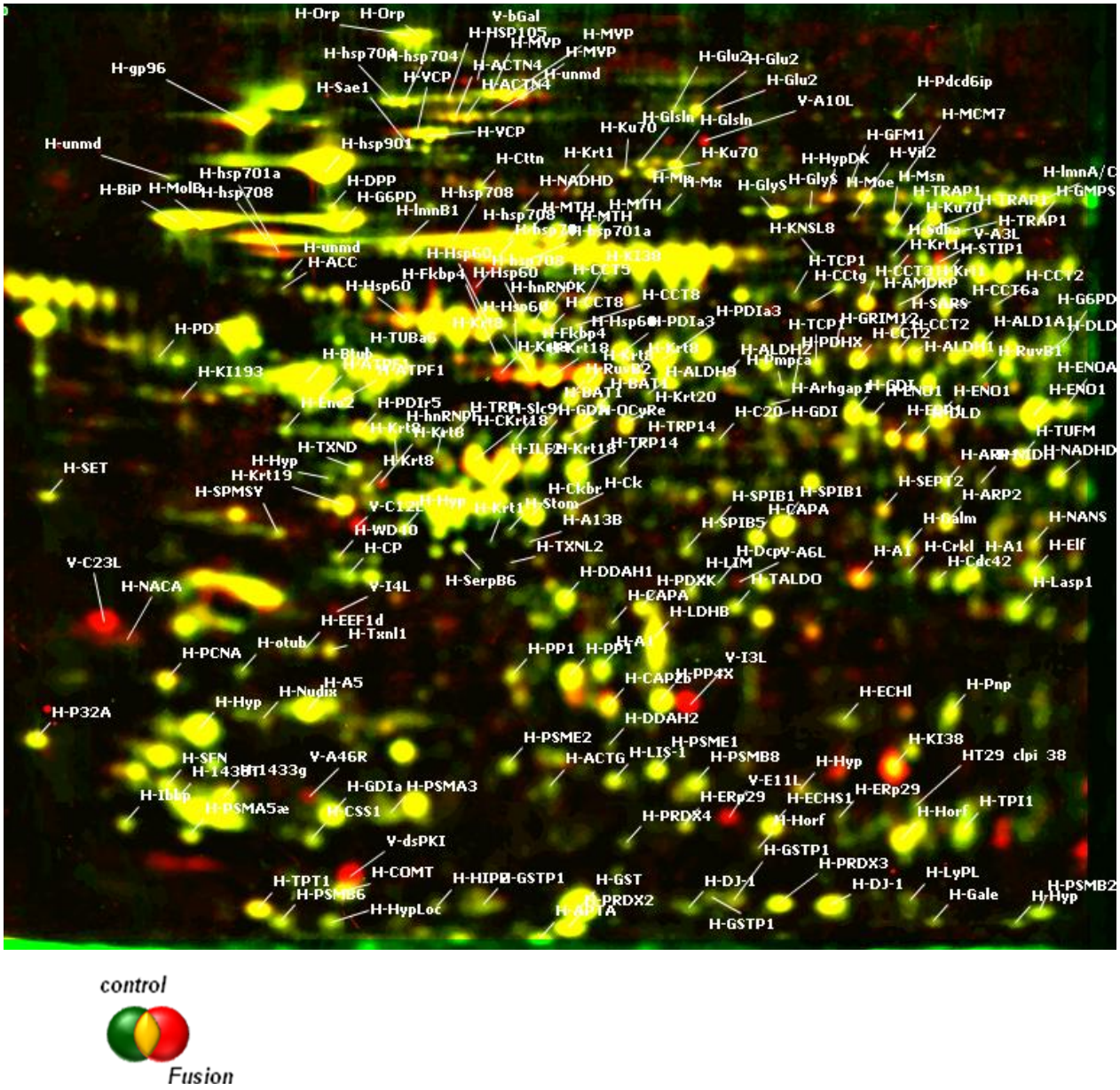

Figure 34. **The differences in protein patterns** of uninfected **HT-29 cells** (green) and VACV GLV-1h68 infected **HT-29 cells** (red) were illustrated by the Dual channel images of 2D-gels produced with Delta 2D Software.

Figure 35. **The differences in protein patterns** of **HT-29 tumor** uninfected (green) and the HT-29 tumor infected with VACV GLV-1h68 (red) were illustrated by the Dual channel images of 2D-gels produced with Delta 2D Software.

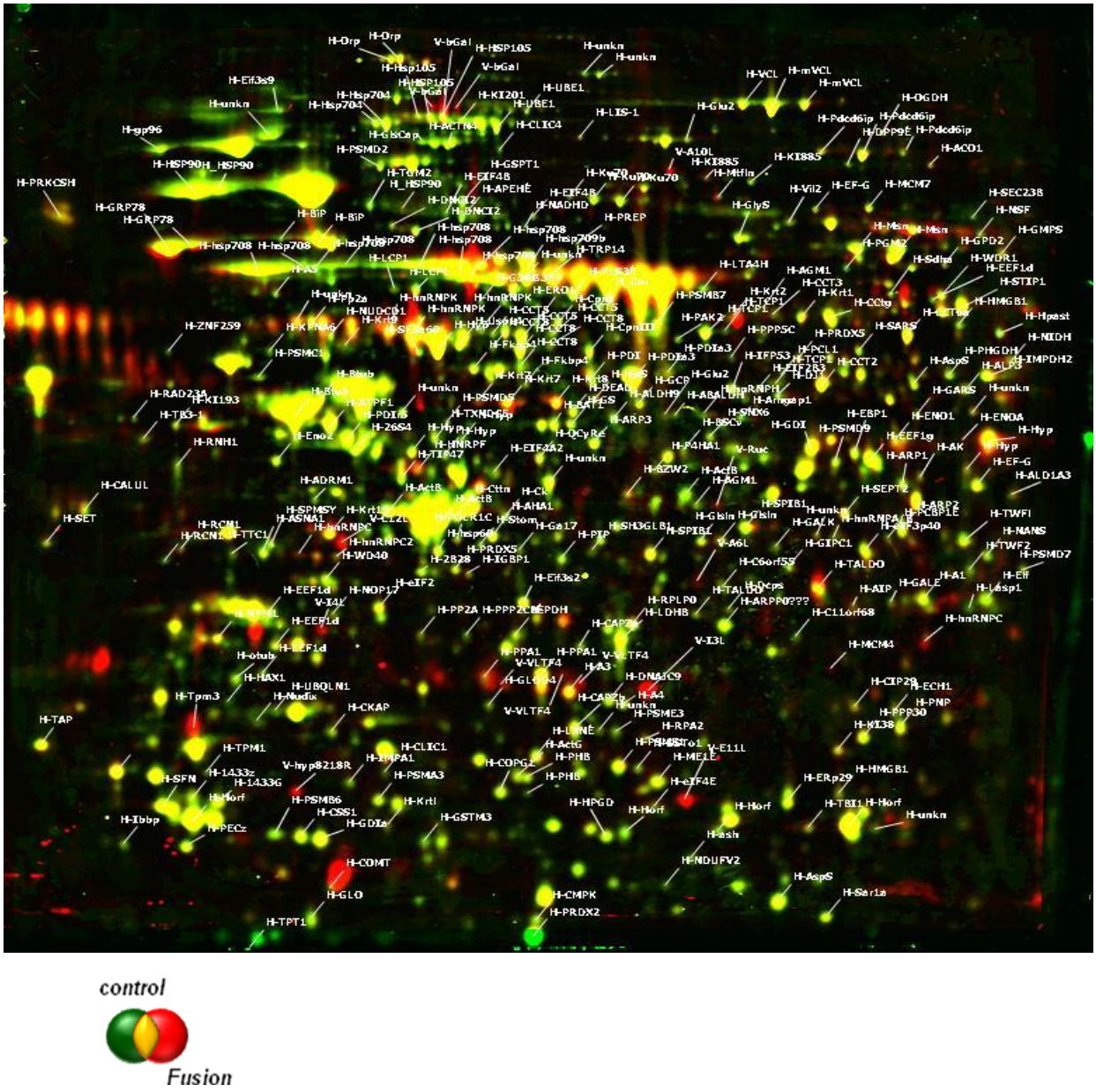

Figure 36. **The differences in protein pattern** of **PC-3 cells** uninfected (green) and the PC-3 cells infected VACV GLV-1h68 (red) were illustrated by the Dual channel images of 2D-gels produced with Delta 2D Software.

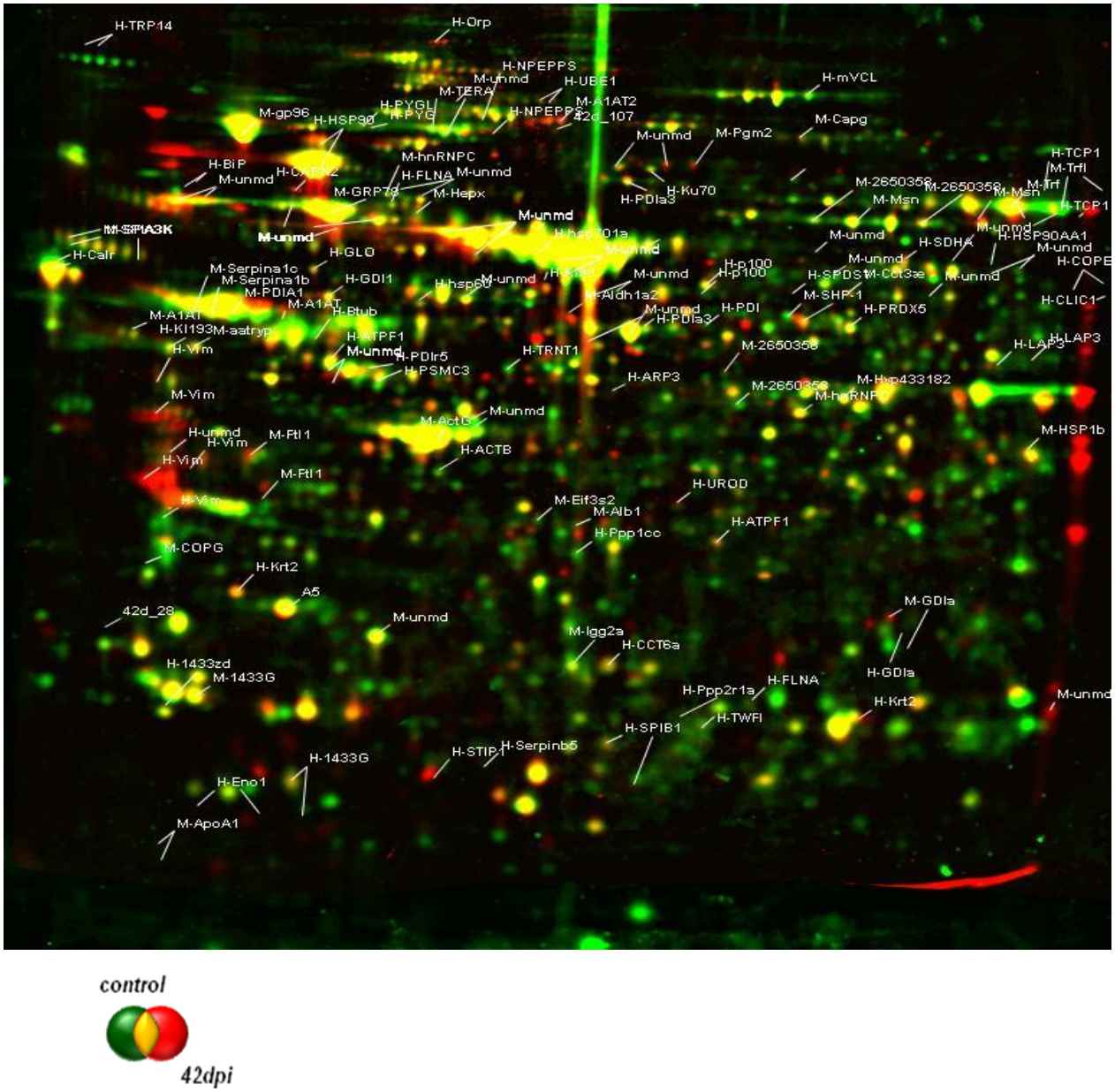

control

42dpi

Figure 37. **The differences in protein patterns** of **PC-3 tumor** uninfected (green) and the PC-3 tumor infected with VACV GLV-1h68 (red) were illustrated by the Dual channel images of 2D-gels produced with Delta 2D Software.

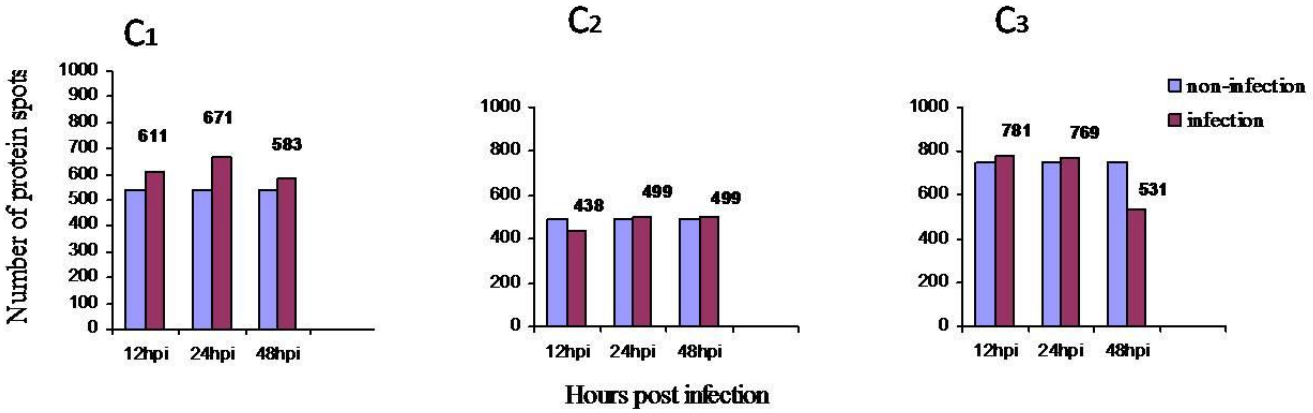

Figure 38. Protein spots number in infected cells. Protein spots number of VACV GLV-1h68 infected GI101-A cells separated in 2-DE (A), infected HT-29 cells (B), infected PC-3 cells (C).

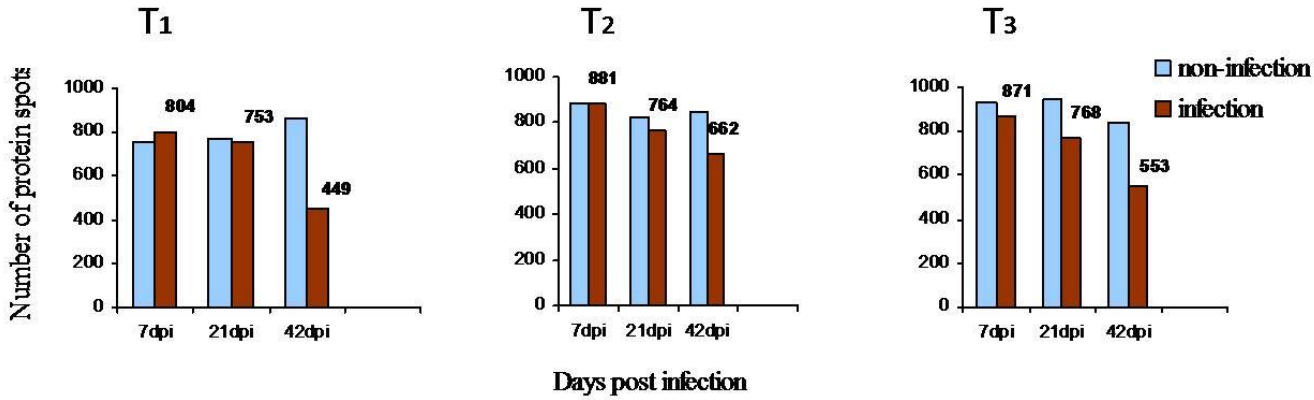

Figure 39. Protein spots number in infected tumors. Protein spots number of VACV GLV-1h68 infected GI101-A tumors separated in 2-DE (A), infected HT-29 tumors (B), infected PC-3 tumors (C).

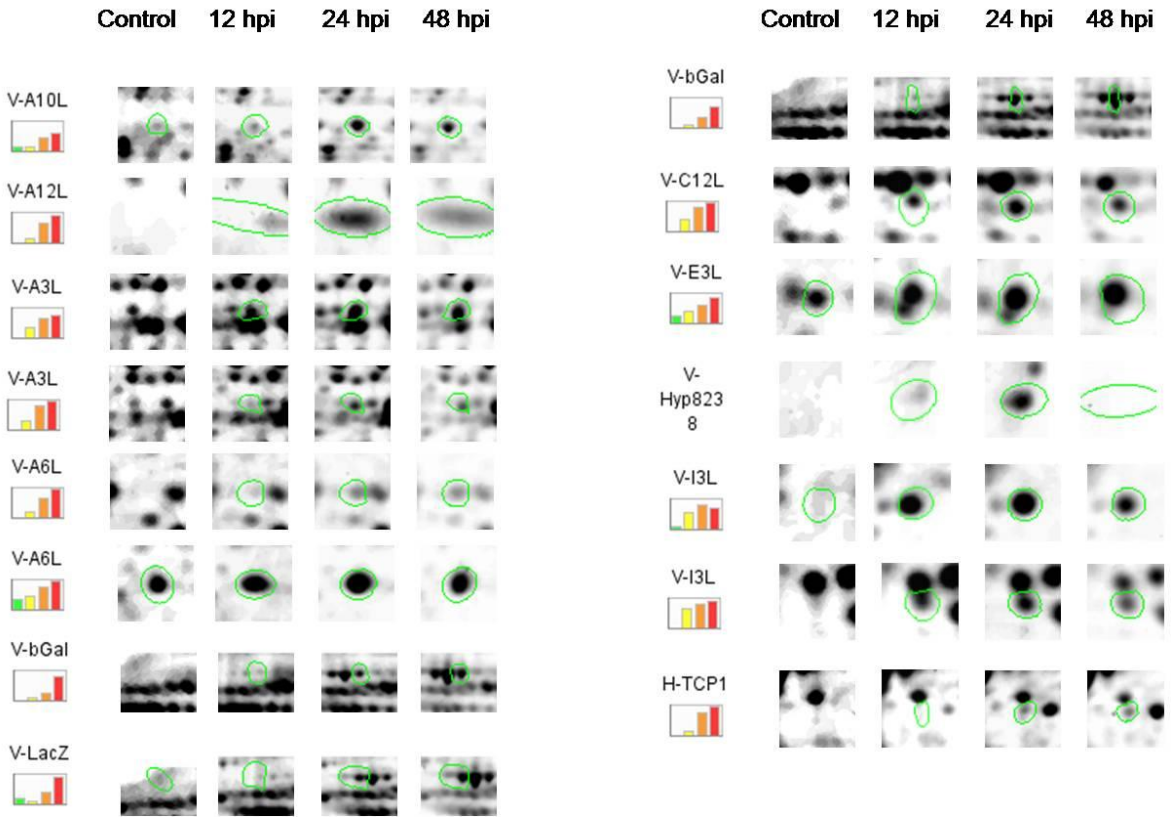

Figure 40A. Viral protein expression in the infected GI-101A cells separated in 2-DE

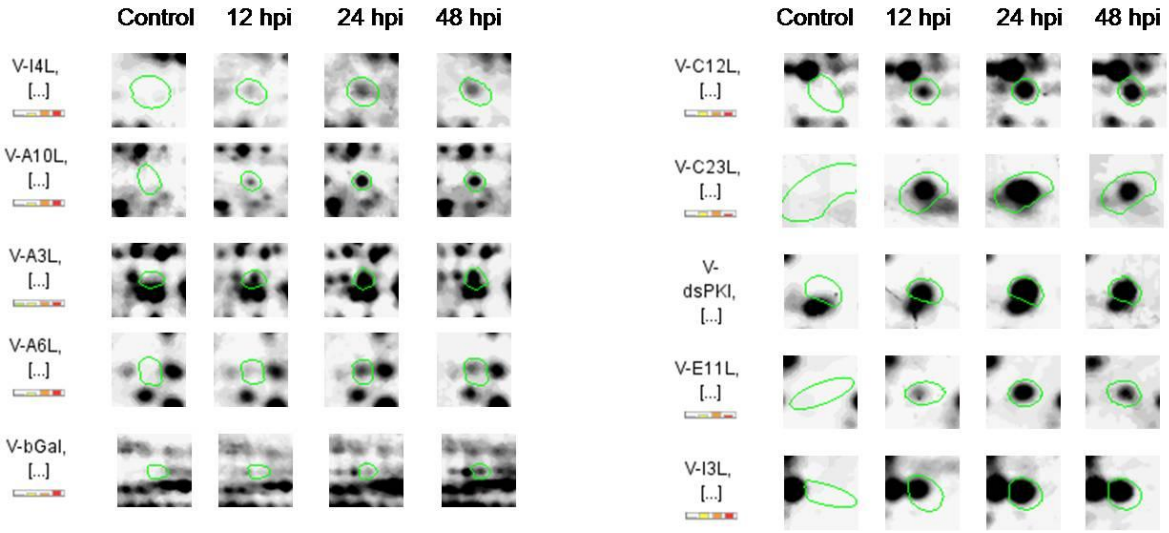

Figure 40B. Viral protein expression in the infected HT-29 cells separated in 2-DE

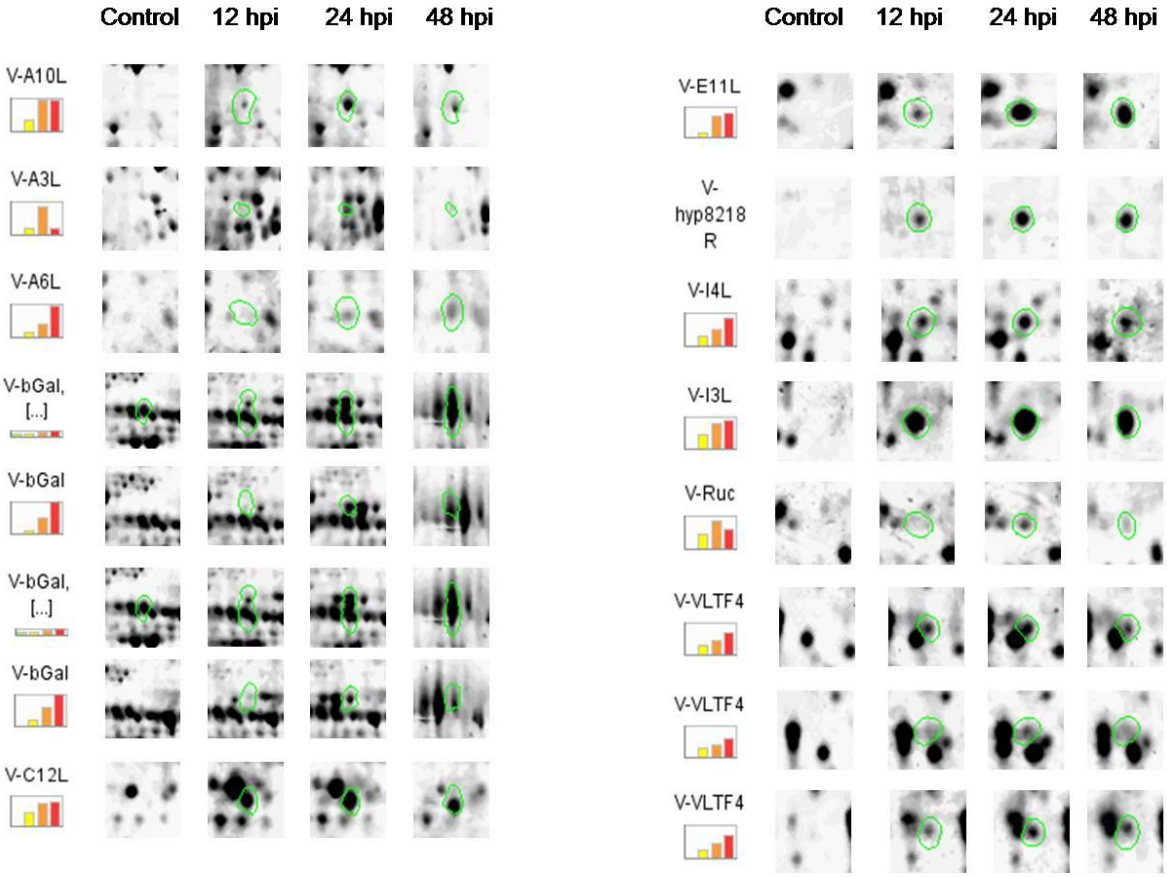

Figure 40C. Viral protein expression in the infected PC-3 cells separated in 2-DE

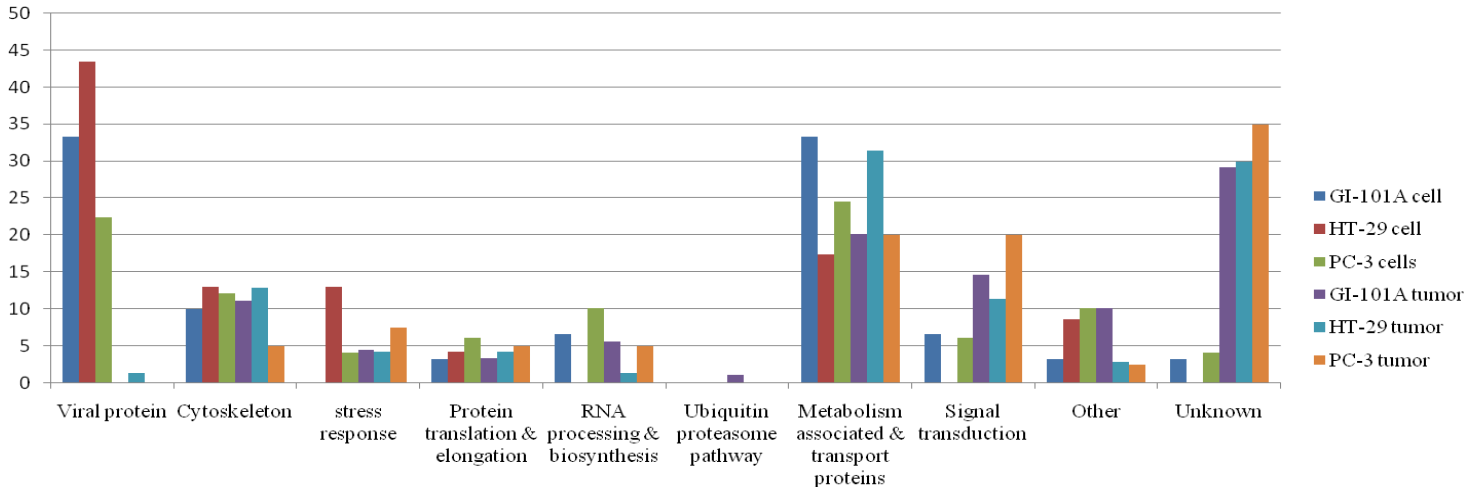

Figure 41. **Functional classification of up-regulated proteins spots in the human tumor cells with and without VAVC GLV-1h68 treatment**; time points were taken 12, 24 and 48 hours after virus infected cells and subcutaneous tumors in nude mice with and without VAVC GLV-1h68 treatment; time point were taken 7, 21 and 42 days after virus intravenous injection; >2 fold of enhancement of protein expression after virus treatment were considered.

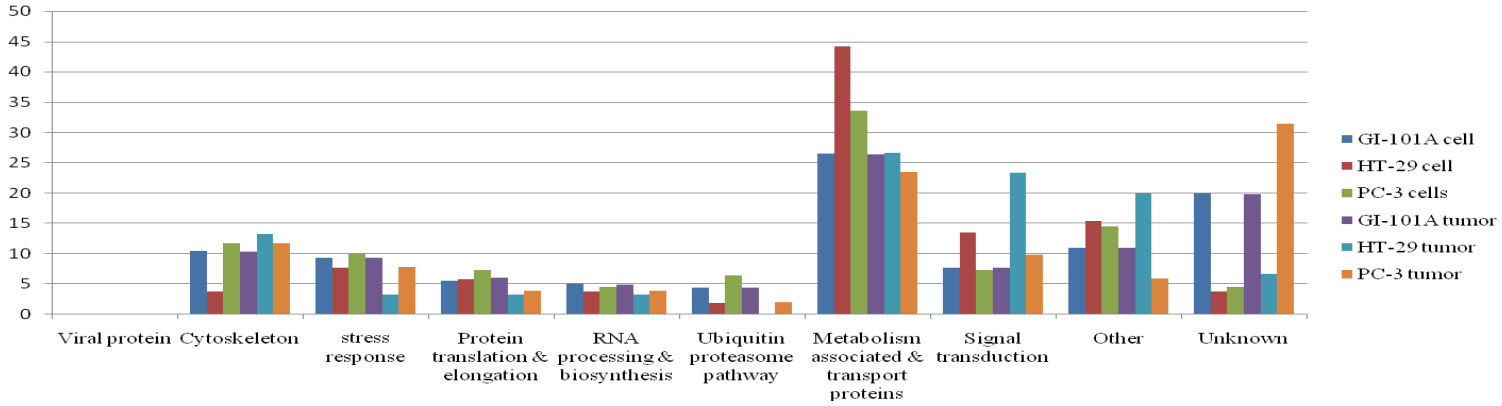

Figure 42. **Functional classification of down-regulated proteins spots in the human tumor cell lines with and without VAVC GLV-1h68 treatment;** time points were taken 12, 24 and 48 hours after virus infected cells and subcutaneous tumors in nude mice with and without VAVC GLV-1h68 treatment; time point were taken 7, 21 and 42 days after virus intravenous injection; >2 fold of reduction of protein expression after virus treatment were considered.

DISCUSSION

In this study, increasing evidence emphasizes comparative proteomics to screen the differentially expressed proteins associated with host tumor cellular responded processes of virus infection (Seet BT. and McFadden G. 2002). From the literature, it appears that very few studies have been performed to analyze the interplay between vaccinia virus and host cells using proteomic analysis. In our study, we obtained a dynamic overview of the altered protein expression of tumor cells responding to VACV GLV-1h68. The identified cellular proteins function in translational regulation, UPP, cytoskeleton organization, signal transduction, stress response, macromolecular biosynthesis, and as metabolic enzymes (Table 1, 2, 3, 4, 5, 6). In general, in the cell lines, the proteins found to be differentially regulated are most often associated with metabolic processes, in particular with primary energy metabolism (glucose catabolism, TCA and lactate production). In tumors, the responses cover a much broader panel of cellular processes, including signalling (e.g., cell death), transport (in particular of iron ions) and migration. A common pathway to be upregulated in both tumors and cell lines is the "unfolded protein response".

4.1 VACV GLV-1h68 infection hijacking of the host translation apparatus

In practical terms, it would be important to understand what is changed insight tumors where VACV GLV-1h68 replicate specifictly. Then some tumors could be eliminated through viral oncolysis, while others are resistant. It appears that the degree of viral replication *in vivo* is a key determinant. Protein data in this study indicated that protein profile changes associated with viral replication precede tumor destruction by a

substantial amount of time. For instance, viral replication was quite active at day 21 and keeping their growth before tumor shrinkage at day 42 for GI-101A xenografts (regressive tumors); at the same late time significant shut down of cancer cell metabolism and simultaneous activation of the mouse response (Table 1).

Interestingly, homo sapiens eukaryotic translation initiation factor 2, subunit 1 alpha, 36kDa (*H-eIF2*) is part of the heterotrimeric complex eIF2, which in a GTP-bound form binds methionyl-initiator tRNA (Met-tRNAMeti) is a eukaryotic translation initiation factor that participates in cap-dependent translation by binding the initiator tRNA to the 40S ribosomal subunit (Merrick, W. C. 2004) and plays a central role in the maintenance of a rate-limiting step in cellular mRNA translation (Kimball, S. R. 1999). The reported data showed that the host translational machinery was turned off by down-regulating EIF4A2 in cells infected with influenza virus type A, poliovirus, herpes simplex virus, and enterovirus 71 (Leong, P. W. et al., 2002; Kuyumcu-Martinez, N. M. et al., 2004). One of the best characterized mechanisms for regulating protein synthesis is the reversible phosphorylation of the a subunit of eukaryotic protein synthesis initiation factor 2, eIF2α (Hershey, J. W. B. 1993; Merrick, W. C. 1992). Phosphorylation of eIF2α increases the stability of complexes formed between eIF2α and eIF-2B (Safer, B. 1983). Since *eIF-2B* is required for the exchange of GDP for GTP in the recycling of *eIF2* in the formation of the eIF2-GTP Met-tRNA ternary complex and exists in cells in relatively low molar quantities with respect to eIF2, phosphorylation of only a limited amount (i.e., 20-25%) of eIF2α is sufficient to sequester virtually all of the eIF-2B, resulting in inhibition of protein synthesis (Safer, B. 1983). Interestingly, *H-eIF2α* was considerably down-regulated in VACV GLV-1h68 infected GI-101A cells and tumor xenografts (Table 1, 4). Hence, this may be inferred that VACV GLV-1h68 turns off the host translational machinery for initiating its viral translation in infected cells by down-regulating eIF2α but not EIF4A2.

A number of cellular stress conditions, such as perturbation in calcium homeostasis or redox status, elevated secretory protein synthesis, expression of misfolded proteins, sugar/glucose deprivation, altered glycosylation, and overloading of cholesterol can interfere with oxidative protein folding and subsequently lead to accumulation of unfolded or misfolded proteins in the ER lumen, which constitutes a fundamental threat

to the cells. The ER has evolved highly specific signaling pathways to alter transcriptional and translational programs to cope with the accumulation of unfolded or misfolded proteins in the ER lumen. This adaptive response, which couples the ER protein folding load with the ER protein folding capacity, is termed the unfolded protein response (UPR) (David Ron. 2002; Patil C. and Walter P. 2001). A transient inhibition of protein synthesis occurs during the unfold protein response (UPR), which is achieved by activation of PKR-like endoplasmic reticulum (ER) kinase (PERK) that phosphorylates eIF2α (Harding, H. P. et al., 1999; Shi, Y. et al. 1998). Among other things, this leads to the loss of cyclin D1 from cells (Brewer, J. W. and Diehl, J. A. 2000), causing a G1 arrest that prevents the propagation of cells experiencing ER stress. Paradoxically, the block in translation specifically allows the activating transcription factor 4 (ATF4) to be synthesized (Brewer, J. W. and Diehl, J. A. 2000) and transactivate downstream genes, like GADD34 (Ma, Y. and Hendershot, L. M. 2003), which is the regulatory subunit of the PP1 phosphatase that acts on *eIF2α* and reverses the translation arrest, and C/EBP-homologous protein (CHOP) (Ma, Y. et al., 2002), which has been implicated in apoptosis. Evidence of down-regulated eIF2α could be explained for inhibiting tumor follow apoptosis branch which could contribute for GI-101A tumor regression.

Among protein differentially expressed in the GI-101A xenografts from VACV GLV-1h68 infected animals, the large majority were down-regulated, particularly, in xenografts excised at day 42 suggesting that viral replication depresses cellular metabolism (Table 1).

Comparison of GI-101A xenografts differential protein expression identified, which involve in anti-apoptosis mediate pathway in the tumor cells, they conclude 12 proteins down regulated. Among them, including positive regulatiton *NK-αB* (*H-PRDX3*, *H-PRDX4*), signal transduction *H-GDIa* (*Rho GDP dissociation inhibitor (GDI) alpha*), *H-eIF2* (*Eukaryotic translation initiation factor 2, subunit 1 alpha, 35kDa*), *H-A1 (Annexin A1), H-A5 (annexin A5), M-1433T (Ywhaq protein),* other metabolism and transport proteins *H-TPT1 (Tumor protein, translationally-controlled), M-Ppp2cb (Similar to Serine/threonine-protein), phosphatase 2A catalytic subunit beta isoform (PP2A), H-ACTN1 (Actinin, alpha 1), H-DDAH2 (Dimethylarginine dimethylaminohydrolase 2), M-Alb1 (Mouse albumin 1).* In contrast, group of protease

inhibitors show up-regulated (*M-KngnI, M-SPIA3K, H-SPIB5, M-Serp1c)* (Table 1). What does role of protease inhibitor in tumor? In *in vitro* study demonstrate that combination of ER stress and proteasome inhibitors greatly promoted the destructive elements of the UPR, including *CASPASE-12* cleavage and apoptosis. Proteasome inhibitors are being used to successfully treat patients with multiple myeloma (Adams, J. 2004). Although proteasome inhibitors have a myriad of effects including a weak activation of the UPR, and it has not been demonstrated that the UPR is activated in myeloma cells, it is possible that an unbalanced stress response in these cells could contribute to tumor death. These studies would support for evidence of regressing in GI-101A xenografts by down regulated proteasome inhibitor level. Unfortunately, in the HT-29 xenografts (non-responding), proteins which involved in anti-apoptosis pathway and protease inhibitor group show to be actually opposite difference. In principle, ER stress has been implicated in, and could potentially have opposing roles during, several different stages of tumor development. During early tumorigenesis and before angiogenesis occurs, activation of UPR could activate the unfolded protein response (UPR) then induce a G1 arrest and activate p38, both of which would promote a dormant state. If the apoptotic branches of the UPR are also activated during this stage of tumor development, cancer cells will be selected that have mutated elements of the apoptotic machinery to evade the alternative fate of death. ER stress also induces anti-apoptotic *NF-κB* and inhibits p53-dependent apoptotic signals. If the balance of early cancer development tilts against cell death, ER stress can further promote the aggressive growth of these cancer cells by enhancing their angiogenic ability, for example through GRP170 induction and increased vascular endothelial growth factor (*VEGF*) secretion. In HT-29 xenografts situation, combination of high anti-apoptosis related proteins level and the low proteasome inhibition protein level with changing of cellular metabolism process which occurs in the early tumor phase (7 dpi). VACV GLV-1h68 replication was even activated at 21 dpi but metabolism process changes insight infected tumors tend to adverse physiological condition. In PC-3 xenografts (non regressing), where we could see the differential protein expression model of deceasing anti-apoptosis and increase of proteasome inhibitors seems similar to GI-101A xenogaft. This would be suggest that protein profile changes associated with viral replication precede tumor destruction slower

than GI-101A tumors, somehow PC-3 xenografts can resist longer from structural collapse. It is appropriate that investigation on cytoskeletal proteins, there are 20 dow-regulated cytoskeletal proteins in GI-101A tumor. On the contrary, only 7 cytoskeletal proteins were found to be dow-regulated express by HT-29 and PC-3 xenografts from infected compared to non-infected animals.

4.2 Alteration of cytoskeleton networks

Studied GI-101A tumors, revealed features on microfilament-associated and microtubule-associated proteins that many actin and tubulin proteins were up-regulated (*H-ACTB, H-Btub, H-FLNA, H-Krt2, H-Krt8, H-LRPPRC, M-Myl1, M-Vim)* whereas *Microfilament-associated proteins (H-ACTN1, H-ARP2, H-Glsln, H-Moe, H-Tpm2, H-TUBB2C*) were down-regulated (Table 1). Unlike microfilament-and microtubule-associated cytoskeleton, *Gelsolin isoform b (H-Glsln)* was greatly decreased. Although these proteins may not be specific to VACV GLV-1h68, most of the cytoskeleton alterations detected in VACV GLV-1h68 infected tumors were caused by VACV GLV-1h68. IFA clearly demonstrated that the *β-tubulin* networks collapse and disperse in IBDV-infected cells (Xiaojuan Zheng et al., 2008).The same result was obtained in this study in which human β-tubulin was down-regulated in the GI-101A infected cells (Table 4), PC-3 infected cells (Table 6) and PC-3 infected tumors (Table 3). Hence, we speculate that cytoskeletal disruption may be a critical mechanism of VACV-GLV-1h68 particle release from infected cells. Recent evidence demonstrates that various viruses manipulate and utilize the host cytoskeleton to promote that viral infection (Radtke, K. et al., 2006). Several studies have shown that human immunodeficiency virus (HIV) type 1 protease cleaves the IF vimentin and induces the collapse of vimentin in infected cells (Xiaojuan Zheng et al., 2008; Alexander Rassmann et al., 2006). Further elucidation is required to determine if IBDV protease VP4 uses an HIV-like strategy to cleave vimentin, resulting in highly decreased expression and the collapse of the vimentin network. Here we found decreased expression human vimentin in PC-3 infected tumor

only (Table 3). However, human vimentin in PC-3 xenografts was dow-regulated dispersely at 21 dpi only then seems remodeled at 42 dpi by up-regulated expression.

In this study, mouse *Apolipoprotein A-I (M-Apoa1)* expression was up-regulated in GI101-A and PC-3 infected tumors. In contrast, the signal transduction protein *Rho-GDP dissociation inhibitor beta (M-GDIa)* was considerably down-regulated (Table 1, 3 respectively). Primary reported that Apoa1, a major constituent of high-density lipoproteins, alters plasma membrane morphology by participating in the reverse transport of cholesterol binding with ATP-binding cassette transporter A1 (Wang, N. et al., 2000), and activates the small GTP-binding protein Cdc42-associated signaling including Apoa1-induced cholesterol efflux, protein kinases, and actin polymerization (Nofer, J. R. et al., 2006). Cumulative evidence also shows that the GTPases of the Rho family are key regulatory molecules of the actin cytoskeleton (Hall, A. 1998), and that Cdc42-activated GTPase induced the collapse of the vimentin network (Nofer, J. R. et al., 2006). Rho-GDI was also reported to be members of the Rho-GTPase regulator family that regulate a wide variety of cellular functions by binding and inhibiting Rho GTPases (Van Aelst, L., and D'Souza-Schorey, C. 1997). Thus, the activity of GTPase regulating the cytoskeletal networks may have been interfered with by the high expression of *Apoa1* and down-regulation of *Rho-GDI* during infection.

In 1989, a computer-based analysis of 2DE gels reported a total of 8 polypeptide differences between cancerous and normal breast epithelial cells in tissue culture (Patil C. and Walter P. 2001). More precise characterization of such polypeptide differences was published in the early 90’s with the demonstration that normal breast epithelial cells produce keratins K5, K6, K7 and K17, whereas tumor cells produce mainly keratins K8, K18 and K19 (Giometti, C. S. et al., 1995). This distribution was secondarily confirmed in tumor samples (Daniel R. et al., 2005) and cytokeratin immunodetection is now eventually used to help discriminate benign from malignant cells on histopathological slides. In infected GI-101A tumors, Keratin 19 was dispersed and greatly decreased at 42 dpi.

4.3 Ubiqitin proteasome pathway (UPP) disorders in VACV GLV-1h68 infected tumor cells

Ubiquitin was described as a heat shock protein playing an important role both during and after stress in chicken embryo fibroblast (Bond, U. et al., 1998). UPP, a major intracellular protein degradation pathway, has recently been implicated in viral infections, including avoidance of host immune surveillance, viral maturation, viral progeny release, efficient viral replication, and reactivation of virus from latency (Gao, G., and Luo, H. 2006). One reports considered that the replication of pea seed-borne mosaic virus induces polyubiquitin and HSP70 expression (Aranda, M. A. et al., 1996). In this study, six UPP-linked proteins were identified as differentially expressed cellular proteins following VACV GLV-1h68 the down-regulated *[Proteasome alpha 3 subunit isoform 2 (H-PSMA3), Proteasome (prosome, macropain) subunit, beta type, 7 (H-PSMB8), Proteasome activator subunit 1-PA28 alpha (H-PSME1), Ubiquitin activating enzyme E1 (H-UBE1), Proteasome subunit, alpha type 6 (M-Psma6), Proteasome subunit, beta type 2 (M-Psmb2)]* and one up-regulated *Proteasome activator hPA28 subunit beta (H-PA28b*) (Table 1). 4 UPP-linked proteins in GI-101A cells [*Proteasome activator subunit 2 (H-PSME2, Chain B-Proteasome Activator Reg-α (H-PARegA), Proteasome beta-subunit (H-PSMB), and Proteasome 26S non-ATPase subunit 5 (H-PSMD5)]* (Table 4), 1 in HT-29 cells is *otubain 1 (H-otub)* (Table 5), 7 in PC-3 cells [*ubiquitin activating enzyme E1 (H-UBE1), proteasome 26S ATPase subunit 4 isoform 1 (H-26S4), otubain 1 (H-otub), proteasome subunit Y (H-PSMB6), Proteasome (prosome, macropain) 26S subunit, ATPase, 1 (H-PSMC1), human 26S proteasome subunit p97 (H-PSMD2)* and *proteasome 26S non-ATPase subunit 5 (H-PSMD5)]* (Table 6) were all identified as differentially expressed cellular proteins following VACV GLV-1h68 the down-regulated. Notably, after VACV GLV-1h68 infection, most of the UPP-associated proteins involved in ubiquitination and deubiquitination were down-regulated, and *H-UBE1* was completely inhibited. These data indicate that VACV GLV-1h68 infection results in functional disorders of UPP system as a "cell cleaner" though the reason for this is unknown. Xiaojuan Zheng *et al*. (Xiaojuan Zheng et al., 2008) reported the down-regulation of *PSMA6, PSMA6, PSMB, PSMD5* in Infectious Bursal Disease virus-

infected cells, suggesting that VACV GLV-1h68 resemble to Infectious Bursal Disease virus in how it disturbs cellular UPP.

4.4 VACV GLV-1h68 alter stress response proteins

Exposure of cells to conditions of environmental stress-including heat shock, oxidative stress, heavy metals, or pathologic conditions, such as ischemia and reperfusion, inflammation, tissue damage, infection, and mutant proteins associated with genetic diseases, results in the inducible expression of heat shock proteins that function as molecular chaperones or proteases. Molecular chaperones are a class of proteins that interact with diverse protein substrates to assist in their folding; with a critical role during cell stress to prevent the appearance of folding intermediates that lead to misfolded or otherwise damaged molecules. Consequently, heat shock proteins assist in the recovery from stress either by repairing damaged proteins (protein refolding) or by degrading them, thus restoring protein homeostasis and promoting cell survival. The events of cell stress and cell death are linked, such that molecular chaperones induced in response to stress appear to function at key regulatory points in the control of apoptosis. On the basis of these observations-and on the role of molecular chaperones in the regulation of steroid aporeceptors, kinases, caspases, and other protein remodeling events involved in chromosome replication and changes in cell structure-it is not surprising that the heat shock response and molecular chaperones have been implicated in the control of cell growth. Caroline Jolly *et al.* (Morimoto RI. 1991) addressed some of the molecular and cellular events initiated by cell stress, the interrelationships between stress signaling, cell death, and oncogenesis-and chaperones as potential targets for cancer diagnosis and treatment.

Cells or tissues from a wide range of tumors have been shown to express atypical levels of one or more HSPs (Morimoto RI. 1991; Fuller KJ et al., 1994). HSPs are overexpressed in a wide range of human cancers and are implicated in tumor cell proliferation, differentiation, invasion, metastasis, death, and recognition by the immune system. Elevated expression of members of the Hsp70 family has also been reported in high-grade malignant tumors (Kaur J. and Ralhan R. 1995; Santarosa M et al., 1997). In

general, HSPs were found down-regulated in both three infected tumor cells. Interestingly, they were found with 12 different HSPs in GI-101A xenografts, in contrast there is only 3 in PC-3 xenografts and 2 HSPs in HT-2 xenografts. This indicated that stress response which was induced in primary tumor cells now changed with evidence of down-regulated HSPs in GI-101A tumors. HSPs what could contribute for tumor cell survival were inhibited at the time viral replication activation occurs. Cellular metabolism process responded to HSPs changing here may lead to disease resolution in GI-101A tumors. Why HSPs were little found in HT-29 and PC-3 xenografts while they were clearly found at *in vitro*? It is possible that at *in vivo,* HSPs might not induce stronger in HT-29 and PC-3 xenografts than GI-101A xenografts therefore observation of identified HSP set in these non-regressing is obstacle or HSPs might be inhibited by mouse protease inhibitors.

In addition, another stress response protein, activator of *Heat shock 90kDa protein* (*H-HSP90*), was down-regulated or inhibited during VACV GLV-1h68 infections (Table 1, 3, 4, 5, 6). Previous studies have shown that HSP90 was a co-chaperone that stimulates Hsp90 ATPase activity and may affect a step in the endoplasmic reticulum-to-Golgi trafficking, and that this Hsp90-associated ATP/GTPase may participate in the regulation of complex formation of *Hsp90* (Panaretou, B. et al., 2002). Consequently, inhibiting H-HSP90 in VACV GLV- 1h68 infected cells may lead to impairment of intracellular protein trafficking in infected cells what happened in GI-101A and PC-3 xenografts.

4.5 Infection effect to anti-apoptosis pathways in cancer cells

Apoptosis is an active cellular process of self-destruction defined by morphological and biological criteria (Kerr JF et al., 1972). Apoptosis protects an organism by ridding it of individual cells whose survival could be detrimental to the organism as a whole (Shen Y and Shenk TE. 1995; Williams GT. 1991). Viral infection often leads to an apoptotic response by a cell, thereby defending other cells from a similar fate (Teodoro JG and Branton PE. 1997) and limiting viral spread. Improving viral propagation in cancer cells is a potential approach to enhance efficacy of oncolytic viral therapy. Many cancer cells have evolved to evade apoptosis (D. Hanahan and R.A.

Weinberg 2000; T.C. Liu and D. Kirn 2005). During evolution of host–pathogen interactions, viruses have also evolved mechanisms to evade apoptosis in order to assist their replication. In the term of infection, the viral genes encoding anti-apoptosis functions or viral induce anti-apoptosis function proteins are therefore theoretically expendable in cancer cells but essential for viral replication in normal cells (E. White 2006; F.H. Igney and P.H. Krammer 2002) illustrates the interactions of cellular apoptosis signaling pathways with a number of viral proteins derived from Ad, HSV and VV (F.H. Igney and P.H. Krammer 2002; W. Schneider-Brachert et al., 2006). Therefore, specific replicating of oncolytic viruses in tumor cell, spreading to others and finally being annihilated before cell die is success in using oncolytic viral therapy.

As shown in table 1, evidence for using VACV GLV-1h68 to eradicate GI-101A xenografts in mice is 12 proteins associated with anti-apoptosis function were found down-regulated, including *Tumor protein, translationally-controlled (H-TPT1), Rho GDP dissociation inhibitor (GDI) alpha (H-GDIa), Ywhaq protein (M-1433T), H-PRDX4, Serine/threonine-protein phosphatase 2A catalytic subunit beta isoform PP2A (M-Ppp2cb), Eukaryotic translation initiation factor 2, subunit 1 alpha, 35kDa (H-eIF2), H- actinin-α1 (ACTN1), annexin A1 (H-A1), annexin A5 (H-A5), mouse albumin 1 (M-Alb1), Dimethylarginine dimethylaminohydrolase 2 (H-DDAH2).* In PC-3 xenografts, anti-apoptosis expression is lesser than those in GI-101A cells, however 3 anti-apoptosis associated proteins were down-regulated such as *ARP3 actin-related protein 3 homolog (H-ARP3), Human FLNA protein, Rho GDP dissociation inhibitor (GDI) alpha (H-GDIa).* In contrast, in HT-29 xenografts, there are several anti-apoptosis associated proteins show even up-regulated; they mostly belong to peroxiredoxin proteins.

In mammalian cells, intracellular redox status has been linked to cellular differentiation, immune response, growth control, tumor promotion, and apoptosis, as well as activation of viruses, notably HIV-1 from latency (Schreck R. et al., 1991; Kalebic T. et al., 1991). One redox-regulated protein is NF-kB. The NF-kB transcription factor promotes cell survival in response to several apoptotic stimuli (figure 44). NF-kB is a member of the Rel family of transcription factors that exist ambiently in the cytoplasm *via* association with inhibitor protein, IkB (Verma I. M. 1995. Baeuerle P. A. 1996). A wide variety of stimuli including tumor necrosis factor-a (TNF-a), phorbol

ester, bacterial lipopolysaccharide, and virus infection can activate NF-kB. One pathway of NF-kB activation involves site-specific phosphorylation of IkB-a on serine residues 32 and 36. It has been suggested that serine phosphorylation targets IkB to the ubiquitin-proteasome pathway for degradation (Palombella V. J. e al., 1994; Traenckner E. B. M. et al., 1995; Chen Z. J. 1996). IkB inactivation, without proteolytic degradation, has also been reported to occur as a consequence of tyrosine phosphorylation on residue 42 (Imbert V. et al., 1996). In both instances, phosphorylation results in an unmasking of the NF-kB nuclear localization signal facilitating nuclear entry of proteins. Thus, for stimuli such as oxidative stress, which potently and rapidly modulates the nuclear activity of NF-kB, IkB-a may represent a critical activation target (Schreck R. et al., 1991). Other hand, phosphorylation and activation of its positive regulator IkB kinase leads to phosphorylation and degradation of IkB, an inhibitor of NF-kB, promoting nuclear translocation of NF-kB and activation of its target genes (351). Dong-Yan et al., (1997) provide the first evidence that the AOE372 class of peroxiredoxins functions through cytoplasmic IkB-a to regulate nuclear activity of NF-kB, peroxiredoxins demonstrated as redox regulators of signal transduction (Baeuerle, P. A., 1996). Cells have multiple pathways to transduce extracellular signals into the nuclear compartment, these pathways are complex networks that ultimately modulate gene expression NF-kB is redox-regulated (2, 50). Several peroxiredoxins were greatly increased in HT-29 tumor such as H-PRDX4, H-PRDX2, and H-PRDX3 suggesting that these peroxiredoxins may participate negative regulation IkB inhibitors to keep up NF-kB pathway activation that cause a continued cell survival.

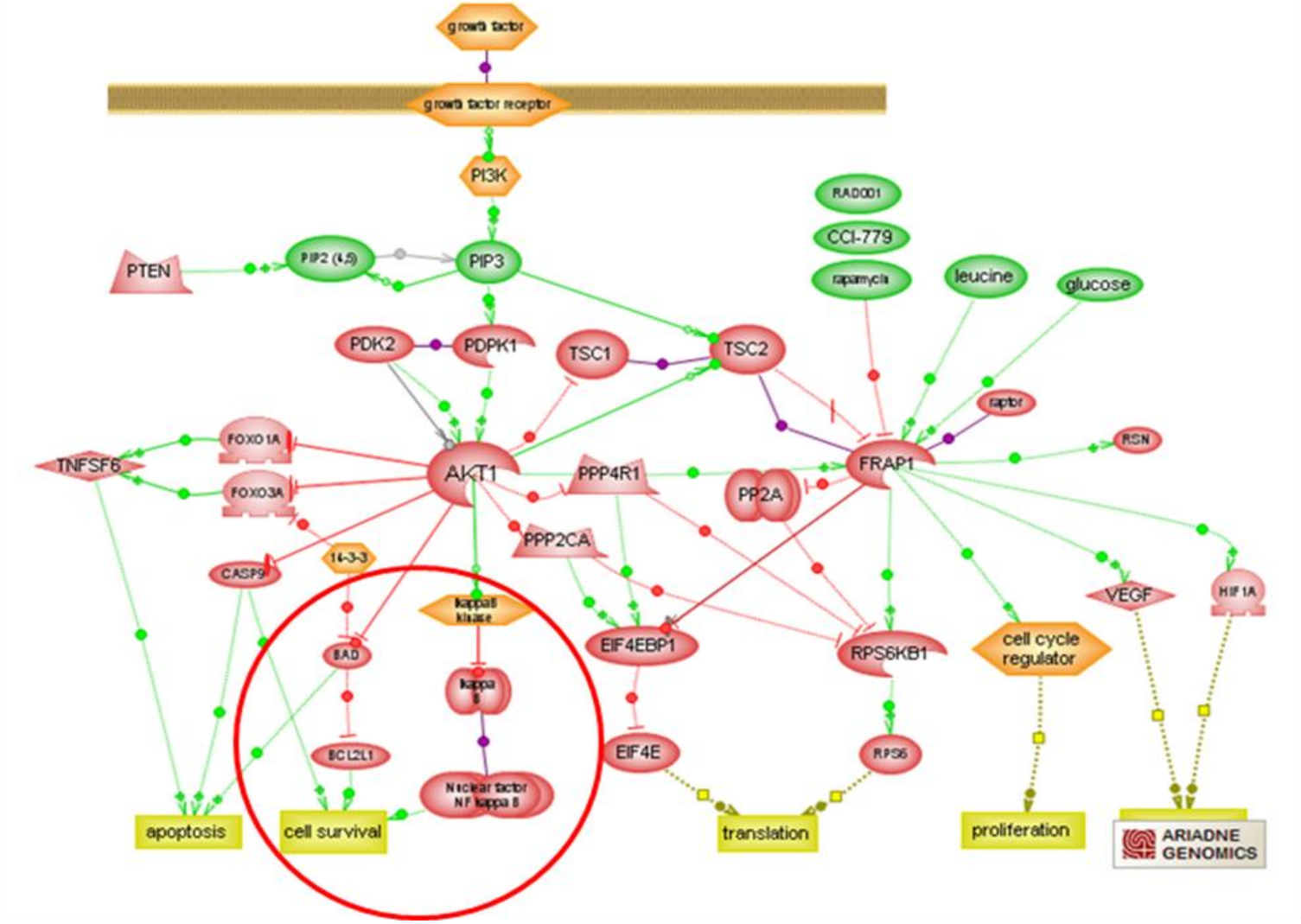

Figure 43. **mTOR pathway**, which is one of the main tumor related pathway, describes inhibiting kappa kinase B (IkB) induces NF-kB release and activation that support cell survival (in red cycle)

4.6 Infection effect to activated EGFR or Ras pathways

Epithelium growth factor (EGFR) is overexpressed in various tumor types, and its expression correlates with metastatic behavior and poor prognosis. Growth factor binding to EGFR induces receptor oligomerization and activation of tyrosine kinase signaling. In

tumor cells, high levels of EGFR lead to hyperactivation of the signaling pathways and activation of Ras signaling downstream. The Ras family of proteins consists of three isoforms, H-, K-, and N-Ras, which play critical roles in control of normal and transformed cell growth. Mutated K-ras is one of the most frequent genetic events in human cancer, with the highest incidences in pancreatic carcinomas (90%), colorectal tumors (50%), lung carcinomas (30%) and myeloid leukemia (25%) (Lexander H. et al., 2005,Jensen, S.L. et al., 1996). Activated K-Ras may not only promote tumor initiation, but also tumor progression and metastasis formation (Xie,Y. and Meier, K.E. 2004; Anna Walduck et al., 2004). The human reovirus is a naturally occurring OV that specifically targets cancer cells with an activated Ras pathway (Roberto Mazzanti et al., 2006; Jellum E et al., 1984). A single intratumoral injection of virus resulted in regression of tumors in 65 to 80% of mice in pre-clinical studies (Roberto Mazzanti et al., 2006). Systemic reovirus therapy of metastatic cancer has also been studied in immune-competent mice (Tracy RP. et al., 1982). In this study, *Ras GTPase-activating-like protein IQGAP1 (H-Iqgap1)* and *Guanine monophosphate synthetase variant (H-GMPS)* were known as proteins activate Ras which were down regulated in GI-101A regressive tumor phase but did not find in HT-29 and PC-3 xenografts. This result supports for shrinking of GI-101A xenografts by effect onto Ras pathways.

4.7 Infection effect to the hypoxic tumor environment

About evidence for activation of the UPR, in principle, neoplastic progression requires several genetic alterations that allow the cell to ignore growth controls and disable apoptotic signalling. As the tumor becomes larger, it experiences increasing hypoxia, nutrient starvation and acidosis until the microenvironment becomes limiting. Cells respond by producing pro-angiogenic factors to initiate the formation and attraction of new blood vessels to the tumor. Although many studies have focused on the hypoxic state of tumors, the stabilization of hypoxia inducible factor-1α (HIF1α), and the activation of protective downstream responses, there is increasing evidence to show that the UPRs can also be activated in tumors. Although no direct link between these two pathways has been established, they share several downstream targets, and it is

conceivable that the two pathways could synergize in some cases and be antagonistic in others (Yanjun Ma and Linda M.Hendershot. 2004).

HIF-1a has a dual role in that it is important for tumor growth but also apoptosis. HIF-1a may exert its proapoptotic effects through stabilisation of p53 or upregulation of BNIP3 (Greijer AE and van der Wall E. 2004). Hypoxia-induced HIF-1-mediated apoptosis might promote the survival of cells that express mutations in tumor suppressor genes and so contribute to their selection. Such a mechanism is supported by evidence that p53-null tumor cells are clonally selected and overgrow similar cells expressing wild-type p53 in hypoxic tumor regions (Graeber et al., 1996). In addition, group of genes induced by HIF-1 was reported (Shalini Patiar and Adrian L Harris 2006) such as iron metabolism associated proteins (ceruloplasmin, transferrin), glucose metabolism associated protein (triosephosphate isomerase). Proteins encoded by these genes were found up-regulated in GI-101A xenografts, only triosephosphate isomerase was found in HT-29, only transferrin was found in PC-3 xenografts, all of them derived from mice. This expression different between different types of tumors suggests that effect may be specific for GI-101A tumor that related to hypoxia-induced HIF-1-mediated apoptosis.

4.8 Chemokines in cell homing to cancer

In order to develop efficient cellular vehicles for oncolytic viruses as well as effective cancer immunotherapy, it is extremely important to develop a systematic understanding of the molecular basis of cell trafficking and biodistribution of candidate carrier cells. Two classes of molecules, chemokines and adhesion molecules such as integrins, have been shown to be important for cell trafficking within immune systems and into tumors (L.M. Ebert et al., 2005; T. Kinashi 2007). Chemokines are a large family of small, generally secreted polypeptides which guide lymphocyte movement throughout the body by controlling integrin avidity and inducing migration. Cancer cells express a number of chemokines which may attract certain types of cells to tumor (F. Balkwill 2004). Host's involvement-derived chemokine RANTES (CCL5) in tumor may play dual roles in tumor growth. In fact that the host's involvement in the tumor phases of the oncolytic process are still intriguing. Here GI-101A, HT-29 and PC-3 xenografts were

further analysis by using enzyme linked immunoabsorbent assay using a "two-site" sandwich detection assay to determine chemokines such as CCL2/MCP-1 (*Macrophage chemotactic protein-1)*, CCL5/RANTES (*Regulated upon activation, normal T-cell expressed and secreted*) and VCAM-1.

In the breast cancer, elevated levels of the chemokine CCL5/RANTES (regulated upon activation, normal T cell expressed and secreted) have been frequently observed in advanced stage breast carcinoma (Riethdorf L. et al., 1996) and this potentiates the invasiveness of the breast cancer cells. The reciprocal interactions between breast tumor cells and TAMs through soluble mediators such as inflammatory cytokines, MMPs and angiogenic factors form a vicious cycle. For example, TNF-a released from TAMs can stimulate the expression of the chemokines CCL2 and CCL5 in breast cancer cells which attracts even more TAMs, thus completing the vicious cycle (Wong MP. et al., 1998). Also, the mRNA for the chemokine CCL5 has been shown to be expressed in the human prostate cancer cell lines including PC-3, DU-145 and LNCaP and also in primary prostate adenocarcinoma cells (Jensen, S.L. et al., 1996). CCL5 induces proliferation and stimulation of invasive power of prostate cancer cells and this effect is inhibited by the CCR5 antagonist TAK-779 (Jensen, S.L. et al., 1996). In this study, interstingly, CCL5 level was shown greatly decrease in GI-101A tumor in the first state, greatly decrease in PC-3 tumors but in the late state and insignificant decreased in HT-29 tumors. This can refer that infection by VACV GLV-1h68 may activate expression of antagonist TAK-779 to inhibits CCL5 which induces proliferation and stimulation of invasive. However, this result may be a significant effect when inhibition of CCL5 occur in early tumor phase.

The chemokine CCL2/MCP-1 is highly expressed in breast tumor (Virchow R. 1863) and stromal cells. Tumor-associated macrophages (TAM) in the tumor stroma exhibit elevated expression of CCL2 and high TAM accumulation correlates with disease recurrence and poor prognosis (Van Ravenswaay et al., 1992, Stephens TC et al., 1978). Further, neutralizing antibodies to CCL2 prevented the formation of the lung metastases in mice bearing CCL2-expressing MDAMB-231 human breast carcinoma xenografts (McBride WH. 1986). This suggests that CCL2 contributes to the metastasis of breast carcinoma cells. In estrogen receptor (ER)-negative breast tumor cells, the cancer-associated membrane glycoprotein, dysadherin, promotes invasion of tumor cells into the

matrigel through regulation of CCL2 expression in vitro and lung metastasis in an *in vivo* animal model (Mantovani A. 1994). Thus, increased CCL2 expression as a result of overexpression of dysadherin may facilitate breast tumor progression and metastasis. Similar to CCL5, CCL2 is also involved in proliferation and migration of prostate cancer cells by acting in an autocrine and paracrine manner and this effect can be abrogated by directing neutralizing antibodies against CCL2 (Roberto Mazzanti et al., 2006). In colon cancer, genes reported to be up-regulated include chemokines (CCL2 and CXCL1), cyclooxygenase-2 (COX-2), growth factors (VEGF and TGF-b2), and cytokines (IL-6) (Hsiao JC et al., 1999,Wang, Y. et al., 2001–Yu YA. et al., 2004). In a mouse model of colitis-associated cancer, IKKb3, an upstream activator of NF-jB, has been reported to link inflammation with tumorigenesis as the conditional knockout of IKKb in colonic epithelial cells significantly attenuated the tumor incidence and deletion in myeloid cells significantly reduced the tumor size (Stephen McCraith et al., 2000). NF-jB activation transcriptionally up-regulates many chemokines involved in tumor progression and metastasis. In this study, CCL2 level shows decreased at the second state of GI-101A. For HT-29 tumor, CCL2 decreases at the first and late state whereas significant increases at second state. For PC-3 tumors, CCL2 shows significant increase at second tumor phase. A similar model of increasing CCL2 in HT-29 and PC-3 xenografts seems to be adverse factor to cancer therapeutic experiment by using oncolytic virus VACV GLV-1h68. For VCAM-1, there is no change remarkably. In summary, role of chemokines and their receptors in tumor pathophysiology is still complex such as some chemokines favor tumor growth and metastasis, while others may enhance anti-tumor immunity. These diverse functions of chemokines establish them as key mediators between the tumor cells and their microenvironment.

REFERENCES

Acres B, Dott K, Stefani L and Kieny MP (1994). Directed cytokine expression in tumour cells in vivo using recombinant vaccinia virus, *Ther. Immunol. 1*. 17–23.

Adams J (2004). The development of proteasome inhibitors as anticancer drugs. *Cancer Cell 5*, 417–421.

Alaiya A, Roblick U, Egevad L, Carlsson A, Franzén B, Volz D, Huwendiek S, Linder S, Auer G (2000). Polypeptide expression in prostate hyperplasia and prostate adenocarcinoma. *Anal Cell Pathol; 21*. 1–9.

Alaiyaa AA, Oppermannb M, Langridgec J, Roblicka U, Egevadd L, Brändstedtd S, Hellstro M, Lindera S, Bergmanb T, Jörnvall H and Auera G (2001). Identification of proteins in human prostate tumor material by two-dimensional gel electrophoresis and mass spectrometry. *Cell Mol Life Sci; 58.* 307-311.

Alan Hall (1998). Rho GTPases and the Actin Cytoskeleton**.** *Science* 279, 509.

Alcami A, Symons JA, Collins PD, Williams TJ, Smith GL (1998). Blockade of chemokine activity by a soluble chemokine binding protein from vaccinia virus. *J Immunol.; 160*. 624–633.

Alessandro R and Kohn EC (2002). Signal transduction targets in invasion. *Clin Exp Metastasis, 19.* 265-273.

Alexander Rassmann, Andreas Henke, Monica Zobawa, Marc Carlsohn, Hans-Peter Saluz, Susanne Grabley, Friedrich Lottspeich and Thomas Munder (2006). Proteome alterations in human host cells infected with coxsackievirus B3. *Journal of General Virology, 87*. 2631–2638.

Alfonso P, Rivera J, Hernaez B., Alonso C and Escribano JM (2004). Identification of cellular proteins modified in response to African swine fever virus infection by proteomics. *Proteomics 4.* 2037-2046.

Allavena P et al., (2005). Anti-inflammatory properties of the novel antitumor agent yondelis (trabectedin): inhibition of macrophage differentiation and cytokine production. *Cancer Res. 65.* 2964–2971.

Allinen M, Beroukhim R, Cai L, Brennan C, Lahti-Domenici J, Huang H, Porter D, Hu M, Chin L, Richardson A, Schnitt S, Sellers WR and Polyak K (2004). Molecular characterization of the tumor microenvironment in breast cancer. *Cancer Cell, 6*, 17–32.

Altenberg B and Greulich KO (2004). Genes of glycolysis are ubiquitously overexpressed in 24 cancer classes. *Genomics 84.* 1014–1020.

Anderson KM, Baranowski J, Olson L and Economou SG (1983). The distribution of acidic coomassie blue-stained proteins from uninvolved human liver, hepatoma, normal colon, primary colon cancer, and colon metastases to the liver, determined by 2D-protein electrophoresis. *J Surg Oncol 24.* 184–191.

Anna Walduck, Andrea Schmitt, Bernadette Lucas, Toni Aebischer, Thomas F Meyer (2004). Transcription profiling analysis of the mechanisms of vaccine-induced protection against *H. pyloriThe FASEB Journal* express article 10.1096/fj.04-2321fje. Published online September 28, 2004.

Aranda MA, Escaler M, Wang D and Maule AJ (1996). Induction of HSP70 and polyubiquitin expression associated with plant virus replication. *Proc Natl Acad Sci U S A 93*, 15289-15293.

Asenjo A, Calvo E and Villanueva N (2006). Phosphorylation of human respiratory syncytial virus P protein at threonine 108 controls its interaction with theM2-1 protein in the viral RNA polymerase complex. *J. Gen. Virol., 87*, 3637–3642.

Avirup Bose, Debabrata Saha, and Naba K Gupta (1997). Regulation of Protein Synthesis during Vaccinia Viral Infection of Animal Cells. *Archives of Biochemistry and Biophysics.*Vol. *342*, No. 2, June 15, pp. 362–372, Article No. BB970138.

Baeuerle PA and Baltimore D (1996). *Cell* 87, 13–20.

Baier PK, Eggstein S, Wolff-Vorbeck G, Baumgartner U and Hopt UT (2005). Chemokines in human colorectal carcinoma, *Anticancer Res. 25.* 3581–3584.

Balkwill F (2004). Cancer and the chemokine network, *Nat. Rev. Cancer 4.* 540–550.

Bartlett DL, Driever HP and Rabkin SD (2001). Vaccinia virus, in: Replication-Competent Viruses for Cancer Therapy, *Monograph Virology, 22,* Karger, 130–159.

Bini L, Magi B, Marzocchi B, Arcuri F, Tripodi S, Cintorino M, Sanchez JC, Frutiger S, Hughes G, Pallini V, Hochstrasser DF and Tosi P (1997). Protein expression profiles in human breast ductal carcinoma and histologically normal tissue. *Electrophoresis, 18.* 2832-2841.

Blachere NE, Li Z, Chandawarkar RY, Suto R, Jaikaria NS, Basu S, Udono H and Srivastava PK (1997). Heat shock protein-peptide complexes, reconstituted in vitro, elicit peptide-specific cytotoxic T lymphocyte response and tumor immunity. *J Exp Med; 186:* 1315-22

Blume-Jensen P and Hunter T(2001). Oncogenic kinase signalling. *Nature, 411.* 355-365.

Bond U, Agell N, Haas AL, Redman K and Schlesinger MJ (1988). Ubiquitin in stressed chicken embryo fibroblasts. *J Biol Chem 263,* 2384-2388.

Bonin-Debs AL, Boche I, Gille H and Brinkmann U (2004). Development of secreted proteins as biotherapeutic agents. *Expert Opin.Biol. Ther. 4*. 551–8.

Brasier AR, Spratt H, Wu Z, Boldogh I, Zhang Y, Garofalo RP, Casola A, Pashmi J, Haag A, Luxon B and Kurosky A (2004). Nuclear heat shock response and novel nuclear domain 10 reorganization in respiratory syncytial virus-infected a549 cells identified by high-resolution two-dimensional gel electrophoresis. *J Virol 78.* 11461-11476.

Brewer JW and Diehl JA (2000). PERK mediates cell-cycle exit during the mammalian unfolded protein response. *Proc. Natl Acad. Sci. USA 97,* 12625–12630.

Brian D Wolf, Surbhi Desai, Steve Shiflett and Peter A Bell (2007). A Sensitive Infrared Fluorescent Protein Stain for Protein Detection in Polyacrylamide Gels. *Part of thermo Fisher Scientific.*

Bruce T Seet, Johnston JB, Craig R Brunetti, John W Barrett, Helen Everett, Cheryl Cameron, Joanna Sypula, Steven H Nazarian, Alexandra Lucas and Grant McFadden (2003). Poxviruses and immune evation. *Annu. Rev. Immunol. 21.* 377–423.

Bucca G, Carruba G, Saetta A, Muti P, Castagnetta L and Smith CP (2004). Gene expression profiling of human cancers. Annals of the New York Academy of Sciences.

Buller RM, Chakrabarti S, Cooper JA, Twardzik DR and Moss B (1988). Deletion of the vaccinia virus growth factor gene reduces virus virulence, *J. Virol. 62.* 866–874.

Buller RM, Smith GL, Cremer K, Notkins AL and Moss B (1985). Decreased virulence of recombinant vaccinia virus expression vectors is associated with a thymidine kinase-negative phenotype, *Nature 317.* 813–815.

Calvo E, Escors D, López JA, González JM, Álvarez A, Arza E and Enjuanes L (2005). Phosphorylation and subcellular localization of transmissible gastroenteritis virus nucleocapsid protein in infected cells. *J. Gen. Virol, 86.* 2255–2267.

Casado-Vela J, Selles S and Martinez RB (2006). Proteomic analysis of tobacco mosaic virus-infected tomato (Lycopersicon esculentum M.) fruits and detection of viral coat protein. *Proteomics 6 Suppl 1,* S196-206.

Chalikonda S, Kivlen MA, O'Malley ME, Dong XD, McCart JA, Gorry MC, Yin XY, Brown CK, Zeh HJ, Guo ZS and Bartlett DL (2008). Oncolytic virotherapy for ovarian carcinomatosis using a tumor-selective oncolytic vaccinia virus armed with a yeast cytosine deaminase gene, *Cancer Gene Ther. 15.* 115–125.

Chalmers MJ, Kolch W, Emmett MR, Marshall AG and Mischak H (2004). Identification and analysis of phosphopeptides.J. Chromatogr. B Analyt. Technol. Biomed. *Life Sci., 803.* 111–120.

Chavey C, Bibeau F, Bourgade SG, Burlinchon S, Boissiere F and Laune D, Roques S and Lazennec G (2007). Oestrogen receptor negative breast cancers exhibit high cytokine content, *Breast Cancer Res. 9*: *R15.*

Chen ZJ, Parent L and Maniatis T (1996). *Cell 84*, 853–862.

Chi JT, Wang Z, Nuyten DS, Rodriguez EH, Schaner ME, Salim A, Wang Y, Kristensen GB, Helland A, Borresen- Dale AL Giaccia A, Longaker MT, Hastie T, Yang GP, Vijver MJ, Brown PO (2006). Gene Expression Programs in Response to Hypoxia: Cell Type Specificity and prognostic Significance in Human Cancers. *PLoS Medicine 3***.** *e47.*

Chiu ST, Hsieh FJ, Chen SW, Chen CL, Shu HF and Li H (2005). Clinicopathologic correlation of up-regulated genes identified using cDNA microarray and real-time reverse transcription-PCR in human colorectal cancer, Cancer Epidemiol. *Biomarkers Prev. 14.* 437–443.

Chung CS, Hsiao JC, Chang YS and Chang W (1998). A27L protein mediates vaccinia virus interaction with cell surface heparin sulfate. *J Virol.72*.1577–1585.

Condeelis J and Pollard JW (2006). Macrophages: obligate partners for tumor cell migration, invasion, and metastasis. *Cell*, *124*, 263–6.

Cooray S, Bahar MW, Abrescia NG, McVey CE, Bartlett NW, Chen RA, Stuart DI, Grimes JM and Smith GL (2007). Functional and structural studies of the vaccinia virus virulence factor N1 reveal a Bcl-2-like anti-apoptotic protein, *J. Gen. Virol. 88.* 1656–1666.

Craig MJ and Loberg RD (2006). CCL2 (Monocyte Chemoattractant Protein-1) in cancer bone metastases, *Cancer Metastasis Rev.*

D. Hanahan, R.A. Weinberg, (2000). The hallmarks of cancer, *Cell 100.* 57–70.

Daniel R Ciocca and Stuart K Calderwood (2005). Heat shock proteins in cancer: diagnostic, prognostic, predictive, and treatment implications. *Cell Stress & Chaperones 10 (2).* 86–103.

David Ron (2002). Translational control in the endoplasmic reticulum stress response. Skirball Institute of Biomolecular Medicine, Department of Medicine and Department of Cell Biology, New York, New York, USA *J. Clin. Invest. 110*:1383–1388 doi:10.1172/JCI200216784.

Davies MV, Chang H-W, Jacobs BL and Kaufman RJ (1993). The E3L and K3L vaccinia virus gene products stimulate translation through inhibition of the double-stranded RNA-dependent protein kinase by different mechanisms. *J. Virol. 67*. 1688–92.

Dong-Yan Jin, Ho Zoon Chae, Sue Goo Rhee and Kuan-Teh Jeang (1997). Regulatory Role for a Novel Human Thioredoxin Peroxidase in NF-kB Activation. *The journal of Biologycal chemistry Vol. 272*, No. 49, Issue of December 5, pp. 30952–30961,

Earnshaw WC, Martins LM and Kaufmann SH (1999). Mammalian caspases: structure, activation, substrates, and functions during apoptosis. Annu. Rev. Biochem. 68, 383±424.

Ebert LM, Schaerli P and Moser B (2005). Chemokine-mediated control of T cell traffic in lymphoid and peripheral tissues, *Mol. Immunol. 42*. 799–809.

Elgert KD, Alleva DG and Mullins DW (1998) Tumor-induced immune dysfunction: the macrophage connection. *J Leukoc Biol*; *64***:**275-90

Ellgaard L, Molinari M and Helenius A (1999). Setting the standards: quality control in the secretory pathway. *Science 286.* 1882–1888.

Esposito JJ and Frenner F (2001). Poxviruses, 4th ed., Lippincott Williams & Wilkins, Philadelphia.

Evan P Adler, Charles A Lemken, Nicholas S Katchen and Robert A Kurt (2003). A dual role for tumor-derived chemokine RANTES (CCL5). *Immunology Letters 90.* 187–194.

Everly DN, Jr, Feng P, Mian IS and Read GS (2002). mRNA degradation by the virion host shutoff (Vhs) protein of herpes simplex virus: genetic and biochemical evidence that Vhs is a nuclease. *J Virol 76*. 8560-8571.

Fenn JB, Mann M, Meng CK, Wong SF and Whitehouse CM (1989). Electrospray ionization for mass spectrometry of large biomolecules. *Science, 246.* 64–71.

Fentiman IS, Rubens RD and Hayward JL (l986). A comparison of intracavitary talc and tetracycline for the control of pleural effusion secondary to breast cancer. *Eur J Cancer Clin Oncol; 9:* 1079-81.

Ficarro SB, McCleland ML, Stukenberg PT and Burke DJ et al., (2002). Phosphoproteome analysis by mass spectrometry and its application to Saccharomyces cerevisiae. *Nat. Biotechnol. , 20.* 301–305.

Fidler IJ (2003). The pathogenesis of cancer metastasis: the 'seed and soil' hypothesis revisited. *Nat Rev Cancer, 3.* 453-458.

Finkel TH, Tudor-Williams G and Banda NK, Cotton MF, Curiel T, Monks C, Baba TW, Ruprecht RM, Kupfer A (1995). Apoptosis occurs predominantly in bystander cells and not in productively infected cells of HIV- and SIV-infected lymph nodes. *Nat Med;1.* 129–34.

Fontana S, Pucci-Minafra I, Becchi M, Freyria AM and Minafra References S (2004). Effect of collagen substrates on proteomic modulation of breast cancer cells. *Proteomics, 4.* 849-860.

Friedman DB, Hill S, Keller JW, Merchant NB, Levy SE, Coffey RJ and Caprioli RM (2004). Proteome analysis of human colon cancer by two-dimensional difference gel electrophoresis and mass spectrometry. *Proteomics, 4.* 793-811.

Fuller KJ, Issels RD, Slosman DO, Guillet JG, Soussi T and Polla BS (1994). Cancer and the heat shock response. *Eur J Cancer*; *30A*:1884–91.

Gao G and Luo H (2006). The ubiquitin-proteasome pathway in viral infections. *Can J Physiol Pharmacol 84,* 5-14.

Garc MA, Meurs EF and Esteban M (2007). The dsRNA protein kinase PKR: Virus and cell control. *Biochimie 89.* 799-811.

Garfinkel MS and Katze MG (1992). Translational control by influenza virus. Selective and cap-dependent translation of viral mRNAs in infected cells. *J Biol Chem 267*. 9383-9390.

Gatenby RA and Gillies RJ (2004). Why do cancers have high aerobic glycolysis? *Nat. Rev. Cancer 4.* 891–899.

Smith GL (1999). Vaccinia virus immune evasion. *Immunology Letters Volume 65, Issues 1-2*. 55-62.

Gil J and Esteban M (2000). Induction of apoptosis by the dsRNA-dependent protein kinase (PKR): mechanism of action. *Apoptosis 5*.107–14.

Giometti CS, Tollaksen SL, Chubb C, Williams C and Huberman E (1995). Analysis of proteins from human breast epithelial cells using two-dimensional gel electrophoresis. *Electrophoresis 16.* 1215–12.

Giovanni Candiano, Maurizio Bruschi, Luca Musante, Laura Santucci, Gian Marco Ghiggeri, Barbara, arnemolla Paola Orecchia, Luciano Zardi, Pier Giorgio Righetti (2004). Blue silver: A very sensitive colloidal Coomassie G-250 staining for proteome analysis. *Electrophoresis, 25,* 1327–1333.

Girish J Kotwal and Bernard Moss (1989). Vaccinia Virus Encodes Two Proteins That Are Structurally Related to Members of the Plasma Serine Protease Inhibitor Superfamily. *Journal of Virology, 63*. 600-606.

Gnant MF, **Noll LA**, **Irvine KR**, **Puhlmann M**, **Terrill RE**, **Alexander HR Jr**, **Bartlett DL**. **(1999).** tumor-specific gene delivery using recombinant vaccinia virus in a rabbit model of liver metastasis. *J. Natl.cancer Inst.91*. 1744-1750.

Godfraind C, Holmes KV and Coutelier JP (1995). Thymus involution induced by mouse hepatitis virus A59 in BALB/c mice. *J Virol; 69.* 6541–7.

Görg A and Weiss W (2000). 2D electrophoresis with immobilized pH gradients. In: Proteome Research: Two-Dimensional Electrophoresis and Identification Methods *(Ed: Rabilloud T), Springer*, 57-106.

Grabbe S, Bruvers S, Beissert S and Granstein RD (1994). Interferon-gamma inhibits tumor antigen presentation by epidermal antigen-presenting cells. *J Leukoc Biol; 55***:** 695-701

Graves DT, Jiang YL, Williamson MJ and Valente AJ (1989). Identification of monocyte chemotactic activity produced by malignant cells. *Science; 245.* 1490–1493.

Greijer AE and van der Wall E (2004). The role of hypoxia inducible factor 1 (HIF-1) in hypoxia induced apoptosis. *Journal of Clinical Pathology. 57*: 1009–1014.

Greten FR, Eckmann L, Greten TF, Park JM, Li ZW and Egan LJ et al., (2004). IKKbeta links inflammation and tumorigenesis in a mouse model of colitis-associated cancer. *Cell 118.* 285–296.

Groux H, Torpier G, Monte D, Mouton Y, Capron A and Ameisen JC (1992). Activation-induced death by apoptosis in CD4_ T cells from human immunodeficiency virus-infected asymptomatic individuals. *J Exp Med; 175* 331–40.

Gruenheid S and Finlay BB (2003). Microbial pathogenesis and cytoskeletal function. *Nature, 422.* 775–781.

Guo ZS and Bartlett DL (2004). Vaccinia as a vector for gene delivery, *Expert Opin. Biol. Ther. 4.* 901–917.

Guo ZS, Naik A, O'Malley ME, Popovic P, Demarco R, Hu Y, Yin X, Yang S, Zeh HJ, Moss B, Lotze MT and Bartlett DL (2005). The enhanced tumor selectivity of an oncolytic vaccinia lacking the host range and anti-apoptosis genes SPI-1 and SPI-2, *Cancer Res. 65.* 9991–9998.

Gygi SP, Rochon Y, Franza BR and Aebersold R (1999). Correlation between protein and mRNA abundance in yeast. *Mol Cell Biol 19.*1720-1730.

Hall A (1998). Rho GTPases and the actin cytoskeleton. *Science* 279, 509-514.

Harding HP et al., (2000). Regulated translation initiation controls stress-induced gene expression in mammalian cells. *Mol. Cell 6*, 1099–1108.

Harding HP, Zhang Y and Ron D (1999). Protein translation and folding are coupled by an endoplasmic-reticulum-resident kinase. *Nature 397*, 271–274.

Henzel WJ, Billeci TM, Stults JT, Wong SC, Grimley C and Watanabe C (1993). Identifying proteins from two-dimensional gels by molecular mass searching of peptide fragments in protein sequence databases. *Proc Natl Acad Sci USA, 90.* 5011-5015.

Herrmann PC, Liotta LA, Petricoin EF 3rd (2001). Cancer proteomics: the state of the art. *Dis Markers, 17.* 49-57.

Hershey JWB (1993). Semin. *Virol. 4,* 201-207.

Hovanessian A (1993). Interferon-induced dsRNA-activated protein kinase (PKR): Antiproliferative, antiviral and antitumoral functions. *Semin. Virol. 4,* 237–245.

Hsiao JC, Chung CS and Chang W (1999). Vaccinia virus envelope D8L protein binds to cell surface chondroitin sulfate and mediates the adsorption of intracellular mature virions to cells. *J Virol.*;*73.* 8750–8761.

Humrich JY, Thumann P, Greiner S, Humrich JH, Averbeck M, Schwank C, Kämpgen E , Schuler G , Jenne (2007). Vaccinia virus impairs directional migration and chemokine receptor switch of human dendritic cells. *Eur. J. Immunol. 37.* 954–965.

Igney FH, Krammer PH (2002). Death and anti-death: tumour resistance to apoptosis, *Nat. Rev. Cancer 2.* 277–288.

Imbert V, Rupec RA, Livolsi A, Pahl HL, Traenckner EBM, Mueller-Dieckmann,

C, Farahifar D, Rossi B, Auberger P, Baeuerle PA and Peyron JF (1996). *Cell 86,* 787–798.

Inoue Y, Yasukawa M and Fujita S (1997). Induction of T-cell apoptosis by human herpesvirus 6. *J Virol; 71:* 3751–9.

Isidoro A, Martinez M, Fernandez PL, Ortega AD, Santamaria G, Chamorro M, Reed JC and Cuezva JM (2004). Alteration of the bioenergetic phenotype of mitochondria is a hallmark of breast, gastric, lung and oesophageal cancer. *Biochem. J. 378.* 17–20.

Jaramillo ML, Abraham N and Bell JC (1995). The interferon system:Areview with emphasis on the role of PKR in growth control. *Cancer Inv. 13,* 327–338.

Jeffrey LB, Eric DW, Maria ED, Jennifer LG, Kristina BK and Ardythe AM (1999). The requirement for molecular chaperones during endoplasmic reticulum-associated protein degradation demonstrates that protein export and import are mechanistically distinct. *J. Biol. Chem. 274,* 3453–3460.

Jellum E, Thorsrud AK, Vatn MH, Grimstad IA, Brennhovd I, Tveit KM and Pihl A (1984). Detection of cancer-related proteins by 2D-electrophoresis. *Ann NY Acad Sci 428.* 173–185.

Jenner E (1798). An Inquiry into the Causes and Effects of the Variolae Vaccinae, a Disease Discovered in Some of the Western Counties of England, Particularly Near Gloucestershire, and Known by the Name of the Cow Pox. *Dover, New York.*

Jensen SL, Wood DP, Jr, Banks ER and Veron M et al., (1996). Increased levels of nm23H1/ nucleoside diphosphate kinase A mRNA associated with adenocarcinoma of the prostate. *Wold J Uro 14 Suppl 1.* S21-5.

Ji H, Reid GE, Moritz RL, Eddes JS, Burgess AW and Simpson RJ (1997). A two-dimensional gel database of human colon carcinoma proteins. *Electrophoresis 18.* 605–613.

Jiang HY et al., (2003). Phosphorylation of the α-subunit of eukaryotic initiation factor 2 is required for activation of NF-κB in response to diverse cellular stresses. *Mol. Cell. Biol. 23,* 5651–5663

John M Taylor and Michele Barry (2006). Near death experiences: Poxvirus regulation of apoptotic death. *Virology 344.* 139 – 150.

Johnston JB and Grant McFadden (2003). Poxvirus Immunomodulatory Strategies: Current Perspectives. *Journal of Virology.* 6093–6100.

Jose G Teodoro and Philip E Branton (1997). Regulation of Apoptosis by Viral Gene Products. *Journal of Virology.* 1739–1746.

Kahn RA, Fu H and Roy CR (2002). Cellular hijacking: a common strategy for microbial infection. *Trends Biochem. Sci., 27.* 308–314.

Kaitlyn J Kelly, Yanghee Woo, Peter Brader, Zhenkun Yu, Christopher Riedl, Shu-Fu Lin, Nanhai Chen, Yong A Yu, Valerie W Rusch, Aladar A Szalay and Yuman Fong (2008). Novel Oncolytic Agent GLV-1h68 Is Effective Against Malignant Pleural Mesothelioma. *Human gene therapy 19*:774–782 (August) © Mary Ann Liebert, Inc. DOI: 10.1089/hum.2008.036

Kalebic T, Kinter A, Poli G, Anderson ME, Meister A and Fauci AS (1991). *Proc. Natl. Acad. Sci. U. S. A. 88,* 986–990.

Kaur J and Ralhan R (1995). Differential expression of 70-kDa heat shock-protein in human oral tumorigenesis. *Int J Cancer*; *63*:774–9.

Keesee SK, Meneghini MD, Szaro RP and Wu YJ (1994). Nuclear matrix proteins in human colon cancer. *Proc Natl Acad Sci USA 91.* 1913–1916.

Keller K, Kolbe H, Lange K and Zimmermann B with technical assistance of Bachmann D, GaiBer H and Monden I (1978). Release of Glyeolytic Enzymes from Cultivated Tumor Cells. *Z. Krebsforsch. 92,* 275-286.

Kelley A Parato, Donna Senger, Peter AJ Forsyth and John C Bell (2005). Recent progress in the battle between oncolytic viruses and tumors. *Nat Rev Cancer; 5 (12):*965-976.

Kerr JF, Wyllie AH and Currie AR (1972). Apoptosis: a basic biological phenomenon with wide-ranging implications in tissue kinetics. *Br J Cancer .26.* 239–57.

Kibler KV, Shors T, Perkins KB, Zeman CC, Banaszak MP, Biesterfeldt J, Langland JO and Jacobs BL (1997). Doublestranded RNA is a trigger for apoptosis in vaccinia virus-infected cells. *J. Virol. 71*:1992–2003.

Kimball SR (1999). Eukaryotic initiation factor eIF2. *Int J Biochem Cell Biol 31,* 25-29.

Kinashi T (2007). Integrin regulation of lymphocyte trafficking: lessons from structural and signaling studies, Adv. *Immunol. 93*.185–227.

Kobayashi H, Boelte KC and Lin PC (2007). Endothelial cell adhesion molecules and cancer progression. *Curr Med Chem. 14.* 377–86.

Kondo K et al., (2002). Inhibition of HIF is necessary for tumor suppression by the von Hippel-Lindau protein. *Cancer Cell 1*, 237–246.

Krystyna W. Nahlik, Anna K. Mleczko, Magdalena K Gawlik and Hanna B Rokita (2003). Modulation of GAPDH expression and cellular localization after vaccinia virus infection of human adherent monocytes .Vol. *50*.667–676.

Kuyumcu-Martinez NM, Van Eden ME, Younan P and Lloyd RE (2004). Cleavage of poly(A)-binding protein by poliovirus 3C protease inhibits host cell translation: a novel mechanism for host translation shutoff. *Mol Cell Biol 24*, 1779-1790.

Laude H, Masters PS in: Siddell SG (1995). The Coronavirus Nucleocapsid Protein, *Plenum Press, New York.* 141–163.

Lee AS (1992). Mammalian stress response: induction of the glucose-regulated protein family. *Curr. Opin. Cell Biol. 4*, 267–273.

Lee AS (2001). The glucose-regulated proteins: stress induction and clinical applications. *Trends Biochem. Sci. 26*, 504–510.

Lee CJ, Liao CL and Lin YL (2005). Flavivirus activates phosphatidylinositol 3-kinase signaling to block caspasedependent apoptotic cell death at the early stage of virus infection. *J. Virol. 79*, 8388–8399.

Leek RD and Harris AL (2002). Tumor-associated macrophages in breast cancer. *J. Mammary Gland Biol. Neoplasia*, *7*, 177–89.

Leong PW, Liew K, Lim W and Chow VT (2002). Differential display RT-PCR analysis of enterovirus-71-infected rhabdomyosarcoma cells reveals mRNA expression responses of multiple human genes with known and novel functions. *Virology 295*, 147-159.

Leong WF and Chow VT (2006). Transcriptomic and proteomic analyses of rhabdomyosarcoma cells reveal differential cellular gene expression in response to enterovirus 71 infection. *Cell Microbiol 8.* 565-580.

Leung SY, Wong MP, Chung LP, Chan ASY and Yuen ST (1997). Monocyte chemoattractant protein-1 expression and macrophage infiltration in gliomas. *Acta Neuropathol; 93.* 518–527.

Lewis C and Murdoch C (2005). Macrophage responses to hypoxia: implications for tumor progression and anti-cancer therapies. *Am. J. Pathol.167.* 627–635.

Lewis DE, Tang DS, Adu-Oppong A, Schober W and Rodgers JR (1994). Anergy and apoptosis in CD8_ T cells from HIV-infected persons. *J Immunol;153.* 412–20.

Lexander H, Hirschberg D, Hell Ström M, Bergman T, Jörnvall H, Auer G and Egevad L (2005). Differentical protein expression in anatomical zones of prostate. *Proteomics; 5.* 2570-2576.

Ley K, Laudanna C, Cybulsky MI and Nourshargh S (2007). Getting to the site of inflammation: the leukocyte adhesion cascade updated, *Nat. Rev. Immunol. 7.* 678–689.

Li XM, Patel BB, Blagoi EL, Patterson MD, Seeholzer SH, Zhang T, Damle S, Gao Z, Boman B and Yeung AT (2004). Analyzing alkaline proteins in human colon crypt proteome. *J. Proteome Res. 3.* 821–833

Lin EY and Pollard JW *(*2007). Tumor-associated macrophages press the angiogenic switch in breast cancer. *Cancer Res. 67.* 5064–6.

Lin SF, Yu Z, Riedl C, Woo Y, Zhang Q, Yu YA, Timiryasova T, Chen N, Shah JP, Szalay AA, Fong Y and Wong RJ (2007). *Treatment of anaplastic thyroid carcinoma in vitro with a mutant vaccinia virus.* Surgery Volume 142, Issue 6, December. *976-983.*

Liu TC and Kirn D (2005). Viruses with deletions in antiapoptotic genes as potential oncolytic agents, *Oncogene 24*. 6069–6079.

Luboshits G, Shina S, Kaplan O, Engelberg S, Nass D, Mercer BL, Chaitchik S, Keydar I, and Baruch AB (1999). Elevated expression of the CC chemokine regulated on activation, normal T cell expressed and secreted (RANTES) in advanced breast carcinoma, *Cancer Res. 59.* 4681–4687.

Luo Y, Zhou H, Krueger J, Kaplan C, Lee SH, Dolman C, Markowitz D, Wu W Liu C, Reisfeld RA and Xiang R (2006). Targeting tumor-associated macrophages as a novel strategy against breast cancer. *J. Clin. Invest., 116*, 2132–41.

Luo Y, Zhou H, Krueger J, Kaplan C, Lee SH, Dolman C, Markowitz D, Wu W, Liu C, Reisfeld RA and Xiang R (2006). Targeting tumor-associated macrophages as a novel strategy against breast cancer. *J. Clin. Invest., 116.* 2132–41.

Ma Y and Hendershot LM (2003). Delineation of the negative feedback regulatory loop that controls protein translation during ER stress. *J. Biol. Chem. 278*, 34864–34873.

Ma Y and Hendershot LM (2004). ER chaperone functions during normal and stress conditions. *J. Chem. Neuro. 28,* 51–65.

Ma Y and Hendershot LM (2004). Herp is dually regulated by both the endoplasmic reticulum stress-specific branch of the unfolded protein response and a branch that is shared with other cellular stress pathways. *J. Biol. Chem. 279,* 13792–13799.

Ma Y, Brewer J W, Diehl JA and Hendershot LM (2002). Two distinct stress signaling pathways converge upon the CHOP promoter during the mammalian unfolded protein response. *J. Mol. Biol. 318,* 1351–1365.

Mahalingam S and Karupiah G (2000). Modulation of chemokines by poxvirus infections. *Curr Opin Immuno ; 12* .409–412.

Mantovani A (1994). Tumour-associated macrophages in neoplastic progression: a paradigm for the in vivo function of chemokines. *Lab Invest; 71.* 5–16.

Mantovani A, Allavena P and Sica A (2004). Tumour-associated macrophages as a prototypic type II polarised phagocyte population: role in tumour progression. *Eur. J. Cancer. 40.* 1660–1667.

Margo H Furman and Hidde L Ploegh (2002). Lessons from viral manipulation of protein disposal pathways. *J. Clin. Invest. 110.* 875–879.

Maxwell KL and Frappier L (2007). Viral proteomics. *Microbiol Mol Biol Rev 71*, 398-411.

McBride WH (1986). Phenotype and functions of intratumoral macrophages. *Biochim Biophys Acta; 865.* 27–41.

McCart JA, Ward JM, Lee J, Hu Y, Alexander HR, Libutti SK, Moss B and Bartlett DL (2001). Systemic cancer therapy with a tumor-selective vaccinia virus mutant lacking thymidine kinase and vaccinia growth factor genes, *Cancer Res. 61*. 8751–8757.

McCormick F (1999). Signalling networks that cause cancer. *Trends Cell Biol, 9***.** M53-56.

McIntosh AAG and Smith GL (1996). Vaccinia virus glycoprotein A34R is required for infectivity of extracellular enveloped virus. *J Virol.;70.* 272–281.

Melillo G (2007). Targeting hypoxia cell signaling for cancer therapy, *Cancer Metastasis Rev. 26.* 341–352.

Meredith DM, Lindsay JA, Halliburton IW and Whittaker GR (1991). Posttranslational modification of the tegument proteins (VP13 and VP14) of herpes simplex virus type 1 by glycosylation and phosphorylation. *J Gen Virol 72 (Pt 11).* 2771-2775.

Meriane M, Mary S, Comunale F, Vignal E, Fort P and Gauthier-Rouviere C (2000). Cdc42Hs and Rac1 GTPases induce the collapse of the vimentin intermediate filament network. *J Biol Chem 275,* 33046-33052.

Merrick WC (1992). *Microbiol. Rev. 56,* 291-315.

Merrick WC (2004). Cap-dependent and cap-independent translation in eukaryotic systems. *Gene 332,* 1-11.

Meyaard L, Miedema F (1995). Programmed death of T cells in the course of HIV infection. *Adv Exp Med Biol; 374*:115–20.

Meyaard L, Otto SA, Jonker RR Mijnster MJ, Keet RP, and Miedema F (1992). Programmed death of T cells in HIV-1 infection. *Science (Wash DC); 257*:217–9.

Mills CD, Shearer J, Evans R and Caldwell MD (1992). Macrophage arginine metabolism and the inhibition or stimulation of cancer. *J Immunol*; *149*: 2709-14

Mitsuyama K, Tsuruta O, Tomiyasu N, Takaki K, Suzuki A, Masuda J, Yamasaki H, Toyonaga A and Sata M (2006). Increased circulating concentrations of growth-related oncogene (GRO)-alpha in patients with inflammatory bowel disease, *Dig. Dis. Sci***.** *51*. 173–177.

Morimoto RI (1991). Heat shock: the role of transient inducible responses in cell damage, transformation, and differentiation. *Cancer Cells; 3:* 295–301.

Moss B (2001). Poxviridae: the Viruses and Their Replication, 4th ed. *Lippincott Williams & Wilkins, Philadelphia.*

Moss B and Earl PL (1998). Expression of proteins in mammalian cells using vaccinia viral vectors. *Curr Prot Mol Biol*.;43-16.

Nakagawa H, Liyanarachchi S, Davuluri RV, Auer H, Martin Jr EW, de la Chapelle A and Frankel WL. **(2004).** Role of cancerassociated stromal fibroblasts in metastatic colon cancer to the liver and their expression profiles, *Oncogene 23.* 7366–7377.

Nalty TJ, Taylor CW and Yeoman LC. (1988). Variation in cytosolic protein expression between human colon tumors that differ with regard to differentiation class. *Clin Chem 34.* 71–75.

Nam JS, Kang MJ, Suchar AM, Shimamura T, Kohn EA, Michalowska AM, Jordan VC, Hirohashi Sand Wakefield LM (2006). Chemokine (C-C motif) ligand 2 mediates the prometastatic effect of dysadherin in human breast cancer cells, *Cancer Res***.** *66.* 7176–7184.

Negus RP, Stamp GW, Relf MG, Burke F, Malik ST, Bernasconi S, Allavena P, Sozzani S, Mantovani A, and Balkwill FR (1995). The detection and localisation of monocyte hemoattractant protein-1 in human ovarian cancer. *J Clin Invest; 95.* 2391–2396.

Neumann G, Castrucci MR and Kawaoka Y (1997). Nuclear import and export of influenza virus nucleoprotein. *J. Virol., 71.* 9690–9700.

Nofer JR, Remaley AT, Feuerborn R, Wolinnska I, Engel T, von Eckardstein A, and Assmann G (2006). Apolipoprotein A-I activates Cdc42 signaling through the ABCA1 transporter. *J Lipid Res 47*, 794-803.

Noltmann EA (1972). Aldose ketose isomerases. *Enzymes 1*:271-353.

Oyaizu N, Adachi Y, Hashimoto F, McCloskey TW, Hosaka N, Kayagaki N, Yagita H and Pahwa S (1997). Monocytes express Fas ligand upon CD4 cross-linking and induce CD4_ T cells apoptosis: a possible mechanism of bystander cell death in HIV infection. *J Immunol;158*: 2456–63.

Palombella VJ, Rando OJ, Goldberg AL and Maniatis T (1994). *Cell* 78, 773–785.

Panaretou B, Siligardi G, Meyer P, Maloney A, Sullivan JK, Singh S, Millson SH, Clarke PA, Naaby-Hansen S, Stein R, Cramer R, Mollapour M, Workman P, Piper PW, Pearl LH and Prodromou C (2002). Activation of the ATPase activity of hsp90 by the stress-regulated cochaperone aha1. *Mol Cell 10*, 1307-1318.

Pandey A and Mann M (2000). Proteomics to study genes and genomes. *Nature, 405.* 837-846.

Parajuli P and Singh SM (1996). Alteration in IL-1 and arginase activity of tumor-associated macrophages: a role in the promotion of tumor growth. *Cancer Lett*; *107***:** 249-56

Pardoll D (2003). Does the immune system see tumors as foreign or self? *Annu. Rev. Immunol. 21*. 807-839.

Patil C and Walter P (2001). Intracellular signaling from the endoplasmic reticulum to the nucleus: the unfolded protein response in yeast and mammals**.** *Current Opinion in Cell Biology. 13:* 349-355(7).

Pawson T and Scott JD (1997). Signaling through scaffold, anchoring, and adaptor proteins. *Science, 278.* 2075–2080.

Peng J and Gygi SP (2001). Proteomics: the move to mixtures. *J Mass Spectrom, 6.* 31083-31091.

Peplinski GR, Tsung AK, Casey MJ, Meko JB, Fredrickson TN, Buller RM and Norton JA (1996). In vivo murine tumor gene delivery and expression by systemic recombinant vaccinia virus encoding interleukin-1beta, *Cancer J. Sci. Am. 2.* 21–27.

Peter Scriven, Nicola J Brown, Graham Pockley A and Lynda Wyld (2007). The unfolded protein response and cancer: a brighter future unfolding? *J Mol Med. 85*:331–341

Petricoin EF, Zoon KC, Kohn EC, Barrett JC and Liotta LA (2002). Clinical proteomics: translating bench side promise into bedside reality. *Nat Rev Drug Discov, 1.* 683-695.

Petruzzelli L, Takami M and Humes HD (1999). Structure and function of cell adhesion molecules. *Am J Med; 106.* 467–76.

Pouyssegur J, Dayan F and Mazure NM (2006). Hypoxia signaling in cancer and approaches to enforce tumour regression, *Nature 441.* 437–443.

Pucci-Minafra I, Fontana S, Cancemi P, Alaimo G and Minafra S (2002). Proteomic patterns of cultured breast cancer cells and epithelial mammary cells. *Ann NY Acad Sci, 963.* 122-139.

Pucci-Minafra I, Fontana S, Cancemi P, Basiricò L, Caricato S and Minafra S (2002). A contribution to breast cancer cell proteomics: detection of new sequences. *Proteomics, 2.* 919-927.

Puhlman M, Brown CK, Gnant M, Huang J, Libutti SK, Alexander HR and Bartlett DL (2000). Vaccinia virus as a vector for tumor directed gene therapy: biodistribution of the thymidine kinase deleted mutant. *Cancer Gen Ther 7.* 66-73.

Puhlmann M, Brown CK, Gnant M, Huang J, Libutti SK, Alexander HR, Bartlettt DL (2000). Vaccinia as a vector for tumor-directed gene therapy: biodistribution of a thymidine kinase-deleted mutant, *Cancer Gene Ther***.** *7***.** 66–73.

Pupa SM, Menard S, Forti S and Tagliabue E (2002). New insights into the role of extracellular matrix during tumor onset and progression. *J. Cell Physiol., 192*, 259–67.

Radtke K, Dohner K and Sodeik B (2006). Viral interactions with the cytoskeleton: a hitchhiker's guide to the cell. *Cell Microbiol 8*. 387-400.

Radtke K, Dohner K and Sodeik B (2006). Viral interactions with the cytoskeleton: a hitchhiker's guide to the cell. *Cell Microbiol 8*, 387-400.

Ralhan R and Kaur J (1995). Differential expression of Mr 70,000 heat shock protein in normal, premalignant, and malignant human uterine cervix. *Clin Cancer Res; 1*: 1217–22.

Ramaswamy S, Ross KN, Lander ES and Golub TR (2003). A molecular signature of metastasis in primary solid tumors. *Nat Genet 33.* 49–54.

Ramiro-Ibanez F, Ortega A, Brun A, Escribano JM and Alonso C (1996). Apoptosis: a mechanism of cell killing and lymphoid organ impairment during acute African swine fever virus infection. *J Gen Virol*; 77: 2209–19.

Reboredo M, Greaves RF and Hahn G (2004). Human cytomegalovirus proteins encoded by UL37 exon 1 protect infected fibroblasts against virus-induced apoptosis and are required for efficient virus replication. *J. Gen. Virol. 85,* 3555–3567

Rhoads RE (1991) *Translation in Eukaryotes* (Trachsel, H., ed) pp. 109–148, CRC Press, Boca Raton, FL

Rhoads RE (1993) J. Biol. *Chem. 268*, 3017-3020.

Riccardo Alessandro, Simona Fontana, Elise Kohn, and Giacomo De Leo.(2005). Proteomic strategies and their application in cancer research. *Tumori, 91.* 447-455.

Riethdorf L, Riethdorf S, Gutzlaff K, Prall F and Loning T (1996). Differential expression of the monocyte chemoattractant protein-1 gene in human papillomavirus-16-infected squamous intraepithelial lesions and squamous cell carcinomas of the cervix uteri. *Am J Pathol; 149.* 1469–1476.

Roberto Mazzanti, Michela Solazzo, Ornella Fantappie´, Sarah Elfering, Pietro Pantaleo, Paolo Bechi, Fabio Cianchi, Adam Ettl, and Cecilia Giulivi (2006). Differential expression proteomics of human colon cancer. *Am J Physiol Gastrointest Liver Physiol 290.* G1329–G1338.

Robinson SC, Scott KA, Wilson JL, Thompson RG, Proudfoot AEI and Balkwill FR(2003). A chemokine receptor antagonist inhibits experimental breast tumor growth. *Cancer Res. 63.* 8360–8365.

Roblick UJ, Bader FG, Hammarstedt L, Habermann JK, Hellman U, Becker S,

Sundmacker A, Gemoll T, Zimmermann K, Auer G and Munck-Wikland E. (2008). Proteomic analysis of protein expression in human tonsillar cancer - differentially expressed proteins characterize human tonsillar cancer**.** ***Acta Oncol. Aug 29:*****1-9.**

Roblick UJ, Hirschberg D, Habermann JK, Palmberg C, Becker S, Kruger S, Gustafsson M, Bruch HP, Franzen B, Ried T, Bergmann T, Auer G and Jornvall H (2004). Sequential proteome alterations during genesis and progression of colon cancer. *Cell Mol Life Sci, 61.* 1246-1255.

Rodriguez JM, Salas ML and Santaren JF (2001). *Proteomics, 1,* 1447–1456.

Romashkova JA and Makarov SS (1999). NF-kappaB is a target of AKT in anti-apoptotic PDGF signalling. *Nature*; *401*: 86–90.

Rowley A, Choudhary JS, Marzioch M, Ward MA, Weir M, Solari RCE and Blackstock WP(2000). Applications of protein mass spectrometry in cell biology. *Methods, 20.* 383-397.

Safer B (1983). *Cell 33,* 7-8.

Saji H, Koike M, Yamori T, Saji S, Seiki M and Matsushima K et al., (2001). Significant correlation of monocyte chemoattractant protein-1 expression with neovascularization and progression of breast carcinoma, *Cancer 92.* 1085–1091.

Salcedo R, Ponce ML, Young HA, Wasserman K, Ward JM, Kleinman HK Oppenheim JJ, **Murphy WJ (2000).** Human endothelial cells express CCR2 and respond to MCP-1: direct role of MCP-1 in angiogenesis and tumor progression, *Blood 96.* 34–40.

Samuel CE, Kuhen KL, George CX, Ortega LG, Rende-Fournier R and Tanaka H (1997). The PKR protein kinase: An interferon-inducible regulator of cell growth and differentiation. *International J. Hematol.* 65, 227–237.

Santarosa M, Favaro D, Quaia M and Galligioni E (1997). Expression of heat shock protein 72 in renal cell carcinoma: possible role and prognostic implications in cancer patients. *Eur J Cancer*; *33*:873–7.

Sato K, Kuratsu J, Takeshima H, Yoshimura T and Ushio Y (1995). Expression of monocyte hemoattractant protein-1 in meningioma. *J Neurosurg; 82.* 874–878.

Schlee M, Krug T, Gires O, Zeidler R, Hammerschmidt W, Mailhammer R, Laux G, Sauer G, Lovric J and Bornkamm GW (2004). Identification of Epstein-Barr virus (EBV) nuclear antigen 2 (EBNA2) target proteins by proteome analysis: activation of EBNA2 in conditionally immortalized B cells reflects early events after infection of primary B cells by EBV. *J Virol 78*.3941-3952.

Schneider-Brachert W, Tchikov V, Merkel O, Jakob M, Hallas C, Kruse ML, Groitl P, Lehn A, Hildt E, Held-Feindt J, Dobner T, Kabelitz D, Krönke M and Schütze S (2006). Inhibition of TNF receptor 1 internalization by adenovirus 14.7K as a novel immune escape mechanism, *J. Clin. Invest. 116.* 2901–2913.

Schreck, R., Rieber, P., and Baeuerle, P. A. (1991). *EMBO J. 10,* 2247–2258.

Secchiero P, Flamand L, Gibellini D, Falcieri E, **Robuffo I**, **Capitani S**, **Gallo RC**, **Zauli G (1997).** Human herpesvirus 7 induces CD4(_) T-cell death by two distinct mechanisms: necrotic lysis in productively infected cells and apoptosis in uninfected or nonproductively infected cells. *Blood; 90:* 4502–12.

Seet BT and McFadden G (2002). Viral chemokine-binding proteins. *J Leukoc Biol.;72*.24–34.

Selak MA, Armour SM, MacKenzie ED, Boulahbel H, Watson DG, Mansfield KD, Pan Y, Simon MC, Thompson CB and Gottlieb E (2005). Succinate links TCA cycle dysfunction to oncogenesis by inhibiting HIF-_ prolyl hydroxylase. *Cancer Cell 7*. 77–85

Semenza GL (2001). Hypoxia-inducible factor 1: oxygen homeostasis and disease pathophysiology. *Trends in Molecular Medicine 7.* 345–350.

Sen CK and Packer L (1996). *FASEB J.* 10, 709–720.

Shackelford J and Pagano JS (2005). Targeting of host-cell ubiquitin pathways by viruses. *Essays in biochemistry 41*.139-156.

Shalini Patiar and Adrian L Harris (2006). Role of hypoxia-inducible factor-1a as a cancer therapy target Endocrine-Related *Cancer 13*. S61–S75.

Shen Y and Nemunaitis J (2005). Fighting cancer with vaccinia virus: teaching new tricks to an old dog, *Mol. Ther. 11.* 180–195.

Shen Y and Shenk TE (1995). Viruses and apoptosis. *Curr Opin Genet Dev;5.*105–11.

Shi Y, Vattem KM, Sood R, An J, Liang J, Stramm L, and Wek RC (1998). Identification and characterization of pancreatic eukaryotic initiation factor 2α-subunit kinase, PEK, involved in translational control. *Mol. Cell. Biol. 18,* 7499–7509.

Sica A, Saccani A, Bottazzi B, Bernasconi S, Allavena P, Gaetano B, Fei F, LaRosa G, Scotton C, Balkwill F and Mantovani A (2000). Defective expression of the monocyte chemotactic protein-1 receptor CCR2 in macrophages associated with human ovarian carcinoma. *J Immunol; 164.* 733–738.

Simpson RJ, Connolly LM, Eddes JS, Pereira JJ, Moritz RL, and Reid GE (2000). Proteomic analysis of the human colon carcinoma cell line (LIM 1215): development of a membrane protein database. *Electrophoresis 21.* 1707–1732.

Sirinarumitr T, Zhang Y, Kluge JP, Halbur PG and Paul PS (1998). A pneumovirulent United States isolate of porcine reproductive and respiratory syndrome virus induces apoptosis in bystander cells both in vitro and in vivo. *J Gen Virol;79.* 2989–95.

Sivakumar A (2002). 2D gels and bioinformatics--an eye to the future. *In Silico Biol, 2.* 507-510.

Srinivas PR, Verma M, Zhao Y and Srivastava S (2002). Proteomics for cancer biomarker discovery. *Clinical Chemistry, 48.* 1160- 1169.

Staal FJT, Anderson MT and Herzenberg LA (1995). *Methods Enzymol. 252,* 168–174

Stephen McCraith, Ted Holtzman, Bernard Moss, and Stanley Fields (2000). Genome-wide analysis of vaccinia virus protein–protein interactions. *PNAS April 25, vol. 97 no. 9.* 4879-4884.

Stephens TC, Currie GA and Peacock JH (1978). Repopulation of gamma-irradiated Lewis lung carcinoma by malignant cells and host macrophage progenitors. *Br J Cancer; 38.* 573–582.

Stulik J, Koupilova K, Osterreicher J, Knizek J, Macela A, Bures J, Jandik P, Langr F, Dedic K and Jungblut PR (1999). Protein abundance alterations in matched sets of macroscopically normal colon mucosa and colorectal carcinoma. *Electrophoresis 20.* 3638–3646.

Sunderkotter C, Steinbrink K, Goebeler M, Bhardwaj R and Sorg C (1994). Macrophages and angiogenesis. *J Leukoc Biol; 55:* 410-22

Susana Guerra, Luis A. Lo´pez-Ferna´ndez, Raquel Conde, Alberto Pascual-Montano (2004). Microarray Analysis Reveals Characteristic Changes of Host Cell Gene Expression in Response to Attenuated Modified Vaccinia Virus Ankara Infection of Human HeLa Cells. *J. of Virology, 78.* 5820–5834.

Szymczyk P, Krajewska WM, Jakubik J, Berner A, Janczukowicz J, Mikulska U, Berner J and Kilianska ZM (1996). Molecular characterization of cellular proteins from colorectal tumors. *Tumori.* 82(4):376-81.

Takahiko Ito, Rosemary jagust and Stratford May W (1994). Interleukin 3 stimulates protein synthesis by regulating. *Proc. Nati. Acad. Sci. USA Vol. 91. 7455-7459.*

Takeshi Tomonaga, Kazuyuki Matsushita, Seiko Yamaguchi,1 Masamichi Oh-Ishi, Yoshio Kodera, Tadakazu Maeda, Hideaki Shimada, Takenori Ochiai and Fumio Nomura (*2004*). Identification of Altered Protein Expression and Post-Translational Modifications in Primary Colorectal Cancer by Using Agarose Two-Dimensional Gel Electrophoresis Clinical Cancer Research 2007- *Vol. 10, 2007–2014.*

Tang H, Peng T and Wong-Staal F (2002). Novel technologies for studying virus-host interaction and discovering new drug targets for HCV and HIV. *Curr Opin Pharmacol 2*. 541-547.

Teodoro JG and Branton PE (1997). Regulation of apoptosis by viral gene products. *J Virol; 71*:1739–46.

Thompson CB (1995). Apoptosis in the pathogenesis and treatment of disease. *Science 267*, 1456±1462.

Thorne SH, Bartlett DL and Kirn DH (2005). The use of oncolytic vaccinia viruses in the treatment of cancer: a new role for an old ally*? Curr. Gene Ther. 5*. 429–443.

Thorne SH, Hwang TH, O'Gorman BE, Bartlett DL, Sei S, Adatia F, Brown C, Werier J, Jo JH, Lee DE, Wang Y, Bell J and Kirn DH (2007). Rational strain selection and engineering creates a broad spectrum systemically effective oncolytic poxvirus JX-963, *J. Clin. Invest. 117*. 3350–3358.

Timiryasova TM, Li J, Chen B, Chong D, Langridge WH, Gridley DS and Fodor I (1999). Antitumor effect of vaccinia virus in glioma model, *Oncol Res. 11*. 133–144.

Tracy RP, Wold LE, Currie RM and Young DS (1982). Patterns for normal colon mucosa and colon adenocarcinoma compared by two-dimensional gel electrophoresis. *Clin Chem 28.* 915–919.

Traenckner EBM, Pahl HL, Henkel T, Schmidt KN, Wilk S and Baeuerle PA (1995) *EMBO J.* 14, 2876–2883

Trask DK, Band V, Zajchowski DA, Yaswen P, Suh T and Sager R (1990). Keratins as markers that distinguish normal and tumor-derived mammary epithelial cells. *Proc. Natl. Acad. Sci. U. S. A. 87***,** 2319–2323

Tymiryasova T,Yu YA, Shabahang S, Fordor I and Szalay AA (2000). In the proceedings of the 11th international Symposium on Bioluminescence and Chemiluminescence. *Pacific Grove,CA, September 6-10, (eds. Case. J.F.et al) 457-460 (Wold Scientific, Singapore, 2001).*

Ueno T, Masakazu T, Saji H, Muta M, Bando H, Kuro K, Koike M, Inadera H and Matsushima K(2000). Significance of macrophage chemo-attractant protein-1 on macrophage recruitment, angiogenesis and survival in human breast cancer. *Clin Cancer Res; 6.* 3282–3289.

Ueno T, Toi M, Saji H, Muta M, Bando H and Kuroi K, Koike M, Inadera H and Matsushima K (2000). Significance of macrophage chemoattractant protein- 1 in macrophage recruitment, angiogenesis, and survival in human breast cancer, *Clin. Cancer Res. 6.* 3282–3289.

Ullrich CK, Groopman JE and Ganju RK (2000). HIV-1 gp120- and gp160-induced apoptosis in cultured endothelial cells is mediated by caspases. *Blood 96.*1438–42.

Vaday GG, Peehl DM, Kadam PA and Lawrence DM (2006). Expression of CCL5 (RANTES) and CCR5 in prostate cancer, *Prostate 66.* 124–134.

Van Aelst L and D'Souza-Schorey C (1997). Rho GTPases and signaling networks. *Genes Dev* 11, 2295-2322.

Van Ravenswaay, Claasen HH, Kluin PM and Fleuren GJ (1992). Tumour infiltrating cells in human cancer. On the possible role of CD16+ macrophages in anti-tumour cytotoxicity. *Lab Invest; 6.* 166–174.

Ventelon-Debout M, Delalande F, Brizard JP, Diemer H, Van Dorsselaer A and Brugidou C (2004). Proteome analysis of cultivar-specific deregulations of Oryza sativa indica and O. sativa japonica cellular suspensions undergoing rice yellow mottle virus infection. *Proteomics **4***, 216-225.

Verma IM, Stevenson JK, Schwarz EM, Antwerp DV and Miyamoto S (1995). *Genes Dev.* 9, 2723–2735.

Verma M, Kagan J, Sidransky D and Srivastava S (2003). Proteomic analysis of cancer-cell mitochondria. *Nat. Rev. Cancer 3.* 789–795.

Virchow R (1863). Aetologie der neoplastichen Geschwulste/Pathogenie der neoplastischeneschwulste. Die Krankhaften Geschwulste. Berlin: Verlag von August Hirschwald; 57-101.

Vrubel F, Mraz J, Nemecek R, Papousek F and Hanselova M (1979). Carcinoma of the prostate. I. Histochemical examination as an aid in evaluating prostate carcinoma. *Int Urol Nephrol; 11.* 295-299.

Waltregny D, de Leval L, Menard S, de Leval J and Castronovo V (1997). Independent prognostic value of the 67-kd laminin receptor in human prostate cancer. *J Natl Cancer Inst; 89.* 1224-1227.

Wang D, Wang H, Brown J, Daikoku T, Ning W and Shi Q et al., (2006). CXCL1 induced by prostaglandin E2 promotes angiogenesis in colorectal cancer, *J. Exp. Med. 203.* 941–951.

Wang FL, Wang Y, Wong WK, Liu Y, Addivinola FJ, Liang P, Chen LB, Kantoff PW and Pardee AB (1996). Two differentially expressed genes in normal human prostate tissue and in carcinoma. *Cancer Res;56.* 3634-3637.

Wang N, Silver DL, Costet P and Tall AR (2000). Specific binding of ApoA-I, enhanced cholesterol efflux, and altered plasma membrane morphology in cells expressing ABC1. *J Biol Chem* 275, 33053-33058.

Wang Y, Wang G, O'Kane D.J and Szalay AA (2001). Chemiluminescence energy transfer to study protein-protein interaction in the living cell. *Mol. Gen. Genet. 264.* 578-587.

Wang Y, Wang G, O'Kane D.J and Szalay AA I (1996). Proceeding of the 9th international symposium on Bioluminescence, Woods Hole MA October 4-8.

Wang Y, Wang G, O'Kane DJ and Szalay AA (2001). Chemilunescence energy transfer to study protein- protein interaction in living cell. *Mol.Gen. Genet. 264.* 578-587.

Wang Y, Wang G, O'Kane DJ and. Szalay AA (1996). In proceedings oft he 9th international Symposium on Bioluminescence and Chemiluminescence, Woods Hole. *MA, October 4-8. (eds.Hasting. J.W.et al)419-422 (Wiley, Chichester, UK, 1996).*

Wang Y, Yu Y, Shabahang S, Wang G and Szalay AA (2002). Functional Renilla-lucifrase Aequorea GFP(RUC-GFP) fusion protein as a novel dual reporter for image of gene expression in the cell cultures and the live animals. *Mol.Gen.Genet.268.*160-168.

Wang Y,Yu YA, Shabahang S, Fordor I and Szalay AA (2002). Functional Renilla Luciferase-Aequorea GFP (RUC-GFP) fusion protein as a novel dual reporter for imaging of gene expression in the cell cultures and in live animals. *Mol. Gen. Gent 268.* 160-168.

Warburg O (1956). On the origin of cancer cells. *Science 123.* 309–314.

Washburn MP, Wolters D and Yates JR III (2001) Large-scale analysis of the yeast proteome by multidimensional protein identification technology. Nat. Biotechnol., 19, 242–247.

Washburn MP, Wolters D and Yates JR III (2001). Large-scale analysis of the yeast proteome by multidimensional protein identification technology. *Nat. Biotechnol., 19.* 242–247.

Wasilenko ST, Banadyga L, Bond D and Barry M (2005). The vaccinia virus F1L protein interacts with the proapoptotic protein Bak and inhibits Bak activation, *J. Virol. 79* 14031–14043.

White E (2006). Mechanisms of apoptosis regulation by viral oncogenes in infection and tumorigenesis, *Cell Death Differ. 13.*1371–1377.

Wiesner A (2004). Detection of tumor markers with ProteinChip technology. *Curr Pharm Biotechnol, 5.* 45-67.

Wilkins MR, PasqualiC, Appel RD, Ou K, Golaz O, Sanchez JC, Yan JX, Gooley AA, Hughes G, Smith IH, Williams KL and Hochstrasser DF (1996). From proteins to proteomes: large scale protein identification by two-dimensional electrophoresis and amino acid analysis. *Biotecnology (NY),14.* 61-5.

Williams BRG (1997). Role of the double-stranded RNAactivated protein kinase (PKR) in cell regulation. *Biochem. Soc. Trans.* 25, 509–513.

Williams GT (1991). Programmed cell death: apoptosis and oncogenesis. *Cell;65.* 1097–8.

Wiseman BS and Werb Z (2002). Stromal effects on mammary gland development and breast cancer. *Science, 296,* 1046–9.

Wong MP, Cheung KN, Yuen ST, Fu KH , Chan ASY , Leung SY , Chung L.P (1998). Monocyte chemoattractant protein-1 (MCP-1) expression in primary lymphoepithelioma-like carcinomas (LELCs) of the lung. *J Pathol; 186.* 372–377.

Worland PJ, Bronzert D, Dickson RB, Lippman ME, Hampton L, Thorgeirsson SS and Wirth PJ (1989). Secreted and cellular polypeptide patterns of MCF-7 human breast cancer cells following either estrogen stimulation or v-H-ras transfection. *Cancer Res. 49,* 51–57.

Wright CW, Means JC, Penabaz T and Clem RJ (2005). The baculovirus anti-apoptotic protein Op-IAP does not inhibit *drosophila* caspases or apoptosis in *drosophila* S2 cells and instead sensitizes S2 cells to virus-induced apoptosis. *Virology 335,* 61–71

Wu T-C (2007). The Role of Vascular Cell Adhesion Molecule-1 in Tumor Immune Evasion. *Cancer Res; 67(13).* 6003–6

Wu X, Gong X, Foley HD, Schnell MJ and Fu ZF (2002). Both viral transcription and replication are reduced when the rabies virus nucleoprotein is not phosphorylated. *J. Virol., 76.* 4153–4161.

Xiangzhi Meng, Addie Embry, Debbi Sochia and Yan Xiang (2007). Vaccinia Virus A6L Encodes a Virion Core Protein Required for Formation of Mature Virion-*Journal of Virology, Vol.81*. 1433–1443.

Xiaojuan Zheng, Lianlian Hong, Lixue Shi, Junqing Guo, Zhen Sun, Jiyong Zhou *(*2008). Proteomic Analysis of Host Cells Infected with Infectious Bursal Disease Virus. *Molecular & Cellular Proteomics 7:*612-625.

Xie Y and Meier KE (2004). Lysophospholipase D and its role in LPA production. *Cell signal 16.* 975-81.

Xu RH, Pelicano H, Zhou Y, Carew JS, Feng L, Bhalla KN, Keating MJ and Huang P (2005). Inhibition of glycolysis in cancer cells: a novel strategy to overcome drug resistance associated with mitochondrial respiratory defect and hypoxia. *Cancer Res. 65.* 613-621.

Xuezhi Bi, Qingsong Lin, Tet Wei Foo, Shashikant Joshi, Tao You, Han-Ming Shen, Choon Nam Ong, Peh Yean Cheah, Kong Weng Eu and Choy-Leong Hew (2006). Proteomic Analysis of Colorectal Cancer Reveals Alterations in Metabolic Pathways. *Molecular & Cellular Proteomics 5:1119-1130*

Yaal-Hahoshen N, Shina S, Leider-Trejo L, Barnea I, Shabtai EL, Azenshtein E Greenberg I, Keydar I and Baruch AB (2006). The chemokine CCL5 as a potential prognostic factor predicting disease progression in stage II breast cancer patients, *Clin. Cancer Res. 12*. 4474–4480.

Yang ST, Guo ZS, O'Malley ME, Yin XY, Zeh HJ and Bartlett DL (2007). A new recombinant vaccinia with targeted deletion of three viral genes: its safety and efficacy as an oncolytic virus, *Gene Ther. 14.* 638–647.

Yanjun Ma and Linda M Hendershot (2004). The role of the unfolded protein response in tumor development: friend or foe? *Nature reviews, cancer volume 4.*

Yarden Y, (2001). The EGFR family and its ligands in human cancer: signallingmechanisms and therapeutic opportunities, *Eur. J. Cancer 37(Suppl 4).* S3-S8.

Yoo NK, Pyo CW, Kim Y, Ahn BY and Choi SY (2008). Vaccinia virus-mediated cell cycle alteration involves inactivation of tumour suppressors associated with Brf1 and TBP, *Cell Microbiol. 10.* 583–592.

Yu YA, Shabahang S, Timiryasova TM, Zhang Q, Beltz R, Gentschev I, Goebel W & Szalay AA (2004). Visualization of tumors and metastases in live animals with bacteria and vaccinia virus encoding light-emitting proteins. *Nat Biotechnol;22.*313–20.

Yunping Luo, He Zhou, Jörg Krueger, Charles Kaplan, Sung-Hyung Lee, Carrie Dolman, Dorothy Markowitz, Wenyuan Wu, Cheng Liu, Ralph A Reisfeld, and Rong Xiang (2006). Targeting tumor-associated macrophages as a novel strategy against breast cancer. *J. Clin. Invest. 116.* 2132–2141

Zhang L, Zhou W, Velculescu VE, Kern SE, Hruban RH, Hamilton SR, Vogelstein B, and Kinzler KW (1997). Gene expression profiles in normal and cancer cells. *Science 276.* 1268–1272.

Zhang Q, Yu YA, Wang E, Chen N, Danner RL, Munson PJ, Marincola FM, AA Szalay (2007). Eradication of solid human breast tumors in nude mice with an intravenously injected light-emitting oncolytic vaccinia virus, *Cancer Res. 67.*10038–10046.

TABLES (inthe next version)

CURRICULUM VITAE

Full name	**Le Thu Ha**
Gender	Female
Date of birth	18.07.1969
Place of birth	Quang ninh- Viet nam
Marital status	Married
Nationality	Vietnamese

Education background

1976-1982	Quang yen primary school, Yen hung district, Quang ninh province, Vietnam.
1982-1986	Tran phu high school, Hai phong province, Vietnam.
1987-1993	Ha noi medical university, Vietnam. *(Medical doctor, Avergae, average score: 6.7).*
2000-2002	Military medical university, Hanoi, Vietnam. *(MSc in Medicine, good, average score: 9.8)*

Work experience

1994-2000	Researcher at National epidermic and hygien Institue, Hanoi, Vietnam
2000-2002	MD-master student in Military academy of medical university, Hanoi, Vietnam.
2002-2004	Researcher at National epidermic and hygien Institue, Ha noi, Viet nam
2004-Present	Postgraduate student, Microbiologycal department of Bio-centre-University of Würzburg.

Würzburg …… ……

(Thu Ha Le)

Publications

1. **The occurrence of precore regional mutation in hepatitis B virus genome in young carriers and HBV-DNA detection rate in asymptomatic carriers and patients with chronic active hepatitis**. *Journal of Military Parmaco-Medicine Vol 345 /GP-BVHTT345 (2002)*
   Nguyen Xuan Thanh, Le Thu Ha, Vu Chien Thang, Doan Trong Tuyen (Vietnamese).

2. **Four-color labeling of cell culture and tumors of live mice upon infection with: GFP-Ruc and RFP-CBG99 expressing Vaccinia virus strains. 2007 In: Proceedings of the 14th International Symposium on Bioluminescence &** *Chemiluminescence: Chemistry, Biology and Applications. World Scientific: Singapore, 2007: 197-200.*
   Raab V, Horbaschek C, Chen N, Zhang Q, Yu YA, Seubert C, Geissinger U, Worschech A, Tietze CJ, Zellner E, Le TH, Grummt F, Stritzker J, Szalay AA.

Table 1. Differential expression proteins in GI-101A tumors (Protein profiling using 2-DE; Delta2D software; MALDI-TOF).

(Subcutaneous GI-101A tumors in nude mice with and without VAVC GLV-1h68 treatment; time points were taken 7, 21 and 42 days after intravenous injection of the virus; fold of enhancement or reduction of protein expression after virus injection are shown; highly expression in red and down-regulated in blue)

Fold of enhancement	Fold of suppression
>5	>5
3 to 5	3 to 5
2 to3	2 to 3

Protein name	Abbr	Accession	MW	*p*I	7dpi (+)fold	21dpi (+)fold	42dpi (+)fold	7dpi (-)fold	21dpi (-)fold	42dpi (-)fold
Cytoskeleton proteins										
ACTB protein	H-ACTB	gi|15277503	40194,07031	5,55		1,54	5,21	0,93		
ACTB protein	H-ACTB	gi|15277503	40194,07031	5,55				0,40	0,72	0,59
actin-like	M-Actl	gi|8850209	43572,48047	5,11	1,16				0,32	0,40
ARP2 actin-related protein 2 homolog	H-ARP2	gi|15778930	44732,25	6,3				0,87	0,99	0,26
capping protein alpha 1 subunit	M-CAPZA1	gi|595917	32731,24023	5,34	1,40				0,92	0,27
capping protein alpha 1 subunit	M-CAPZA1	gi|595917	32731,24023	5,34	1,46	1,55				0,56
dynein, cytoplasmic, intermediate chain 2	M-DYNC1I2	gi|6753658	68351,65625	5,16		1,13		0,76		0,40
fascin homolog 1, actin bundling protein	M-Fscn1	gi|113680348	54473,92969	6,44	1,07	1,05				0,22
fascin homolog 1, actin bundling protein	M-Fscn1	gi|113680348	54473,92969	6,44	1,52	1,22				0,34
FLNA protein	H-FLNA	gi|15779184	88534,4063	5,93	2,06	1,22				0,36
gamma-actin	M-ActG	gi|809561	40992,46875	5,56	3,25	1,43	2,13			

gamma-actin	M-ActG	gi|809561	40992,46875	5,56				0,64	0,67	0,06
gamma-actin	M-ActG	gi|809561	40992,46875	5,56		1,14		0,78		0,07
gelsolin isoform b	H-Glsln	gi|38044288	80590,50781	5,58	1,12				0,43	0,13
gelsolin-like capping protein	M-GDIb	gi|110227377	38744,67188	6,47			1,64		0,31	
gsn protein	M-Gsn	gi|18606238	80712,38281	5,52	1,45				0,83	0,58
actinin, alpha 1	H-ACTN1	gi|30585329	103105,711	5,25		1,03		0,68		0,49
keratin 19	H-Krt19	gi|34783124	45586,96875	5,11	2,11	1,76	1,84			
keratin 19	H-Krt19	gi|34783124	45586,96875	5,11	2,76	2,14	1,89			
keratin 2	H-Krt2	gi|47132620	65393,21094	8,07	2,73	1,83				0,33
keratin, type I cytoskeletal 19 (Cytokeratin-19)	H-Krt19	gi|75041620	44038,07813	5,04				0,81	0,98	0,07
keratin, type I cytoskeletal 19 (Cytokeratin-19)	H-Krt19	gi|75041620	44038,07813	5,04	1,09	1,10				0,39
KRT19 protein	H-Krt19	gi|39644709	45870,17188	5,16					0,89	0,00
KRT19 protein	H-Krt19	gi|45709960	46179,37109	5,16		1,06		0,99		0,26
KRT8 protein	H-Krt8	gi|33875698	55787,17188	5,62	7,06	1,47				0,23
leucine-rich PPR motif-containing protein	H-LRPPRC	gi|31621305	157805,1094	5,81	1,34	2,05	3,97			
moesin	H-Moe	gi|4505257	67777,78906	6,08	1,20				0,98	0,32
myosin, light polypeptide 1	M-Myl1	gi|29789016	20581,41016	4,98		1,22	8,37	0,48		
put. beta-actin (aa 27-375)	M-ActA	gi|49868	39160,64063	5,78		1,35		0,70		0,08
tropomyosin 2 (beta) isoform 1	H-Tpm2	gi|42476296	32830,57031	4,66		1,12	1,65	0,57		
TUBB protein	H-TUBB	gi|16198437	30339,59961	4,77	1,20	1,35				0,38
TUBB2C protein	H-TUBB2C	gi|14124960	25858,39063	4,95	1,13	1,09				0,05
TUBB2C protein	H-TUBB2C	gi|14124960	25858,39063	4,95	1,14	1,47				0,05
tubulin, beta, 2	H-Btub	gi|5174735	49799	4,79		2,16		0,82		0,90
vimentin	M-Vim	gi|2078001	51533,08984	4,96	4,53		12,82		0,80	
vimentin	M-Vim	gi|2078001	51533,08984	4,96	1,33		2,39		0,44	
WD repeat domain 1	M-Wdr1	gi|29144967	72068,32031	8,66	1,17	1,18				0,46

WD repeat-containing protein 1 isoform 1 variant	H-WDR1	gi|62897087	66185,85156	6,17		1,71				0,25
Stress response										
chaperonin (HSP60)	H-Hsp60	gi|306890	60986,3711	5,7				0,73	0,97	0,29
chaperonin containing TCP1, subunit 2 (beta)	H-CCT2	gi|54696792	57565,21094	6,01		1,39		0,90		0,17
chaperonin containing TCP1, subunit 3 (gamma)	H-CCT3	gi|55960506	57935,03125	6,46		2,84		0,94		0,13
chaperonin containing TCP1, subunit 5 (epsilon)	H-CCT5	gi|24307939	59632,80859	5,45		1,10		0,60		0,52
chaperonin containing TCP1, subunit 6A isoform a variant	H-CCT6a	gi|62089036	57725,46094	6,25		1,40		0,91		0,20
chaperonin containing TCP1, subunit 8 (theta)	H-CCT8	gi|48762932	59582,5	5,42		1,49		0,60		0,00
heat shock 70kDa protein 4 isoform a	H-Hsp704	gi|38327039	94271,24219	5,11		1,57		0,73		0,14
heat shock 70kDa protein 4 isoform a	H-Hsp704	gi|38327039				1,20		0,36		0,07
heat shock 70kDa protein 8 isoform 1	H-Hsp708	gi|5729877	70854,21875	5,37				0,22	0,16	0,36
heat shock protein 60	H-Hsp60	gi|77702086	61174,4492	5,7	1,04	1,26				0,33
heat shock protein 70 - human	H-Hsp70	gi|2135328	78945,29688	5,13	2,25		1,43		0,88	
HSP90AA1 protein	H-HSP90	gi|83318444	68328,78125	5,11				0,87	0,53	0,36
HSP90AA1 protein	H-HSP90	gi|83318444	68328,78125	5,11	1,15				0,95	0,37
Hspd1 protein	M-Hspd1	gi|76779273	59387,98828	8,09	1,54	1,05				0,24
KIAA0002	H-KI002	gi|1136741	58465,14844	5,75				0,87	0,99	0,26
peroxiredoxin 3	H-PRDX3	gi|54696872	27788,2598	7,67		1,98		0,88		0,40
PRDX4	H-PRDX4	gi|49456297	30570,8496	5,86	1,28	1,12				0,40
protein disulfide isomerase associated 4	M-PDIa4	gi|86198316	72324,64063	5,08	1,40	1,31	2,44			
protein disulfide isomerase associated 6	M-PDIa	gi|60502437	48626,60156	5,05				0,84	0,85	0,55
stress-induced-phosphoprotein1 (Hsp70/Hsp90-organizing protein)	H-STIP1	gi|5803181	62599,39844	6,4	1,00	1,00				0,26
t-complex polypeptide 1	H-TCP1	gi|36796	60355,75	6,03	2,01	2,07				0,55
t-complex polypeptide 1	H-TCP1	gi|36796	60355,75	6,03	1,22	1,87				0,31

Translation associated proteins										
acidic ribosomal phosphoprotein P0	M-ARPP0	gi|13277927	34164,73828	5,91		1,49		0,84		0,05
ATP-dependent DNA helicase II	H-Ku70	gi|10863945	82652,27344	5,55	1,22	2,10	2,26			
ATP-dependent DNA helicase II	H-Ku70	gi|10863945	82652,27344	5,55	1,11				0,95	0,05
ATP-dependent DNA helicase II, 70 kDa subunit	H-Ku70	gi|4503841	69799,04688	6,23	1,17	1,17				0,34
endothelial cell growth factor 1 (platelet-derived)	H-Ecgf1	gi|4503445	49924,17188	5,36		1,03		0,98		0,41
eukaryotic translation initiation factor 3, subunit 2 (beta)	M-Eif3s2	gi|9055370	36437,58984	5,38		1,71		0,98		0,51
eukaryotic translation initiation factor 3, subunit 3 gamma	H-Eif3s3	gi|60825606	40018,14063	6,09				0,90	0,84	0,10
eukaryotic translation initiation factor 2, subunit 1 alpha, 35kDa	H-eIF2	gi|30584065	36202,4609	5,01	1,22	1,24				0,15
human elongation factor-1-delta	H-EEF1D	gi|38522	31201,8594	4,95	2,55	1,14				0,08
KIAA0111	H-KI111	gi|40788956	46954,26172	6,33		1,05		0,69		0,21
PPA1 protein	H-PPA1	gi|38181963	35859,91016	6,28	2,43	1,18				0,01
pyrophosphatase 1	H-PP1	gi|11056044	32639,15039	5,54	1,18	1,21				0,03
tu translation elongation factor, mitochondrial	H-TUFM	gi|34147630	49843,32031	7,26		1,30		0,75		0,13
RNA processing										
asparaginyl-tRNA synthetase variant	H-AsnS	gi|62897229	62870,53906	5,9	4,85	2,01				0,14
aspartyl-tRNA synthetase	H-AspS	gi|45439306	57100,03125	6,11				0,83	0,70	0,12
aspartyl-tRNA synthetase	H-AspS	gi|78394948	57088	6,11	1,08				0,78	0,17
Chromosome 17 open reading frame 25	H-GLOD4	gi|16198390	33193,57813	5,4	1,83	1,09				0,25
glycyl-tRNA synthetase	H-GlyS	gi|493066	77463,34375	5,88				0,66	0,52	0,15
heme binding protein 2	H-HEBP2	gi|7657603	22861,18945	4,58	1,05				0,91	0,08
heterogeneous nuclear ribonucleoprotein D-like	M-HnrpdlÊ	gi|7710036	33538,08984	6,85	1,29	2,02				0,35

HLA-B-associated transcript 1A	M-Bat1a	gi|9790069	49003,96875	5,44	1,01				0,91	0,39
HLA-B-associated transcript 1A	M-Bat1a	gi|9790069	49003,96875	5,44	1,08	1,06				0,43
PA2G4 protein	H-PA2G4	gi|33879698	41654,28125	7,14				0,99	0,88	0,41
prolyl endopeptidase	H-PREP	gi|41349456	80648,03125	5,53	1,27	1,47	5,61			
PRP19/PSO4 pre-mRNA processing factor 19 homolog	H-PRPF19	gi|7657381	55146,33984	6,14				0,84	0,81	0,31
TARS protein	H-TARS	gi|56789234	78555,42969	6,45	1,11	2,01				0,19
tryptophanyl-tRNA synthetase isoform b	H-TrpS	gi|47419918	48820,39844	6,03		1,14				0,21
Ubiquitin proteasome pathway										
proteasome (prosome, macropain) subunit, beta type, 7	H-PSMB8	gi|30585303	30112,40039	8,19	1,19	1,00				0,14
proteasome (prosome, macropain) subunit, beta type 2	M-Psmb2	gi|31981327	22851,73047	6,43	1,50				0,88	0,07
proteasome activator hPA28 suunit beta	H-PA28b	gi|1008915	27331,31055	5,44	2,26	1,48				0,16
proteasome alpha 3 subunit isoform 2	H-PSMA3	gi|23110939	27629,74023	5,19				0,69	0,79	0,23
ubiquitin activating enzyme E1	H-UBE1	gi|35830	117715,3438	5,57				0,59	0,93	0,07
ubiquitin activating enzyme E1	H-UBE1	gi|35830	117715,3438	5,57				0,62	0,98	0,15
ubiquitin activating enzyme E1	H-UBE1	gi|35830	117715,3438	5,57		1,04		0,67		0,17
ubiquitin activating enzyme E1	H-UBE1	gi|35830	117715,3438	5,57		1,25		0,80		0,40
ubiquitin carboxyl-terminal hydrolase 5	H-USP5								0,92	0,47
Metabolism associated and transport proteins										
3-phosphoglycerate dehydrogenase	H-PHGDH	gi|5771523	56628,42188	6,29	1,05				0,87	0,09
acetyl-Coenzyme A acetyltransferase 2	H-Acat2	gi|5174389	41269,30859	6,27				0,43	0,69	0,09
Adenosine kinase	H-AK	gi|13097732	38712,60156	6,23		1,01		0,86		0,01
adenylate kinase 1	M-ADK1	gi|10946936	23101,78906	5,7		1,85	10,97	0,73		
aldehyde dehydrogenase 1A3	H-ALD1A3	gi|4502041	55973,73828	6,64	1,48				0,61	0,11

aldo-keto reductase family 1, member B8	M-Akr1b8	gi|6679791	36097,60938	5,97	4,16	1,36				0,28
aminopeptidase puromycin sensitive	H-NPEPPS	gi|15451907	98440,95313	5,23				0,54	0,93	0,51
annexin A1	H-A1	gi|54696610	38803,0586	6,57	1,46	1,22				0,48
apoa1 protein	M-ApoA1	gi|61402210	23007,91016	7				0,25	0,85	0,33
apolipoprotein A-I	M-ApoA1	gi|2145135	30497,60938	5,64	1,84	1,01	2,38			
asparaginyl-tRNA synthetase variant	H-Nars	gi|62897229	62870,53906	5,9	2,82	1,29				0,15
brain glycogen phosphorylase	H-Pygb	gi|21361370	96634,52344	6,4	1,76	1,89				0,12
branched chain ketoacid dehydrogenase E1, beta polypeptide	M-BCKDHB	gi|40353220	35481,98047	5,33		2,36		0,97		0,50
calpain, small subunit 1	H-CSS1	gi|4502565	28297,73047	5,05	1,11				0,99	0,25
ceruloplasmin isoform b	M-Ceru	gi|110347564	121074,1875	5,53	1,53		2,28		0,76	
ceruloplasmin isoform b	M-Ceru	gi|110347564	121074,1875	5,53	1,67		2,55		0,77	
ceruloplasmin isoform b	M-Ceru	gi|110347564	121074,1875	5,53	1,97		2,60		0,95	
dihydropyrimidinase-like 2	H-DPYSL2	gi|4503377	62254,57031	5,95	1,13	1,09				0,08
dimethylarginine dimethylaminohydrolase 2	H-DDAH2	gi|7524354	29625,4492	5,66	1,66	1,55				0,17
eno3	M-Eno3	gi|71059715	46968,21875	6,29			4,26	0,99	0,72	
enolase 1 variant	H-Eno1	gi|62896593	47111,28906	7,01	1,15				0,71	0,32
enoyl Coenzyme A hydratase 1, peroxisomal	H-ECH1	gi|16924265	35735,37891	8,47		1,40		0,85		0,37
ferritin heavy chain 1	M-Fth1	gi|6753912	21053,25977	5,53		1,37	5,22	0,80		
ferritin light chain 1	M-Ftl1	gi|18044716	20745,4707	5,66	2,38	1,11	5,41			
glucosidase II	H-Glu2	gi|2274968	106832,6484	5,71		1,20		0,71		0,13
glutamate carboxypeptidase	H-GCP	gi|15620780	52818,91016	5,71		1,22		0,73		0,02
glutathione S-transferase	H-GST	gi|2204207	23367,03906	5,43	1,08	1,09				0,14
glutathione S-transferase M3	H-GSTM3	gi|23065552	26542,14063	5,37				0,88	0,83	0,08
glutathione synthetase	H-GS	gi|4504169	52352,26172	5,67		1,26		0,87		0,36
guanine monophosphate synthetase variant	H-GMPS	gi|62898359	76647,90625	6,24	1,17				0,54	0,05

guanine nucleotide binding protein (G protein), alpha inhibiting activity polypeptide 3	H-GNAI3	gi|5729850	40506,26953	5,5	1,05	2,17				0,05
cathepsin D (lysosomal aspartyl protease)	H-Ctsd	gi|30584113	44636,71094	6,1	1,20	1,04				0,40
glucose-6-phosphate dehydrogenase	H-G6PD	gi|30584817	59332,07031	6,39	1,37				0,41	0,23
hypothetical protein	H-hyp	gi|21740140	27244,63086	5,66				0,98	0,55	0,17
inosine monophosphate dehydrogenase 2	H-IMPDH2	gi|66933016	55769,64844	6,44	1,32				0,43	0,09
LAP3 protein	H-LAP3	gi|37588925	54354,73828	6,8				0,64	0,58	0,14
LAP3 protein	H-LAP3	gi|37588925	54354,73828	6,8	1,18				0,84	0,20
leukotriene A4 hydrolase	H-LTA4H	gi|4505029	69241,24219	5,8				0,68	0,95	0,56
major vault protein	M-MVP	gi|13879460	95865,17188	5,43				0,72	0,83	0,28
mitochondrial ATP synthase, H+ transporting F1 complex beta subunit	H-ATPF1	gi|89574029	48083,03906	4,95		1,24	1,18	0,57		
mKIAA0573 protein	M-KI573	gi|50510531	49685,71875	5		1,72		0,73		0,50
N-acetylneuraminic acid phosphate synthase	H-NANS	gi|12056473	40281,44922	6,29	1,09				0,44	0,18
NAPRT1 protein	H-NARP	gi|33991172	54958,73828	5,74				0,81	0,75	0,26
oxidized protein hydrolase	H-OPH	gi|7144648	81200,64063	5,29				0,73	0,92	0,00
peroxiredoxin 6	H-PRDX6	gi|4758638	25019,18945	6	1,07	1,22				0,08
peroxiredoxin 6	M-PRDX6	gi|6671549	24810,98047	5,98	3,66				0,76	0,87
Pgm2 protein	M-Pgm2	gi|33416468	63414,58984	6,02			1,92	0,87	0,54	
Ppp2cb protein	M-PPP2CB	gi|17512397	32037,6797	5,48	2,42	1,68				0,30
similar to Serine/threonine-protein phosphatase 2A catalytic subunit beta isoform (PP2A-	M-Ppp2cb	gi|94383336	34903,0703	5,45	1,48	1,64				0,04
proteasome (prosome, macropain) activator subunit 1 (PA28 alpha)	H-PSME1	gi|54695540	28818,09961	5,78				0,89	0,86	0,17
proteasome (prosome, macropain) subunit, alpha type 6	M-Psma6	gi|6755198	27354,80078	6,34	1,10	1,44				0,51
protein disulfide isomerase-associated 4	H-PDIa4	gi|4758304	72886,96875	4,96	1,09	2,40	2,74			
purine nucleoside phosphorylase	M-PNP	gi|388921	32253,10938	5,93	1,23	2,16				0,78
pyridoxal kinase	H-PDXK	gi|4505701	35079,91016	5,75	1,29	1,25				0,15

ribonuclease/angiogenin inhibitor variant	H-RNH1					1,11		0,91		0,29
ribonuclease/angiogenin inhibitor variant	H-RNH1	gi|62087972	34524,33984	4,83	1,52	1,14				0,50
selenium binding protein 1	H-SBP1	gi|16306550	52357,62109	5,93				0,89	0,89	0,25
sulfotransferase family, cytosolic, 1A, phenol-preferring, member 4	H-SULT1A4	gi|84040296	34303,14063	5,68	1,91	2,36				0,37
TALDO1 protein	H-TALDO	gi|48257056	37385,42188	6,35	2,13				0,96	0,28
TALDO1 protein	H-TALDO	gi|48257056	37385,42188	6,35	1,31				0,79	0,14
thioredoxin peroxidase 1-like	H-PRDX1l	gi|62901916	24796,53906	6,05	1,02	1,04				0,29
transferrin	M-Trf	gi|20330802	76673,71875	6,94	3,37	1,10	2,13			
triosephosphate isomerase	M-TPI1	gi|1864018	22491,6308	5,62				0,93	0,43	0,42
triosephosphate isomerase	M-TPI1	gi|1864018	22491,63086	5,62	1,87		2,81		0,99	
triosephosphate isomerase 1	H-TPI1	gi|4507645	26652,74023	6,45	1,19	1,33				0,22
tumor protein, translationally-controlled 1	H-TPT1	gi|15214610	19644,5996	4,84		1,12		0,65		0,17
TXNDC5 protein	H-TXDC5	gi|12654715	36155	5,32		1,09		0,82		0,15
Ublcp1 protein	M-Ublcp1	gi|34784378	24285,68945	9,19		1,17		0,97		0,06
UMP-CMP kinase 2, mitochondrial	M-Tyki				1,20				0,77	0,33
vitamin D-binding protein	M-DBP	gi|193446	53050,69141	5,26	1,24	1,01	2,35			
Signal transduction										
annexin A3	H-A3	gi|4826643	36352,66016	5,63		2,43		0,83		0,01
annexin A5	H-A5	gi|60824338	35932,3594	4,94	2,49	1,51				0,40
annexin A5	H-A5	gi|60833746	36029,4297	4,89	1,17				0,85	0,02
arhgap1 protein	M-Arhgap1	gi|13879250	50393,10156	5,97		3,15		0,95		0,66
cathepsin Z	M-Ctsz	gi|11066226	34153,21875	6,13	7,76	2,54	1,39			
chain B, Cathepsin B (E.C.3.4.22.1)	H-Ctsb	gi|999909	22401,3301	5,2	1,94	2,09				0,25
chloride intracellular channel 1	H-CLIC1	gi|55961458	26167,26953	4,95	1,14	1,25				0,37
ER-60 protein	H-ER-60	gi|2245365	56747,73047	5,88		1,03		0,88		0,12

fibrinogen, B beta polypeptide	M-Fibrb	gi|33859809	54717,69141	6,68	14,42	1,65	4,92			
haptoglobin	M-Hpgn	gi|8850219	38727,48047	5,88	1,80	1,15	2,04			
HMW kininogen-I variant	M_KngnI	gi|40715900	53171,87109	4,88			8,00	0,68	0,88	
HMW kininogen-I variant	M_KngnI						1,78	0,54	0,53	
HMW kininogen-I variant	M-KngnI						8,00	0,68	0,88	
HMW kininogen-I variant	M-KngnI							1,78	0,54	0,53
serine (or cysteine) proteinase inhibitor, clade B (ovalbumin), member 1	H-SPIB1	gi|30584099	42827,78906	5,9	1,53				0,97	0,31
IQGAP1 protein	H-Iqgap1	gi|40674640	107472,1406	5,64				0,99	0,98	0,00
IQGAP1 protein	H-Iqgap1	gi|40674640	107472,1406	5,64	1,08	1,31				0,00
iqgap1 protein	M-Iqgap1	gi|27370648	106421,3906	5,61		1,44		0,86		0,26
kininogen 1	M-Kngn	gi|12963497	47867,60156	5,74			3,45	0,51	0,59	
kininogen 1	M-Kngn	gi|12963497	47867,60156	5,74			4,42	0,55	0,69	
kininogen 1	M-Kngn	gi|12963497	47867,60156	5,74			4,98	0,77	0,89	
kininogen 1	M-Kngn							0,18	0,55	0,75
kininogen 1	M-Kngn						1,94	0,19	0,58	
rho GDP dissociation inhibitor (GDI) alpha	H-GDIa	gi|4757768	23192,6992	5,02		1,12		0,92		0,59
serine (or cysteine) peptidase inhibitor, clade A, member 3K	M_SPIC3K	gi|16741103	46869,96094	5,05	2,67	2,60	2,23			
serine (or cysteine) peptidase inhibitor, clade A, member 3K	M-SPIA3K	gi|16741103			5,36		2,56		0,86	
serine (or cysteine) peptidase inhibitor, clade A, member 3K	M-SPIA3K	gi|16741103			6,49	1,15	3,41			
serine (or cysteine) peptidase inhibitor, clade A, member 3K	M-SPIA3K	gi|16741103	46869,96094	5,05	6,95	2,23	8,25			
serine (or cysteine) peptidase inhibitor, clade A, member 3K	M-SPIA3K				3,18				0,39	0,12
serine (or cysteine) peptidase inhibitor, clade A, member 3K	M-SPIA3K				4,14		1,20		0,70	
serine or cysteine proteinase inhibitor clade B member	H-SPIB5	gi|60817455	42083,42188	5,72		2,07		0,73		0,13

5										
serpina1c protein	M-Serp1c	gi|15929675	45593,39844	5,31	3,88	2,84	5,56			
serpina1c protein	M-Serp1c				2,33	1,60				0,60
tyrosine 3-monooxygenase/tryptophan 5-monooxygenase activation protein, beta polypeptide	M-1433e	gi|31543974	28068,85938	4,77		1,19		0,79		0,54
ywhaq protein	M-1433T	gi|51593617	29920,93945	4,87		1,33		0,81		0,33
Other proteins										
albumin 1	M-Alb1	gi|33859506	68677,71875	5,75	1,27		1,16		0,31	
annexin A8	H-A8	gi|60652779	36970,73047	5,56	1,85	1,01				0,56
chain A, crystal Structure of Fkbp52 C-Terminal domain	H-FKBP	gi|50513270	38216,17188	6,38		1,03	2,17	0,96		
chain A, crystal structure of murine coronin-1	M-Coro1	gi|83754025	44317,33984	6,03		1,08		0,62		0,56
complement C3 precursor (HSE-MSF)	M-C3	gi|1352102	186364,6875	6,39	3,85	2,05	1,95			
complement C3 precursor (HSE-MSF)	M-C3							0,76	0,66	0,34
crocalbin-like protein	H-CALUL	gi|8515718	34968,32031	4,39		5,07				0,22
FK506-binding protein 4	H-Fkbp4	gi|4503729	51772,07031	5,35				0,95	0,96	0,51
HP95	H-HP95	gi|13375569	95936,1094	6,13				0,72	0,54	0,19
hypothetical protein FLJ41407 variant	H-Hyp41407	gi|62088022	59575,87109	8,54				0,60	0,86	0,04
KIAA0158	H-KI158	gi|40788885	42119,53906	6,05		1,61		0,66		0,31
mFLJ00343 protein	M-FLJ	gi|47847514	205197,625	5,6	1,22				0,84	0,39
mFLJ00343 protein	M-FLJ343	gi|47847514	205197,625	5,6	6,12	2,22				0,73
mFLJ00343 protein	M-FLJ343				3,54	1,15				0,57
otubain 1	M-otub	gi|19527388	31250,40039	4,85	1,85	1,21				0,45
serum amyloid P-component precursor (SAP)	M-SAP	gi|134198	26230,26953	5,98	2,43	1,39	3,54			
SET	M-SET	gi|3953617	24348,0293	4,97				0,90	0,41	0,09
SET	M-SET	gi|3953617	24348,0293	4,97	1,81	1,24				0,57

stress-induced phosphoprotein 1	M-Stip1	gi|13277819	62528,37891	6,4	1,33				0,96	0,29
thrombospondin	M-Thbs	gi|554390	53810,44922	6,16	7,68	1,15	4,47			
TPMsk1	H-TPMsk1	gi|19072647	23740,13086	4,72			2,70	0,49	0,92	
villin 2	H-Vil2	gi|21614499	69369,74219	5,94	1,16				0,81	0,19
villin 2	H-Vil2	gi|46249758	69198,63281	5,94	10,53	25,08				0,48
villin 2	H-Vil2	gi|46249758	69198,63281	5,94	4,16	1,40				0,45
villin 2	H-Vil2	gi|46249758	69198,63281	5,94				0,16	0,64	0,01
villin 2	H-Vil2	gi|46249758	69198,63281	5,94				0,44	0,68	0,03
villin 2	H-Vil2	gi|46249758	69198,63281	5,94				0,61	0,71	0,17
villin 2	H-Vil2	gi|46249758	69198,63281	5,94	1,75				0,90	0,25
vinculin	H-VCL	gi|60812071	116776,4219	5,83	1,21	1,30				0,26
vinculin	M-VCL	gi|31543942	116644,2969	5,77	2,01	3,74	3,06			
vinculin	M-VCL	gi|31543942	116644,2969	5,77	1,99	1,03				0,25
Unknown proteins										
unknown	H-unkn	gi|63991119	36035,26953	5,96	2,36				0,82	0,38
unknown	H-unkn	gi|63991119	36035,26953	5,96	2,39	1,24	2,07			
unknown	H-unkn	gi|62288384	64990,55078	5,59	2,65	1,44	2,19			
unknown (protein for IMAGE:5068183)	H-unkn	gi|116283668	106891,7188	5,69	1,31				0,64	0,02
unknown (protein for IMAGE:3529287)	H-unkn	gi|52790434	37696,98047	8,56	1,38				0,79	0,31
unknown (protein for IMAGE:3592890)	H-unkn	gi|14250269	69103,8125	6,38				0,55	0,63	0,01
unknown (protein for IMAGE:3592890)	H-unmd	gi|14250269	69103,8125	6,38	2,55	1,31				0,57
unnamed protein product	H-unmd	gi|7022978	91550,79688	5,22				0,86	0,60	0,09
unnamed protein product	H-unmd	gi|10435669	26938,83008	5,34				0,97	0,73	0,43
unknown (protein for IMAGE:3592890)	H-unmd	gi|14250269	69103,8125	6,38	1,15	1,21				0,43
unknown (protein for IMAGE:3592890)	M-unkn	gi|14250269	69103,8125	6,38	5,86	2,02	5,34			

unnamed protein product	M-unkn	gi|74151835	35893,12109	5,43	1,20				0,63	0,25
unknown (protein for IMAGE:2650358)	M-unkn	gi|116283288	51882,26172	8,84	1,24				0,77	0,45
unnamed protein product	M-unmd	gi|74198890	22130,38086	8,26	8,59	14,15	11,16			
unnamed protein product	M-unmd	gi|53141	3842,189941	9,78	3,27	4,21	9,30			
unnamed protein product	M-unmd	gi|74198200	47292,98047	5,61	2,24	2,58	7,57			
unnamed protein product	M-unmd	gi|12845061	43003,78125	6,58	2,61	2,64	8,52			
unnamed protein product	M-unmd	gi|12845061	43003,78125	6,58	2,98	3,03	8,96			
unnamed protein product	M-unmd	gi|74204932	26277,78906	5,16	1,21	1,43	2,07			
unnamed protein product	M-unmd	gi|26344461	22933,64063	5,2	1,22	1,43	2,09			
unnamed protein product	M-unmd	gi|26341410	20290,49023	9,8	1,27	1,44	2,11			
unnamed protein product	M-unmd	gi|12851441	33155,16016	5,22	1,27	1,48	2,13			
unnamed protein product	M-unmd	gi|74224797	36487,08984	6,47	1,32	1,51	2,22			
unnamed protein product	M-unmd	gi|74214038	34524,53906	6,06	1,37	1,52	2,29			
unnamed protein product	M-unmd	gi|74222627	33100,94141	5,83	1,38	1,59	2,29			
unnamed protein product	M-unmd	gi|12845061	43003,78125	6,58	1,44	1,73	2,40			
unnamed protein product	M-unmd	gi|74197204	19477,58008	4,76	1,44	1,80	2,46			
unnamed protein product	M-unmd	gi|74178174	92418,25	4,74	1,51	2,09	2,68			
unnamed protein product	M-unmd	gi|74219251	51285,17969	7,92	1,59	2,14	2,85			
unnamed protein product	M-unmd	gi|74224797	36487,08984	6,47	1,70	2,30	2,90			
unnamed protein product	M-unmd	gi|26346108	47145,35938	5,67	1,74	2,35	3,08			
unnamed protein product	M-unmd	gi|74139792	56517,78125	7,53	1,75	2,49	3,50			
unnamed protein product	M-unmd	gi|74139792	56517,78125	7,53	1,82	2,52	3,74			
unnamed protein product	M-unmd	gi|74194251	46717,28125	5,09	1,94	2,53	6,37			
unnamed protein product	M-unmd	gi|12847394	33036,17969	4,91				0,61	0,64	0,18
unnamed protein product	M-unmd	gi|74204185	46256,64844	5,49				0,63	0,64	0,21
unnamed protein product	M-unmd	gi|74185120	42704,23047	5,4				0,63	0,75	0,22
unnamed protein product	M-unmd	gi|74185796	42541,16016	5,53				0,63	0,78	0,22

unnamed protein product	M-unmd	gi|74185796	42541,16016	5,53				0,64	0,80	0,24
unnamed protein product	M-unmd	gi|74183311	42983,17188	5,08				0,66	0,82	0,25
unnamed protein product	M-unmd	gi|74194251	46717,28125	5,09				0,66	0,84	0,27
unnamed protein product	M-unmd	gi|50815	42157,89844	6,56				0,69	0,85	0,29
unnamed protein product	M-unmd	gi|12850141	38331,92188	5,01				0,73	0,85	0,29
unnamed protein product	M-unmd	gi|50815	42157,89844	6,56				0,73	0,85	0,31
unnamed protein product	M-unmd	gi|12846758	49607,96094	4,78				0,74	0,89	0,35
unnamed protein product	M-unmd	gi|74147276	48647,14063	5,72				0,77	0,92	0,37
unnamed protein product	M-unmd	gi|12846039	12923,26953	4,82				0,79	0,93	0,38
unnamed protein product	M-unmd	gi|74141821	49667,01172	4,82				0,82	0,93	0,39
unnamed protein product	M-unmd	gi|74138546	59225,75	5,97				0,82	0,94	0,45
unnamed protein product	M-unmd	gi|74138891	56950,75	4,79				0,83	0,95	0,51
unnamed protein product	M-unmd	gi|26353794	56589,58984	5,78				0,85	0,97	0,51
unnamed protein product	M-unmd	gi|26341396	64960,71094	5,49				0,88	0,98	0,53
unnamed protein product	M-unmd	gi|74219490	59645,98047	5,72		1,00		0,91		0,59
unnamed protein product	M-unmd	gi|74200069	42169,55078	4,57		1,01		0,94		0,60
unnamed protein product	M-unmd	gi|74184034	29177,75	6,14	1,19				0,32	0,00
unnamed protein product	M-unmd	gi|74197204	19477,58008	4,76				0,19	0,44	0,06
unnamed protein product	M-unmd	gi|74181386	26518,15039	4,69				0,45	0,45	0,07
unnamed protein product	M-unmd	gi|74137638	26380,18945	4,74				0,46	0,52	0,07
unnamed protein product	M-unmd	gi|74151976	35760,21875	4,83				0,51	0,56	0,11
unnamed protein product	M-unmd	gi|74142393	35716,14844	4,79				0,55	0,60	0,12
unnamed protein product	M-unmd	gi|74151784	32887,64844	5,69				0,59	0,61	0,15
unnamed protein product	M-unmd	gi|12834035	31441,7793	5,7				0,59	0,61	0,15

Table 2. Differential expression proteins in HT-29 tumors (Protein profiling using 2-DE; Delta2D software; MALDI-TOF).

(Subcutaneous HT-29 tumors in nude mice with and without VAVC GLV-1h68 treatment; time points were taken 7, 21 and 42 days after intravenous injection of the virus; fold of enhancement or reduction of protein expression after virus injection are shown; highly expression in red and down-regulated in blue)

Fold of enhancement	Fold of suppression
>5	>5
3 to 5	3 to 5
2 to3	2 to 3

Protein name	Abbr	Accession	MW	*p*I	12hpi (+)fold	24hpi (+)fold	48hpi (+)fold	12hpi (-)fold	24hpi (-)fold	48hpi (-)fold
Viral proteins										
GUS23	V-Gus	gi|8515916	68346,70313	5,29	∞		1,51		0,94	
Cytoskeleton proteins										
Actr2 protein	H-Actr2	gi|29126784	44601,19141	6,31	2,41		1,03		0,92	
keratin 1	H-Krt1	gi|17318569	66027	8,16		2,37	1,50	0,89		
keratin 18	H-Krt18	gi|12653819	48002,53125	5,39	2,50				0,37	0,89
keratin 2	H-Krt2	gi|47132620	65393,21094	8,07	3,32	1,30	1,74			
keratin 20	H-Krt20	gi|60811060	48570	5,52	∞		1,50		0,72	
keratin 8	H-Krt8	gi|60826349	53784,21875	5,52		2,70	1,74	0,48		
keratin 8	H-Krt8	gi|4504919	53671,12891	5,52		2,95	2,14	0,44		
gelsolin-like capping protein	M-GlsCap	gi|110227377	38744,67188	6,47	2,98				0,86	0,63
myosin A1 catalytic light chain, skeletal muscle - mouse	M-MyoA1				2,32	1,28				0,41
myosin A1 catalytic light chain, skeletal muscle - mouse	M-MyoA1	gi|91114	20580,44922	4,98		70,32	2,48	0,89		

alpha actinin	H-Actna	gi|3157976	105158,6797	5,47	1,36	1,10				0,49
keratin, type II cytoskeletal 1 (Cytokeratin-1) (CK-1) (Keratin-1) (K1) (67 kDa cytokeratin) (Hair	H-Krt1	gi|1346343	65977,97656	8,16	∞				0,55	0,35
keratin 1	H-Krt1	gi|17318569	66027	8,16	13,04				0,68	0,56
keratin 1	H-Krt1	gi|17318569	66027	8,16	35,16				0,63	0,46
KRT8 protein	H-Krt8	gi|39645331	55874,19922	5,62				0,88	0,60	0,55
KRT8 protein	H-Krt8	gi|33875698	55787,17188	5,62				0,87	0,74	0,57
65-kDa macrophage protein	M-LCP-1	gi|984636	70156,8125	5,28	1,58	1,17				0,56
Stress response										
chaperonin containing TCP1, subunit 2	H-CCT2	gi|5453603	57452,12891	6,01		1,12	2,24	0,54		
Hspd1 protein	M-Hspd	gi|76779273	59387,98828	8,09		2,29		0,60		0,35
T-complex protein 1 subunit beta (TCP-1-beta) (CCT-beta)	M-TCP1	gi|22654291	57441,10938	5,97	1,12				0,78	0,47
Translation associated proteins										
eukaryotic translation elongation factor 1 gamma	H-EEF1g	gi|15530265	50115,17188	6,25	2,68		1,74		0,85	
elongation factor 2[Mus musculus	M-EF2	gi|192989	29870,07031	6,2	∞				0,23	0,25
acidic ribosomal phosphoprotein P0	M-ARPP0	gi|13277927	34164,73828	5,91	2,27	1,33	1,45			
PP856	H-PP856	gi|10834730	43805,32813	6,05	1,08		1,10		0,59	
RNA processing										
asparaginyl-tRNA synthetase	H-AsnS	gi|4758762	62902,51172	5,9	60,87				0,61	0,92
PREDICTED: similar to zinc finger protein 658B	H-ZNF658B	gi|113421082	94170,64063	8,86	1,05		1,57		0,50	
Metabolism associated and transport proteins										
peroxiredoxin 2 isoform a	H-PRDX2	gi|32189392	21878,24023	5,66	∞	∞	∞			
peroxiredoxin 3	H-PRDX3	gi|14250063	27705,15039	7,11	∞	18,18	14,29			
peroxiredoxin 3	H-PRDX3	gi|14250063	27705,15039	7,11	2,14	6,64				0,77
peroxiredoxin 4	H-PRDX4	gi|60834541	30635,83984	5,74	2,36	1,16	1,27			

peroxiredoxin 4	H-PRDX4	gi|60834541	30635,83984	5,74	2,27		1,01		0,99	
TALDO1 protein	H-Tal1	gi|48257056	37385,42188	6,35	2,01				0,76	0,84
TALDO1 protein	H-Tal1	gi|48257056	37385,42188	6,35	2,36				0,73	0,79
TALDO1 protein	H-Tal1				3,72				0,69	0,71
TALDO1 protein	H-Tal1	gi|16307182	35306,44922	9,07	∞				0,31	0,70
annexin A13 isoform a variant	H-A13	gi|62898309	35321,16016	5,59	2,22		1,25		0,37	
acetyl-CoA acetyltransferase, cytosolic variant	H-Acat	gi|62087566	42108,78906	7,2	2,35				0,69	0,78
dihydropyrimidinase-like 2 variant	H-DPYSL2	gi|62087970	68141,52344	5,85	2,03		1,12		0,94	
glutathione-S-transferase omega 1	H-GSTo1	gi|4758484	27548,03906	6,23	2,04				0,83	0,94
IDI1 protein	H-IDI1	gi|48257312	27585,17969	6,02	∞		1,31		0,30	
chain A, Structure Of Importin Beta Bound To The Ibb Domain Of Importin Alpha	H-Imp	gi|5107666	97172,07031	4,71	3,38	1,14				0,98
peroxiredoxin 1	H-Mccc2	gi|55959887	18963,66992	6,41	∞				0,81	0,44
peroxiredoxin 1	H-Mccc2	gi|6754976	22162,34961	8,26	1,58	211,68	1,66			
malate dehydrogenase (EC 1.1.1.37), cytosolic - human	H-MDH	gi|7431153	36391,94922	5,92	6,36	1,57	1,11			
protein disulfide isomerase-associated 4	H-PDIa4	gi|4758304	72886,96875	4,96	3,73	1,16	1,13			
chain A, triosephosphate Isomerase (Tim) (E.C.5.3.1.1) Complexed With 2-Phosphoglycolic Acid	H-TPI1	gi|999892	26521,69922	6,51	∞	110,01				0,24
abhydrolase domain containing 14B	M-Abhd	gi|14249382	22331,56055	5,94	24,90	3,30	1,01			
adenylate kinase 1	M-ADK1	gi|10946936	23101,78906	5,7		2,55		0,60		0,72
alpha-fetoprotein	M-AFP	gi|191765	47194,94922	5,47		55,97		0,67		0,46
apolipoprotein A-I	M-Apoa1	gi|2145135	30497,60938	5,64	3,89		1,22		0,74	
Apoa1 protein	M-ApoA1	gi|61402210	23007,91016	7	5,81	3,12	1,92			
Eno3	M-ENO3	gi|71059715	46968,21875	6,29	605,22	2,36				0,04
Eno3	M-Eno3	gi|71059715	46968,21875	6,29		6,23		0,13		0,12
rho, GDP dissociation inhibitor (GDI) beta	M-GDIa	gi|33563236	22836,49023	4,97	2,19	1,17				0,88
Purine nucleoside phosphorylase (Inosine phosphorylase) (PNP)	M-PNP	gi|1346738	32256,06055	5,78	4,46	1,01	2,22			
RAB14, member RAS oncogene family	M-RAB	gi|18390323	23881,92969	5,85	∞	113,87	3,17			
annexin A13 isoform a variant	H-A13	gi|62898309	35321,16016	5,59	1,36		1,41		0,50	
S-adenosylhomocysteine hydrolase Human	H-AHCY	gi|178277	47684,21875	6,03	1,86		1,33		0,52	
aldo-keto reductase family 7, member A2	H-akrf7	gi|41327764	39563,69922	6,7	1,47				0,56	0,73

aldehyde dehydrogenase 9A1	H-ALDH9	gi|115387104	56255,42969	6,23	1,68		1,46		0,50	
clusterin	H-Clu	gi|61365285	52575,03906	5,73		1,21		0,80		0,58
glycerol-3-phosphate dehydrogenase 1	H-GPD1	gi|60810758	37656,39844	5,81	1,95		1,23		0,55	
AICAR formyltransferase/IMP cyclohydrolase bifunctional enzyme (Homo sapiens)	M-AICAR	gi|1263196	64425,26172	6,39				0,72	0,97	0,45
chromatin modifying protein 4B	M-CMP4B	gi|28077049	24920,56055	4,76	1,13				0,38	0,81
Signal transduction										
DJ-1 protein	H-DJ-1	gi|31543380	19878,49023	6,33	2,32	5,69	1,23			
PREDICTED: similar to Proteasome subunit alpha type 6 (Proteasome iota chain)	H-PSMA6	gi|109083331	28129,24023	6,35	2,32		2,82		0,81	
fibrinogen, B beta polypeptide	M-Fibrg	gi|33859809	54717,69141	6,68	2,58	1,27				0,78
haptoglobin	M-Hpgn	gi|8850219	38727,48047	5,88	1,00	2,42				0,65
proteasome (prosome, macropain) subunit, alpha type 1	M-PSMA1	gi|33563282	29527,82031	6	11,17				0,66	0,74
proteasome (prosome, macropain) 26S subunit, non-ATPase, 7	M-PSMD7	gi|6754724	36517,21094	6,29	12,78	1,05				0,89
serine (or cysteine) peptidase inhibitor, clade A, member 3K	M-SPIA3K				2,15	1,10				0,31
serine (or cysteine) peptidase inhibitor, clade A, member 3K	M-SPIA3K	gi|15079234	46835,96875	5,05	∞				0,59	0,09
serine (or cysteine) peptidase inhibitor, clade A, member 3K	M-SPIA3K	gi|16741103	46869,96094	5,05		2,04		0,38		0,91
serine (or cysteine) peptidase inhibitor, clade A, member 3K	M-SPIA3K	gi|15079234	46835,96875	5,05		3,81	1,00	0,07		
HMW kininogen-I variant	M-KngnI	gi|40715900	53171,87109	4,88		1,35	2,17	0,56		
serine (or cysteine) proteinase inhibitor, clade B (ovalbumin), member 6	H-SPIB6	gi|41152086	42594,05859	5,18		1,16		0,54		0,82
fibrinogen gamma-chain	M-Fibrg	gi|15593267	20752,91016	5,17		1,29	1,07	0,57		
fibrinogen gamma-chain	M-Fibrg	gi|15593267	20752,91016	5,17		1,32	1,10	0,57		
haptoglobin	M-Hpgn	gi|8850219	38727,48047	5,88	1,14	1,08				0,53
LMW K-kininogen precursor	M-Kng	gi|205077	35672,78906	7,21		1,97	1,67	0,59		
kininogen 1	M-KngnI	gi|12963497	47867,60156	5,74		1,15	1,44	0,58		

HMW kininogen-I variant	M-KngnI				1,48				0,59	0,42
pregnancy zone protein	M-PZP	gi|110347469	165747,7969	6,24	1,59	1,29				0,52
serine (or cysteine) peptidase inhibitor, clade A, member 3K	M-SPIA3K	gi|16741103	46869,96094	5,05		1,69		0,57		0,87
HMW kininogen-I variant	M-SPIA3K				1,01	1,15				0,45
HMW kininogen-I variant	M-SPIA3K					1,28		0,87		0,47
Others										
Ig gamma-1 chain C region (15C5) - mouse (fragment)	M-IgGc	gi|110077	17304,51953	8,76	6,90				0,23	0,20
albumin 1	M-Alb1	gi|33859506	68677,71875	5,75		2,39	1,10	0,59		
albumin 1	M-Alb1	gi|33859506	68677,71875	5,75		23,40	1,15	0,39		
tumor rejection antigen (gp96) 1 variant	H-gp96					1,11		0,67		0,56
tumor rejection antigen (gp96) 1 variant	H-gp96	gi|62088648	65912,28906	5,08		1,22	1,28	0,27		
PAP-inositol-1,4-phosphatase	H-PIP	gi|6688197	33401,21094	5,46	1,23		1,02		0,60	
thioredoxin reductase	H-PRDX5	gi|2832346	54511,85156	6,07	1,55	1,14				0,42
albumin 1	M-Alb1	gi|33859506	68677,71875	5,75	1,16	1,11				0,12
albumin 1	M-Alb1	gi|33859506	68677,71875	5,75	1,11	1,12				0,39
albumin 1	M-Alb1	gi|33859506	68677,71875	5,75		1,17		0,94		0,44
complement component 3	M-CompC3	gi|23956044	186363,7031	6,44		1,44		0,77		0,51
complement component 3	M-CompC3	gi|23956044	186363,7031	6,44				0,95	0,78	0,45
otub1 protein	M-Otub	gi|32484336	30977,28906	4,85				0,60	0,87	0,48
Unknown proteins										
unnamed protein product	H-unmd	gi|10434142	65265,12109	8,96		1,34	1,70	0,51		
unknown (protein for IMAGE:3832468)	H-3832468	gi|33988037	38802,42969	9,37	2,65				0,97	0,58
unnamed protein product	H-unmd	gi|28317	59491,87109	5,17	43,13		1,02		0,77	
	H-unmd				∞				0,35	0,93
unknown (protein for IMAGE:3592890)	M-3592890	gi|14250269	69103,8125	6,38	∞				0,21	0,26
unknown (protein for IMAGE:3592890)	M-3592890	gi|14250269	69103,8125	6,38		8,89	2,56	0,16		
unnamed protein product	M-unmd	gi|26345182	30596,64063	5,51	2,18				0,84	0,66

unnamed protein product	M-unmd	gi|26354961	60505,82813	7,63	5,05				0,84	0,63
unnamed protein product	M-unmd	gi|74219251	51285,17969	7,92	10,98				0,83	0,59
unnamed protein product	M-unmd	gi|26354961	60505,82813	7,63	12,06				0,77	0,59
unnamed protein product	M-unmd	gi|26361821	22151,18945	7,11	16,66				0,75	0,52
unnamed protein product	M-unmd	gi|26361821	22151,18945	7,11	21,61				0,72	0,52
unnamed protein product	M-unmd	gi|26345182	30596,64063	5,51	129,63				0,72	0,52
unnamed protein product	M-unmd	gi|26364516	12070,15039	6,28	323,36				0,60	0,44
unnamed protein product	M-unmd	gi|52181	25730,48047	7,59	568,02				0,57	0,40
unnamed protein product	M-unmd	gi|26341410	20290,49023	9,8	759,74				0,53	0,38
	M-unmd				∞				0,01	0,11
unnamed protein product	M-unmd	gi|74216905	16492,63086	6,14	∞				0,21	0,22
unnamed protein product	M-unmd	gi|26344461	22933,64063	5,2		2,72	1,47	0,56		
unnamed protein product	M-unmd	gi|74139512	36303,55859	5,61		3,07	1,55	0,55		
unnamed protein product	M-unmd	gi|12845061	43003,78125	6,58		5,52	1,86	0,53		
unnamed protein product	M-unmd	gi|26341396	64960,71094	5,49		9,32	2,34	0,26		
unnamed protein product	H-unmd	gi|34039	44079,12109	5,04			1,69	0,59	0,95	
unknown (protein for IMAGE:3529287)	H-3529287	gi|52790434	37696,98047	8,56			1,05	0,44	0,98	

Table 3. Differential expression proteins in PC-3 tumors (Protein profiling using 2-DE; Delta2D software; MALDI-TOF).

(Subcutaneous PC-3 tumors in nude mice with and without VAVC GLV-1h68 treatment; time points were taken 7, 21 and 42 days after intravenous injection of the virus; fold of enhancement or reduction of protein expression after virus injection are shown; highly expression in red and down-regulated in blue)

Fold of enhancement	Fold of suppression
>5	>5
3 to 5	3 to 5
2 to3	2 to 3

Protein name	Abbr	Accession	MW	*p*I	7dpi (+)fold	21dpi (+)fold	42dpi (+)fold	7dpi (-)fold	21dpi (-)fold	42dpi (-)fold
Cytoskeleton proteins										
ACTB protein	H-ACTB	gi|15277503	40194,07031	5,55		1,82				0,36
ARP3 actin-related protein 3 homolog	H-ARP3	gi|5031573	47340,98047	5,61				0,86	0,47	0,97
FLNA protein	H-FLNA	gi|15779184	88534,4063	5,93	1,01				0,60	0,41
moesin	M-Msn	gi|199765	66440,10938	5,94			1,57	0,46	0,57	
tubulin, beta, 4 variant	H-Btub	gi|62897639	50340,19922	4,83	1,23				0,66	0,24
VIM	H-Vim	gi|47115317	53547,05859	5,09	1,79	2,39				0,33
vimentin	M-Vim	gi|2078001	51533,08984	4,96			8,94		0,15	
vimentin	H-Vim	gi|37852	53653,05859	5,06			###	0,86	0,50	
vimentin	H-Vim	gi|37852	53653,05859	5,06	1,79		3,59		0,78	
vimentin	H-Vim	gi|62414289	53619,07813	5,06			1,53	0,84	0,00	
Stress response										

CCT2	H-TCP1	gi|48146259	57424,05859	6,01		1,57				0,24
heat shock protein 1, beta	M-HSP1b	gi|40556608	83229,10938	4,97			3,12	0,44	0,72	
HSP90AA1 protein	H-HSP90AA1	gi|83318444	68328,78125	5,11				0,92	0,82	0,14
T-complex protein 1 subunit beta (TCP-1-beta) (CCT-β)	H-TCP1						2,32	0,81	0,77	
Translation associated proteins										
ATP-dependent DNA helicase II	H-Ku70	gi|10863945	82652,27344	5,55		2,44				0,88
BiP protein	H-BiP	gi|6470150	70887,52344	5,23		1,57		0,21		0,21
Ribosomal protein, large, P0	H-RPLP0	gi|12654583	34252,73828	5,42	1,73	2,63				0,95
stress-induced-phosphoprotein 1 (Hsp70/Hsp90)	H-STIP1	gi|5803181	62599,39844	6,4			4,35	0,70	0,23	
RNA processing										
	H-p100						3,82	0,93	0,81	
alpha isoform of regulatory subunit A, protein phosphatase 2	H-Ppp2r1a	gi|21361399	65266,9102	5				0,84	0,93	0,51
calreticulin=calcium binding protein [human, placenta, Peptide Partial, 31 aa, segment 1 of 5]	H-Calr	gi|913149	3736,72998	6,86			5,29	0,87	0,95	
calreticulin=calcium binding protein [human, placenta, Peptide Partial, 31 aa, segment 1 of 5]	H-Calr	gi|913148	3736,72998	6,86	1,18	1,13				0,17
heterogeneous nuclear ribonucleoprotein C	M-hnRNPC	gi|8393544	34363,85938	4,92	1,15				0,85	0,23
Hnrpc protein	M-hnRNPC	gi|13435678	32256,88086	5,01			1,35	0,93	0,53	
tRNA nucleotidyl transferase, CCA-adding, 1 isoform 1	H-TRNT1	gi|7705763	46329,14063	6,3					0,90	0,22
Metabolism associated and transport proteins										
aldehyde dehydrogenase family 1, subfamily A2	M-Aldh1a2	gi|6677665	54690,87109	5,83		1,29	4,05			
apolipoprotein A-I	M-ApoA1	gi|2145139	30525,60938	5,51	1,66				0,35	0,00
apolipoprotein A-I	M-ApoA1	gi|2145139	30525,60938	5,51	∞	2,70				0,00
copg protein	M-COPG	gi|14250257	70573,60938	4,78					0,78	0,40
EBNA-2 co-activator variant	H-p100	gi|62088600	107366,2734	7,36		1,07				0,15

enolase 1 variant	H-Eno1	gi|62897945	47167,32031	7,01				0,70	0,65	0,09
enolase 1 variant	H-Eno1	gi|62897945	47167,32031	7,01				0,87	0,76	0,43
epsilon subunit of coatomer protein complex isoform c	H-COPE	gi|40805827	28754,59961	5,11				0,32	0,51	0,00
epsilon subunit of coatomer protein complex isoform c	H-COPE	gi|40805827	28754,59961	5,11		1,01				0,02
ferritin light chain 1	M-Ftl1	gi|18044716	20745,4707	5,66				0,96	0,81	0,19
glycogen phosphorylase	H-PYG	gi|3170407	97061,86719	6,31	1,11				0,67	0,32
LAP3 protein	H-LAP3	gi|37588925	54354,73828	6,8			3,70	0,44	0,38	
LAP3 protein	H-LAP3	gi|37588925	54354,73828	6,8				0,88	0,80	0,23
liver transferrin Musculus	M-Trf	gi|198848	14644,24023	4,94			2,50	0,57	0,83	
liver transferrin Musculus	M-Trf	gi|198848	14644,24023	4,94		1,02		0,99		0,04
liver transferrin Musculus	M-Trf	gi|198848	14644,24023	4,94			9,48	0,52	0,72	
mitochondrial ATP synthase, H+ transporting F1 complex beta subunit	H-ATPF1	gi|89574029	48083,03906	4,95			4,54	0,84	0,58	
Pgm2 protein	M-Pgm2	gi|33416468	63414,58984	6,02		2,20	1,53			
Phosphorylase, glycogen; liver (Hers disease, glycogen storage disease type VI)	H-PYGL	gi|112180335	96955,97656	6,71	1,44				0,46	0,28
PREDICTED: similar to Transitional endoplasmic reticulum ATPase (TER ATPase) (15S Mg(2+)-ATPase p97 Mouse	M-TERA	gi|94408013	58740,21875	5,62				0,98	0,96	0,58
rab GDP dissociation inhibitor alpha	M-GDIa	gi|13936441	50494,07031	4,96			4,49		0,72	
rho GDP dissociation inhibitor (GDI) alpha	M-GDIa	gi|31982030	23392,81055	5,12	1,27				0,92	0,00
transferrin	M-Trf	gi|20330802	76673,71875	6,94		1,19		0,96		0,06
twinfilin-like protein	H-TWFl	gi|6005846	39523,26953	6,37		1,10		0,78		0,55
ubiquitin activating enzyme E1	H-UBE1	gi|35830	117715,34375	5,57				0,36	0,67	0,68
uroporphyrinogen decarboxylase	H-UROD	gi|71051616	40760,82813	5,77			2,54	0,98	0,59	
signal transduction										
	M-SHP-1						2,17	0,62	0,75	
alpha-1 protease inhibitor 2	M-A1AT2	gi|191844	44746,85938	5,33	2,12	1,13	1,83			
alpha-1-antitrypsin	M-A1AT	gi|192094	22826,7793	5,98	1,08				0,95	0,46

chain A, Crystal Structure Of 14-3-3 Gamma In Complex With A Phosphoserine Peptide Human	H-1433G	gi|82407948	28153,8691	4,8	###		###		0,68	
chain A, crystal Structure Of 14-3-3 gamma in complex with a phosphoserine peptide	H-1433G	gi|82407948	28153,8691	4,8	1,17				0,00	0,11
nuclear chloride channel	H-CLIC1	gi|4588526	26906,73047	5,02				0,24	0,36	0,11
rho GDP dissociation inhibitor (GDI) alpha	H-GDIa	gi|4757768	23192,6992	5,02	1,30				0,83	0,50
Serine (or cysteine) peptidase inhibitor, clade A, member 3K	M-SPIA3K	gi|16741103	46869,96094	5,05		6,78		0,77		0,28
serine (or cysteine) proteinase inhibitor, clade B (ovalbumin), member 5	H-Serpinb5	gi|4505789	42111,44922	5,72		2,93		0,28		0,38
serine (or cysteine) proteinase inhibitor, clade B (ovalbumin), member 1 variant	H-SPIB1	gi|62898301	42742,71094	5,9	1,72	2,61				0,71
serine (or cysteine) proteinase inhibitor, clade B (ovalbumin), member 5	M-SPIA3K					1,71	8,15	0,68		
serine (or cysteine) proteinase inhibitor, clade B (ovalbumin), member 5	H-SPIB1					1,01		0,42		0,29
serpina1b protein	M-Serpina1b	gi|15929675	45593,39844	5,31	1,07	2,06				0,84
SH2 phosphatase 1	M-SHP-1	gi|4097668	67675,25	7,66	1,53				0,83	0,46
calpain 2, large subunit	H-CAPN2	gi|4502563	79955,82031	4,92	2,23		5,20		0,25	
Others proteins										
chain L, Igg2a Fab Fragment (50.1) Complex With 16-Residue Peptide (Residues 311-328 Of Hiv-1 Gp120 (mus culus)	M-Igg2a	gi|442937	23956,59961	5,07				0,96	0,81	0,49
protein phosphatase 1, catalytic subunit, gamma isoform	H-Ppp1cc	gi|4506007	36959,71875	6,13		1,09		0,87		0,45
transformation-related protein 14	H-TRP14					2,66				0,06
transformation-related protein 14	H-TRP14	gi|33415057	42791,69141	5,49		2,31		0,86		0,01
vinculin isoform meta-VCL	H-mVCL	gi|7669550	123721,8125	5,5		1,04		0,93		0,19
Unknown proteins										
unnamed protein product	H-unmd	gi|21757045	52406,42188	4,99		1,11	3,20			
unknown (protein for IMAGE:2650358)	M-2650358	gi|116283288	51882,26172	8,84					0,85	0,46

unknown (protein for IMAGE:2650358)	M-2650358	gi|116283288	51882,26172	8,84					0,92	0,52
unnamed protein product	M-unmd	gi|51452	58833,12891	5,48		1,01	5,66			
unnamed protein product	M-unmd	gi|26341396	64960,71094	5,49		1,05	4,97			
unnamed protein product	M-unmd	gi|74137565	68687,71875	5,78		1,12	4,10			
unnamed protein product	M-unmd	gi|74137565	68687,71875	5,78		1,16	3,69			
unnamed protein product	M-unmd	gi|26341396	64960,71094	5,49		1,18	3,54			
unnamed protein product	M-unmd	gi|74220592	70647,97656	5,22		1,20	2,64			
unnamed protein product	M-unmd	gi|74198645	56293,51172	5,25		1,23	2,47			
unnamed protein product	M-unmd	gi|26341396	64960,71094	5,49		1,23				0,05
unnamed protein product	M-unmd	gi|74208631	70827,17188	5,32		1,25				0,11
unnamed protein product	M-unmd	gi|74219251	51285,17969	7,92		1,27				0,18
unnamed protein product	M-unmd	gi|74143673	56857,73828	5,43		1,29				0,31
unnamed protein product	M-unmd	gi|74220199	68455,45313	5,15		1,31				0,34
unnamed protein product	M-unmd	gi|74179916	27358,78906	6,34		2,34				0,78
unnamed protein product	M-unmd	gi|12845061	43003,78125	6,58		2,46				0,83
unnamed protein product	M-unmd	gi|74178174	92418,25	4,74		2,64				0,84
unnamed protein product	M-unmd						2,18	0,36	0,41	
unnamed protein product	M-unmd	gi|26341396	64960,71094	5,49		1,01	2,20	0,97		
unnamed protein product	M-unmd						1,69	0,42	0,49	
unnamed protein product	M-unmd							0,80	0,69	0,40
unknown (protein for IMAGE:2650358)	M-unmd	gi|116283288	51882,26172	8,84				0,89	0,80	0,41
unnamed protein product	M-unmd						1,90	0,37	0,67	
unnamed protein product	M-unmd						1,78	0,40	0,74	
unnamed protein product	M-unmd						1,60	0,49	0,75	
unnamed protein product	M-unmd						1,57	0,51	0,79	
unnamed protein product	M-unmd	gi|26341396	64960,71094	5,49			1,40	0,53	0,79	
unnamed protein product	M-unmd	gi|74143673	56857,73828	5,43			1,32	0,59	0,85	
unnamed protein product	M-unmd	gi|50815	42157,89844	6,56	3,48	9,61				0,93

Table 4. Differential expression proteins in GI-101A cells (Protein profiling using 2-DE; Delta2D software; MALDI-TOF).

(GI-101A cells with and without VAVC GLV-1h68 treatment; time points were taken 12, 24 and 48 hours after virus infection; fold of enhancement or reduction of protein expression after virus infection are shown; highly expression in red and down-regulated in blue)

Fold of enhancement	Fold of suppression
>5	>5
3 to 5	3 to 5
2 to3	2 to 3

Protein name	Abbr	Accession	MW	*p*I	12hpi (+)fold	24hpi (+)fold	48hpi (+)fold	12hpi (-)fold	24hpi (-)fold	48hpi (-)fold
Viral proteins										
20 kDa virion core protein	V-A12L	gi|137349	20506,2207	9,57	4,50	21,61	30,84			
30k DNA binding phosphoprotein	V-I3L	gi|2772696	30008,4707	5,68	1,91	2,53	2,83			
beta-galactosidase	V-bGal	gi|37780061	117625,8672	5,37	1,11	2,63	6,27			
beta-galactosidase	V-bGal	gi|644832	116130,9531	5,28		1,79	4,67	0,59		
dsRNA dependent PK inhibitor	V-E3L	gi|2772689	21490,82031	5,19	1,64	2,33	3,53			
hypothetical protein m8238R	V-Hyp8238	gi|56713587	24638,28906	6,35	2,44	10,45				0,72
hypothetical protein VACWR125	V-A6L	gi|66275922	43146,62109	8,08	1,31	2,88	4,48			
lacZ [Integrative translation probe vector pTP1]	V-LacZ	gi|91983328	115411,6875	5,3		1,23	2,82	0,35		
major core protein	V-A10L	gi|56713513	102184,5391	5,83		2,55	3,42	0,89		
major core protein P4b	V-A3L	gi|2772718	72577,88281	6,37	1,10	2,42	2,71			
p4b precursor of core protein 4b	V-A3L	gi|66275919	72577,84375	6,28	1,52	2,44	3,18			

putative 43.1k protein	V-A6L	gi|2772720	43072,44141	5,71		2,27	2,89	0,87		
ssDNA-binding phosphoprotein	V-I3L	gi|37551517	29994,44922	5,68	5,05	7,22	6,47			
Cytoskeleton proteins										
ARP3 actin-related protein 3 homolog	H-ARP3	gi|5031573	47340,98047	5,61	1,43	1,94	2,03			
chromosome 20 open reading frame 3	H-C20	gi|24308201	46450,85156	5,82				0,83		0,57
keratin 18	H-Krt18	gi|12653819	48002,5313	5,4				0,48		0,50
keratin 8, isoform CRA_d	H-Krt8	gi|119617060	62105,26953	5,79				0,61		0,44
radixin	H-Rdx	gi|4506467	68521,39063	6,03	2,46	2,20	2,52			
tropomodulin 3	H-TMOD3	gi|6934244	39556,28125	5,08				0,50		0,60
tropomyosin 4 Human	H-TPM4	gi|54696134	28617,57031	4,67	1,82	2,00	2,60			
tubulin, beta polypeptide	H-Btub	gi|57209813	47735,98828	4,7				0,85		0,51
Stress response										
chaperonin containing TCP1, subunit 8 (theta) variant	H-CCT8	gi|62896539	59612,51172	5,42				0,70		0,43
gamma subunit of CCT chaperonin	H-CCtg	gi|671527	60292,25	6,23		1,31		0,56		0,69
heat shock 70kDa protein 1A variant	H-hsp701a	gi|62089222	77447,71094	5,97				0,10		
heat shock 70kDa protein 1A variant	H-hsp701a	gi|62089222	77447,71094	5,97		1,05		0,58		0,68
heat shock 70kDa protein 4-like	H-HSPA4L	gi|31541941	94452,52344	5,63				0,99		0,50
HSP90AA1 protein	H-HSP90AA1	gi|12654329	64349,69922	5,1				0,63		0,32
HSPA9 protein	H-HSPA9	gi|21040386	73807,9531	6				0,51		0,48
t-complex polypeptide 1	H-TCP1	gi|36796	60355,75	6,03	1,12	2,82	3,72			
t-complex polypeptide 1	H-TCP1	gi|36796	60355,75	6,03		1,02		0,33		0,75

Translation associated proteins										
eukaryotic translation initiation factor 3, subunit 2 beta,	H-Eif3s2	gi|54696060	36591,69922	5,38				0,65		0,55
eukaryotic translation initiation factor 4B	H-EIF4B	gi|49256408	69125,25781	5,55	1,86	2,18	1,90			
eukaryotic translation initiation factor 4B	H-EIF4B	gi|49256408	69125,25781	5,55	1,99	3,18	2,96			
eukaryotic translation initiation factor 2, subunit 1 alpha, 35kDa [synthetic construc	H-eIF2	gi|30584065	36202,4609	5				0,73		0,48
pyrophosphatase 1	H-PP1	gi|11056044	32639,15039	5,54				0,41		0,35
RNA processing										
heterogeneous nuclear ribonucleoprotein U (scaffold attachment factor A)	H-henuriU	gi|55859528	79793,85156	8,06	1,77	2,03	2,47			
prohibitin	H-PHB	gi|46360168	29801,92969	5,57				0,31		0,27
thyroid hormone binding protein precursor Homosapiens	H-TRBP	gi|339647	57068,67188	4,82	3,41	2,19	1,17			
Ubiquitin proteasome pathway										
chain B, proteasome activator reg(Alpha) (Homo sapiens)	H-PARegA	gi|2780871	16284,66992	7,14				0,76		0,33
proteasome 26S non-ATPase subunit 5	H-PSMD5	gi|4826952	56160,35938	5,35				0,38		0,25
proteasome activator subunit 2	H-PSME2	gi|30410792	27384,31055	5,54				0,25		0,19
proteasome activator subunit 2	H-PSME2	gi|30410792	27384,31055	5,54				0,80		0,21
proteasome beta-subunit - human	H-PSMB	gi|631345	25892,85938	5,7				0,97		0,45
Metabolism associated proteins										
annexin A1	H-A1	gi|61356735	38718,0117	6,6				0,69		0,41

Chain A, Human B Lactate Dehydrogenase Complexed With Nad+ And 4- Hydroxy-1,2,5-Oxadiazole-3-Carbox	H-LDHB	gi|49259209	36516,1406	5,86	1,07	2,00				0,82
chain A, human B lactate dehydrogenase complexed with Nad+ And 4- Hydroxy-1,2,5-Oxadiazole-3-Carbox	H-LDHB	gi|49259209	36516,1406	5,86				0,65		0,58
creatine kinase, muscle	H-Creatine	gi|13938619	43039,91016	6,77	4,30					0,45
cytosolic malate dehydrogenase	H-MDH1	gi|5174539	36403,01953	6,91	4,30	5,86				0,93
dimethylarginine dimethylaminohydrolase 2	H-DDAH2	gi|55961454	19946,4297	5,6				0,90		0,41
enolase 1 variant	H-ENO1	gi|62897945	47167,32031	7,01	2,02	2,33	1,32			
enolase 1 variant	H-Eno1	gi|62896593	47111,28906	7,01				0,92		0,24
glucose-6-phosphate dehydrogenase	H-G6PD	gi|30584817	59332,07031	6,39				0,35		0,46
Hpast	H-Horf	gi|2529707	60664,67188	6,49				0,81		0,52
PDZ and LIM domain 1 (elfin)	H-PDZ	gi|13994151	36049,03906	6,56				0,63		0,43
peroxiredoxin 2	H-PRDX2	gi|60654143	21991,3203	5,7				0,40		0,42
peroxiredoxin 6	H-PRDX6	gi|4758638	25019,18945	6	1,30	2,16	2,61			
PGAM1	H-PGAM1	gi|49456447	28816,83984	6,67	3,15	6,74				0,01
phosphoribosyl pyrophosphate synthetase 2 isoform 2	H-PRPS2	gi|4506129	34746,98047	6,15	2,75	2,08	1,97			
protein disulfide isomerase-associated 4	H-PDIa4	gi|4758304	72886,96875	4,96				0,77		0,46
spermidine synthase	H-SPDSY	gi|63253298	33802,71094	5,3	2,17	1,71	1,38			
TALDO1 protein	H-TALDO	gi|48257056	37385,42188	6,35				0,28		0,15
triosephosphate isomerase 1	H-TPI1	gi|4507645	26652,74023	6,45	2,78	2,56	1,27			
TXNDC4	H-TXDC4	gi|37183214	46897,4102	5,1				0,71		0,59
Signal transduction										
COP9 signalosome subunit 4	H-CSN	gi|38373690	46239,6719	5,6	1,01					0,46
human rab GDI	H-GDI	gi|285975	50631,85938	5,94				0,80		0,45

mitogen-activated protein kinase kinase 2	H-MKK2	gi|33304081	34317,0117	7,66	1,13					0,48
rho GTPase activating protein 1	H-Arhgap1	gi|4757766	50404,19141	5,85	1,30	2,02	2,55			
serine protease inhibitor-like SPI-1	V-C12L	gi|37551651	40392,98828	5,08	16,68	35,52	41,96			
serpin peptidase inhibitor, clade B (ovalbumin), member 6, isoform CRA_d	H-SERPINB6	gi|119575506	42996,25	5,18				0,52		0,26
YWHAZ protein	H-1433zd	gi|49119653	29928,8203	4,7				0,58		0,45
Other proteins										
CAPNS1 protein	H-CAPNS1	gi|40674605	28211,67969	4,96	1,56	2,29	2,89			
FK506 binding protein 4 59kDa	H-Fkbp4	gi|61355277	51802,07813	5,35				0,47		0,34
FK506 binding protein 4 59kDa	H-Fkbp4							0,75		0,50
ribosomal protein SA, isoform CRA_c	H-RPSA	gi|119584991	19625,26953	8,37				0,64		0,45
Unkown proteins										
unknown	H-unkn	gi|158261809	59691,80078	5,34	1,59	1,95	2,71			
unknown	H-unkn	gi|62630180	88890,34375	5,44				0,43		0,52

Table 5. Differential expression proteins in HT-29 cells (Protein profiling using 2-DE; Delta2D software; MALDI-TOF).

(HT-29 cells with and without VAVC GLV-1h68 treatment; time points were taken 12, 24 and 48 hours after virus infection; fold of enhancement or reduction of protein expression after virus infection are shown; highly expression in red and down-regulated in blue)

Fold of enhancement	Fold of suppression
>5	>5
3 to 5	3 to 5
2 to3	2 to 3

Protein name	Abbr	Accession	MW	*p*I	12hpi (+)fold	24hpi (+)fold	48hpi (+)fold	12hpi (-)fold	24hpi (-)fold	48hpi (-)fold	Protein name
Viral proteins											
30k DNA binding phosphoprotein	V-I3L	gi|2772696	30008,4707	5,68	10,65	######	12,78	12,05			
chemokine-binding protein	V-C23L	gi|66275798	26349,5293	4,49	13,40	######	18,03	8,72			
dsRNA dependent PK inhibitor	V-dsPKI	gi|2772689	21490,82031	5,19	6,04	864.671	8,65	6,54			
hypothetical protein VACWR125	V-A6L	gi|66275922	43146,62109	8,08	3,50	706.686	7,07	5,82			
major core protein	V-A10L	gi|56713513	102184,5391	5,83	3,87	734.005	7,34	7,26			
p4b precursor of core protein 4b	V-A3L	gi|66275919	72577,84375	6,28	1,45	209.607	2,10	2,01			
putative DNA-binding virion core protein	V-E11L	gi|56713462	28424,65039	6,03	8,07	######	20,41	11,57			
ribonucleoside-diphosphate reductase	V-I4L	gi|56713400	36922,23828	5,08	5,61	######	10,70	9,63			
serine protease inhibitor-like SPI-1	V-C12L	gi|37551651	40392,98828	5,08	5,30	727.146	7,27	6,82			
toll/IL1-receptor	V-A46R	gi|66275969	27617,65039	4,99	1,93	217.246	2,17	1,23			
Cytoskeleton proteins											
actin, gamma 1 propeptide	H-ACTG	gi|4501887	41765,78906	5,31					0,93	0,52	0,44

ARP1 actin-related protein 1 homolog A, centractin alpha	H-ARP1	gi|5031569	42586,89844	6,19					0,94	0,90	0,38
BiP protein	H-BiP	gi|6470150	70887,52344	5,23					0,41	0,66	0,62
chain A, moesin ferm domain bound to Ebp50 C-terminal peptide	H-Moe	gi|50513540	34896,30859	9,03	2,01		1,93	1,67			
chaperonin (HSP60)	H-Hsp60	gi|306890	60986,3711	5,7	1,15		1,93	2,28			
heat shock 70kDa protein 1A variant	H-hsp701a	gi|62089222	77447,71094	5,97	3,22		1,46	1,37			
heat shock 70kDa protein 4 isoform a	H-hsp704	gi|38327039	94271,24219	5,11					0,58	0,54	0,76
heat shock 70kDa protein 8 isoform 2	H-hsp708	gi|24234686	53484,41016	5,62	31,38	472.297	4,72	16,64			
keratin 1	H-Krt1	gi|17318569	66027	8,16	5,84	478.636	4,79	1,53			
KRT8 protein	H-Krt8	gi|62913980	41082,66016	4,94	1,58		1,48	2,57			
KRT8 protein	H-Krt8	gi|62913980	41082,66016	4,94	2,38	245.634	2,46	3,59			
KRT8 protein	H-Krt8	gi|39645331	55874,19922	5,62	2,79	396.946	3,97	5,95			
PRDX4	H-PRDX4	gi|49456297	30570,8496	5,86					0,81	0,54	0,60
Stress response											
stress-induced-phosphoprotein 1 (Hsp70/Hsp90-organizing protein)	H-STIP1	gi|5803181	62599,39844	6,4					0,86	0,85	0,59
Translation associated proteins											
ATP-dependent DNA helicase II, 70 kDa subunit	H-Ku70	gi|4503841	69799,04688	6,23	1,02					0,58	0,64
G elongation factor, mitochondrial 1	H-GFM1	gi|18390331	83418,4375	6,58	1,09					0,74	0,59
KIAA0038	H-KI38	gi|436226	25468,67969	8,66	3,43	519.819	5,20	5,04			
minichromosome maintenance protein 7 isoform 1	H-MCM7	gi|33469968	81256,57031	6,08					0,87	0,70	0,37
RNA processing											
lamin A/C transcript variant 1	H-lmnA/C	gi|57014043	74036,70313	6,73					0,76	0,71	0,44
lamin B1	H-lmnB1	gi|5031877	66367,61719	5,11					0,99	0,78	0,31

otubain 1	H-otub	gi|109148508	31264,41992	4,85					0,88	0,82	0,47
Ubiquitin proteasome pathway											
Metabolism associated and transport proteins											
2-phosphopyruvate-hydratase alpha-enolase; carbonate dehydratase	H-ENOA	gi|693933	47079,28125	7,01					0,10	0,64	0,40
annexin A1	H-A1	gi|54696610	38803,0586	6,57	1,81	#####	3,04	2,72			
annexin A1	H-A1	gi|1421662	36308,6484	5,63					0,66	0,65	0,52
annexin A13 isoform b	H-A13B	gi|51896029	39719,26172	5,38					0,78	0,11	0,06
calpain, small subunit 1	H-CSS1	gi|18314496	28281,74023	5,05					0,91	0,60	0,54
chain A, the crystal structure of dihydrolipoamide dehydrogenase and dihydrolipoamide dehydrogenase	H-DLD	gi|83753870	50142,91016	6,5					0,56	0,92	0,34
chain A, ubiquitin-conjugating enzyme E2-25 kda (Huntington Interacting Protein 2)	H-HIP2	gi|60594411	22536,61914	5,33	1,05					0,63	0,34
chain E, crystal structure of human pnp At 2.3a resolution	H-Pnp	gi|37926571	31996,13086	6,49					0,84	0,64	0,56
dimethylarginine dimethylaminohydrolase 1	H-DDAH1	gi|6912328	31101,92969	5,53					0,64	0,73	0,55
dimethylarginine dimethylaminohydrolase 2	H-DDAH2	gi|7524354	29625,4492	5,66					0,89	0,77	0,40
enolase 1 variant	H-ENO1	gi|62896593	47111,28906	7,01					0,60	0,90	0,69
enolase 2	H-Eno2	gi|5803011	47239	4,91					0,84	0,60	0,27
galactose mutarotase (aldose 1-epimerase)	H-Galm	gi|20270355			1,57		1,03				0,59
glucosidase II	H-Glu2	gi|2274968	106832,6484	5,71	2,56		1,40	2,12			
glucose-6-phosphate dehydrogenase	H-G6PD	gi|30584817	59332,07031	6,39					0,40	0,65	0,22
hypothetical protein	H-Hyp	gi|12052754	20432,64063	6,29					0,31	0,47	0,19
hypothetical protein	H-Hyp	gi|31873364	33087,82813	8,14					0,73	0,71	0,59
kinesin-like 8 isoform a	H-KNSL8	gi|41871946	68597,61719	5,82					0,52	0,71	0,63
lasp-1 protein - human	H-Lasp1	gi|2135552	29786,19922	6,11					0,60	0,61	0,38
mRNA decapping enzyme	H-Dcp	gi|7661734	38585,01953	5,93	1,09					0,39	0,56

N-acetylneuraminic acid phosphate synthase	H-NANS	gi|12056473	40281,44922	6,29					0,91	0,93	0,56
NADH dehydrogenase (ubiquinone) Fe-S protein 1, 75kDa (NADH-coenzyme Q reductase)	H-NADHD	gi|21411235	79388,5	5,8					0,67	0,77	0,42
NADP-dependent isocitrate dehydrogenase	H-NIDH	gi|3641398	46658,53906	6,34					0,86	0,92	0,49
nascent-polypeptide-associated complex alpha polypeptide	H-NACA	gi|5031931	23369,71094	4,52	4,66		1,73	1,06			
peptidase (mitochondrial processing) alpha	H-Pmpca	gi|24308013	58215,60156	6,45					0,94	0,28	0,65
platelet-activating factor acetylhydrolase, isoform Ib, beta subunit 30kDa	H-LIS-1	gi|4505585	25553,11914	5,57	1,09					0,82	0,53
triosephosphate isomerase 1	H-TPI1	gi|4507645	26652,74023	6,45					0,61	0,80	0,51
TXNL2 protein	H-TXNL2	gi|48257132	32594,74023	5,36		257.026	2,57		0,63		0,69
Signal transduction											
serine or cysteine proteinase inhibitor clade B member 5	H-SPIB5	gi|60817455	42083,42188	5,72	1,04		1,15				0,57
interferon-induced Mx protein Homo sapiens	H-Mx	gi|188901	75530,25	5,65	1,04					0,67	0,48
thioredoxin reductase GRIM-12	H-GRIM12	gi|3820535	54579,92969	6,36	1,51		1,63				0,27
rho GTPase activating protein 1	H-Arhgap1	gi|4757766	50404,19141	5,85					0,90	0,54	0,35
DJ-1 protein	H-DJ-1	gi|31543380	19878,49023	6,33					0,85	0,62	0,50
DJ-1 protein	H-DJ-1	gi|31543380	19878,49023	6,33					0,95	0,76	0,57
interferon-induced Mx protein Human	H-Mx	gi|188901	75530,25	5,65					0,87	0,41	0,45
proteasome (prosome, macropain) subunit, beta type, 2	H-PSMB2	gi|30585195	22934,75977	6,51					0,56	0,47	0,43
proteasome activator subunit 2	H-PSME2	gi|30410792	27384,31055	5,54					0,68	0,98	0,56
serine (or cysteine) proteinase inhibitor, clade B (ovalbumin), member 1 variant	H-SPIB1	gi|62898301	42742,71094	5,9					0,85	0,68	0,49
Other proteins											
chain A, molecular basis for the recognition of phosphorylated and phosphoacetylated histone H3 by	H-MolB	gi|83754467	29242,32031	4,97					0,97	0,89	0,46
hypothetical protein	H-Hyp	gi|59016665	32559,26953	6,31					0,46	0,48	0,23

hypothetical protein DKFZp762H157.1 - human (fragment)	H-HypDK	gi|11276938	73890,09375	6,46	2,01		1,93	1,62			
hypothetical protein LOC79017	H-HypLoc	gi|13129018	20994,33008	5,07					0,93	0,58	0,57
integrin beta 4 binding protein isoform a	H-Ibbp	gi|4504771	26582,18945	4,56					0,73	0,73	0,54
KIAA0193	H-KI193	gi|20521842	49370,12109	4,83	1,97	237.479	2,37				0,72
programmed cell death 6 interacting protein	H-Pdcd6ip	gi|22027538	95963,1172	6,13					0,95	0,89	0,45
RuvB-like 1	H-RuvB1	gi|4506753	50196,30859	6,02					0,59	0,49	0,56
transformation-related protein 14	H-TRP14	gi|33415057	42791,69141	5,49					0,00	0,15	0,23
transformation-related protein 14	H-TRP14	gi|33415057	42791,69141	5,49					0,32	0,27	0,35
tumor necrosis factor type 1 receptor associated protein TRAP-1 - human	H-TRAP1	gi|1082886	75294,8672	8,43					0,58	0,68	0,53
Unknown proteins											
unnamed protein product	H-unmd	gi|34534595	65922,46094	4,45					0,44	0,45	0,01
unnamed protein product	H-unmd	gi|22760040	34008,57813	5,31					0,87	0,60	0,26

Table 6. Differential expression proteins in PC-3 cells (Protein profiling using 2-DE; Delta2D software; MALDI-TOF).

(PC-3 cells with and without VAVC GLV-1h68 treatment; time points were taken 12, 24 and 48 hours after virus infection; fold of enhancement or reduction of protein expression after virus infection are shown; highly expression in red and down-regulated in blue)

Fold of enhancement	Fold of suppression
>5	>5
3 to 5	3 to 5
2 to3	2 to 3

Protein name	Abbr	Accession	MW	*p*I	12hpi (+)fold	24hpi (+)fold	48hpi (+)fold	12hpi (-)fold	24hpi (-)fold	48hpi (-)fold
Viral proteins										
30k DNA binding phosphoprotein	V-I3L	gi|2772696	30008,4707	5,68	6,41	11,09	12,59			
beta galactosidase [UAS-less reporter vector pMELbeta]	V-bGal	gi|37812657	118482,3672	5,49		6,55	13,27			
beta-galactosidase	V-bGal	gi|595694	123444,8281	5,37		3,61	6,37	0,95		
beta-galactosidase	V-bGal	gi|644832	116130,9531	5,28		1,80	2,69	0,74		
hypothetical protein m8218R	V-hyp8218R	gi|56713567	27620,60938	4,85	8,52	17,00	21,52			
major core protein	V-A10L	gi|56713513	102184,5391	5,83		4,42	4,78			
morphogenesis-related, substrate of B1R kinase	V-VLTF4	gi|66275900	22286,59961	6,86	5,14	7,58	12,08			
morphogenesis-related, substrate of B1R kinase	V-VLTF4	gi|66275900	22286,59961	6,86	5,51	9,91	12,36			
p4b precursor of core protein 4b	V-A3L	gi|66275919	72577,84375	6,28		3,30				0,70
putative 43.1k protein	V-A6L	gi|2772720	43072,44141	5,71		1,60	3,76	0,46		
putative DNA-binding virion core protein	V-E11L	gi|56713462	28424,65039	6,03	3,47	17,19	19,77			
renilla luciferase/neomycin phosphotransferase fusion protein [CMV hRluc-neo Flexi Vector pF9A]	V-Ruc	gi|114054347	65953,07031	5,15		2,80	2,14			

ribonucleoside-diphosphate reductase	V-I4L	gi|56713400	36922,23828	5,08	2,99	5,37	8,90			
serine protease inhibitor-like SPI-1	V-C12L	gi|37551448	38215,5	4,69	8,42	14,80	14,56			
Cytoskeleton proteins										
tropomyosin 3 isoform 2	H-Tpm3	gi|24119203	29014,74023	4,75			9,79		0,74	
keratin, type I cytoskeletal 9 (Cytokeratin-9) (CK-9) (Keratin-9) (K9)	H-Krt9	gi|81175178	62091,91016	5,19	2,26	1,77	1,46			
keratin like	H-Krtl	gi|951272	27379,2793	5,45	2,38		1,18		0,96	
keratin 7	H-Krt7	gi|67782365	51354,30859	5,4	2,42	1,99				0,63
keratin 7	H-Krt7	gi|12803727	51387,35938	5,42	2,61	2,18	1,97			
keratin 8	H-Krt8	gi|49256423	53717,12109	5,52	2,71	2,23				0,62
keratin 19	H-Krt19	gi|34783124	45586,96875	5,11	2,93	2,43				0,67
ACTB protein	H-ActB	gi|15277503	40194,07031	5,55				0,44	0,56	0,54
gamma-actin Homo sapiens	H-ActG	gi|178045	25861,96094	5,65		1,01	1,07	0,53		
alpha actinin 4	H-ACTN4	gi|2804273	102204,398	5,27				0,54	0,49	0,33
ARP2 actin-related protein 2 homolog (yeast)	H-ARP2	gi|15778930	44732,25	6,3				0,85	0,78	0,52
ARP3 actin-related protein 3 homolog	H-ARP3	gi|5031573	47340,98047	5,61				0,55	0,61	0,72
tubulin, beta, 4 variant	H-Btub	gi|62897639	50340,19922	4,83				0,66	0,72	0,60
chain A, crystal structure of soluble form of clic4	H-CLIC4	gi|109157428	29818,2207	5,89				0,47	0,37	0,44
gelsolin (amyloidosis, Finnish type)	H-GlsCap	gi|55960301	28935,71094	7,71				0,90	0,66	0,26
HS1 binding protein (HAX1)	H-HAX1	gi|55663095	28473,43945	4,82				0,79	0,45	0,29
L-plastin variant	H-LCP1	gi|62898171	70214,82813	5,2				0,22	0,11	0,14
L-plastin	H-LCP1	gi|4504965	70244,84375	5,2			1,28	0,56	0,86	
moesin	H-Msn	gi|4505257	67777,78906	6,08				0,99	0,87	0,53
moesin	H-Msn	gi|4505257	67777,78906	6,08				0,73	0,73	0,51
stomatin (EPB72)-like 2 variant	H-Stom	gi|62897765	38524,21094	6,88				0,82	0,90	0,46
Stress reponse										

CCT2	H-TCP1	gi|48146259	57424,05859	6,01		3,97	6,86	0,97		
chaperonin containing TCP1, subunit 5 (epsilon)	H-CCT5	gi|24307939	59632,80859	5,45				0,80	0,66	0,52
chaperonin containing TCP1, subunit 5 (epsilon)	H-CCT5	gi|24307939	59632,80859	5,45				0,67	0,63	0,42
chaperonin containing TCP1, subunit 8 (theta) variant	H-CCT8	gi|62896539	59612,51172	5,42				0,57	0,64	0,56
DnaJ homolog, subfamily C, member 9	H-DNAJC9	gi|27597059	29891,08984	5,58				0,52	0,71	0,97
gamma subunit of CCT chaperonin	H-CCtg	gi|671527	60292,25	6,23				0,88	0,86	0,56
heat shock 70kDa protein 4 isoform a variant	H-Hsp704	gi|62087882	87949,21094	5,44				0,60	0,73	0,50
heat shock 70kDa protein 4 isoform a variant	H-Hsp704	gi|62087882	87949,21094	5,44				0,47	0,65	0,45
heat shock 70kDa protein 8 isoform 1	H-hsp708	gi|5729877	70854,21875	5,37		1,41	2,11	0,99		
heat shock 70kDa protein 8 isoform 1	H-hsp708	gi|5729877	70854,21875	5,37				0,54	0,45	0,37
heat shock 70kDa protein 8 isoform 1	H-hsp708	gi|5729877	70854,21875	5,37				0,65	0,59	0,66
heat shock 70kDa protein 8 isoform 1	H-hsp708	gi|5729877	70854,21875	5,37				0,62	0,52	0,48
heat shock protein HSP 90-alpha (HSP 86) (NY-REN-38 antigen)	H-HSP90	gi|92090606	84606,67969	4,94				0,55	0,34	0,06
HSP90AA1 protein	H-HSP90	gi|12654329	64349,69922	5,1				0,36	0,46	0,24
KIAA0201	H-KI201	gi|40788905	106673,8438	5,82				0,54	0,59	0,59
oxygen regulated protein precursor	H-Orp	gi|5453832	111266,2109	5,16				0,92	0,88	0,10
oxygen regulated protein precursor	H-Orp	gi|5453832	111266,2109	5,16				0,65	0,88	0,05
t-complex polypeptide 1	H-TCP1	gi|36796	60355,75	6,03				0,46	0,57	0,63
Translation associates proteins										
ATP-dependent DNA helicase II	H-Ku70	gi|10863945	82652,27344	5,55				0,48	0,50	0,10
ATP-dependent DNA helicase II	H-Ku70	gi|10863945	82652,27344	5,55				0,71	0,85	0,50

ATP-dependent DNA helicase II	H-Ku70	gi|10863945	82652,27344	5,55				0,64	0,70	0,32
DNA replication licensing factor MCM4	H-MCM4				43,47	22,21	7,36			
elongation factor Tu, mitochondrial precursor (EF-Tu) (P43) Homosapiens	H-EF-G	gi|1706611	49510,17969	7,26		1,05		0,92		0,34
eukaryotic translation elongation factor 1 gamma	H-EEF1g	gi|15530265	50115,17188	6,25				0,73	0,71	0,58
eukaryotic translation initiation factor 3, subunit 9 eta, 116kDa	H-Eif3s9	gi|51094703	88625,02344	4,96				0,23	0,56	0,49
eukaryotic translation initiation factor 4B	H-EIF4B	gi|50053795	69110,28125	5,55				0,26	0,57	0,29
eukaryotic translation initiation factor 4B	H-EIF4B	gi|50053795	69110,28125	5,55				0,04	0,31	0,01
KIAA0038	H-KI38	gi|436226	25468,67969	8,66		1,58	2,02			
minichromosome maintenance protein 7 isoform 1	H-MCM7	gi|33469968	81256,57031	6,08				0,90	0,95	0,34
PPA1 protein	H-PPA1	gi|33875891	35448,64063	5,95	2,73	4,83	8,16			
ribosomal protein, large, P0	H-ARPP0???	gi|12654583	34252,73828	5,42				0,36	0,42	0,35
TB3-1 Homo sapiens	H-TB3-1	gi|338687	47965,16016	9,52					0,56	0,22
RNA processing										
adhesion regulating molecule 1 precursor	H-ADRM1	gi|28373192	42126,80859	4,96				0,69	0,31	0,49
ash protein	H-ash	gi|28876	18567,17969	6,65				0,79	0,43	0,52
aspartyl-tRNA synthetase	H-AspS	gi|45439306	57100,03125	6,11				0,31	0,64	0,46
glycyl-tRNA synthetase	H-GlyS	gi|116805340	83112,60938	6,61				0,59	0,62	0,52
heterogeneous nuclear ribonucleoprotein C (C1/C2)	H-hnRNPC	gi|14249959	32373,91016	5	4,24	13,33	10,74			
heterogeneous nuclear ribonucleoprotein H3 isoform b	H-hnRNPC	gi|14141159	35216,37891	6,36	2,73	3,07	5,67			
heterogeneous nuclear ribonucleoprotein K	H-hnRNPK	gi|55958544	47527,64063	5,46	2,05	2,52	3,43			
hnRNP C2 protein Homo sapiens	H-hnRNPC2	gi|337455	33278,39063	5,11	2,41	2,13	2,76			
HNRPF protein	H-HNRPF	gi|16876910	45670,85938	5,38	2,24	3,86	3,61			
poly(rC) binding protein 1	H-PCBP1Ê	gi|5453854	37501,96875	6,66	2,46	2,00				0,84
SARS protein	H-SARS	gi|111494145	58369,82031	6,05	1,20				0,97	0,46
splicing factor SF3a60	H-SF3a60	gi|551450	58740,23047	5,3	1,16	2,07	2,68			

TALDO1 protein	H-TALDO	gi|48257056	37385,42188	6,35	1,49	2,67	3,76			
Ubiquitin proteasome pathway										
human 26S proteasome subunit p97	H-PSMD2	gi|1060888	100121,7734	5,08				0,48	0,69	0,83
otubain 1	H-otub	gi|109148508	31264,41992	4,85				0,75	0,55	0,57
Proteasome (prosome, macropain) 26S subunit, ATPase, 1	H-PSMC1	gi|16741033	49172,73047	5,92				0,69	0,56	0,67
proteasome 26S ATPase subunit 4 isoform 1	H-26S4	gi|5729991	47336,53906	5,09				0,52	0,62	0,61
proteasome 26S non-ATPase subunit 5	H-PSMD5	gi|4826952	56160,35938	5,35			1,10	0,53	0,56	
proteasome subunit Y	H-PSMB6	gi|558528	25299,40039	4,8				0,79	0,47	0,60
ubiquitin activating enzyme E1	H-UBE1	gi|35830	117715,3438	5,57				0,47	0,61	0,29
ubiquitin activating enzyme E1	H-UBE1	gi|35830	117715,3438	5,57				0,39	0,50	0,16
Metabolism associated and transport proteins										
aconitase 1	H-ACO1	gi|8659555	98336,57813	6,23		2,36				0,37
acylamino acid-releasing enzyme	H-APEHÊ	gi|556514	81240,64844	5,29				0,42	0,50	0,31
adenosine kinase Homosapiens	H-AK	gi|1224125	38714,62891	6,28		2,23	1,54			
AGM1	H-AGM1	gi|56203408	55453,94141	5,76				0,63	0,83	0,59
aryl hydrocarbon receptor interacting protein	H-AIP	gi|4502009	37640,14844	6,09	3,76	2,17	2,11			
chain A, crystal structure of human sar1a in complex with Gdp	H-Sar1a	gi|93279951	23160,89063	7,19				0,01	0,01	0,21
chain A, horf6 a novel human peroxidase enzyme	H-Horf	gi|3318841	25011,19922	6				0,71	0,42	0,34
chain A, horf6 a novel human peroxidase enzyme	H-Horf	gi|3318841	25011,19922	6				0,73	0,69	0,54
COMT protein	H-COMT	gi|33875419	20032,23047	5,36	5,52	10,90	24,97			
copine I	H-CpnI	gi|4503013	59021,53906	5,52				0,65	0,62	0,53
copine III	H-CpnIII	gi|4503015	60092,12891	5,6				0,71	0,75	0,50
creatine kinase	H-Ck	gi|180570	42591,26172	5,34					0,80	0,41

dipeptidylpeptidase 9	H-DPP9Ê	gi|51988902	96551,14844	6,05				0,50	0,63	0,00
endoplasmic reticulum protein 29 isoform 1 precursor	H-ERp29	gi|5803013	28975,15039	6,77				0,88	0,79	0,58
enolase 1 variant	H-ENO1	gi|62896593	47111,28906	7,01	1,88	2,11	1,20			
enolase 2	H-Eno2	gi|5803011	47239	4,91				0,69	0,71	0,59
ERO1-like (S. cerevisiae)	H-ERO1L	gi|14250470	54357,10156	5,62				0,45	0,30	0,19
glucosidase II	H-Glu2	gi|2274968	106832,6484	5,71				0,59	0,89	0,21
glutathione S-transferase M3 (brain)	H-GSTM3	gi|14250650	26556,15039	5,37				0,72	0,45	0,72
glutathione synthetase	H-GS	gi|4504169	52352,26172	5,67				0,55	0,70	0,85
glycerol-3-phosphate dehydrogenase 2 (mitochondrial)	H-GPD2	gi|4504085	80763,53125	6,98	2,25	2,44	1,31			
glyoxalase I	H-GLO	gi|1881782	20764,25	5,12				0,08	0,02	0,76
GSPT1 protein	H-GSPT1	gi|33874734	68403,96094	5,22				0,52	0,55	0,32
guanine monophosphate synthetase	H-GMPS	gi|4504035	76666,95313	6,42		1,82				0,26
heat shock 70kDa protein 5 (glucose-regulated protein, 78kDa)	H-GRP78	gi|16507237	72288,42969	5,07				0,64	0,96	0,32
Hpast	H-Hpast	gi|2529707	60664,67188	6,49		1,33				0,28
hypothetical protein	H-Hyp	gi|31873302	47063,33984	7,57		2,05				0,94
inosine monophosphate dehydrogenase 2	H-IMPDH2	gi|66933016	55769,64844	6,44		1,12				0,51
karyopherin alpha 6	H-KPNA6	gi|6912478	59991,44922	4,89				0,23	0,25	0,15
lasp-1 protein - human	H-Lasp1	gi|2135552	29786,19922	6,11	1,50		1,33		0,47	
leukotriene A4 hydrolase	H-LTA4H	gi|4505029	69241,24219	5,8	1,05				0,68	0,22
mitochondrial ATP synthase, H+ transporting F1 complex beta subunit	H-ATPF1	gi|89574029	48083,03906	4,95				0,79	0,78	0,42
NADH dehydrogenase (ubiquinone) Fe-S protein 1, 75kDa (NADH-coenzyme Q reductase)	H-NADHD	gi|21411235	79388,5	5,8				0,36	0,05	0,02
NDUFV2	H-NDUFV2	gi|48145973	27331,9707	8,22				0,38	0,41	0,54
N-ethylmaleimide-sensitive factor	H-NSF	gi|21040484	82542,07031	6,52	2,35				0,97	0,02
oxoglutarate (alpha-ketoglutarate) dehydrogenase (lipoamide) isoform 1 precursor	H-OGDH	gi|51873036	115861,3984	6,4					0,98	0,37
phosphoglucomutase 2	H-PGM2	gi|14603253	68298,39844	6,17				0,77	0,67	0,54

phosphoglycerate dehydrogenase	H-PHGDH	gi|23308577	56614,39844	6,29		1,06		0,93		0,57
protein disulfide isomerase	H-PDI	gi|860986	56643,71875	6,1				0,70	0,59	0,91
replication protein A2, 32kDa	H-RPA2	gi|56204165	30137,01953	6,45	1,46	1,28	2,04			
SEC23B protein	H-SEC23B	gi|13529299	86407,57031	6,43				0,79	0,31	0,04
spermine synthase	H-SPMSY	gi|21264341	41241,78125	4,87				0,55	0,65	0,83
succinate dehydrogenase complex, subunit A, flavoprotein precursor variant	H-Sdha	gi|62087562	73129,52344	6,94		1,71		0,84		0,27
TALDO1 protein	H-TALDO	gi|48257056	37385,42188	6,35				0,58	0,93	0,65
TPI1 protein (Triosephosphate isomerase)	H-TBI1	gi|47682755	27420,24023	8,48		2,25				0,93
twinfilin-like protein	H-TWFl	gi|6005846	39523,26953	6,37					0,88	0,42
TXNDC5 protein	H-TXNDC5	gi|12654715	36155	5,32				0,77	0,70	0,41
ubiquinol-cytochrome c reductase core I protein Homosapiens	H-QCyRe	gi|515634	52585,42188	5,94				0,72	0,82	0,05
Signal transduction										
ANXA3	H-A3	gi|47115233	36451,73828	5,76	1,30	2,01	2,61			
BiP protein	H-BiP	gi|6470150	70887,52344	5,23			1,10	0,56	0,71	
Chain A, Human Dj-1 With Sulfinic Acid	H-DJ1	gi|50513593	19886,48047	6,33				0,24	0,57	0,90
chloride intracellular channel 1	H-CLIC1	gi|55961458	26167,26953	4,95			2,19	0,88	0,51	
cytidylate kinase	H-CMPK	gi|7706497	25838,34961	8,14			1,09	0,00	0,00	
G3BP	H-G3BP	gi|49168554	52132,10938	5,42				0,44	0,65	0,23
GIPC1 protein	H-GIPC1	gi|33872740	32677,91992	5,89				0,71	0,58	0,51
high-mobility group box 1	H-HMGB1	gi|55958715	22036,3203	9,61	1,27	1,15	2,46			
phosphoglucomutase 1	H-HMGB1	gi|30584157	61444,5117	6,2	1,03	1,12				0,56
P21-activated kinase 2	H-PAK2	gi|47482156	58104,9609	5,78				0,29	0,53	0,54
rho GTPase activating protein 1	H-Arhgap1	gi|4757766	50404,19141	5,85				0,47	0,50	0,20
zinc finger protein 259	H-ZNF259	gi|4508021	50893	4,66				0,23	0,59	0,17

Other proteins										
dendritic cell protein variant	H-Ga17	gi|62896687	42443,82813	5,41				0,64	0,50	0,88
hypothetical protein	H-Hyp	gi|31874844	46340,05078	5,55				0,49	0,46	0,42
hypothetical protein	H-Hyp	gi|51491236	47911,62891	8,12				0,69	0,58	0,57
hypothetical protein	H-Hyp	gi|51476352	42920,98047	5,27				0,75	0,84	0,59
immunoglobulin binding protein 1	H-IGBP1	gi|4557663	39197,5	5,26	1,61	1,10	2,64			
integrin beta 4 binding protein isoform a	H-Ibbp	gi|4504771	26582,18945	4,56				0,75	0,52	0,86
KIAA0885 protein	H-KI885	gi|40788973	91993,1875	5,62		2,76				0,97
KIAA0885 protein	H-KI885	gi|40788973	91993,1875	5,62				0,52	0,56	0,25
leucine aminopeptidase 3	H-ALP3	gi|41393561	56130,80859	8,03					0,88	0,41
mitofilin	H-Mtfln	gi|8131894	68145,28125	5,57	2,23	1,84				0,27
NOP17	H-NOP17	gi|8923598	32342,36914	5,05			2,02	0,82	0,79	
nudC domain containing 1	H-NUDCD1	gi|23618846	66733,28125	4,99	2,12	1,71	1,14			
plastin 3	H-PLS3Ê	gi|7549809	70766,21094	5,41				0,83	0,59	0,46
programmed cell death 6 interacting protein	H-Pdcd6ip	gi|22027538	95963,1172	6,13	1,21	1,29				0,53
programmed cell death 6 interacting protein	H-Pdcd6ip	gi|22027538	95963,1172	6,13	1,06	1,21				0,48
programmed cell death 6 interacting protein	H-Pdcd6ip	gi|22027538	95963,1172	6,13		1,01		0,73		0,38
protein phosphatase 2, catalytic subunit, beta isoform	H-PPP2CBÊ	gi|4758952	35552,32813	5,21			1,07	0,48	0,78	
Protein SET (Phosphatase 2A inhibitor I2PP2A) (I-2PP2A) (Template-activating factor I) (TAF-I) (HLA	H-SET	gi|46397790	33468,69922	4,23	1,29				0,93	0,56
reticulocalbin 1 precursor	H-RCN1	gi|4506455	38866,16016	4,86				0,62	0,61	0,52
tetratricopeptide repeat domain 1	H-TTC1	gi|4507711	33505,17188	4,78			1,06		0,52	
transglutaminase 2 isoform a	H-TGM2	gi|39777597	77279,67188	5,11				0,37	0,44	0,27
tumor rejection antigen (gp96) 1 variant	H-gp96	gi|62088648	65912,28906	5,08				0,12	0,35	0,05
UV excision repair protein RAD23 homolog A variant	H-RAD23A	gi|62089006	41230,51172	4,66	1,23				0,64	0,29
vinculin isoform meta-VCL	H-mVCL	gi|7669550	123721,8125	5,5				0,58	0,65	0,28
vinculin isoform meta-VCL	H-mVCL	gi|7669550	123721,8125	5,5				0,64	0,76	0,44

vinculin isoform VCL	H-VCL	gi|4507877	116649,3203	5,83				0,67	0,75	0,49
Unknown proteins										
unknown (protein for IMAGE:3529287)	H-unkn	gi|52790434	37696,98047	8,56	2,04	2,20	1,11			
unknown [synthetic construct]	H-unkn	gi|62288518	31111,46094	6,3	2,86	2,21	1,39			
unnamed protein product	H-unkn	gi|18676733	28025,11914	6,5				0,55	0,56	0,20
unnamed protein product	H-unkn	gi|34534595	65922,46094	4,45				0,21	0,50	0,16
unnamed protein product	H-unkn	gi|21748975	47011,35938	5,45				0,68	0,59	0,25
unnamed protein product	H-unkn	gi|35218	75811,5625	5,41				0,77	0,73	0,57
unnamed protein product	H-unkn	gi|35218	75811,5625	5,41				0,75	0,62	0,39